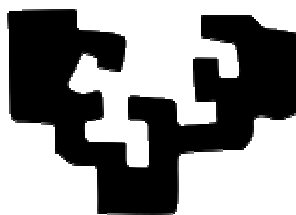


eman ta zabal zazu



Universidad
del País Vasco

Euskal Herriko
Unibertsitatea

FACULTAD DE QUÍMICA DE SAN SEBASTIÁN
DEPARTAMENTO DE QUÍMICA APLICADA
UNIDAD DE QUÍMICA INORGÁNICA

**“LATE TRANSITION METAL Silyl AND ACYL COMPLEXES THROUGH E-H
ACTIVATION: REACTIVITY AND CATALYTIC APPLICATIONS”**

MEMORIA

para optar al grado de Doctor en Ciencias Químicas
que presenta

SUSAN AZPEITIA COSCARÓN

2019

ACKNOWLEDGEMENTS

En primer lugar quisiera agradecer a mis directores, la Dra. M^a Ángeles Garralda Hualde y el Dr. Miguel Ángel Huertos Mansilla, por la confianza depositada y todo su apoyo durante mi formación como investigadora, y por el tiempo dedicado y los consejos prestados, sin los cuales no hubiera sido posible realizar este trabajo.

I would like to express my sincere gratitude to the Chemistry Department of the University of Oxford, for giving me access to their laboratory and research facilities, and especially to Prof. Andrew S. Weller, for the opportunity to join his team and his support during my stay. I would also like to thank all the members of the Weller group I worked with for their help in and outside the lab, and for making me feel so welcome.

Mi agradecimiento al Gobierno Vasco por la financiación durante estos años, con la concesión tanto de la Ayuda a la Formación de Personal Investigador como la Ayuda de Movilidad para la Estancia en el extranjero, las cuales me han permitido realizar parte de este trabajo.

Agradezco a todas aquellas personas que han colaborado o han estado presentes en la realización de este trabajo, y en particular a la Dra. Lourdes Ibarlucea y a la Dra. Montserrat Barquín.

Quiero también agradecer a todos mis compañeros de laboratorio por la ayuda y apoyo que me habéis ofrecido durante toda mi investigación y por los buenos ratos compartidos, a los que ya estaban cuando me incorporé: Ainara, Itziar Oyarzabal, Itziar Zumeta, Virginia y Jorge, y a los que han ido llegando: Borja, Andoni, Ane, Estitxu, Maider, Uxua, Eder y Unai. En especial a Itxaso y a Naroa, sin las que estos cuatro años no habrían sido lo mismo.

A mi familia, por todo su cariño y paciencia. Por animarme y apoyarme en todas mis decisiones, aguantar mis nervios y estar ahí siempre que los he necesitado. Y a David, por hacerme ver siempre las cosas buenas.

LIST OF ABBREVIATIONS

ampy	2-aminomethylpyridine
aqui	8-aminoquinoline
bipy	2,2`-bipyridine
cod	1,5-cyclooctadiene
coe	cyclooctene
Cp*	pentamethylcyclopentadienyl
m/z	mass-to-charge ratio
nbd	Bicyclo[2.2.1]hepta-2,5-diene
nbyl	norbornenyl
ntyl	nortricyclyl
hpz	pyrazole
phen	1,10-phenantroline
4-pic	4-methylpyridine or 4-picoline
py	pyridine
THF	tetrahydrofuran

INDEX

I.	INTRODUCTION	17
I.1.	ORGANOMETALLIC COMPLEXES IN E-H BOND ACTIVATION	19
I.1.1.	TRANSITION-METAL CATALYSED C-H ACTIVATION	23
I.1.2.	TRANSITION-METAL CATALYSED SI-H ACTIVATION	25
I.2.	BIBLIOGRAPHY	28
II.	RESULTS AND DISCUSSION.....	31
II.1.	ACTIVATION OF THE SILICON-HYDROGEN BOND.....	33
II.1.1.	INTRODUCTION.....	33
II.1.2.	SYNTHESIS OF SILYL-THIOETHER MULTIDENTATE PRELIGANDS AND THEIR REACTIVITY WITH DIOLEFINIC RHODIUM(I) AND IRIIDIUM(I) COMPLEXES	38
II.1.2.1.	Synthesis of ligands	39
II.1.2.2.	Reactivity of ligands L1 and L2 with [Rh(cod)Cl] ₂ . Synthesis of Rh(III) complexes via Rh(I)/Rh(III) mixed-valent and cyclooctenyl intermediates	41
II.1.2.3.	Reactivity of ligand L2 with [Rh(cod)Cl] ₂ , [Ir(cod)Cl] ₂ and [Rh(nbd)Cl] ₂ dimers. Study of the olefin insertion and β-hydride elimination processes	48
II.1.2.3a.	<i>Reactivity of L2 with [Rh(cod)Cl]₂ and [RhCl(PPh₃)₃]</i>	48
II.1.2.3b.	<i>Reactivity of L2 with [Ir(cod)Cl]₂</i>	52
II.1.2.3c.	<i>Reactivity of L2 with [Rh(nbd)Cl]₂</i>	58
II.1.2.4.	Reactivity of ligand L3 with [Rh(cod)Cl] ₂ , [Rh(nbd)Cl] ₂ , [Ir(cod)Cl] ₂ and [Rh(coe) ₂ Cl] ₂ dimers.....	63
II.1.2.4a.	<i>Reactivity of L3 with [Rh(cod)Cl]₂, [Rh(nbd)Cl]₂ and [Ir(cod)Cl]₂</i>	63
II.1.2.4b.	<i>Reactivity of L3 with [Rh(coe)₂Cl]₂</i>	69
II.1.3.	SYNTHESIS AND CATALYTIC APPLICATIONS OF SILYL-HYDRIDE RHODIUM(III) AND IRIIDIUM(III) COMPLEXES DERIVED FROM L1 AND L2	74
II.1.3.1.	Synthesis of rhodium and iridium catalysts	78
II.1.3.2.	Dehydrogenative coupling of L2 using Wilkinson's catalyst	83
II.1.3.3.	Tandem isomerisation-hydrosilylation of alkenes.....	88
II.1.3.3a.	<i>Rhodium-catalysed alkene tandem isomerisation-hydrosilylation</i>	88
II.1.3.3b.	<i>Rhodium and iridium catalysed alkene tandem isomerisation- hydrosilylation or dehydrogenative silylation</i>	98
II.1.4.	BIBLIOGRAPHY	103
II.2.	ACTIVATION OF THE CARBON-HYDROGEN BOND IN ALDEHYDES	108

II.2.1.	INTRODUCTION	108
II.2.2.	REACTIVITY OF PHOSPHINE-ALDEHYDE $\text{PPh}_2\text{CH}(\text{Ph})\text{CH}_2\text{CHO}$ WITH DIOLEFINIC RHODIUM(I) COMPLEXES.....	120
II.2.2.1.	Reactivity with $[\text{Rh}(\text{cod})\text{Cl}]_2$	123
	II.2.2.1a. Synthesis, characterization and reactivity of neutral acylhydridorhodium(III) complexes.....	123
	II.2.2.1b. Synthesis and characterization of cationic acylhydridorhodium(III) complexes with NN bidentate or PNN-terdentate ligands	132
II.2.2.2.	Reactivity with $[\text{Rh}(\text{nbd})\text{Cl}]_2$. Alkyl(phosphinoacyl)- and Alkyl(phosphinoester)-rhodium(III) complexes.....	138
II.2.3.	THE REACTION OF $[\text{Rh}(\text{nbd})\text{Cl}]_2$ WITH QUINOLINE-8-CARBALDEHYDE AND PYRAZOLE. REACTIVITY AND CATALYTIC APPLICATIONS.....	144
II.2.3.1.	Synthesis of alkyl-quinolineacyl-pyrazole rhodium complexes	149
II.2.3.2.	Reactivity of alkyl-quinolineacyl-pyrazole rhodium(III) complexes with monodentate P-donor ligands, PPh_3 or PPh_2OH	156
II.2.3.3.	Catalytic activity of alkyl-quinolineacyl-pyrazole rhodium(III) complexes in the hydrolysis of ammonia-borane for hydrogen liberation.....	163
	II.2.3.3a. Optimization of reaction conditions	166
	II.2.3.3b. Hydrolysis of ammonia-borane catalysed by complexes $[\text{RhCl}(\text{C}_9\text{H}_6\text{NCO})(\text{Hpz})(\text{nbyl})]_2$, $[\text{RhCl}(\text{C}_9\text{H}_6\text{NCO})(\text{Hpz})_2(\text{nbyl})]$, $[\text{Rh}(\text{C}_9\text{H}_6\text{NCO})(\text{Hpz})_3(\text{nbyl})]\text{BPh}_4$ or $[\text{RhCl}(\text{C}_9\text{H}_6\text{NC}(\text{nbyl})\text{OH})(\text{Hpz})(\text{Ph}_2\text{PO})]$...	167
II.2.4.	BIBLIOGRAPHY	172
III.	CONCLUSIONS	179
IV.	EXPERIMENTAL SECTION	185
IV.1.	INSTRUMENTAL TECHNIQUES.....	187
IV.2.	SYNTHESIS OF STARTING MATERIAL	189
IV.3.	SYNTHESIS AND CHARACTERISATION OF COMPLEXES	192
IV.4.	CATALYTIC PROCEDURES	215
IV.4.1.	DEHYDROCOUPLING OF SILANES	215
IV.4.2.	TÁNDEM ISOMERISATION-HYDROSILYLATION OR TÁNDEM ISOMERISATION-DEHYDROGENATIVE SILYLATION.....	216
IV.4.3.	DEHYDROGENATIO OF AMMONIA BORANE	219
IV.5.	BIBLIOGRAPHY	220
V.	RESUMEN	221

I. INTRODUCTION

I.1. ORGANOMETALLIC COMPLEXES IN E-H BOND ACTIVATION

The discovery of the π -sandwich structure of ferrocene in the early 1950s served as a driving force for the rapid development that organometallic chemistry has experienced to date, and subsequent advances led to deep conceptual changes in our understanding of chemical bonding, structural features and reaction mechanisms.¹ This multidisciplinary science also laid the basis for a number of revolutionary processes in diverse areas, such as in polymer industry, pharmaceuticals, refinery, agriculture or medicine.² The large variety of ligands that can coordinate to a metal centre allow organometallic complexes to adopt very different structural geometries, and late second and third row transition metals grant the access to multiple stable oxidation states, thus enabling the multielectron transformation of a substrate under mild conditions.³ Consequently, organometallic compounds have been vastly used as catalysts for organic and polymer syntheses to date.

Industrial catalysis has been dominated by precious metal based complexes for decades, due to several unique properties they exhibit as catalysts.⁴ A great resistance to corrosion or oxidation allows them to work under acidic and alkaline conditions or without the strict need of an air-free environment in a variety of reactions, and the low ligand lability of these complexes also contributes to their overall stability. Moreover, their enhanced activity and selectivity for a certain type of transformation or product, and their facile and straightforward characterisation by well-established techniques including NMR spectroscopy, an extraordinarily helpful tool due to the formation of diamagnetic derivatives, ensures a predictable reactivity.

Among noble metals, ruthenium, palladium and rhodium have by far been the most employed as organometallic catalysts both in laboratory and industrial scale, especially in fine chemical syntheses. Rhodium-based homogeneous catalysts are known to participate in an enormous range of synthetically important organic reactions. The discovery of Wilkinson's catalyst $[\text{RhCl}(\text{PPh}_3)_3]$ proved to be a major breakthrough in the 1960s, leading to numerous successful applications including the hydrogenation of olefins with molecular hydrogen.⁵ At present, the use of this catalyst and its derivatives is well established for the hydroacylation, hydroboration, hydrosilylation or isomerisation of olefins.⁶ In contrast, iridium complexes are not so often applied in industrial chemistry as are their rhodium analogues, although they have proved to be very efficient in the production of fine chemicals as highly chemo and enantioselective catalysts.⁷ They have also been successfully used as model compounds for the stoichiometric study of the steps of numerous transition metal-catalysed reaction mechanisms.⁸ The

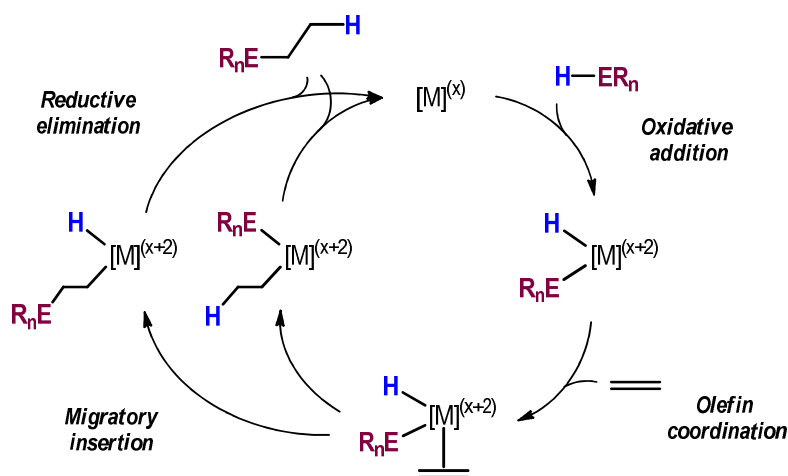
iridium(I) square planar $[\text{IrCl}(\text{CO})(\text{PPh}_3)_2]$ complex, commonly known as Vaska's compound, is representative of the latter application. First synthesised in 1961, its ability to undergo oxidative addition of a range of small molecules such as HCl, H_2 or O_2 encouraged the study of this key process and contributed to the development of many homogeneous catalysts.⁹

Despite their numerous advantages, the limited availability of precious metals and the demand of a more sustainable chemistry have recently encouraged the development of homogeneous catalysts based on first-row transition metals, due to their abundance and less toxic nature. However, their sensitivity to oxidising conditions, weak carbon-metal bonding and the tendency to generate radical intermediates are still important challenges to overcome.

While the choice of metal heavily influences the catalyst activity, the role played by the different ligands around the metal centre has also proved to be crucial. The formation of a metal-ligand bond modulates both the electronic properties of the metal and the steric environment of the coordination sphere, which enables some control of the structure and reactivity of the complex. It is well known that the formation of a chelate makes the resulting complex more stable.¹⁰ The use of multidentate ligands with mixed hard and soft donor atoms can also enhance the catalytic activity, as the weaker donor atom can often undergo facile decoordination to form an unsaturated species and allowing the substrate binding. This dynamic ability is known as hemilability.¹¹ Additionally, the coordination environment of a complex can also affect the selectivity of a certain reaction. A good example of this is the use of chiral ligands to obtain a certain enantiomeric product, commonly known as asymmetric catalysis.¹² Chiral phosphine ligands play an important role in this catalysis, in which chirality can be present in the backbone or in the phosphorus atom.¹³ In this manner, the selection of a particular ligand can directly affect the pathway of catalytic mechanisms.

Most catalytic pathways for electron-rich transition metals involve the cleavage and formation of new bonds in oxidative addition and reductive elimination steps.¹⁴ These cycles start with the activation of relatively inert non-polar E-E' and E-H bonds promoted by an organometallic complex (e.g. for E = C, Si, B, N, H). The activation of E-H bonds by oxidative addition is a key step in numerous important catalytic functionalization processes such as hydroacylation (E = acyl group),¹⁵ hydrosilylation (E = SiR_3),¹⁶ hydroboration (E = BR_2),¹⁷ hydroamination (E = NR_2),¹⁸ hydrophosphination (E = PR_2)¹⁹ or hydrogenation (E = H).²⁰ These hydroelementation processes imply the addition of the E-H bond to an unsaturated bond. A generally accepted mechanism for transition-metal centres in low oxidation states involves the oxidative addition of the E-H bond, coordination of the substrate by a multiple bond, the migratory insertion of this bond

and the reductive elimination of the product and catalyst regeneration (Scheme I1).¹⁴ In these mechanisms, the activation of the E-H bond by the metal centre leads to a hydride complex.

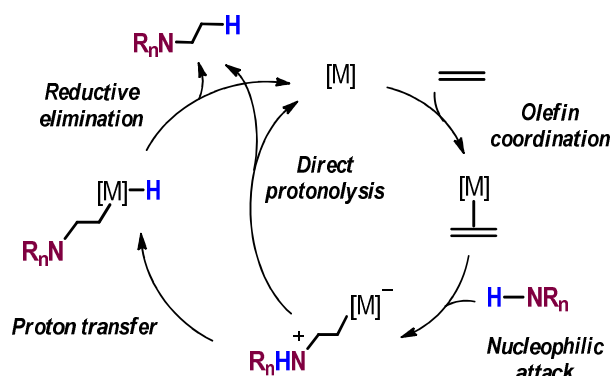


Scheme I1. Simplified catalytic cycle for a hydroelementation reaction by addition of an E-H bond to a double bond.

In 1965, Wilkinson's catalyst was found to catalyse the hydrogenation of olefins and acetylenes by the initial activation of the H-H bond of molecular hydrogen.²¹ This publication also discussed the attack of the olefin to the formed hydride species and the subsequent insertion into the M-H bond. In the same year, Chalk and Harrod described a similar mechanism for the hydrosilylation of olefins initiated by the activation of the Si-H bond by the metal centre, and followed by the activation of the olefin by coordination.²² In 1982, Milstein proposed the steps depicted in Scheme I1 for the intramolecular hydroacylation reaction of 4-pentenal to afford cyclopentanone, *via* the oxidative addition of the C-H bond in the aldehyde.²³

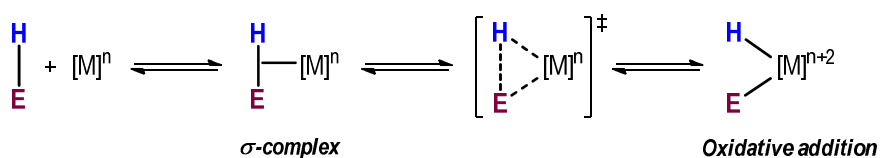
In contrast, the reaction pathway and selectivity of both hydroboration and hydroamination processes has proved to be heavily influenced by the type of catalyst.²⁴ Although the oxidative addition of the B-H bond in catecholborane to Wilkinson's catalyst was described in 1975 by Kono, Ito and Nagai,²⁵ it was not until the late 1980s that the mechanism involving olefin insertion into the M-H bond and product liberation by reductive elimination was proposed.²⁶ This E-H activation pathway was first proposed by Milstein et al. for the hydroamination reaction of norbornene with aniline, catalyzed by an iridium complex.²⁷ However, the most common observed mechanism for this reaction involves the initial activation of the olefin by coordination to the metal centre, followed by a nucleophilic attack by the N-H containing molecule on the olefin. Liberation of the final product then occurs by protonolysis, by direct

proton transfer to the M-C bond or by transfer of the proton to the metal centre with subsequent reductive elimination to form a C-H bond (Scheme 12).²⁸



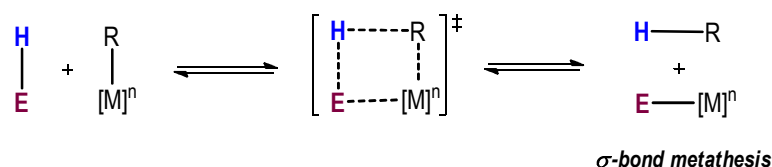
Scheme 12. Catalytic cycle for the hydroamination of an alkene by nucleophilic attack.

The formation of a metal-hydride species by the oxidative addition of the E-H to a metal centre can be preceded by a variety of metal-hydrogen interactions, including the η^2 -coordination of the E-H bond as a ligand to give σ -bond complexes (Scheme 13).²⁹ This reactivity has been the subject of intense research over the past years,³⁰ as it gives an insight into the E-H bond activation process by transition metals. Silane σ -bond complexes were the first to be isolated,³¹ and they represent the second largest class of σ -bond complexes apart from molecular hydrogen systems. They are currently used as a model for the binding and activation of their much more ephemeral alkane σ -analogues.^{30a,30d} Borane σ -complexes have also been recently well-characterised, with a coordination chemistry similar to that observed for silanes.^{30f,30h}



Scheme 13. Example of a reaction pathway for oxidative addition via a σ -complex intermediate.

The ability of E-H bonds to coordinate in a η^2 -manner also enables other types of reactivity such as σ -bond metathesis, where a ligand exchange is produced at the metal centre *via* a four-centre transition state, without a formal oxidative addition occurring (Scheme 14).³² This reaction pathway is usually observed with transition metal complexes unable to support an oxidation state increase by oxidative addition.



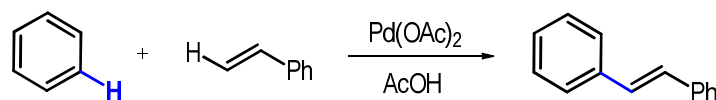
Scheme 14. Reaction pathway for a σ -bond metathesis.

The importance of σ -complexes and transition-metal hydride complexes is well established, as they are known to participate in practically all aforementioned catalytic hydroelementation reactions, as well as in olefin isomerisations, hydroformylations and in some oligomerisation and polymerisation processes. Due to the remarkable lability of the M-H moiety, it can participate in a wide range of important catalytic steps, such as migration, insertion or reductive elimination reactions, as depicted in Scheme 11. Therefore, the study of the formation and reactivity of transition-metal hydride complexes is necessary to give insight into the processes where they are involved.

I.1.1. TRANSITION-METAL CATALYSED C-H ACTIVATION

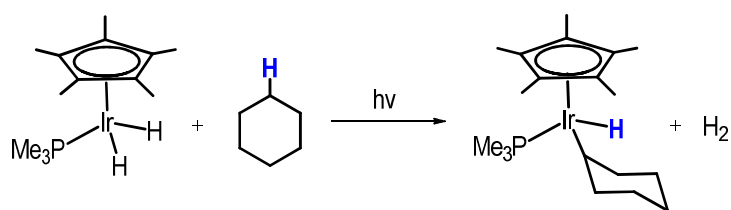
The selective functionalization of poorly reactive alkanes and alkyl moieties remains as one of the most challenging goals of modern chemistry. The possibility of producing more complex molecules by formation of new C-C and C-E bonds from abundant and traditionally inert saturated hydrocarbons has attracted considerable interest, although the usually large bond dissociation energy of C-H bonds makes it particularly difficult. However, transition-metal based catalysts have proved to be a powerful tool for this purpose.

It was well established that C(sp²)-H bonds in arenes were more readily activated than C(sp³)-H bonds in alkanes, due to their more electron-rich nature, and the ability to coordinate more strongly to a transition metal. One of the first examples of aryl C(sp²)-H activation was reported in 1965 by Chatt and Davidson, who described the oxidative addition of naphthalene to a ruthenium zero-valent complex to give the hydride derivative.³³ Another early contribution in aromatic C-H bond activation was the arylation of olefins by the stoichiometric coupling reaction of Pd(II)-olefin complexes with various arenes (Scheme 15), reported in late 1960s by Moritani and Fujiwara.³⁴ The study was later expanded to palladium-catalysed coupling between two benzenes to form biphenyl.³⁵



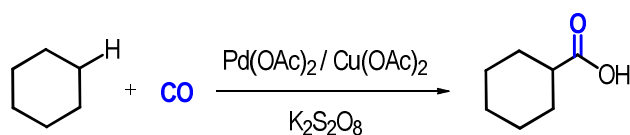
Scheme 15. Example of olefin arylation reported by Moritani and Fujiwara.

The first example of an alkane addition to a transition-metal complex was reported by Bergman and co-workers in 1982.³⁶ This publication describes the C(sp³)-H bond activation by oxidative addition of the simple alkane to an iridium complex to form stable alkyl hydrides (Scheme 16). Irradiation of the iridium Cp*Ir(PMe₃)₂ in neat cyclohexane as a solvent led to the loss of dihydrogen to form the reactive [Cp*Ir(PMe₃)] species, which readily cleaved the C–H bond of cyclohexane. Since then, several studies have been reported where the oxidative addition of an alkane is promoted by an unsaturated metal complex produced by photochemical or thermal loss of H₂ from dihydride species, RH from hydridoalkyl precursors or CO.³⁷



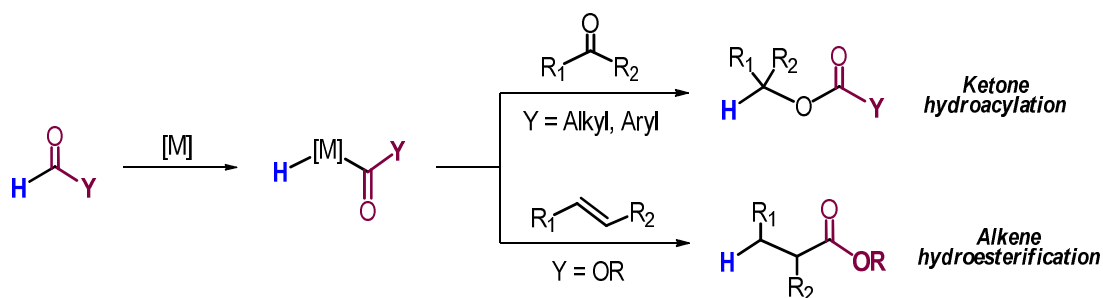
Scheme 16. C-H oxidation of cyclohexane by an iridium complex reported by Bergman et al.

The transition-metal mediated activation of C(sp)-H, C(sp²)-H and C(sp³)-H bonds by carboxylation has proved to be a powerful method for the synthesis of esters and derivatives, extensively used in pharmaceuticals or materials chemistry or as building blocks for numerous organic transformations.³⁸ In 1980, the first direct carboxylation of arenes was reported by Fujiwara and co-workers,³⁹ which was performed in the presence of stoichiometric amounts of Pd(OAc)₂. C-H activation in the arene, leading to benzoyl-palladium intermediates and to AcOH, allows the final formation of benzoic acid. The first transition-metal catalysed carboxylation of alkanes was also reported by Fujiwara et al. in 1989, performed on cyclohexane with pressured CO to afford cyclohexanecarboxylic acid (Scheme 17).⁴⁰ Since then, numerous studies using other esterification reagents to substitute carbon monoxide have been reported, such as azodicarboxylates,⁴¹ alkyl chloroformates,⁴² glyoxylates,⁴³ α-keto esters,⁴⁴ formates,⁴⁵ or carbon dioxide.⁴⁶



Scheme 17. C-H activation of cyclohexane by carboxylation with CO, reported by Fujiwara et al.

The aldehydic C-H bond activation is another important method for the synthesis of esters. The cleavage of the C-H bond in an aldehyde leads to a hydride-acyl metal species, which can be added across a C=O bond in ketones to form an ester product (Scheme 18). The intramolecular ketone hydroacylation to form 7-membered lactones is one of the most extensively studied application of this reaction.⁴⁷ The C-H activation of a formate can also yield an ester product through alkene hydroesterification, *via* the oxidative addition to a metal centre and subsequent addition to the C=C bond (Scheme 18).



Scheme 18. Synthesis of ester products through aldehyde or ester C-H activation.

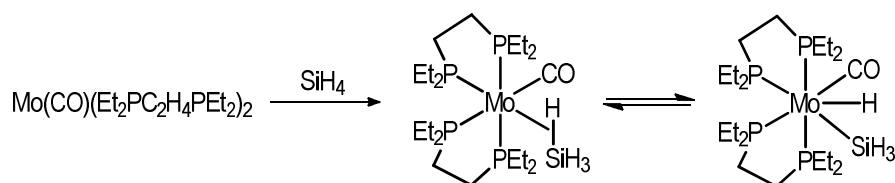
Metal acyl-hydride complexes formed by activation of the C-H bond in aldehydes are of particular interest, as they are known to be intermediates in numerous organic transformations involving the formation of new C-C bonds, as in olefin hydroacylation, or the formation of C-O bonds as in ketone hydroacylation. They can also promote the cleavage of C-C bonds as in decarbonylation reactions. The activation of aldehyde C-H bonds and the reactivity of resulting acyl-hydride metal complexes will be addressed further and discussed in this thesis.

I.1.2. TRANSITION-METAL CATALYSED SI-H ACTIVATION

The synthesis of the iron $\text{Cp}(\text{CO})_2\text{Fe-SiMe}_3$ compound by Wilkinson and co-workers in 1956 marked the beginning of the silyl transition-metal chemistry,⁴⁸ and it has become an area of intensive research since then.⁴⁹ For years, the study of the reactivity and properties of Si-M complexes has allowed a comparison with related C-M systems,⁵⁰ in addition to giving insight

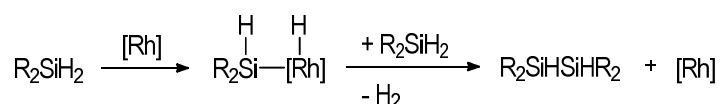
into the elementary steps of catalytic reactions for Si-C bond formation, such as hydrosilylation,⁵¹ or Si-Si bond formation as in dehydrogenative coupling of primary, secondary and tertiary silanes.⁵²

For instance, the binding modes of SiH₄ to transition metal complexes have been studied for a better understanding of the methane activation and transformations.^{50a} The first examples of transition metal η²-SiH₄ complexes were synthesised by reaction of silane with Mo(CO)(R₂PC₂H₄PR₂)₂, which were found to be in equilibrium with the hydridosilyl species formed by oxidative addition (Scheme I9).



Scheme I9. First reported equilibrium between η²-SiH₄ and the hydride species.

In 1965, Chalk and Harrod proposed the formation of a silyl-hydride complex by oxidative addition of the Si-H bond in the substrate to the catalyst, as the first step for the hydrosilylation reaction.²² This mechanism derived from the previous studies on chloroplatinic acid as an efficient catalytic precursor for alkene hydrosilylation by Speier.⁵³ In the same year, they described the formation of a silyl-cobalt compound by activation of the Si-H bond in a variety of silanes.⁵⁴ A later theoretical study on the hydrosilylation reaction of ethylene catalysed by Pt(PH₃)₂ led to the conclusion that this process proceeded through the mechanistic steps proposed by Chalk and Harrod.⁵⁵ In 1973, Ojima and co-workers also proposed the initial oxidative addition of a silane to Wilkinson's catalysts for the silane dehydrogenative coupling reaction, with the formation of a silyl-rhodium intermediate (Scheme I10).⁵⁶



Scheme I10. Route for silane dehydrogenative coupling proposed by Ojima et al.

The early development of silane compounds that can coordinate to the metal centre as ligands *via* oxidative addition has contributed to a better understanding of the activation of Si-H bonds and the nature of the Si-M interactions. Chelating silyl ligands have been successfully

employed for years, due to their stabilising effect and the versatility they exhibit.⁵⁷ A broader coordination opportunities have resulted in more effective catalysts for reactions involving Si-H activation.

The first part of this thesis will be focused on the activation of Si-H bonds in both stoichiometric and catalytic reactions. The synthesis of various silyl ligands containing a Si-H bond and their reactivity with transition-metal complexes is described, as well as the catalytic activity these complexes exhibit in both hydrosilylation and silane dehydrocoupling reactions. In a second part, C-H activations will be discussed, with the focus on aldehyde C-H activation by rhodium complexes and the synthesis of acyl-hydride compounds. Moreover, the reactivity and possible catalytic applications of these acyl-hydride complexes will also be studied.

I.2. BIBLIOGRAPHY

1. D. Astruc, *Organometallic Chemistry and Catalysis. History of Organometallic Chemistry*, Springer, Berlin, **2007**, 5-20.
2. (a) G. W. Parshall, R. E. Putscher, *J. Chem. Educ.*, **1986**, *63*, 189-191; (b) I. Omae, *Applications of Organometallic Compounds*, Wiley, **1998**; (c) R. Whyman, *Applied Organometallic Chemistry and Catalysis*, Oxford University Press, **2001**.
3. R. H. Crabtree, *General Properties of Organometallic Complexes*, Wiley, **2005**.
4. (a) T. Muroi, *Role of Precious Metal Catalysts, Noble Metals, InTech*, **2012**; (b) L. S. Benner, T. Suzuki, K. Meguro, *Precious Metals: Science and Technology*, Allentown Press, **1991**.
5. (a) A. J. Birch, D. H. Williamson, *Org. React.*, **1976**, *24*, 1-2; (b) B. R. James, *Homogeneous Hydrogenation*, New York, Wiley, **1973**; (c) R. C. West, A. F. Hill, M. J. Fink, *Advances in Organometallic Chemistry*, Vol. 55, Elsevier, **2008**.
6. (a) I. Ojima, T. Kogure, *Tetrahedron Lett.*, **1972**, *13*, 5035-5038. (b) C. F. Lochow, R. G. Miller, *J. Am. Chem. Soc.*, **1976**, *98*, 1281-1283; (c) D. A. Evans, G. C. Fu, A. H. Hoveyda, *J. Am. Chem. Soc.*, **1988**, *110*, 6917-6918; (d) K. Burgess, W. A. van der Donk, C. Jun, Y. J. Park, *Encyclopedia of Reagents for Organic Synthesis*, Wiley, **2005**.
7. L. A. Oro, C. Claver, *Iridium Complexes in Organic Synthesis*, Wiley, **2009**.
8. J. S. Merola, *Encyclopedia of Inorganic Chemistry. Iridium: Organometallic Chemistry*, Wiley, **2006**.
9. (a) R. U. Kirss, *Bull. Hist. Chem.*, **2013**, *38*, 52-60; (b) J. A. Labinger, *Organometallics*, **2015**, *34*, 4784-4795.
10. R. H. Crabtree, *The Organometallic Chemistry of the Transition Metals*, Wiley, **2005**.
11. a) C. S. Slone, D. A. Weinberger, C. A. Mirkin, *Prog. Inorg. Chem.* **1999**, *48*, 233-350; (b) P. Braunstein, F. Naud, *Angew. Chem. Int. Ed.* **2001**, *40*, 680-699.
12. J. Seyden-Penne, *Chiral Auxiliaries and Ligands in Asymmetric Synthesis*, Wiley, **1995**.
13. P. A. Evans, *Modern Rhodium-Catalyzed Organic Reactions*, Wiley, **2005**.
14. a) R. Dietiker, P. Chen, *Angew. Chem. Int. Ed.* **2004**, *43*, 5513-5516; (b) D. A. Colby, R. G. Bergman, J. A. Ellman, *Chem. Rev.* **2010**, *110*, 624-655.
15. M. C. Willis, *Chem. Rev.*, **2010**, *110*, 725-748.
16. B. Marciniak, *Hydrosilylation: A Comprehensive Review on Recent Advances*, Springer, **2009**.
17. D. A. Evans, G. C. Fu, B. A. Anderson, *J. Am. Chem. Soc.*, **1992**, *114*, 6679-6685.
18. T. E. Müller, K. C. Hultsch, M. Yus, F. Foubelo, M. Tada, *Chem. Rev.*, **2008**, *108*, 3795-3892.
19. L. Rosenberg, *ACS Catal.*, **2013**, *3*, 2845-2855.
20. P. N. Rylander, *Catalytic Hydrogenation in Organic Syntheses*, Academic Press, **2012**.
21. J. A. Osborn, F. H. Jardine, J. F. Young, G. Wilkinson, *J. Chem. Soc. A*, **1966**, *0*, 1711-1732.
22. A. J. Chalk, J. F. Harrod, *J. Am. Chem. Soc.*, **1965**, *87*, 16-21.
23. D. Milstein, *J. Chem. Soc., Chem. Commun.*, **1982**, 1357-1358.

24. (a) K. D. Karlin, *Progress in Inorganic Chemistry*, Vol. 48, Wiley, **1999**. (b) L. Huang, M. Arndt, K. Gooßen, H. Heydt, L. J. Gooßen, *Chem. Rev.*, **2015**, *115*, 2596-2697.
25. H. Kono, K. Ito, Y. Nagai, *Chem. Lett.*, **1975**, *10*, 1095-1096.
26. D. Männing, H. Nöth, *Angew. Chem. Int. Ed. Engl.*, **1985**, *24*, 878-879.
27. A. L. Casalnuovo, J. C. Calabrese, D. Milstein, *J. Am. Chem. Soc.*, **1988**, *110*, 6738-6744.
28. a) H. M. Senn, P. E. Blochl, A. Togni, *J. Am. Chem. Soc.*, **2000**, *122*, 4098-4107; (b) J. Takaya, J. F. Hartwig, *J. Am. Chem. Soc.*, **2005**, *127*, 5756-5757; (c) Z. Liu, H. Yamamichi, S. T. Madrahimov, J. F. Hartwig, *J. Am. Chem. Soc.*, **2011**, *133*, 2772-2782.
29. G. J. Kubas, *Dihydrogen and Other σ -Bond Complexes. Comprehensive Organometallic Chemistry III*, Elsevier, **2007**, 671-698.
30. (a) S. Geftakis, G. E. Ball, *J. Am. Chem. Soc.*, **1998**, *120*, 9953-9954; (b) M. A. Esteruelas, L. A. Oro, *Adv. Organomet. Chem.*, **2001**, *47*, 1-59; (c) Z. Lin, *Chem. Soc. Rev.*, **2002**, *31*, 239-245. (d) I. Castro-Rodriguez, H. Nakai, P. Gantzel, L. N. Zakharov, A. L. Rheingold, K. Meyer, *J. Am. Chem. Soc.*, **2003**, *125*, 15734-15735; (e) R. H. Crabtree, *J. Organomet. Chem.*, **2004**, *689*, 4083-4091; (f) N. Merle, G. Koicok-Kohn, M. F. Mahon, C. G. Frost, G. D. Ruggiero, A. S. Weller, M. C. Willis, *J. Chem. Soc., Dalton Trans.*, **2004**, 3883-3892; (g) V. I. Bakhmutov, *Eur. J. Inorg. Chem.*, **2005**, 245-255; (h) K. S. Cook, C. D. Incarvito, C. E. Webster, Y. Fan, M. B. Hall, J. F. Hartwig, *Angew. Chem., Int. Ed.*, **2004**, *43*, 5474-5477.
31. W. Jetz, W. A. G. Graham, *J. Am. Chem. Soc.*, **1969**, *91*, 3375-3376.
32. R. Waterman, *Organometallics*, **2013**, *32*, 7249-7263.
33. J. Chatt, J. M. Davidson, *J. Chem. Soc.*, **1965**, 843-855.
34. I. Moritani, Y. Fujiwara, *Tetrahedron Lett.*, **1967**, *8*, 1119-1122.
35. Y. Fujiwara, I. Moritani, K. Ikegami, R. Tanaka, S. Teranishi, *Bull. Chem. Soc. Jpn.*, **1970**, *43*, 863-867.
36. A. H. Janowicz, R. G. Bergman, *J. Am. Chem. Soc.*, **1982**, *104*, 352-354.
37. (a) J. K. Hoyano, W. A. G. Graham, *J. Am. Chem. Soc.*, **1982**, *104*, 3723-3725; (b) W. D. Jones, F. J. Feher, *J. Am. Chem. Soc.*, **1984**, *106*, 1650-1663; (c) M. Hackett, J. A. Ibers, G. M. Whitesides, *J. Am. Chem. Soc.*, **1988**, *110*, 1436-1448; (d) T. Gregory, P. Harper, R. S. Shinomoto, M. A. Deming, T. C. Flood, *J. Am. Chem. Soc.*, **1988**, *110*, 7915-7916; (e) W. A. Kiel, R. G. Ball, W. A. G. Graham, *J. Organomet. Chem.*, **1990**, *383*, 481-496.
38. J. Otera, *Esterification: methods, reactions, and applications*, Wiley-VCH, **2010**.
39. Y. Fujiwara, T. Kawanchi, H. Taniguchi, *J. Chem. Soc., Chem. Commun.*, **1980**, 220-221.
40. Y. Fujiwara, T. Jintoku, Y. Uchida, *New J. Chem.*, **1989**, *13*, 649-650.
41. W. Y. Yu, W. N. Sit, K. M. Lai, Z. Zhou, A. S. C. Chan, *J. Am. Chem. Soc.*, **2008**, *130*, 3304-3306.
42. T. Kochi, S. Urano, H. Seki, E. Mizushima, M. Sato, F. Kakiuchi, *J. Am. Chem. Soc.*, **2009**, *131*, 2792-2793.
43. S. Wang, Z. Yang, J. Liu, K. Xie, A. Wang, X. Chen, Z. Tan, *Chem. Commun.*, **2012**, *48*, 9924-9926.
44. W. Zhou, P. Li, Y. Zhang, L. Wang, *Adv. Synth. Catal.*, **2013**, *355*, 2343-2352.
45. J. Wu, J. Lan, S. Guo, J. You, *Org. Lett.*, **2014**, *16*, 5862-5865.

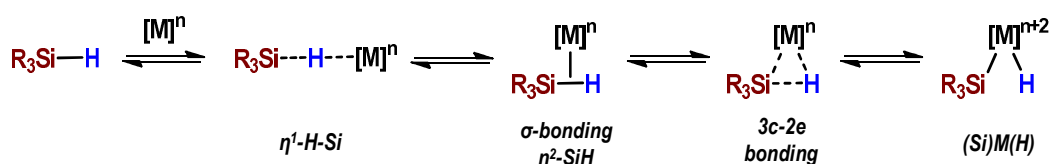
46. K. Sasano, J. Takaya, N. Iwasawa, *J. Am. Chem. Soc.*, **2013**, *135*, 10954-10957.
47. Z. Shen, H. A. Khan, V. M. Dong, *J. Am. Chem. Soc.*, **2008**, *130*, 2916-2917; (b) Z. Shen, P. K. Dornan, H. A. Khan, T. K. Woo, V. M. Dong, *J. Am. Chem. Soc.*, **2009**, *131*, 1077-1091.
48. T. S. Piper, D. Lemal, G. Wilkinson, *Naturwissenschaften*, **1956**, *43*, 129-129.
49. T. D. Tilley, *The Chemistry of Organic Silicon Compounds*, Wiley: New York, **1989**, 1415.
50. (a) S. L. Luo, G. J. Kubas, C. J. Burns, J. C. Bryan, C. J. Unkefer, *J. Am. Chem. Soc.*, 1995, *117*, 1159-1160; (b) S. Fang, H. Chen, H. Wei, *RSC Adv.*, **2018**, *8*, 9232-9242.
51. B. Marciniak, *Hydrosilylation: A Comprehensive Review on Recent Advances*, Springer, **2009**.
52. R. G. Jones, W. Ando, J. Chojnowski, *Silicon-Containing Polymers: The Science and Technology of Their Synthesis and Applications*, Springer, **2013**.
53. J. L. Speier, *Adv. Organomet. Chem.*, **1979**, 407-447.
54. J. F. Harrod, A. J. Chalk, *J. Am. Chem. Soc.*, **1965**, *87*, 1133-1133.
55. S. Sakaki, N. Mizoe, M. Sugimoto, Y. Musashi, *Coord. Chem. Rev.*, **1999**, *190-192*, 933-960.
56. I. Ojima, S. Inaba, T. Kogure, Y. Nagai, *J. Organomet. Chem.*, **1973**, *55*, C7-C8.
57. (a) C. Eaborn, T. N. Metham, A. Pidcock, *J. Organomet. Chem.*, **1973**, *63*, 107-117; (b) J. Grobe, A. Walter, *J. Organomet. Chem.*, **1977**, *140*, 325-348; (c) R. D. Holmes-Smith, S. R. Stobart, T. S. Cameron, K. Jochem, *J. Chem. Soc., Chem. Commun.*, **1981**, 937-939; (d) M. Simon, F. Breher, *Dalton Trans.*, **2017**, *46*, 7976-7997.

II. RESULTS AND DISCUSSION

II. 1. ACTIVATION OF THE SILICON-HYDROGEN BOND

II. 1. 1. INTRODUCTION

Activation of hydrosilanes by organometallic complexes implies the addition of the Si-H bond to the metallic centre in an oxidative addition reaction. In this reaction, the Si-H bond is cleaved and both M-Si and M-H bonds are formed, with the consequent increase of the formal oxidation state and coordination number of the metal. This process is generally promoted by electron-rich and low valent transition metal complexes, such as complexes with metals of groups 9 and 10. Along the Si-H activation pathway, several types of bonding interactions can be distinguished (Scheme 1), from non-classical to full homolytic cleavage of the Si-H bond.

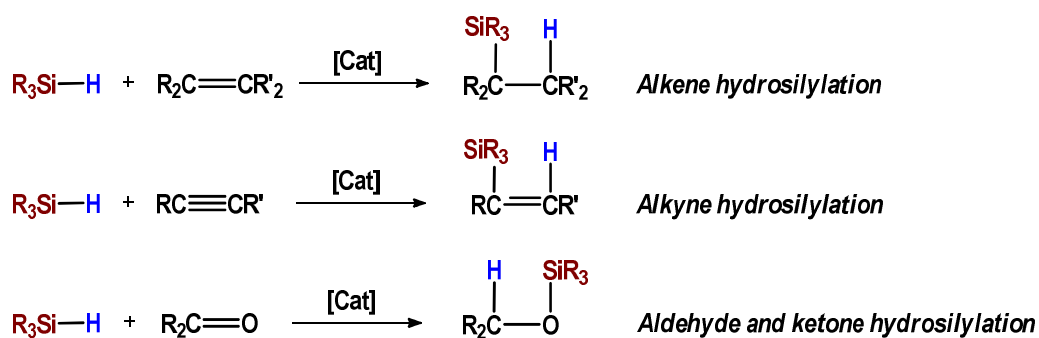


Scheme 1. Different bonding situations for the Si-H oxidative addition to a transition metal complex.

Spectroscopic data support the existence of σ -bonded silyl intermediate complexes before the insertion, in a η^2 -SiH coordination mode.¹ Isolation of such compounds is not rare. The first reported silane σ -complex was synthesised from a rhenium carbonyl compound in 1969,² and numerous examples of (η^2 -SiH) transition metal σ -complexes are known.³ There are also several reports of stable compounds in which the oxidative addition is belated in a stage where the Si-H bond is not completely cleaved, and the M-H and M-Si bonds are not fully formed. This interaction is described as a three-center-two-electron bond (Scheme 1).⁴ The relative stability of the non-classical binding modes is influenced by electronic properties of the metal centre, the auxiliary ligands and by the substituents at the silicon atom.

It is known that the oxidative addition of Si-H bonds to transition metal centres is a key step in multiple metal-catalysed transformations reactions, such as hydrosilylation,⁵ silane alcoholysis,⁶ silane redistribution⁷ or dehydrogenative silane oligomerization.⁸ These reactions have been applied to the development of new materials, polymeric synthesis or biomedical chemistry.⁹ Among these processes involving Si-H bond activation, this chapter will be focused mainly in alkene hydrosilylation and dehydrogenative silane coupling reactions.

Hydrosilylation is the addition of the Si-H bond into an unsaturated substrate (e. g. alkenes, alkynes, aldehydes or ketones). For alkene and alkyne hydrosilylation, this transformation leads to deliverance of alkyl or vinyl silanes as silylated products respectively, with the consequent formation of a new Si-C bond. On the other hand, the hydrosilylation of aldehydes and ketones and the subsequent hydrolysis of these silyl-ether products has become a powerful method for the synthesis of primary and secondary alcohols (Scheme 2).¹⁰ Overall, hydrosilylation represents one of the most important reactions in the silicon chemistry, and is extensively used in industry to produce silicone polymers, such as lubricants, water repellent coatings or resins.¹¹ It has also proved to be an efficient method for the formation of new organosilicon compounds, which can be used in fine chemical synthesis, as they participate in several important organic transformations.¹²



Scheme 2. Hydrosilylation of different unsaturated substrates.

The first hydrosilylation reaction was reported in 1947 by Sommer and co-workers.¹³ This work described a free radical chain reaction of 1-octene with trichlorosilane with the use of peroxides as catalysts, resulting in poor selectivity to the hydrosilylated product. This selectivity was highly improved in 1957 using the transition metal compound $[\text{H}_2\text{PtCl}_6]\cdot\text{H}_2\text{O}$ (Speier's catalyst) as catalyst.¹⁴ The development of the platinum(0) $\text{Pt}_2[(\text{Me}_2\text{SiCH}=\text{CH}_2)_2\text{O}]_3$ compound, which is known as Karstedt's catalyst¹⁵ in 1973 led to an important step forward in transition metal homogeneous catalysis. These two platinum based complexes (Figure 1) have prevailed as the most employed catalysts in industry for decades due to their stability and high activity. However, the demand of cheaper catalysts has recently encouraged the study of first row transition-metal catalysts as a more accessible and sustainable replacement.¹⁶ Nevertheless, unwanted side reactions and the requirement of high temperatures are significant drawbacks for these systems.

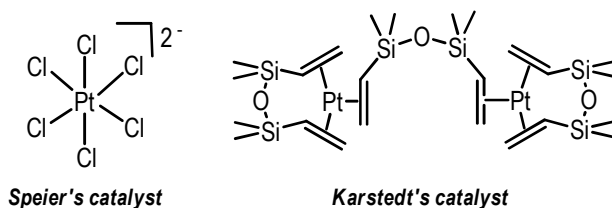


Figure 1. Classic platinum-based hydrosilylation catalysts.

To date, apart from platinum compounds, complexes based on other transition precious metals have been developed as hydrosilylation catalysts. Rhodium complexes with phosphine and carbonyl ligands $[\text{RhCl}(\text{PR}_3)_3]$ and $[\text{RhCl}(\text{CO})(\text{PR}_3)_2]$ are the most employed in this processes due to their high activity.¹⁷ For example, the use of Wilkinson's catalyst $[\text{RhCl}(\text{PPh}_3)_3]$ in the hydrosilylation of alkenes, alkynes and carbonyl substrates has been well established.¹⁸ Rhodium-carbene complexes have also been extensively studied. Particularly, rhodium complexes with strong donating *N*-heterocyclic carbene ligands (NHCs), which were reported by Nile and Hill in 1977.¹⁹ Rhodium complexes with these type of ligands are comparable to complexes with tertiary phosphines in their bonding characteristics as well as in their activity in hydrosilylation processes (Figure 2).²⁰ Other examples of efficient catalysts with NHC ligands based on iridium²¹ have also been reported (Figure 2). In 2004, Chirik and co-workers reported a highly effective alkene hydrosilylation catalysed by an iron complex with a bis(imino)pyridine bis(dinitrogen) ligand (Figure 2).²²

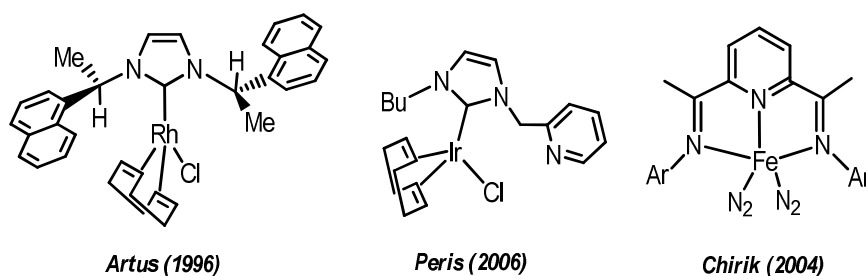
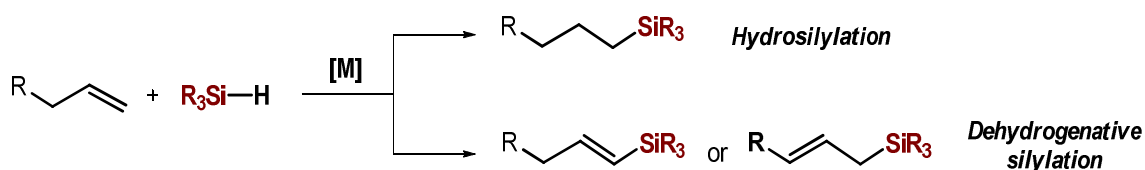


Figure 2. Examples of hydrosilylation catalysts.

In contrast to platinum and rhodium-based catalysts, examples of hydrosilylation reactions catalysed by iridium complexes are scarce. First experiments reported showed the lower activity of iridium complexes in hydrosilylation of alkenes compared to similar rhodium systems.²³ However, recent studies with cationic iridium species containing P,N-indene ligands,²⁴ and pincer PNP supported silyl and silylene iridium species²⁵ afforded hydrosilylated products efficiently. Moreover, iridium complexes such as $[\text{Ir}(\text{cod})(\mu\text{-X})_2]$ ($\text{X} = \text{Cl}, \text{OMe}$) ($\text{cod} =$

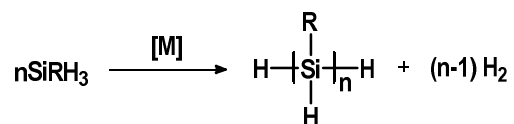
1,5-cyclooctadiene) appeared to be effective for hydrosilylation reactions. The use of this kind of catalysts can also lead to the dehydrogenative silylation reaction.²⁶

In a dehydrogenative silylation reaction, the elimination of the β -Hydrogen in the silylated substrate yields a vinyl or allylsilane product instead of the alkylsilane product (Scheme 3). It is proposed that the β -H elimination is the key step for the two competitive reactions, and the preference for one of the possible pathways is influenced by the nature of the substrate and the catalyst.²⁷



Scheme 3. Representation of alkene hydrosilylation and dehydrogenative silylation reactions.

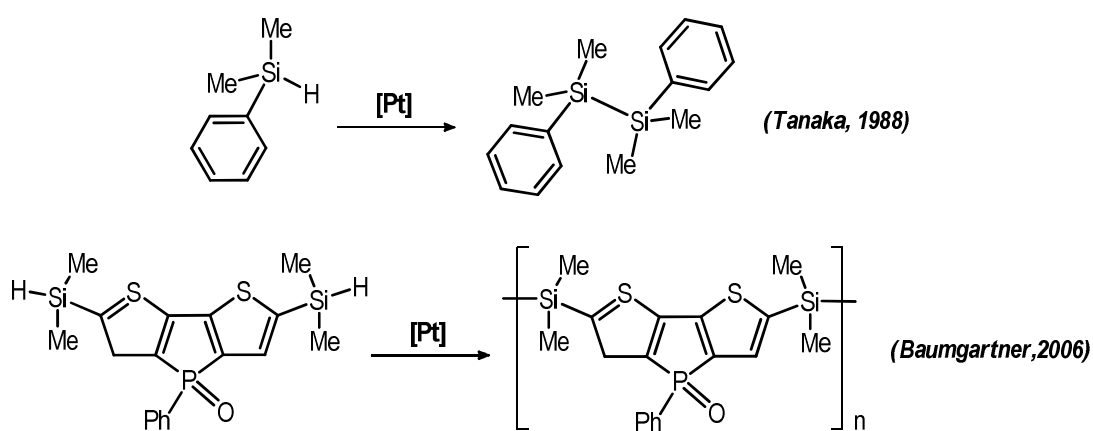
Another relevant process involving the catalytic Si-H bond activation is the dehydrogenative coupling of primary, secondary and tertiary silanes. In this reaction, the activation of a Si-H bond in the substrate leads to the formation of new Si-Si bonds to produce disilanes, oligosilanes and polysilanes (Scheme 4).



Scheme 4. Metal-catalysed dehydrogenative coupling of a primary silane.

The transition-metal catalysed silane dehydrocoupling is one of the routes to synthesise polysilanes. Using this strategy, it is possible to solve the problems encountered in the Wurtz coupling of halosilanes. Some of these problems would be the harsh reaction conditions and the use of alkali metals.²⁸ Early transition metals have been extensively studied as catalysts in dehydrocoupling of hydrosilanes.²⁹ By contrast, late transition metal complexes have been scarcely studied. The lower catalytic activity and the competitive reaction, which yields substituents redistribution, are the most important drawbacks for the use of late transition metal based compounds in dehydrocoupling reactions.³⁰ However, examples of highly active late transition metal catalysts in recent years suggest that these systems are equally valid.³¹

The first reported late metal-catalysed silane dehydrocoupling involved Wilkinson's catalyst.³² In this work, the dehydrogenative condensation of secondary silanes such as Ph_2SiH_2 , PhMeSiH_2 and Et_2SiH_2 , to yield short chained oligosilanes was reported. Since then, $[\text{RhCl}(\text{PPh}_3)_3]$ has proved to be effective in the dehydrocoupling of both primary and secondary silanes.³³ Moreover, rapid removal of hydrogen from the reaction mixture was found to favour dehydrocoupling over redistribution, in order to avoid the presence of disproportionation products.³⁴ In general, efficiency of late transition-metal catalysts in dehydrogenative silane coupling decreases from primary to tertiary silanes. Examples of tertiary silane dehydrocoupling are scarce,³⁵ and limited to platinum-based catalysts (Scheme 5).



Scheme 5. Tertiary silane dehydrocoupling reported by Tanaka and Baumgartner.

This chapter will focus on the synthesis of new silane compounds with thioether moieties containing a Si-H bond. The reactivity of these silanes with various rhodium(I) and iridium(I) compounds will also be studied. This reactivity will involve the coordination of the silyl-thioether to the metal complex as a chelate ligand through the activation of the Si-H bond by oxidative addition. The catalytic activity of the resulting compounds will also be tested for alkene hydrosilylation and silane dehydrocoupling reactions.

II. 1. 2. SYNTHESIS OF SILYL-THIOETHER MULTIDENTATE PRELIGANDS AND THEIR REACTIVITY WITH DIOLEFINIC RHODIUM(I) AND IRIIDIUM(I) COMPLEXES

The study of Si-H bond activation in silanes by a metal centre could give an insight into the mechanism of important catalytic processes. For example, oxidative addition of a Si-H bond to a complex with coordinated olefins would lead to species involved in the hydrosilylation reaction. However, the easy M-Si bond cleavage would prevent the isolation of the resulting silyl-hydride derivatives. For this reason, the stabilization of the silyl group onto the metal centre by the chelating effect in a bidentate,^{33b,36} tridentate³⁷ or tetradentate³⁸ ligand could be necessary.

The use of disilyl $\kappa^2(\text{Si},\text{Si})$ and trisilyl $\kappa^3(\text{Si},\text{Si},\text{Si})$ ligands has been reported.³⁹ However, most examples of silyl multidentate ligands contain pendant phosphane and N-donor groups, PSiP,⁴⁰ NSiN,⁴¹ or mixed donor PSiN⁴² ligands. Examples of these ligands are shown in Figure 3.

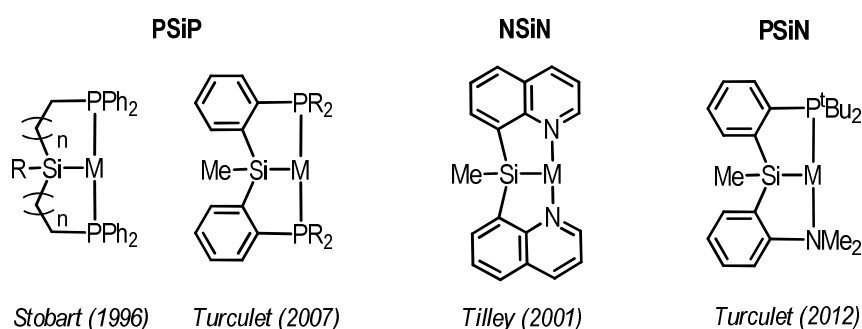


Figure 3. Examples of PSiP, NSiN and PSiN pincer ligands.

The presence of the silyl fragment gives unique properties to the ligand, such as a strong σ -donor character and *trans* influence. This effect results in elongation of the bond *trans* to the silicon atom, and could help to isolate unsaturated complexes with a vacant coordination site.⁴³ Complexes with silyl pincer ligands also show great reactivity towards small molecules and inert bond activation induced by chelating effects,⁴⁴ as well as enhanced catalytic performance.

Research on silyl ligands with thioether moieties is more scarce.⁴⁵ Examples of these ligands are shown in figure 4. The σ -donor and weak π -acceptor nature of the thioether functionalities is likely to ease the exchange of these pendant groups with other ligands.⁴⁶ Hill et al. described the synthesis of ruthenium(II) compounds with a new sulphur donor bis(methylmazoly)silane

tridentate ligand.⁴⁷ Unno and Takeda reported the synthesis of Ir(III) and Pt(II) complexes with a coordinated tripodal tetradentate SiS₃ ligand. Interestingly, the reaction of this ligand with [PdCl₂(PhCN)₂] results in rare Si-C(sp²) bond cleavage to yield a binuclear palladium(II) compound with two [(t-BuSCH₂)C₆H₄]⁻ units.⁴⁸ Peters et al. prepared a series of iron complexes chelated by hybrid silyl ligands that included thioether moieties, or a mixture of sulphur and phosphine donors.⁴⁹

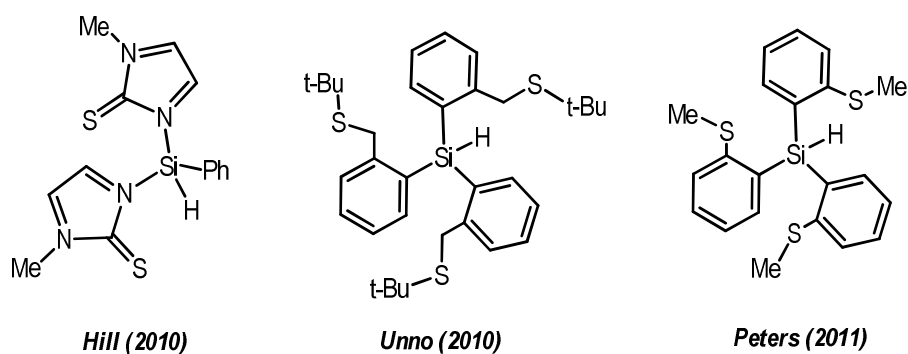
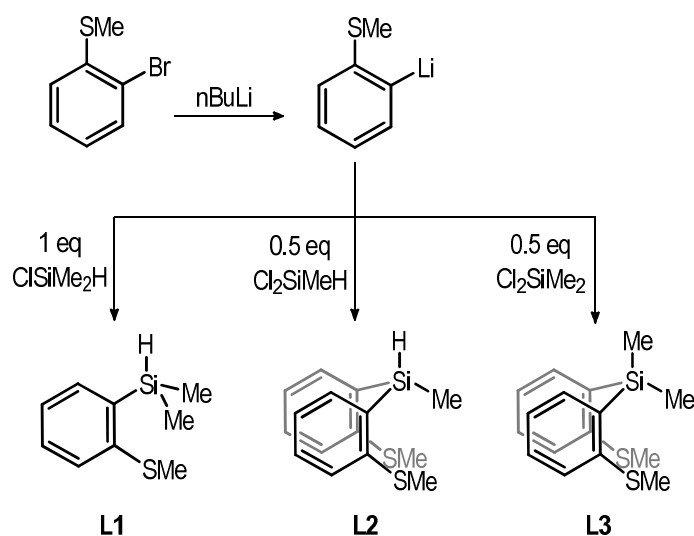


Figure 4. Selected examples of multidentate silyl ligands containing sulphur moieties.

In this part, three new silyl multidentate preligands with thioether pendant moieties have been synthesised (**L1**, **L2** and **L3**, Scheme 6) and their reactivity with rhodium(I) and iridium(I) compounds has been studied.

II. 1.2.1. Synthesis of ligands

The ligands employed in this work were synthesised by reaction of the aryl bromide 2-MeS(C₆H₄Br) with n-buthyllithium at 0°C in diethyl ether, and subsequent addition of the corresponding chlorosilane (Scheme 6).



Scheme 6. Synthesis of the three silyl-thioether ligands employed in this work.

Addition of an equivalent of dimethylchlorosilane over the lithiated product leads to the formation of the bidentate preligand $\text{SiMe}_2\text{H}(o\text{-C}_6\text{H}_4\text{SMe})$ (**L1**) (Scheme 6). The ^1H NMR spectrum for this preligand shows a doublet at 0.43 ppm corresponding to the two equivalent methyl groups bonded to the silicon, and a singlet at 2.48 ppm for the methyl group bonded to the sulphur atom. The Si-H bond of the ligand presents a heptet at 4.56 ppm, with a coupling constant of 3.8 Hz.

Tridentate preligand $\text{SiMeH}(o\text{-C}_6\text{H}_4\text{SMe})_2$ (**L2**) is obtained after the reaction of half equivalent of methylchlorosilane with one equivalent of the lithiated product (Scheme 6). In the ^1H NMR spectrum of the compound, the quartet signal at 5.29 ppm indicates the presence of the Si-H group. The two -SMe moieties are equivalent in solution, showing a singlet at 2.38 ppm, and the methyl group bonded to the silicon atom shows a singlet at 0.78 ppm.

The third preligand $\text{SiMe}_2(o\text{-C}_6\text{H}_4\text{SMe})_2$ is synthesised by addition of half equivalent of dimethyldichlorosilane over one equivalent of the lithiated product (Scheme 6). The ^1H NMR spectrum indicates the presence of the two SiMe equivalent groups with a relative integral 6 H singlet signal at 0.65 ppm, and the other 6 H singlet signal at 2.18 ppm corresponds to the two thioether groups, also equivalent in solution. Slow evaporation of the solvent in a concentrated ligand solution in Et_2O leads to the formation of colourless single crystals that allowed the characterisation of the compound by single crystal X-Ray diffraction. The structure of **L3** in the solid state (Figure 5) is in good agreement with the structure deduced from the NMR spectroscopic data in solution.

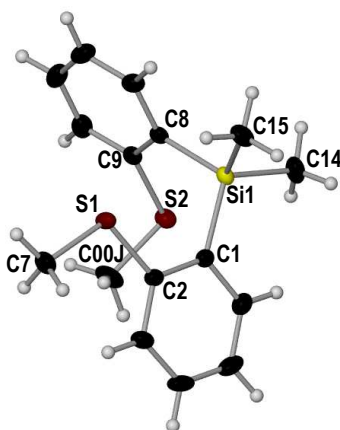
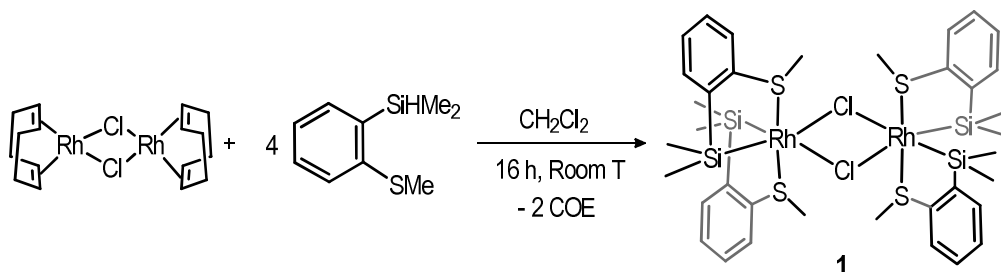


Figure 5. Molecular structure of **L3**. Displacement ellipsoids are drawn at the 50% probability level. Selected bond lengths (Å) and angles (°): Si1–C1 1.893(1), Si1–C8 1.887(1), Si1–C14 1.868(1), Si1–C15 1.875(1), S1–C2 1.771(1), S1–C7 1.792(1), S2–C9 1.783(1), S2–C00J 1.801(1); C1–Si1–C8 110.45(5), C2–S1–C7 104.16(6), C9–S2–C00J 101.14(6).

II. 1.2.2. Reactivity of ligands **L1** and **L2** with $[\text{Rh}(\text{cod})\text{Cl}]_2$. Synthesis of Rh(III) complexes via Rh(I)/Rh(III) mixed-valent and cyclooctenyl intermediates.

The reaction of $[\text{Rh}(\text{cod})\text{Cl}]_2$ with 4 equivalents of the bidentate preligand **L1** in CH_2Cl_2 at room temperature gives the dimeric complex $[\text{Rh}(\text{SiMe}_2(\text{o-C}_6\text{H}_4\text{SMe}))_2\text{Cl}]_2$ (**1**) (Scheme 7).



Scheme 7. Formation of complex **1**.

The $^{29}\text{Si}\{^1\text{H}\}$ NMR spectrum of **1** confirms the coordination of the ligand to the metal centre. This spectrum shows a doublet signal at 44.2 ppm ($J_{\text{Rh-Si}} = 28$ Hz), which is in accordance with a silicon-rhodium bond. The ^1H NMR spectrum of **1** shows a relative integral 12 H signal at 2.97 ppm corresponding to the four S-CH₃ groups in the complex. This fact is indicative of the equivalence of all four ligand units in the complex in solution. The presence of two relative integral 12 H signals (0.63 ppm and -0.24 ppm) corresponding to two different sets of Si-CH₃ moieties indicate that the methyl groups on each silicon atom are not equivalent as a consequence of chelation. A selective NOE experiment was performed in order to confirm this

non-equivalence. The experiment and the labelling of the coordinated ligand are shown in Figure 6.

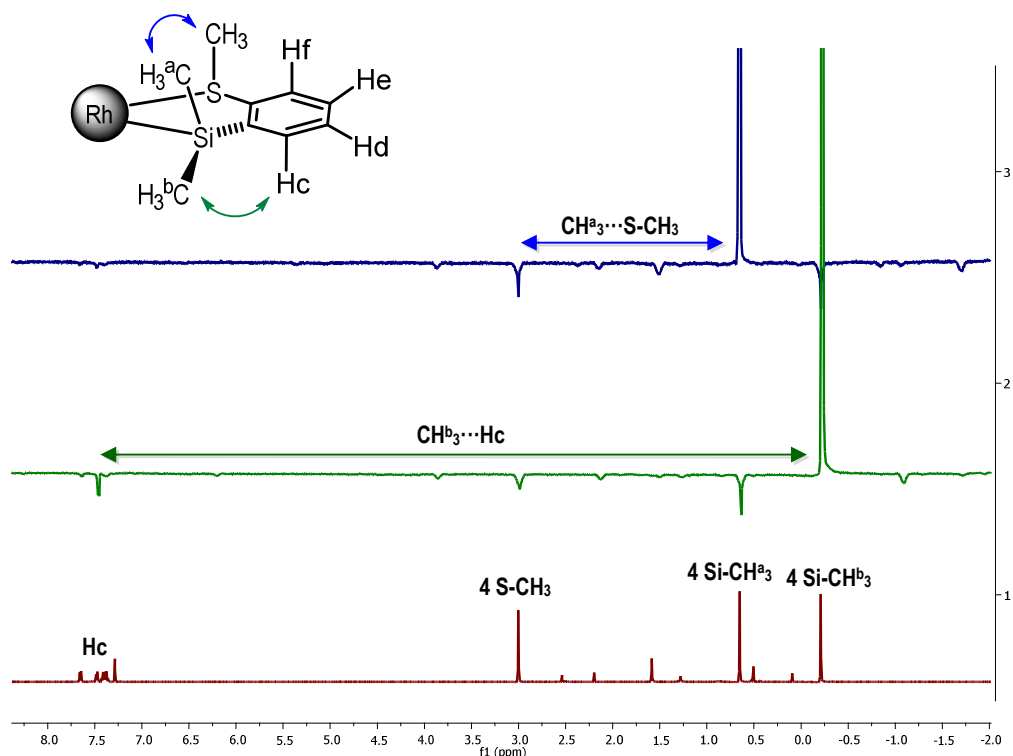


Figure 6. Labelling of the coordinated ligand and selective NOE experiments for **1**.

X-ray quality crystals of compound **1** were obtained, and characterization by single crystal X-ray diffraction could be performed (Figure 7). The resulting molecular structure is in agreement with the structure deduced from the spectroscopic data in solution.

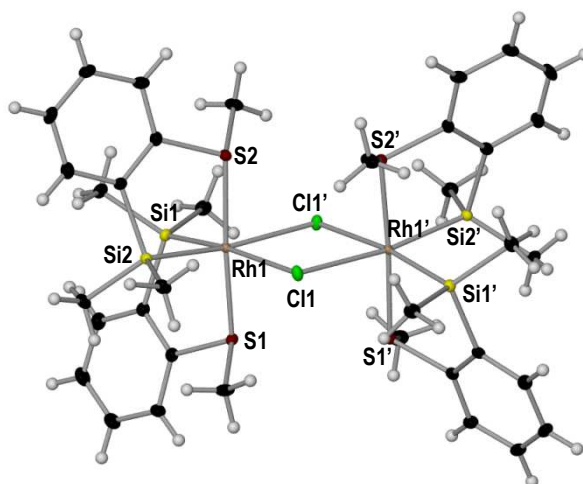


Figure 7. Molecular structure of **1**. Displacement ellipsoids are drawn at the 50% probability level. Selected bond lengths (Å) and angles (°): Rh1–Cl1 2.5846(9), Rh1–Cl1' 2.5760(9), Rh1–S1 2.3025(10), Rh1–S2 2.3071(10), Rh1–Si1 2.3154(11), Rh1–Si2 2.3104(10); S1–Rh1–Si1 85.52(4), S2–Rh1–Si2 85.66(4).

The crystal structure of dinuclear complex **1** consists of two chloride bridges between the two rhodium(III) centres. The geometry around each rhodium atom is a slightly distorted octahedron. The equatorial plane of the dimer is formed by the bridging chloride ligands in *trans* position to the silicon atoms, and the axial positions are occupied by the sulphur atoms, also mutually *trans*. Both Rh–Cl bond lengths of 2.5846(9) and 2.5760(9) Å fall in the range of μ -chlorido–Rh(III) bond lengths found in related compounds.⁵⁰ The Rh–Si bond lengths of 2.3154(11) and 2.3104(10) Å are also consistent with other observed Rh(III)–Si distances.⁵¹ The Rh··Rh separation of 3.9027(6) Å excludes any significant intermetallic interaction.

With the aim to understand the formation process of complex **1**, the reaction of [Rh(cod)Cl]₂ with 4 equivalents of **L1** was performed in a sealed NMR tube and was monitored by ¹H NMR spectroscopy. ¹H NMR spectra were acquired every 30 minutes. A total reaction time of 16 hours was required for the complete transformation of the starting material into **1**. After 8 hours of reaction, the ¹H NMR spectrum (Figure 8) shows the presence of three multiplets at 4.77, 4.61 and 3.68 ppm with a relative integral of 3 H, which are characteristic of (η^3 -cyclooctenyl)-Rh(III) compounds.⁵² The presence of free cyclooctene (coe) can also be observed in this spectrum. This could suggest the formation of η^3 -cyclooctenyl intermediates (**1a** and **1b** in Figure 8) that would afterwards afford cyclooctene.

Additionally, after 8 hours of reaction we were able to isolate by crystallisation the unusual μ -dichlorido bridged Rh(I)/Rh(III) mixed valent compound [(cod)Rh(μ -Cl)₂Rh(SiMe₂(*o*-C₆H₄SMe))₂] (**2**) from the reaction mixture. This compound can also be observed in the ¹H NMR spectra (Figure 8). The presence of this compound allows us to propose that the formation of complex **1** could start with a Si-H bond activation of two molecules of the **L1** ligand on the same rhodium centre, leading to the mixed valent complex **2** as an intermediate *via* (η^3 -cyclooctenyl)-Rh(III) species.

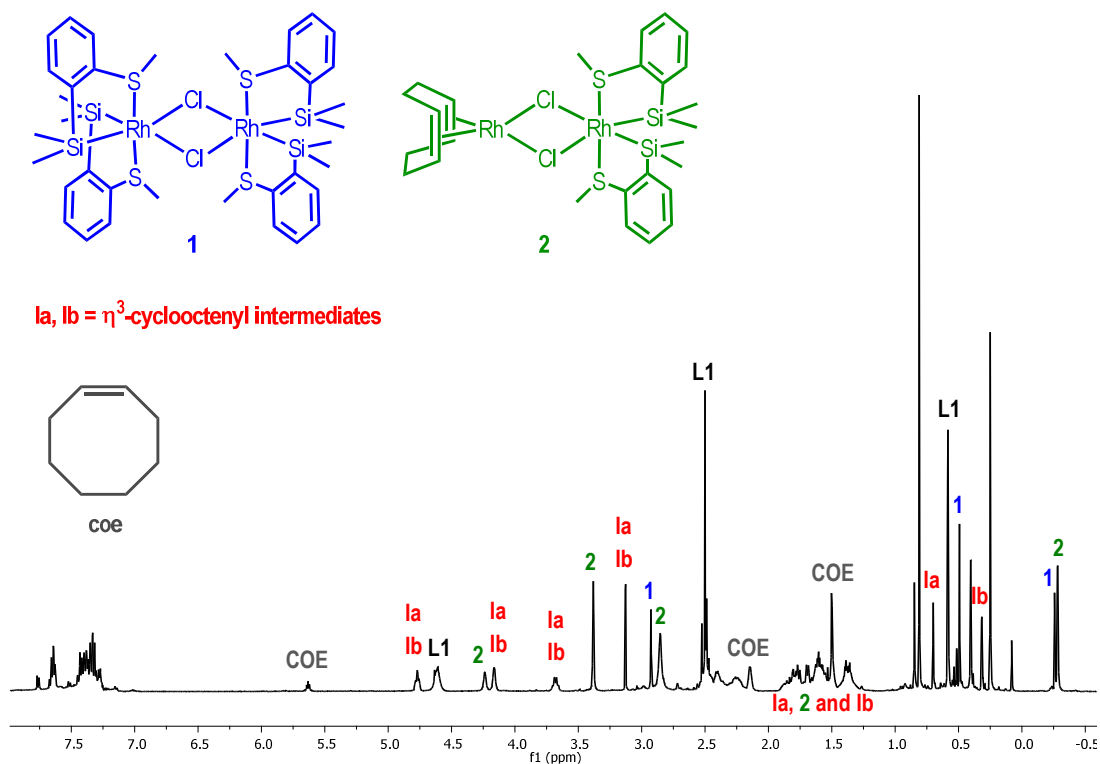


Figure 8. ^1H NMR spectrum of the formation of **1** after 8 hours of reaction in a sealed NMR tube, in CDCl_3 .

Compound **2** was isolated by crystallization, and therefore the molecular structure could be determined by X-ray diffraction (Figure 9). The binuclear Rh(I)/Rh(III) complex **2** is bridged by two μ -chlorine atoms. Complex **2** consists of a Rh(I) square planar centre and a Rh(III) pseudo octahedral centre. In the coordination sphere of the Rh(III) centre there are two ligand units derived from **L1**, where the sulphur atoms are disposed mutually *trans*, and the silicon atoms form the equatorial plane along with the chlorine bridging atoms. A molecule of cyclooctadiene is π^2 -coordinated to the Rh(I) centre. The Rh(I)–Cl distances (2.3888(8) and 2.3789(8) Å) are significantly shorter than the Rh(III)–Cl distances (2.6504(8) and 2.6300(8) Å), a consequence of the differing oxidation states of the metal centres.

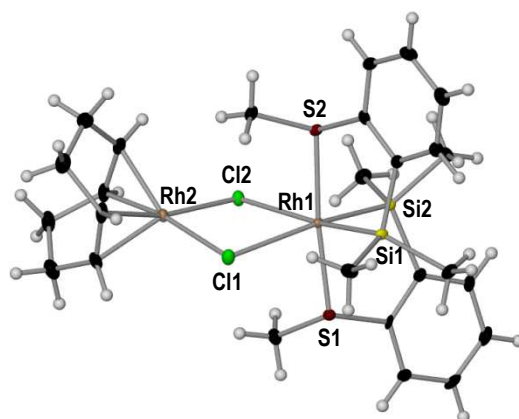


Figure 9. Molecular structure of **2**. Displacement ellipsoids are drawn at the 50% probability level. Selected bond lengths (Å) and angles (°): Rh1–Cl1 2.6504(8), Rh1–Cl2 2.6300(8), Rh2–Cl1 2.3888(8), Rh2–Cl2 2.3789(8), Rh1–Si1 2.2992(9), Rh1–Si2 2.3030(8), Rh1–S1 2.2946(8), Rh1–S2 2.2977(8); S1–Rh1–S2 174.41(3), Si1–Rh1–S1 87.47(3), Si2–Rh1–S2 87.33(3).

Compound **2** was also characterised by NMR spectroscopy (Figure 10). The ^1H NMR spectrum of the isolated compound shows two broad singlets at -0.18 and 0.58 ppm, corresponding to two nonequivalent SiMe groups in the molecule. As in complex **1**, this would be due to magnetically different methyl moieties on each silicon atom as a consequence of chelation. Multiplets at 4.24, 2.47 and 1.77 ppm indicate the presence of the coordinated cyclooctadiene ligand.

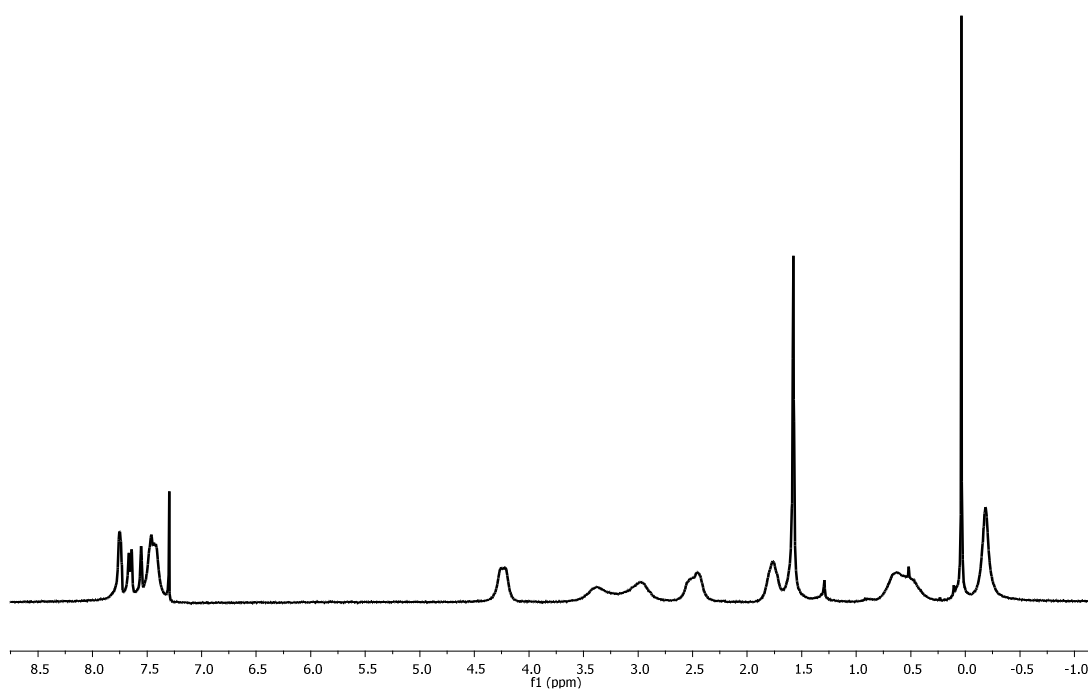
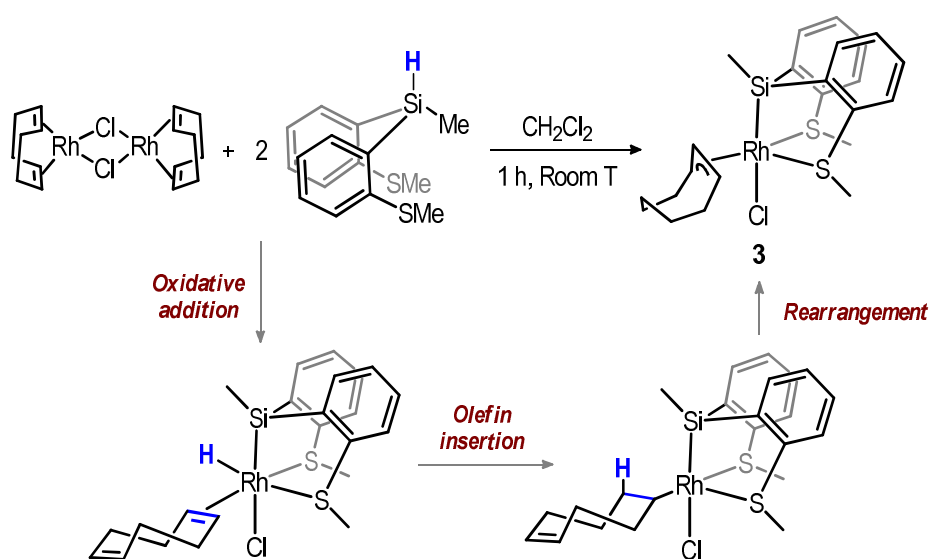


Figure 10. ^1H NMR spectrum of complex **2** in CDCl_3 .

In an attempt to allow a single Si-H bond activation on the Rh centre, which could afford a cyclooctenyl species, we performed the reaction of $[\text{Rh}(\text{cod})\text{Cl}]_2$ with the tridentate ligand **L2**. This reaction was carried out at room temperature in CH_2Cl_2 , and using 2 equivalents of **L2**, to yield the neutral complex $[\text{Rh}(\eta^3\text{-cyclooctenyl})(\text{SiMe}(\text{o-C}_6\text{H}_4\text{SMe})_2\text{Cl})]$ (**3**) (Scheme 8). The formation of this complex can be explained by a chelate-assisted oxidative addition of the Si-H bond of the ligand to the metal to give the unobserved silyl-hydrido-cyclooctadiene-rhodium(III) compound. This would be followed by the insertion of the double bond of the olefin into the Rh-H bond, and the subsequent rearrangement of the σ -alkyl or σ,π -cyclooctenyl into the η^3 -allyl cyclooctenyl species, which is thermodynamically more stable.⁵³



Scheme 8. Formation of complex **3**.

Complex **3** was characterised by NMR spectroscopy. The coordination of the ligand is confirmed by $^{29}\text{Si}\{^1\text{H}\}$ NMR with the presence of a doublet at 44.2 ppm ($J_{\text{Rh-Si}} = 24$ Hz), indicative of a Rh-silyl bond. The SMe groups show magnetic equivalence in solution with a unique singlet signal at 2.90 ppm in the ^1H NMR spectrum. The coordination of the η^3 -cyclooctenyl ligand is suggested by the presence a double triplet signal at 5.14 ppm, with a 1 H relative integral, and a quartet signal at 3.78 ppm with a 2 H relative integral. These signals are characteristic of the η^3 -allyl fragment in the molecule,⁵² and evidence the equivalence of two C-H groups in the moiety. The two-dimensional HSQC experiment correlates these signals with peaks at 96.7 and 66.8 ppm respectively in the $^{13}\text{C}\{^1\text{H}\}$ NMR spectrum. The ESI-MS spectroscopy shows a molecular ion at $m/z = 501.06$, which is in accordance with the $[\text{Rh}(\eta^3\text{-cyclooctenyl})(\text{SiMe}(\text{o-C}_6\text{H}_4\text{SMe})_2)]^+$ ion.

X-ray quality crystals of **3** were obtained from a CDCl_3 solution layered with pentane at $-4\text{ }^\circ\text{C}$. Complex **3** in the solid state (Figure 11) shows a slightly distorted octahedral arrangement around the Rh(III) centre, with the tridentate ligand **L2** located on one of the faces of the octahedron. The ligand is bounded via the silicon atom (Si1–Rh1 2.406(1) Å) and the two SME fragments (S1–Rh1 2.3733(5) Å and S2–Rh1 2.3524(5) Å). The chlorine atom is located *trans* to the silicon, and the long Rh–Cl distance of 2.6216(6) Å evidences the *trans*-labializing effect of the silyl group. The η^3 -cyclooctenyl ligand occupies two coordination positions in the compound. In the allyl fragment of this ligand, the Rh–C distance of the central carbon atom is shorter (C16–Rh1 2.1109(19) Å) than the terminal carbon distances (C17–Rh1 2.1982(19) Å and C20–Rh1 2.2008(19) Å).

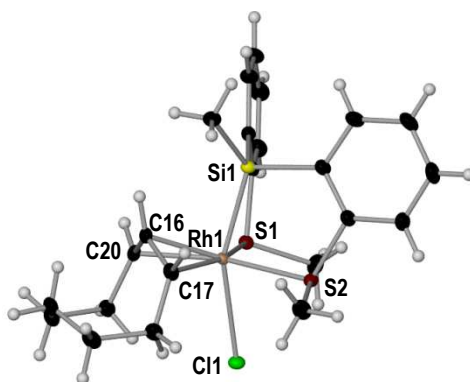
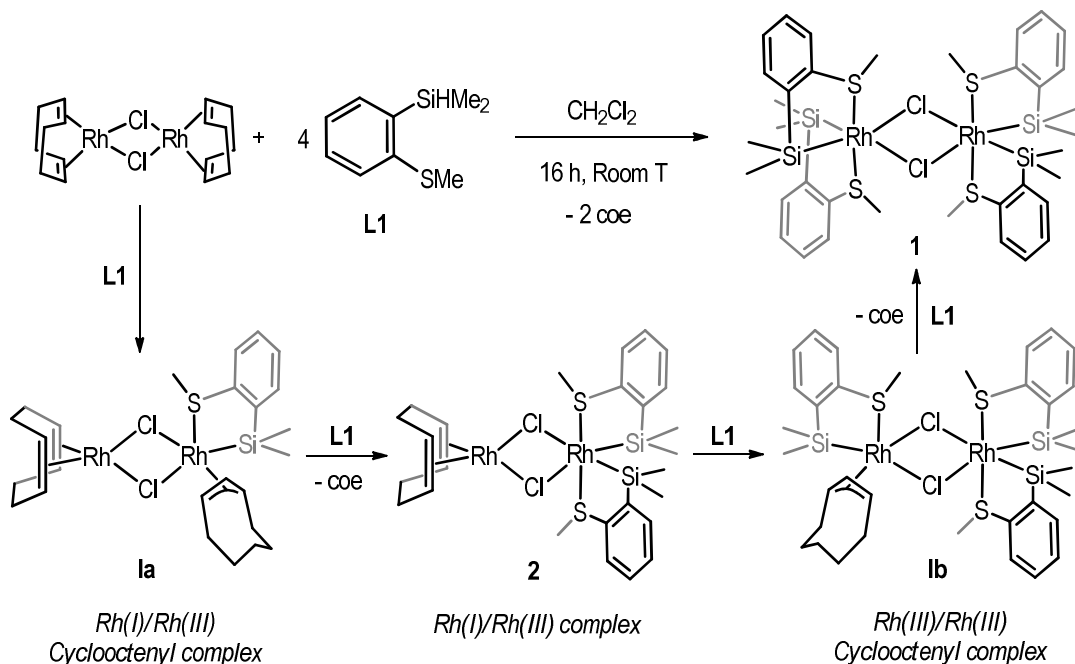


Figure 11. Molecular structure of **3**. Displacement ellipsoids are drawn at the 50% probability level. The solvent molecule is omitted for clarity. Selected bond lengths (Å) and angles ($^\circ$): Rh1–C16 2.1109(19), Rh1–C17 2.1982(19), Rh1–C20 2.2008(19), Rh1–Si1 2.3063(5), Rh1–Cl1 2.6216(5); S1–Rh1–S2 100.051(18), Si1–Rh1–S1 85.009(18), Si1–Rh1–S2 85.533(18).

The isolation and characterisation of the η^3 -cyclooctenyl complex **3** and the evidences of η^3 -cyclooctenyl species observed in the reaction mixture leading to complex **1** enables us to propose a mechanism for the formation of **1** (Scheme 9). The reaction of the first equivalent of **L1** with $[\text{Rh}(\text{cod})\text{Cl}]_2$ would lead to the formation of an unobservable rhodium-hydrido-cyclooctadiene complex. Then the insertion of the cyclooctadiene into the Rh–H bond gives the Rh(I)/Rh(III) cyclooctenyl intermediate (**1a**). The addition of a second molecule of **L1** results in another Si–H activation by the Rh(III) centre, with the subsequent cyclooctene dissociation and the formation of the mixed-valent Rh(I)/Rh(III) compound **2**. This second activation would presumably occur via an σ -complex assisted metathesis (or σ -CAM) process. This is supported by the isolation of compound **2** from the reaction mixture. The second Rh(I) atom would follow the same process with the addition of another unit of **L1**, leading to a Rh(III)/Rh(III)

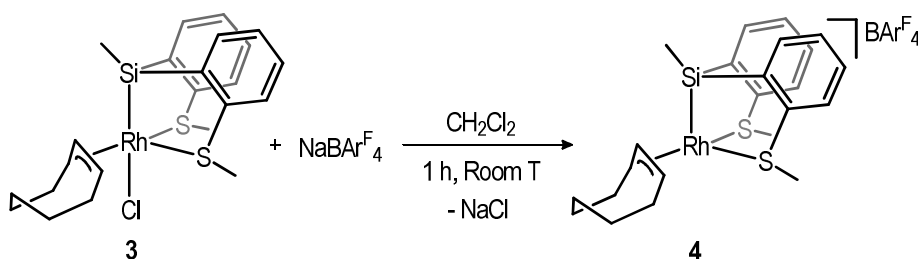
cyclooctenyl intermediate (**1b**). The addition of the last equivalent of **L1** to this intermediate would lead to the final product **1**.



II. 1.2.3. Reactivity of ligand **L2** with $[\text{Rh}(\text{cod})\text{Cl}]_2$, $[\text{Ir}(\text{cod})\text{Cl}]_2$ and $[\text{Rh}(\text{nbd})\text{Cl}]_2$ dimers. Study of the olefin insertion and β -hydride elimination processes.

II. 1.2.3a. Reactivity of **L2** with $[\text{Rh}(\text{cod})\text{Cl}]_2$ and $[\text{RhCl}(\text{PPh}_3)_3]$

The reaction of complex **3** with the sodium tetrakis[3,5-bis(trifluoromethyl)phenyl]borate salt ($\text{NaBAR}^{\text{F}_4}$) in dichloromethane results in the formation of the cationic compound $[\text{Rh}(\eta^3\text{-cyclooctenyl})(\text{SiMe}(\text{o-C}_6\text{H}_4\text{SMe})_2)]\text{BAR}^{\text{F}_4}$ (**4**) (Scheme 10), which contains a coordinative vacancy. Unsaturated complex **4** is stable in solution and in solid state.



The 16 electron compound **4** was characterised by NMR spectroscopy (Figure 12). The tridentate ligand shows signals at 0.78 ppm for the SiMe group, and at 2.58 ppm for the two equivalent SMe groups in the ^1H NMR spectra. The coordination of the η^3 -cyclooctenyl is confirmed with the presence of two doublet of triplets at 5.26 and 4.40 ppm, with 1 H and 2 H relative integrals respectively, corresponding to the η^3 -allyl fragment. 2D experiments correlate these two signals with the two doublets at 105.6 and 75.6 ppm in the $^{13}\text{C}\{^1\text{H}\}$ NMR spectrum. In the ESI-MS spectroscopy, the existence of a molecular ion at $m/z = 501.06$ also evidences the formation of this complex.

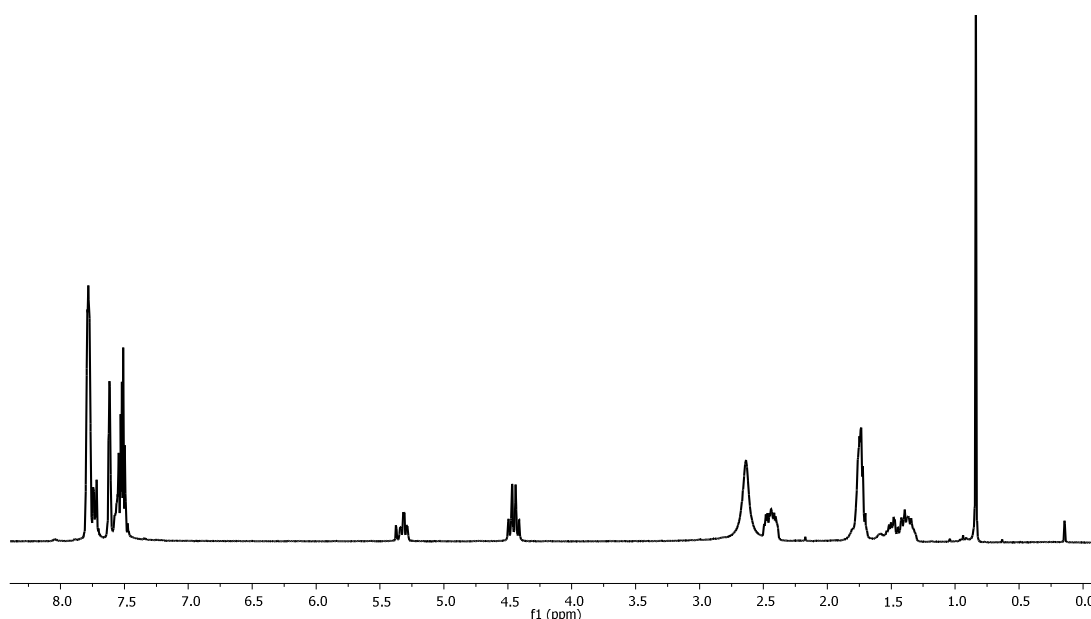
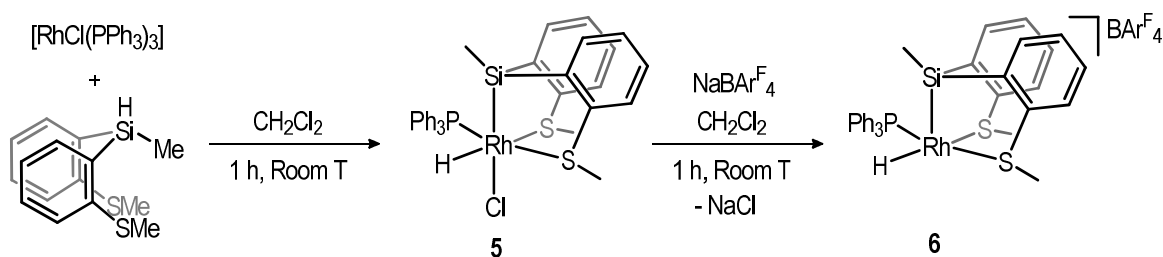


Figure 12. ^1H NMR spectrum of complex **4** in CD_2Cl_2 .

An X-ray analysis of single crystals of compound **4** confirms the proposed structure. Although the low quality of the data did not permit the discussion of bond distances and angles, the disposition of the ligands and the geometry adopted around the metal centre can be analysed (Supporting Information). The solid state structure shows a distorted square pyramidal geometry, with the silyl fragment of the tridentate ligand located in the apical position. The base of the pyramid is occupied by the two SMe moieties and the η^3 -allyl fragment of the cyclooctenyl ligand. The stability showed by this unsaturated compound could be due to the strong *trans* influence displayed by the silicon atom.

Unsaturated rhodium(III) complex **4**, containing a cyclooctenyl ligand was obtained from a 16e cyclooctadiene-rhodium(I) starting material. The possibility of obtaining compound **4** by the addition of an external cyclooctadiene molecule to rhodium(III) species was also studied. For

that purpose, we synthesised an olefin-free unsaturated hydride-rhodium(III) compound from Wilkinson's catalyst $[\text{RhCl}(\text{PPh}_3)_3]$ (Scheme 11).



Scheme 11. Formation of compounds **5** and **6** from Wilkinson's catalyst.

The reaction of $[\text{RhCl}(\text{PPh}_3)_3]$ with an equivalent of the tridentate preligand **L2** in dichloromethane led to the formation of a neutral hydride compound $[\text{RhClH}(\text{SiMe}(o\text{-C}_6\text{H}_4\text{SMe})_2)(\text{PPh}_3)]$ (**5**) after the oxidative addition of the Si-H bond to the rhodium centre. The ^1H NMR spectrum shows the hydride signal at -12.76 ppm. The SiMe group on the ligand presents a signal at -0.07 ppm, and the SMe moieties show two different singlet signals at 3.21 and 2.47 ppm. In the $^{31}\text{P}\{^1\text{H}\}$ NMR spectrum, a doublet at 46.8 ppm ($J_{\text{Rh-P}} = 138.3$ Hz) confirms the presence of the PPh_3 molecule coordinated to a Rh(III) centre.

With the aim of producing a vacant coordination site, complex **5** was treated with an equivalent of $\text{NaBAR}_4^{\text{F}}$ salt in dichloromethane, to yield the cationic and unsaturated 16 electron compound $[\text{RhH}(\text{SiMe}(o\text{-C}_6\text{H}_4\text{SMe})_2)(\text{PPh}_3)]\text{BAR}_4^{\text{F}}$ (**6**) (Scheme 11). The signal of the hydride ligand of **6** appears at -10.91 ppm in the ^1H NMR spectrum, and the $^{31}\text{P}\{^1\text{H}\}$ NMR spectrum shows a doublet at 47.3 ppm that corresponds to PPh_3 .

Compounds **5** and **6** were also characterised in the solid state by single-crystal X-ray structural determination (Figure 13). The resulting molecular structures are in good agreement with the structures deduced from the spectroscopic data in solution. Complex **5** in figure 13a shows a pseudo octahedral structure around a Rh(III) centre. The tridentate ligand, which is bonded to the metal via the silicon atom (Si1-Rh1 2.277(2) Å) and the two sulphur moieties (S1-Rh1 2.350(2) Å and S2-Rh1 2.439(2) Å) is located in one of the faces of the octahedron. The hydride and the triphenylphosphine ligands occupy the positions *trans* to the two SMe groups in the equatorial plane. The chlorine atom is located *trans* to the silyl fragment. The elongated Rh-Cl bond length of 2.536(2) Å is due to the high inductive *trans* effect of the silicon atom.

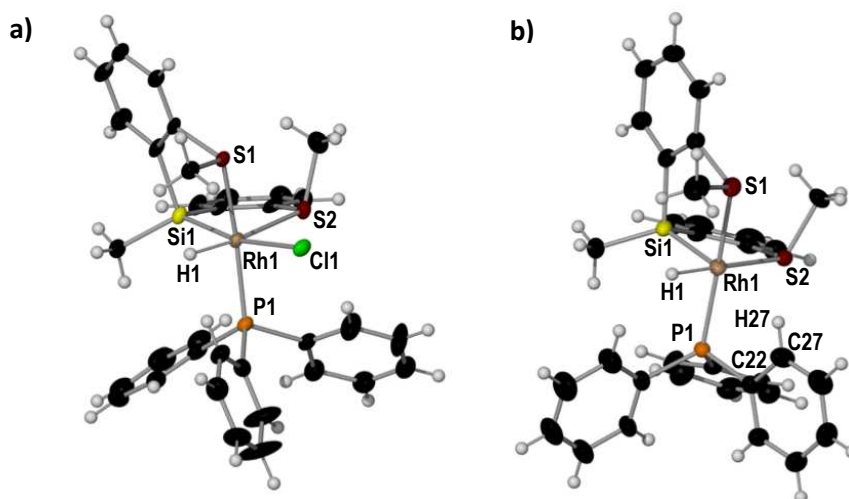
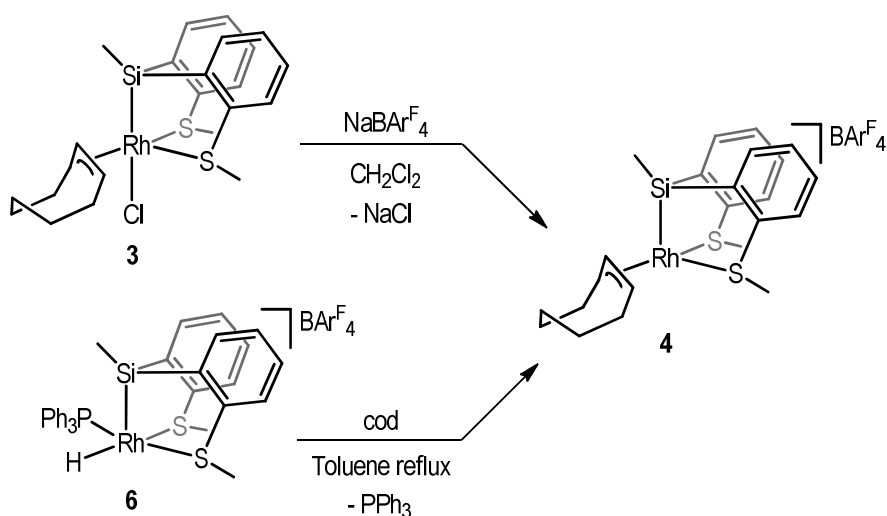


Figure 13. a) Molecular structure of complex **5**. Displacement ellipsoids are drawn at 50 % probability level. Selected bond lengths (Å) and angles (°): Rh1–Cl1 2.5363(16), Rh1–S1 2.3494(16), Rh1–Si1 2.2768(17), Rh1–S2 2.4388(16), S1–Rh1–Si1 86.66(6), S2–Rh1–Si1 86.52(6). b) Molecular structure of compound **6**. The anion is omitted for clarity. Displacement ellipsoids are drawn at 50 % probability level. Selected bond lengths (Å) and angles (°): Rh1–Si1 2.2532(9), Rh1–S1 2.3558(8), Rh1–S2 2.4191(7), Rh1–P1 2.2740(8), S1–Rh1–S2 96.17(3), Si1–Rh1–S1 88.76(3), Si1–Rh1–S2 88.00(3).

In the solid state, complex **6** (Figure 13b) shows an interaction between an aromatic ring of PPh₃ and the rhodium atom leading to a distorted octahedron around the Rh(III) centre, with the [SiMe(*o*-C₆H₄SMe)₂] pincer ligand on one of the octahedron faces. The PPh₃ and the hydride occupy the remaining coordination sites in the equatorial plane. A hydrogen atom of one of the aromatic rings of the triphenylphosphine (H27) occupies the last coordination site *via* a weak Rh⋯H–C interaction⁵⁴ (C27–H27 1.185 Å, Rh1–H27 2.329 Å, Rh1–C27 3.129 Å, Rh1–H27–C27 122.4°). Considering these distances and bond angles, this interaction would be in the border between agostic and anagostic interaction.⁵⁵ Another reason to consider the existence of a M⋯H interaction, is the distortion observed in a Rh–P–C bond angle (Rh1–P1–C22 101.88(10)°), which is shorter than expected.⁵⁶ The Rh⋯H–C interaction is not observed in solution. This could be due to a fast site exchange between all the hydrogen atoms on the *ortho* position of the three phenyl rings. Cooling the solution down to -75 °C did not freeze this process.

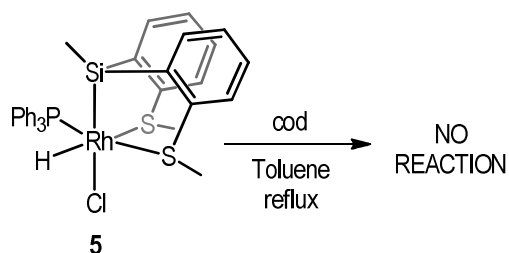
The addition of one equivalent of 1,5-cyclooctadiene to the unsaturated Rh(III)-hydrido compound **6** in toluene at 110 °C resulted in the formation of complex **4** (Scheme 12). The formation of **4** can be explained by the coordination of cod, followed by the insertion of the olefin into the Rh–H bond concomitant with the dissociation of PPh₃. This insertion leads to the formation of a π-olefin/σ-alkyl cyclooctenyl, and the subsequent rearrangement of this ligand

gives the thermodynamically more stable η^3 -cyclooctenyl ligand via successive C–H activation/insertion steps.⁵⁷



Scheme 12. Synthetic path of formation of compound **4** from complexes **3** and **6**.

However, the treatment of the coordinatively saturated chloride-hydrido-Rh(III) compound **5** with cyclooctadiene under the same reaction conditions failed to promote the insertion reaction of the olefin (Scheme 13). This fact evidences that a previous coordination of the cyclooctadiene ligand to the metal centre is necessary for the olefin insertion to occur, and this coordination failed due to the absence of a coordinative vacancy in the coordination sphere of neutral compound **5**.



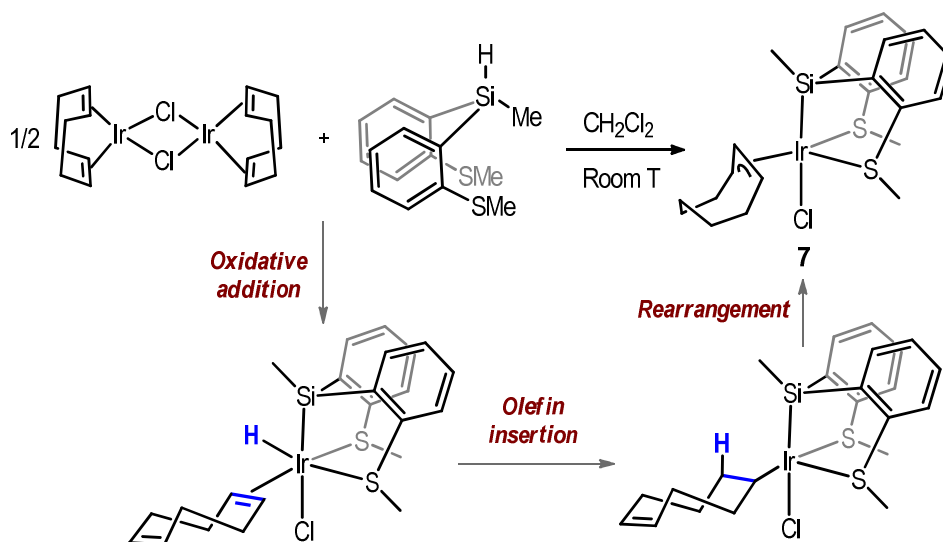
Scheme 13. Attempted reaction of the saturated compound **5** with 1,5-cyclooctadiene.

II. 1.2.3b. Reactivity of L2 with $[\text{Ir}(\text{cod})\text{Cl}]_2$

While diolefinic rhodium complexes containing a Rh–H bond are rare,⁵⁸ stable η^4 -cod-hydride iridium(III) compounds are well known. In the synthesis of η^4 -cod-hydride iridium (III) compounds, 1- σ ,4,5- η^2 -cyclooctenyl insertion products have also been observed.⁵⁹ An equilibrium between species containing both 1- σ ,4,5- η^2 and η^3 -cyclooctenyl isomers has been

observed in solutions of some iridacarboranes.⁶⁰ Based on previously reported results, we decided to study the reactivity of the $[\text{Ir}(\text{cod})\text{Cl}]_2$ dimer with the tridentate preligand **L2**, and thus determine the influence of the metal centre, rhodium or iridium, in the course of these reactions.

Treatment of $[\text{Ir}(\text{cod})\text{Cl}]_2$ with two equivalents of **L2** in dichloromethane at room temperature yielded compound $[\text{IrCl}(\eta^3\text{-cyclooctenyl})(\text{SiMe}_2(o\text{-C}_6\text{H}_4\text{SMe})_2)]$ (**7**). The formation of this compound implies the oxidative addition of the Si-H bond to give the unobserved silyl-hydrido-cyclooctadiene species. The insertion of the cyclooctadiene into the Ir-hydride would lead to an unobserved σ - or σ,π -cyclooctenyl intermediate, and the rearrangement of the ligand in the latter results in the η^3 -cyclooctenyl-Ir(III) complex in **7** (Scheme 14).



Scheme 14. Formation of the saturated compound **7**.

The NMR spectra of complex **7** are consistent with a η^3 -cyclooctenyl species. The signals at 5.15 and 3.68 ppm in the ^1H NMR spectrum, with relative integrals of 1H and 2H, correlate to the 86.9 and 49.0 ppm doublets in the $^{13}\text{C}\{^1\text{H}\}$ NMR spectrum and correspond to the η^3 -allyl fragment of the ligand. The structure is also supported by ESI-MS spectroscopy, with the presence of a molecular ion at $m/z = 591.12$ corresponding to the $[\text{Ir}(\eta^3\text{-cyclooctenyl})(\text{SiMe}_2(o\text{-C}_6\text{H}_4\text{SMe})_2)]^+$ species.

X-ray quality crystals were obtained by layering a CDCl_3 solution of this complex with pentane at room temperature. The structure in the solid state is in agreement with the one proposed from the spectroscopic data in solution (Figure 14). The geometry around the Ir(III) centre is pseudo-octahedral. The S,S,Si tridentate ligand is bonded to the metal via the Si and S atoms

(Si1–Ir1 2.316(1) Å, S1–Ir1 2.345(1) Å and S2–Ir1 2.363(1) Å) occupying one of the faces of the octahedron. The chloride ligand is located *trans* to the silyl fragment. The labilization of this ligand due to the *trans* effect of the silicon is evidenced by the longer distance of Cl1–Ir1 2.579(1) Å. The η^3 -allyl fragment occupies the two remaining coordination sites in the equatorial plane. While the C atoms in the terminal positions show almost identical distances to the metal centre (C2–Ir1 2.197(3) Å and C3–Ir1 2.176(3) Å), the central C atom in the fragment shows a shorter distance of C1–Ir1 2.112(3) Å.

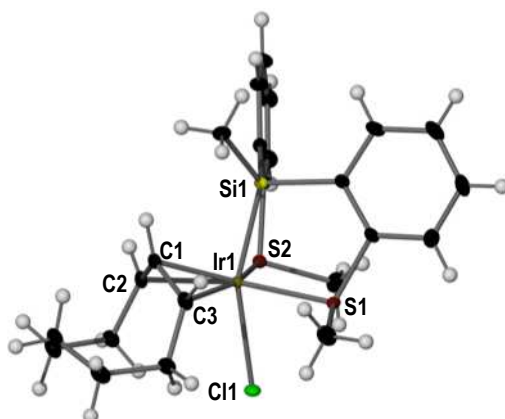
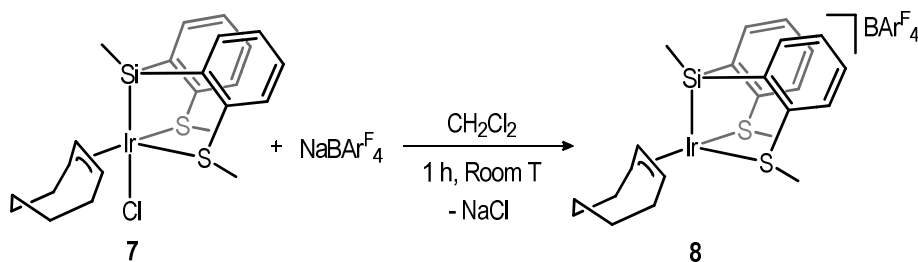


Figure 14. Molecular structure of complex **7**. Displacement ellipsoids are drawn at 50% probability level. The solvent molecule is omitted for clarity. Selected bond lengths (Å) and angles ($^\circ$): Ir1–Si1 2.316(1), Ir1–S1 2.345(1), Ir1–S2 2.363(1), Ir1–C1 2.112(3), Ir1–C2 2.197(3), Ir1–C3 2.176(3); Ir1–Cl1 2.579(1); S1–Ir1–S2 99.30(3), Si1–Ir1–S1 85.63(3), Si1–Ir1–S2 85.34(3).

Reaction of the saturated compound **7** with the $\text{NaBAR}_4^{\text{F}}$ salt in dichloromethane causes the extraction of the chloride ligand, and yields a 16 electron cationic compound $[\text{Ir}(\eta^3\text{-cyclooctenyl})(\text{SiMe}_2(o\text{-C}_6\text{H}_4\text{SMe}_2))]^+\text{BAR}_4^{\text{F}}$ (**8**) (Scheme 15). Unlike $\eta^3\text{-cyclooctenyl-Rh(III)}$ analogue compound **4**, product **8** exhibited low stability in solution at room temperature. For that reason, characterisation by NMR spectroscopy was performed at $-25\text{ }^\circ\text{C}$.



Scheme 15. Formation of the unsaturated compound **8**.

The presence of the η^3 -cyclooctenyl fragment is supported by ^1H NMR spectroscopy with the presence of two signals at 5.20 and 4.41 ppm, with a relative integral of 1H and 2H respectively. X-ray crystallography also confirmed the proposed structure for **8** (Supporting Information), but unfortunately collection of angles and bond lengths was not possible due to the poor quality data of the crystal. However, the relative disposition of the ligands around the metal centre implies a distorted square planar pyramid with the silyl fragment occupying the apical site.

As mentioned above, compound **8** is not stable in solution at room temperature, as stirring in CDCl_3 induces a slow transformation into the saturated and cationic hydride species $[\text{Ir}(\text{H})(\eta^4\text{-cod})(\text{SiMe}_2(o\text{-C}_6\text{H}_4\text{SMe}_2))] \text{BAR}^{\text{F}_4}$ (**9**). This transformation was monitored by ^1H NMR (Figure 15).

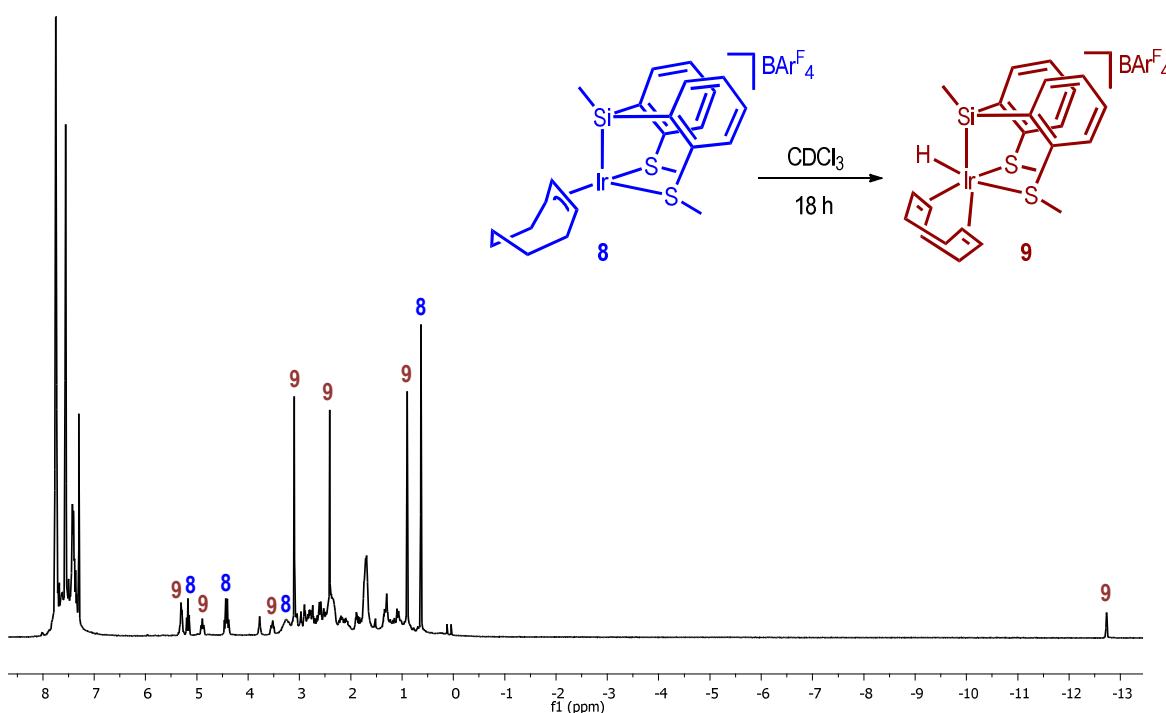
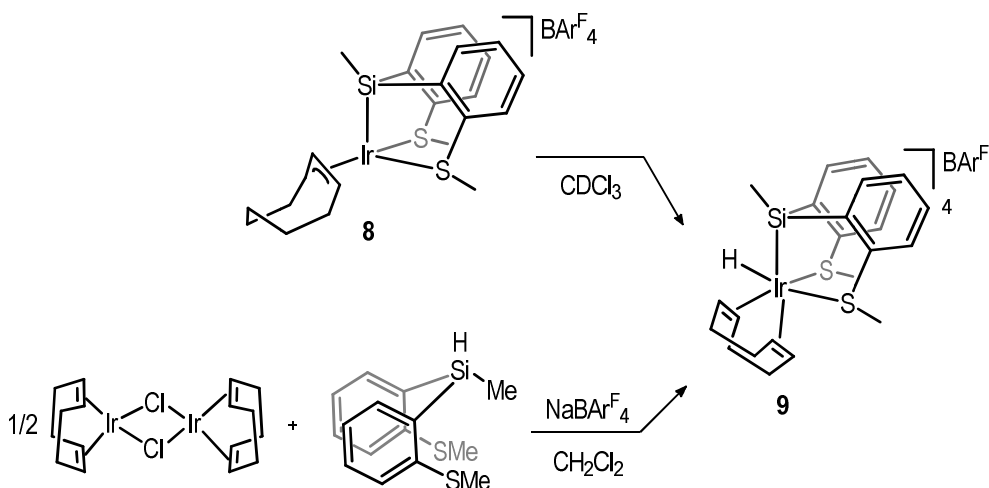


Figure 15. ^1H NMR of compound **8** in CDCl_3 after 18 hours at room temperature. The slow formation of compound **9** can be observed.

The formation of compound **9** was also possible by direct reaction of the $[\text{Ir}(\text{cod})\text{Cl}]_2$ dimer with the tridentate **L2** ligand and the $\text{NaBAR}^{\text{F}_4}$ salt in dichloromethane (Scheme 16). The formation of the η^4 -cyclooctadiene ligand is evidenced by the multiplets observed in the ^1H NMR at 5.29, 4.87 and 3.50 ppm, with a relative integral of 1H, 2H and 1H respectively. These signals correlate with the singlets at 101.9, 97.1, 79.9 and 75.8 ppm found in the $^{13}\text{C}\{^1\text{H}\}$ NMR spectrum. The hydride shows a singlet at -12.75 ppm in the ^1H NMR spectrum.



Scheme 16. Formation of the hydrido- η^4 -cyclooctadiene compound **9**.

The determination of the structure of **9** in the solid state was possible by obtaining X-Ray quality single crystals (Figure 16). The geometry around the Ir(III) centre is pseudo octahedral, with the pincer ligand in one of the faces of the octahedron. The *trans* influence of the silicon atom is evidenced in the different bond lengths of the diolefin carbon atoms (C1, C2, C6 and C7 in Figure 16) bonded to the metal, as the distances between the carbon atoms *trans* to the sulphur atoms (C1–Ir1 2.19(3) Å and C2–Ir1 2.12(2) Å) are shorter than the distances between the carbon atoms *trans* to the silyl fragment (C6–Ir1 2.46(2) Å and C7–Ir1 2.43(2) Å).

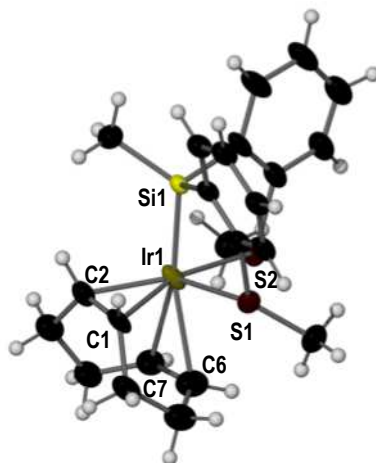


Figure 16. Molecular structure of the cationic unit of compound **9**. Displacement ellipsoids are drawn at 50% probability level. Selected bond lengths (Å) and angles ($^\circ$): Ir1–Si1 2.236(3), Ir1–S1 2.357(4), Ir1–S2 2.404(4), Ir1–C1 2.19(3), Ir1–C2 2.12(2), Ir1–C6 2.46(2), Ir1–C7 2.43(2); Si1–Ir1–S1 87.41(14), Si1–Ir1–S2 87.13(14).

The evolution of **8** into **9** implies a higher stability of 18 electron species for iridium compounds, in contrast with the stability shown by analogous 16 electron rhodium(III) compound **4**. There are some examples of these transformations involving the coordinated cyclooctadiene ligand in iridium complexes that involve a series of β -hydride elimination and olefin insertion steps.⁶¹ That is therefore the more feasible pathway to reach the hydride-cyclooctadiene-iridium(III) complex **9**. Another option is that the process takes place through Ir(V) intermediates.⁶² As the olefin insertion and β -hydride elimination are key processes present in numerous catalytic cycles for alkene functionalization reactions, we considered the importance of studying this transformation further. For that reason, DFT calculations were used to unravel this reaction mechanism.

Multiple reaction pathways were analysed that would transform compound **8** into the more stable **9** (-12.2 kcal/mol) via either Ir(III) or Ir(V) intermediates. Finally, the most plausible route found implies Ir(III) intermediate species and occurs through a series of successive β -hydride elimination and olefin insertion steps. The energetic profile of this process is shown in Figure 17.

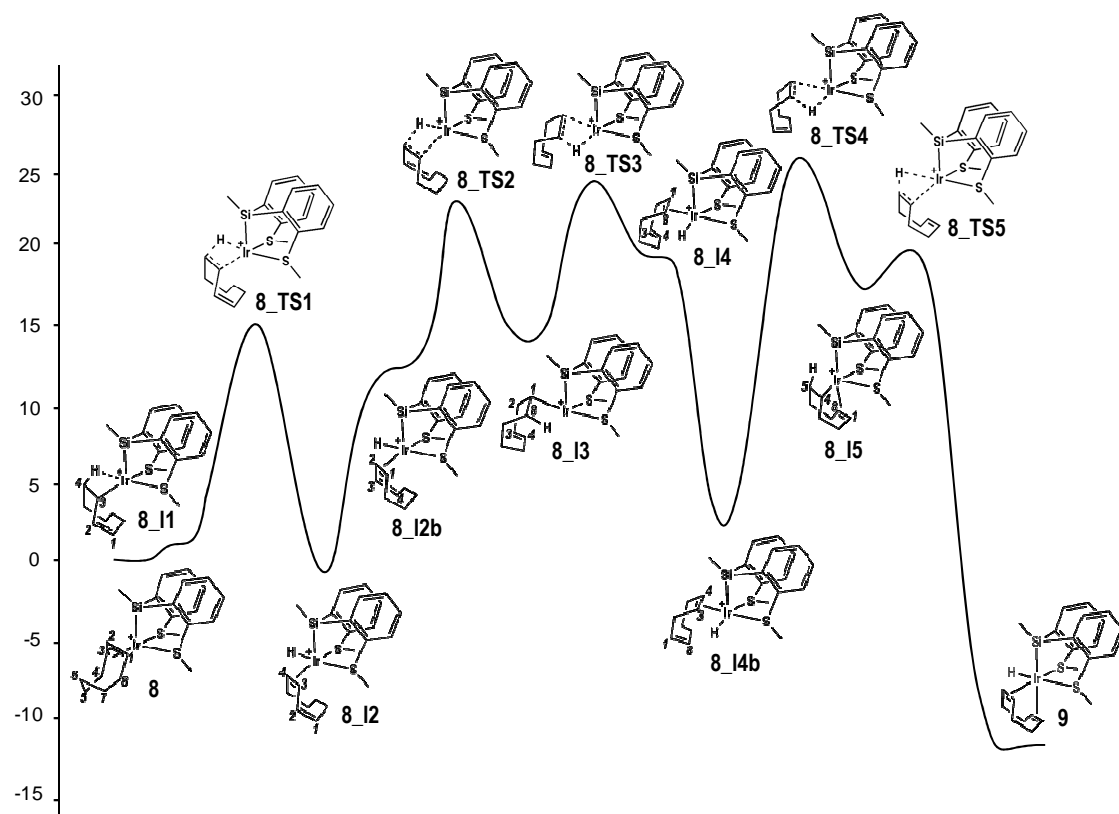


Figure 17. Free energy profile (kcal/mol) of the reaction mechanism from compound **8** to **9** through successive β -hydride elimination and olefin insertion steps. The effects of the solvents have been corrected.

Internal rearrangement of the η^3 -cyclooctenyl fragment in compound **8** leads to energetically higher (0.4 kcal/mol) conformer **8_I1**. In this intermediate, proton H4 is released to form the η^2 -1,3-cyclooctadiene-hydride-iridium species **8_I2** after the first β -hydride elimination process, by overcoming a kinetic barrier of ca. 15.5 kcal/mol associated to transition state **8_TS1**.

A counter clockwise rotation of 1,3-cyclooctadiene in **8_I2** yields intermediate **8_I2b** (13.0 kcal/mol higher in energy). The first olefin insertion into the hydride-iridium bond causes the hydride migration from iridium to atom C2 generating the σ -cyclooctenyl-iridium intermediate **8_I3**. In this species, two simultaneous agostic interactions (C8–H \cdots Ir and C5–H \cdots Ir) are established between the cyclooctenyl and the Iridium centre. Transformation of **8_I2b** into **8_I3** occurs through transition state **8_TS2** with a barrier of ca. 11.4 kcal/mol. Since the two step conversion of **8_I2** into **8_I3** requires a total kinetic barrier of 24.4 kcal/mol, it might therefore be the rate limiting step of the mechanism.

The second β -hydride elimination step proceeds *via* proton (H8) transfer from C8 in **8_I3** to the iridium centre, generating η^2 -1,4-cyclooctadiene-hydride-iridium intermediate **8_I4** through the transition state species **8_TS3**, with a barrier of ca. 10.3 kcal/mol. A clockwise rotation of the η^2 -1,4-cyclooctadiene ligand in **8_I4** yields the thermodynamically more stable conformer **8_I4b**, which is involved in a second olefin insertion step, giving σ,π -cyclooctenyl-iridium intermediate **8_I5**. Finally, **8_I5** promotes a third β -hydride elimination step that yields the final product **9** upon overcoming an associated small kinetic barrier of ca. 1.7 kcal/mol *via* transition structure **8_TS5**.

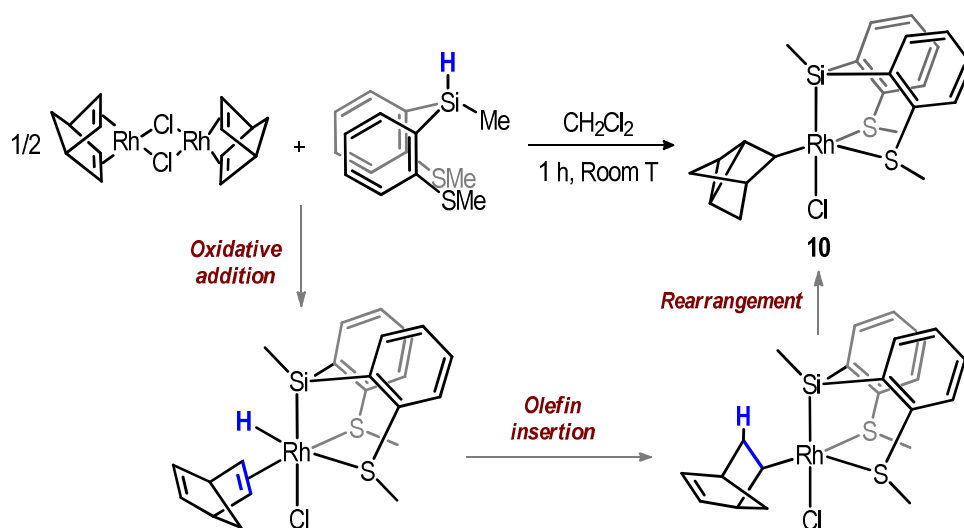
Altogether, the proposed mechanism includes three successive β -hydride elimination and two olefin insertion steps, with all kinetic barriers manageable at experimental conditions, including the rate limiting step with a barrier of 24.14 kcal/mol that might be responsible for the modest reaction rate observed experimentally. Interestingly, the reverse reaction from **9** to **8** would imply overcoming a first barrier of ca. 32.24 kcal/mol with an olefin insertion step to generate intermediate **8_TS5**. This kinetic barrier would be too large to be overcome at room temperature.

II. 1.2.3c. Reactivity of L2 with [Rh(nbd)Cl]₂

In order to extend this research, we envisaged then to study the reactivity of **L2** with a norbornadiene-rhodium(I) complex [Rh(nbd)Cl]₂. Treatment of [Rh(nbd)Cl]₂ with two

equivalents of **L2** in dichloromethane at room temperature resulted in neutral complex $[\text{RhCl}(\text{ntyl})(\text{SiMe}_2(o\text{-C}_6\text{H}_4\text{SMe})_2)]$ ($\text{ntyl} = \sigma\text{-nortricyclyl-C}_7\text{H}_9$) (**10**) as represented in Scheme 17.

It has been established that activation of C-H bonds *via* oxidative addition to rhodium(I) complexes with a coordinated norbornadiene ligand results into the formation of $\sigma\text{-nortricyclyl}$ species, after the insertion of the olefin into the Rh-H bond.⁶³ Formation of 16 electron complex **10** implies the oxidative addition of **L2** to the rhodium(I) dimer, to reach the unobserved hydride- $\eta^2\text{-norbornadiene-rhodium(III)}$ intermediate. The insertion of one of the double bonds in the norbornadiene ligand into the Rh-H bond gives the $\sigma\text{-norborynyl}$ ($\sigma\text{-nbyl}$) species, which then undergoes a double bond shift with a ring closure to yield product **10**. In rhodium(III) complexes with a coordinative vacancy, the transformation of the $\sigma\text{-norborynyl}$ fragment into the $\sigma\text{-nortricyclyl}$ derivative is thermodynamically favoured.⁶⁴



Scheme 17. Formation of the saturated compound **10**.

Characterisation of complex **10** was performed by NMR spectroscopy and ESI-MS. The $\sigma\text{-nortricyclyl}$ ligand shows various multiplet signals from 0.13 to 2.37 ppm in the ^1H NMR spectrum (Figure 18), and there are no signals in the olefin region. The nortricyclyl proton signal at 2.37 ppm correlates to a doublet signal at 44.0 ppm in the $^{13}\text{C}\{^1\text{H}\}$ NMR spectrum, which corresponds to the carbon atom bonded to the rhodium centre ($J_{\text{Rh-C}} = 22$ Hz). The SiMe moiety in the silyl-thioether ligand shows a singlet signal at 1.01 ppm in the ^1H NMR spectrum, and the two non-equivalent SMe groups show different resonances at 2.42 and 2.88 ppm. The presence of the molecular ion at $m/z = 485.03$ in the ESI-MS corresponds to the $[\text{Rh}(\text{ntyl})(\text{SiMe}_2(o\text{-C}_6\text{H}_4\text{SMe})_2)]^+$ fragment, and confirms the pentacoordinated structure proposal for **10**.

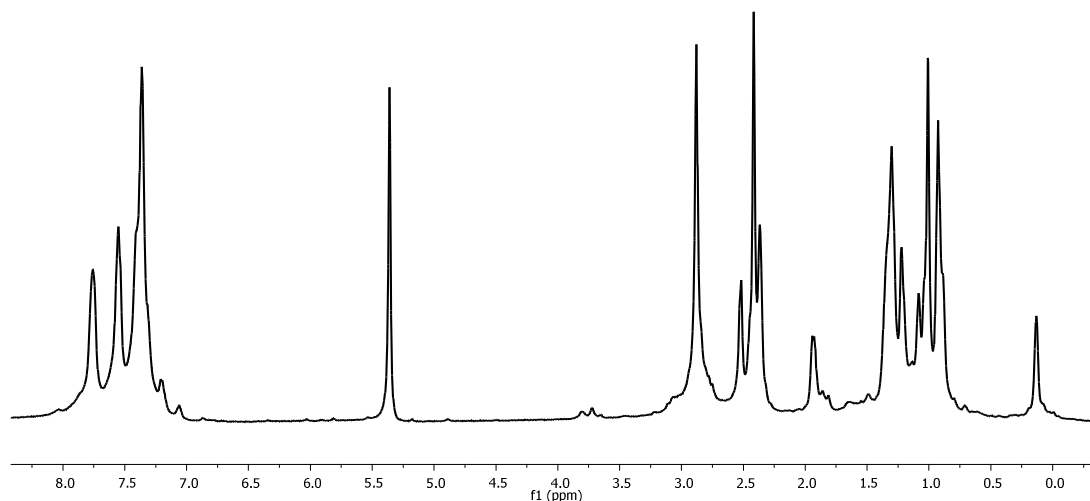
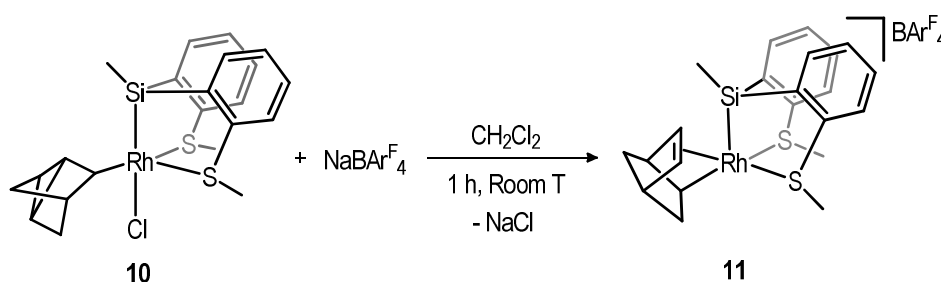


Figure 18. ^1H NMR spectrum of complex **10** in CD_2Cl_2 .

The extraction of the chloride ligand from **10** by addition of the $\text{NaBAR}^{\text{F}}_4$ salt in dichloromethane leads to a cationic 14 electron compound, and induces the reverse rearrangement of the nortricycyl group to form a norbornenyl species. This transformation implies the cleavage of the cyclopropyl fragment, and the formation of a carbon-carbon double bond that would be coordinated to the rhodium(III) centre, to yield complex $[\text{Rh}(\sigma,\pi\text{-nbyl})(\text{SiMe}_2(o\text{-C}_6\text{H}_4\text{SMe}_2))]\text{BAR}^{\text{F}}_4$ (**11**) (Scheme 18). To the best of our knowledge, this would be the first observed transformation of a metal bonded nortricycyl fragment into a norbornenyl derivative.



Scheme 18. Reaction of formation of compound **11**.

The presence of the σ,π -norbornenyl ligand is supported by the ^1H NMR spectrum with the relative integral ^1H signals at 5.50 and 4.45 ppm corresponding to the double bond, which correlate to the resonances at 107.9 and 73.4 ppm in the $^{13}\text{C}\{^1\text{H}\}$ NMR. The proton NMR signal at 2.29 ppm correlates to the carbon NMR doublet at 20.1 ppm ($J_{\text{Rh-C}} = 11.2$ Hz), and corresponds to the carbon atom σ -bonded to the metal in the norbornenyl.

The determination of the solid structure of **11** by single crystal X-ray diffraction was possible (Figure 19). The geometry adopted around the rhodium(III) centre is a distorted octahedron, with the tridentate ligand located in one of the faces. This ligand is bonded *via* the silyl group (Rh1–Si1 2.92(2) Å) and both sulphur atoms (Rh1–S2 2.460(1) Å and Rh1–S3 2.312(2) Å). The equatorial plane is occupied by the two SMe groups and the norbornenyl ligand. The hydrogen atom (H02) of a C-sp³ (C2) of the norbornenyl occupies the last coordination site *trans* to the silicon *via* a weak Rh⋯H–C interaction. The bond distances and angles of the atoms implied (Rh1–H02 = 2.23(9) Å, Rh1–C2 = 2.504(7) Å, Rh1–H02–C2 = 93.2(6) °) suggest this could be an agostic interaction.⁶⁵

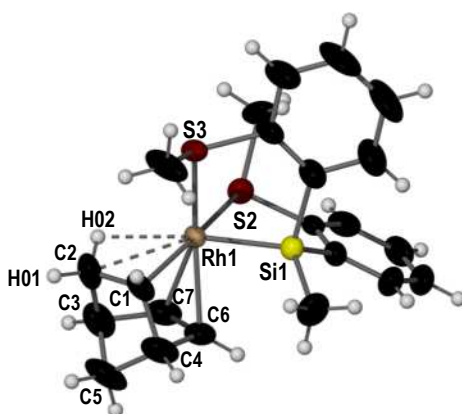


Figure 19. Molecular structure of compound **11**. The anion and a molecule of solvent (CDCl₃) are omitted for clarity. Displacement ellipsoids are drawn at 50% probability level. Selected bond lengths (Å) and angles (°): Rh1–Si1 2.292(2), Rh1–S2 2.460(1), Rh1–S3 2.312(2), Rh1–C1 2.047(6), Rh1–C2 2.504(7), Rh1–H02 2.23(9), C1–C2 1.537(9), C2–H02 1.03(10), Rh1–C6 2.216(6), Rh1–C7 2.271(6); Rh1–H02–C2 93.2(6), S2–Rh1–S3 96.14(6), Si1–Rh1–S2 83.51(3), Si1–Rh1–S3 86.32(6), C1–C2–H02 116(5), Rh1–C1–C2 87.4 (4).

The agostic interaction shown in Figure 19 could also be noticed in solution by a ¹H–¹³C HSQC coupled experiment (Supporting Information). The different value of the C–H coupling constants observed for the two protons bonded to C2 ($J_{C-H} = 144$ Hz and $J_{C-H} = 116$ Hz) could imply one of these hydrogen atoms being involved in a weak interaction with the rhodium centre, although a ring strain could also cause a decrease in a J_{C-H} coupling constant. There are examples of Pd(II) complexes with a coordinated norbornene ligand that show a similar agostic interaction, which also present a difference of 20 Hz between the two agostic and nonagostic proton-carbon coupling constants.⁶⁶

The novelty of the transformation of the σ -nortricyclyl into the σ,π -norbornenyl species motivated a more thorough study of the reaction mechanism. It is usually accepted that the nortricyclyl species are the thermodynamically favoured products, due to the release of strain of the double bond in a rigid bicyclic molecule when the cyclopropyl fragment is formed. However, the free energy difference between the free nortricyclane and norbornene molecules is only 0.9 kcal/mol.⁶⁷ Recent studies on the reaction of hydridoaryltin(II) compounds with norbornadiene propose the formation of σ -norbornenyl or nortricyclyl derivatives depending on the transition states involving only one or both carbon-carbon double bonds, respectively.⁶⁸ In the present case, the removal of the chloride ligand from **10** could have allowed the interaction between the rhodium(III) centre and a carbon-hydrogen bond in the nortricyclyl ligand, and this interaction would promote the cleavage of the cyclopropyl to finally reach the norbornenyl species. The coordination of the double bond to the metal centre and the agostic interaction would then allow the coordinative saturation of compound **11**.

This assumption is reinforced by the study of the reaction mechanism by DFT calculations (Figure 20). This study proposes a two-step mechanism from **10** to **11**, in which a succession of β -hydride elimination and olefin insertion processes are also involved.

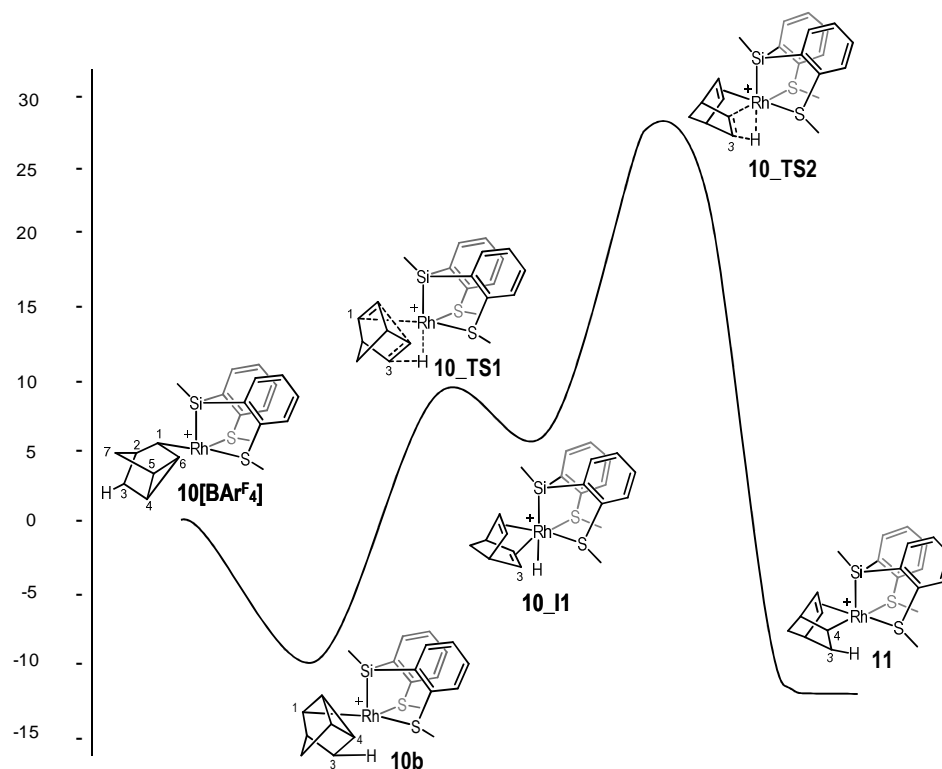


Figure 20. Free energy profile (kcal/mol) of the reaction mechanism from compound **10** to **11** through β -hydride elimination and olefin insertion steps. The effects of the solvents have been corrected.

After the chlorine removal, the new cationic compound **10**[BAr^F₄] experiments a counter-clockwise rotation to form the more stable **10b** conformer (-9.4 kcal/mol). A hydrogen migration from the C3 atom in the nortricyclyl to the rhodium(III) centre leads to the norbornadiene-hydride-rhodium(III) intermediate **10_I1** after the cyclopropyl rupture and the formation of two double bonds. This is possible through the six membered transition state **10_TS1**, by overcoming an energy barrier of 18.7 kcal/mol. In the second step, the insertion of the C3-C4 double bond into the Rh-H bond generates the norbornenyl-rhodium(III) complex **11**, and the agostic interaction is then formed between this migrating hydrogen and the metal (C3-H...Rh). This last transformation presents a barrier of 21.7 kcal/mol *via* the four-membered transition state **10_TS2**.

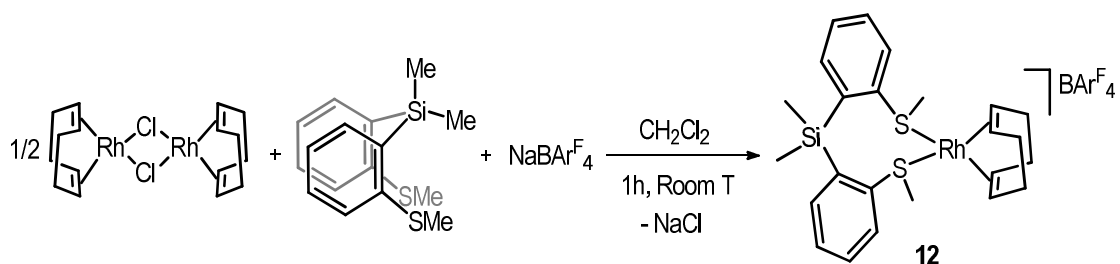
II. 1.2.4. Reactivity of ligand **L3** with [Rh(cod)Cl]₂, [Rh(nbd)Cl]₂, [Ir(cod)Cl]₂ and [Rh(coe)₂Cl]₂ dimers.

The activation of the Si-H bond in the **L1** and **L2** preligands permits the formation of hydride-metal species, which can lead to insertion reactions in the presence of olefins, yielding alkyl-metal complexes. The importance of the alkyl-metal compounds as intermediates in numerous catalytic cycles for alkene functionalization (hydrosilylation⁶⁹, hydroboration⁷⁰ or hydroamination⁷¹) is well known. Up to this point, we have studied the reactivity promoted by the oxidative addition of these ligands to rhodium(I) and iridium(I) complexes with coordinated cyclooctadiene and norbornadiene. Therefore, we considered of interest to study the reactivity derived from a similar ligand incapable of a silicon-hydrogen bond addition.

For this reason, we decided to study the reactivity of rhodium(I) and iridium(I) complexes containing coordinated olefins with the tridentate preligand SiMe₂(*o*-C₆H₄SMe)₂ (**L3**), whose structure is similar to that of **L2**, but with two methyl substituents bonded to the silicon atom.

II. 1.2.4a. Reactivity of **L3** with [Rh(cod)Cl]₂, [Rh(nbd)Cl]₂ and [Ir(cod)Cl]₂

The addition of the preligand **L3** to [Rh(cod)Cl]₂ in dichloromethane at room temperature failed to cleave the chloride bridges of the dimer. The extraction of the chloride by treatment of this mixture with the NaBAr^F₄ salt was necessary to initiate the reaction. The reaction of **L3** with [Rh(cod)Cl]₂ in the presence of NaBAr^F₄ leads to the formation of the cationic 16 electron Rh(I) compound [Rh(cod)SiMe₂(*o*-C₆H₄SMe)₂]⁺BAr^F₄⁻ (**12**) (Scheme 19).



Scheme 19. Formation of cationic compound **12**.

The characterisation of this compound was performed in solution by NMR spectroscopy and ESI-MS, and in solid state by X-ray diffraction. The coordination of the **L3** ligand can be determined by ^1H NMR (Figure 21), in which the presence of a 6H relative integral singlet at 2.31 ppm corresponds to the two SMe groups. The singlet at 0.47 ppm, with a relative integral of 6H, corresponds to the two methyl groups bonded to the silicon atom. The signals assigned to the double bonds in the cyclooctadiene ligand are two multiplets at 4.75 and 4.23 ppm, which correlate with the doublet signals at 86.8 and 91.0 ppm in the $^{13}\text{C}\{^1\text{H}\}$ NMR spectrum (Figure 21), due to the coordination to the rhodium centre. Broad signals at 2.48, 2.20 and 1.91 ppm in ^1H NMR correspond to the CH_2 groups in the cyclooctadiene. The ESI-MS shows a strong molecular ion at $m/z = 515.09$, which corresponds to the $[\text{Rh}(\text{cod})\text{SiMe}_2(\text{o-C}_6\text{H}_4\text{SMe})_2]^+$ unit.

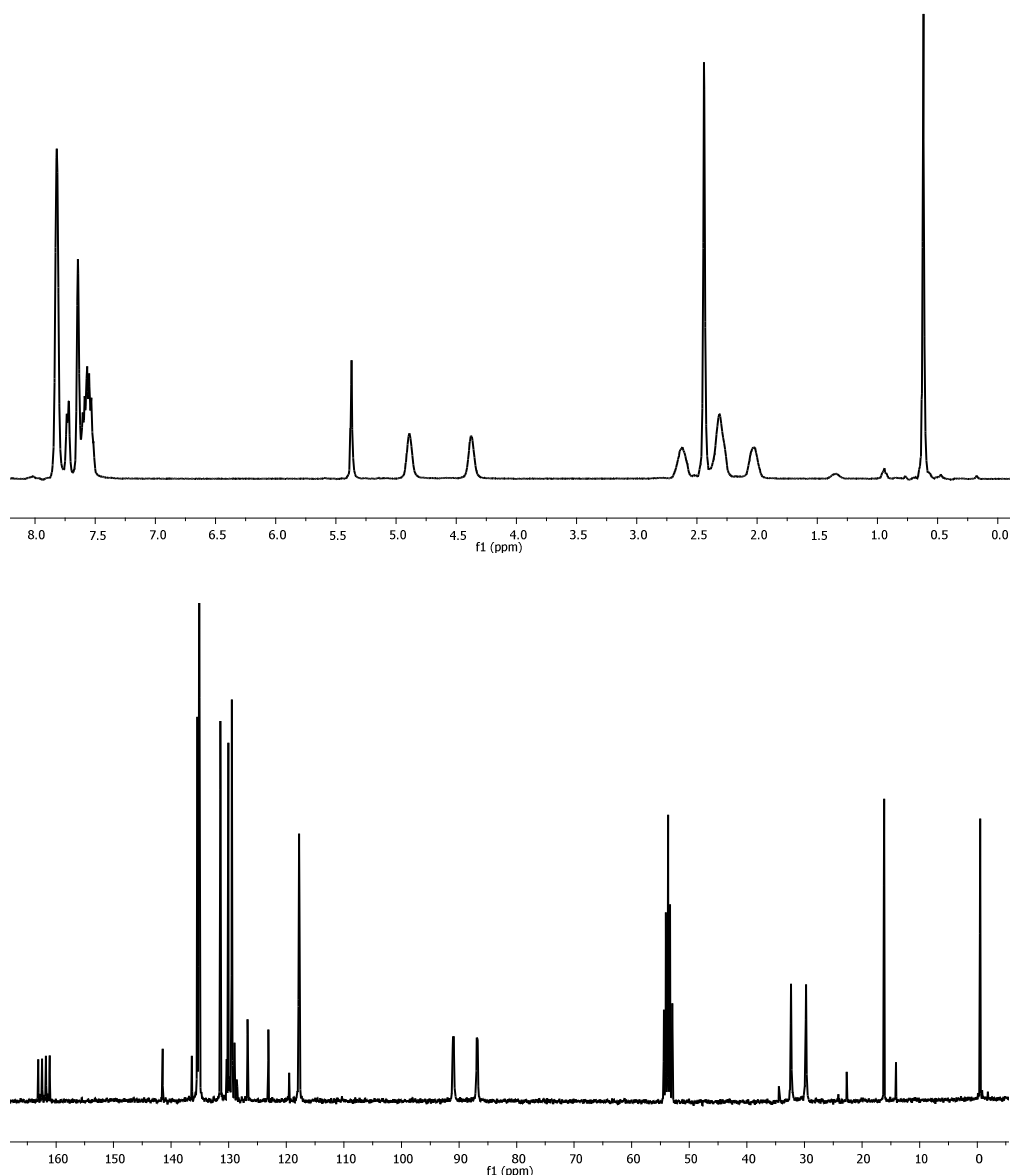


Figure 21. ^1H (top) and $^{13}\text{C}\{^1\text{H}\}$ NMR spectra of complex **12** in CD_2Cl_2 .

Determination of the solid state structure of **12** was also possible by X-ray diffraction, after growing crystals from a dichloromethane solution layered with pentane at room temperature. The resulting structure is in agreement with the one deduced from the spectroscopic data in solution (Figure 22). The Rh(I) centre is in a distorted square planar geometry. **L3** is only coordinated *via* the two SMe moieties (Rh1–S1 2.3967(7) Å and Rh1–S2 2.41(1) Å) to form an eight-membered ring chelate, showing a S1–Rh1–S2 bite angle of 83.3(2)°. The silicon atom is located in the same coordination plane, with the aromatic rings above and below the plane. The cyclooctadiene ligand occupies the two remaining coordination sites *trans* to the sulphur atoms. All bond distances between rhodium and the diolefin carbon atoms are equal (Rh1–C17 2.141(4) Å, Rh1–C18 2.173(4) Å, Rh1–C21 2.148(3) Å, Rh1–C22 2.160(3) Å).

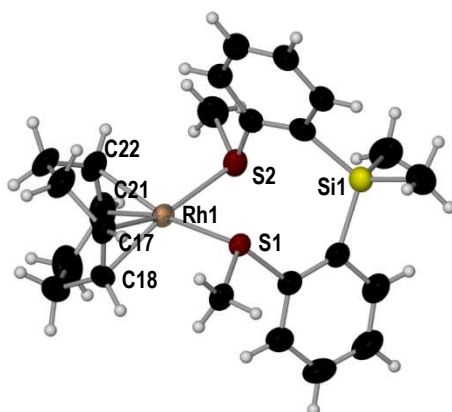
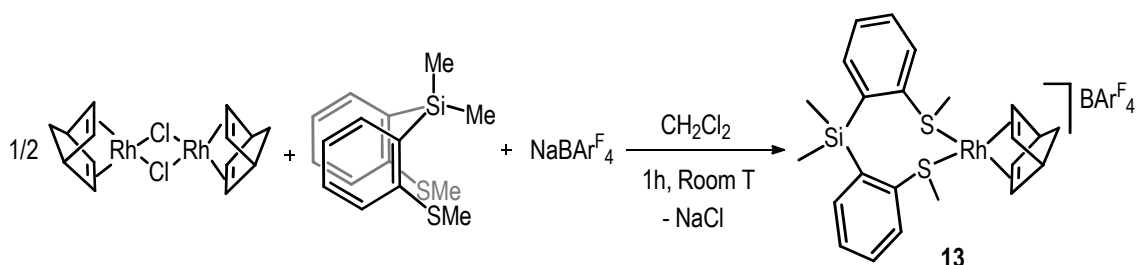


Figure 22. Molecular structure of the cationic unit of compound **12**. Displacement ellipsoids are drawn at 50% probability level. Selected bond lengths (Å) and angles (°): Rh1-S1 2.3967(7), Rh1-S2 2.41(1), Rh1-C17 2.141(4), Rh1-C18 2.173(4), Rh1-C21 2.148(3), Rh1-C22 2.160(3), C21-C22 1.379(6), C17-C18 1.373(5), S1-Rh1-S2 83.3(2).

The presence of the $\text{NaBAR}_4^{\text{F}}$ salt was also necessary for the reaction of the $[\text{Rh}(\text{nbd})\text{Cl}]_2$ and $[\text{Ir}(\text{cod})\text{Cl}]_2$ dimers with **L3**. Treatment of $[\text{Rh}(\text{nbd})\text{Cl}]_2$ with the S,S,Si preligand in the presence of $\text{NaBAR}_4^{\text{F}}$, in dichloromethane at room temperature leads to 16 electron cationic $[\text{Rh}(\text{nbd})\text{SiMe}_2(o\text{-C}_6\text{H}_4\text{SMe})_2]\text{BAR}_4^{\text{F}}$ (**13**) (Scheme 20).



Scheme 20. Formation of cationic compound **13**.

The ^1H NMR spectrum of this compound shows a singlet at 2.16 ppm for the two SME fragments in the chelate ligand, and a singlet at 0.44 ppm corresponding to the methyl groups on the silicon. The broad signal at 4.19 ppm with a 4H relative integral corresponds to the olefinic protons of the norbornadiene fragment. This signal is correlated to two doublet signals at 64.3 and 53.1 ppm in the $^{13}\text{C}\{^1\text{H}\}$ NMR spectrum, due to coordination to the metal centre. The 2H relative integral signal at 3.92 ppm in the ^1H NMR spectrum corresponds to the non-olefinic CH groups in the norbornadiene, and the CH_2 moiety shows a signal at 1.44 ppm. In the ESI-MS, the molecular ion at $m/z = 499.06$ coincides with that calculated for the $[\text{Rh}(\text{nbd})\text{SiMe}_2(o\text{-C}_6\text{H}_4\text{SMe})_2]^+$ species.

Compound **13** was also characterised by single-crystal X-ray diffraction (Figure 23). As in compound **12**, **13** shows a slightly distorted square-planar geometry around the rhodium(I) centre. The **L3** ligand forms an eight-membered chelate-ring, with a S1–Rh1–S2 bite angle of 87.87(1)°, bonded only through the two thioether moieties (Rh1–S1 2.3687(7) Å and Rh1–S2 2.367(1) Å), with the uncoordinated silyl fragment in the same plane. The norbornadiene group occupies the two last coordination sites in the plane. Bond distances between rhodium and the norbornadiene carbon atoms are equal (Rh1–C17 2.145(2) Å, Rh1–C18 2.145(2) Å, Rh1–C20 2.139(2) Å, Rh1–C21 2.138(2) Å).

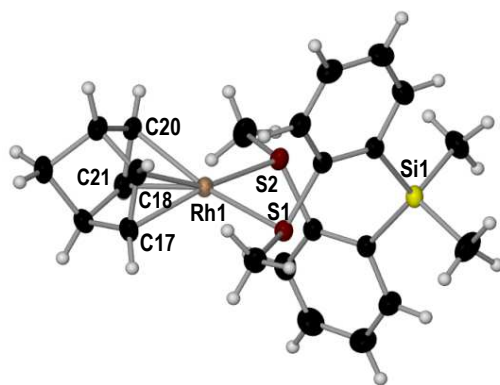
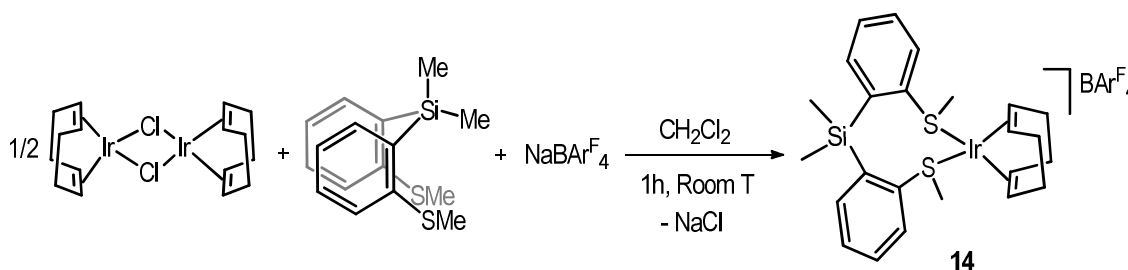


Figure 23. Molecular structure of the cationic unit of compound **13**. Displacement ellipsoids are drawn at 50% probability level. Selected bond lengths (Å) and angles (°): Rh1–S1 2.3687(7), Rh1–S2 2.367(1), Rh1–C17 2.145(2), Rh1–C18 2.145(2), Rh1–C20 2.139(2), Rh1–C21 2.138(2), C21–C20 1.392(3), C17–C18 1.392(3), S1–Rh1–S2 87.87(1).

In the same way, the reaction of the **L3** ligand with $[\text{Ir}(\text{cod})\text{Cl}]_2$ in the presence of $\text{NaBAR}_4^{\text{F}}$ in dichloromethane gives the 16 electron complex $[\text{Ir}(\text{cod})\text{SiMe}_2(\text{o-C}_6\text{H}_4\text{SMe})_2]\text{BAR}_4^{\text{F}}$ (**14**) (Scheme 21). This compound was characterised in solution by NMR spectroscopy.



Scheme 21. Formation of cationic compound **14**.

In the ^1H NMR spectrum, the 6H relative integral singlet signals at 2.55 ppm and 0.51 ppm correspond to the SMe fragments and the two methyl groups in the silicon atom respectively.

The cyclooctadiene ligand exhibits two 2H relative integral multiplets at 4.58 and 3.91 ppm for the olefinic hydrogen atoms in the molecule. The broad signals at 2.32, 2.04 and 1.59 ppm correspond to the remaining CH₂ groups in the cyclooctadiene.

With the aim of testing the catalytic potential of these complexes, we attempted the substitution of the coordinated olefin with a more labile ligand. Hydrogenation of the alkene fragment would lead to the decooordination of the reduced species. For this reason, solutions of compounds **12**, **13** and **14** in fluorobenzene, toluene-d₈ and dichloromethane-d₂ were treated with 4 atm of hydrogen gas (Procedure in experimental section). Rhodium(I) compounds **12** and **13** showed no signs of hydrogenation after 7 days in solution. Iridium(I) compound **14** reached an equilibrium of unidentified products after 24 hours in solution. Heating these solutions at 50 °C resulted in decomposition. The inability of these compounds containing the **L3** ligand to undergo the hydrogenation of the coordinated olefin contrasts with the behaviour observed for similar Rh(I) and Ir(I) complexes with phosphine ligands.⁷²

The decooordination of the diolefin by substitution was then attempted by introducing a coordinating solvent. Compounds **12**, **13** and **14** were dissolved in acetonitrile and stirred for an hour at room temperature. Though rhodium(I) compounds experimented no reaction, iridium(I) complex **14** showed a shift of the cyclooctadiene signals in the ¹H NMR spectrum, along with a singlet at 1.83 ppm that could correspond to a coordinated acetonitrile molecule (Figure 24). The five multiplets corresponding to the diolefin evolved into three broad signals in an intermediate position. This could be a consequence of the coordination of a molecule of acetonitrile to the metal centre to afford a fluxional iridium(I) species.

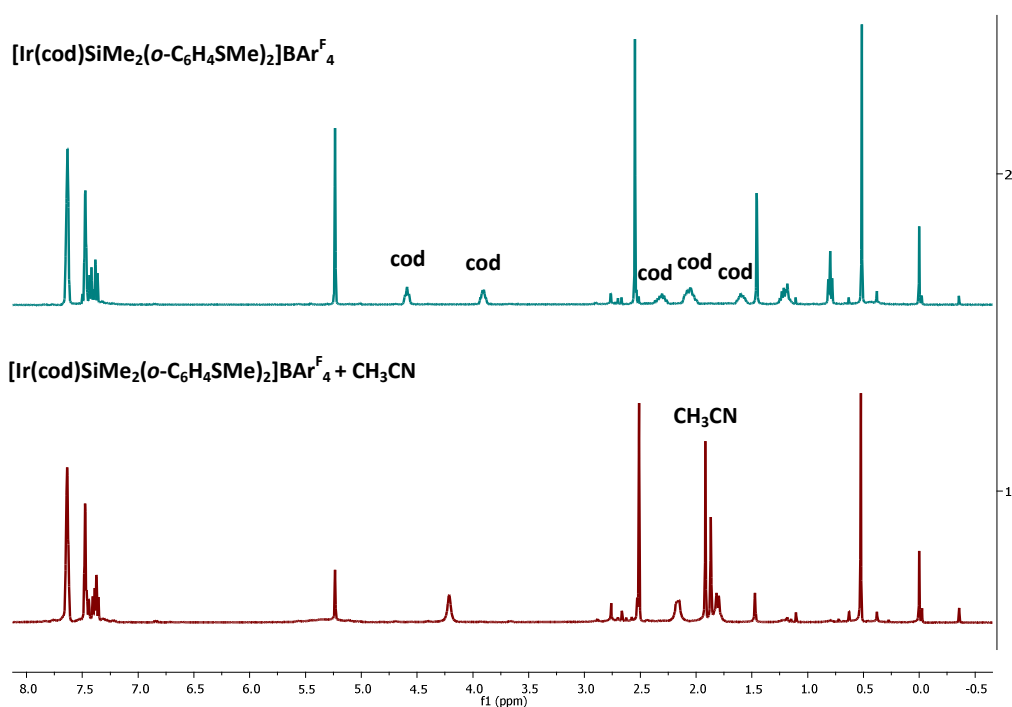


Figure 24. ^1H NMR of compound **14** in CD_2Cl_2 before (top) and after treatment with acetonitrile (bottom).

II. 1.2.4b. Reactivity of **L3** with $[\text{Rh}(\text{coe})_2\text{Cl}]_2$

Since attempts of olefin decoordination on cyclooctadiene complexes **12** and **14**, and on norbornadiene complex **13** proved unsuccessful, the use of the rhodium(I) cyclooctene dimer $[\text{Rh}(\text{coe})_2\text{Cl}]_2$ (coe = cyclooctene) was considered. Treatment of $[\text{Rh}(\text{coe})_2\text{Cl}]_2$ with two equivalents of **L3** in dichloromethane at room temperature gives a yellow precipitate that resulted to be insoluble in several solvents (dichloromethane, benzene, acetone, methanol) but completely soluble in dimethylsulfoxide. The reaction product was therefore dissolved in DMSO-d_6 for its characterisation by NMR spectroscopy (Figure 25). The ^1H NMR spectrum shows two singlet signals at 0.59 and 0.82 ppm, both with a relative integral of 3H, which could correspond to the two methyl groups bonded to the silicon atom in **L3**. Two singlet signals at 2.69 and 2.77 ppm correspond to the two non-equivalent SMe moieties. This would indicate the coordination of the **L3** ligand to the rhodium centre. The absence of signals corresponding to coordinated or free cyclooctene indicates that the loss of coe is produced in the formation of the insoluble product by reaction of $[\text{Rh}(\text{coe})_2\text{Cl}]_2$ with **L3**.

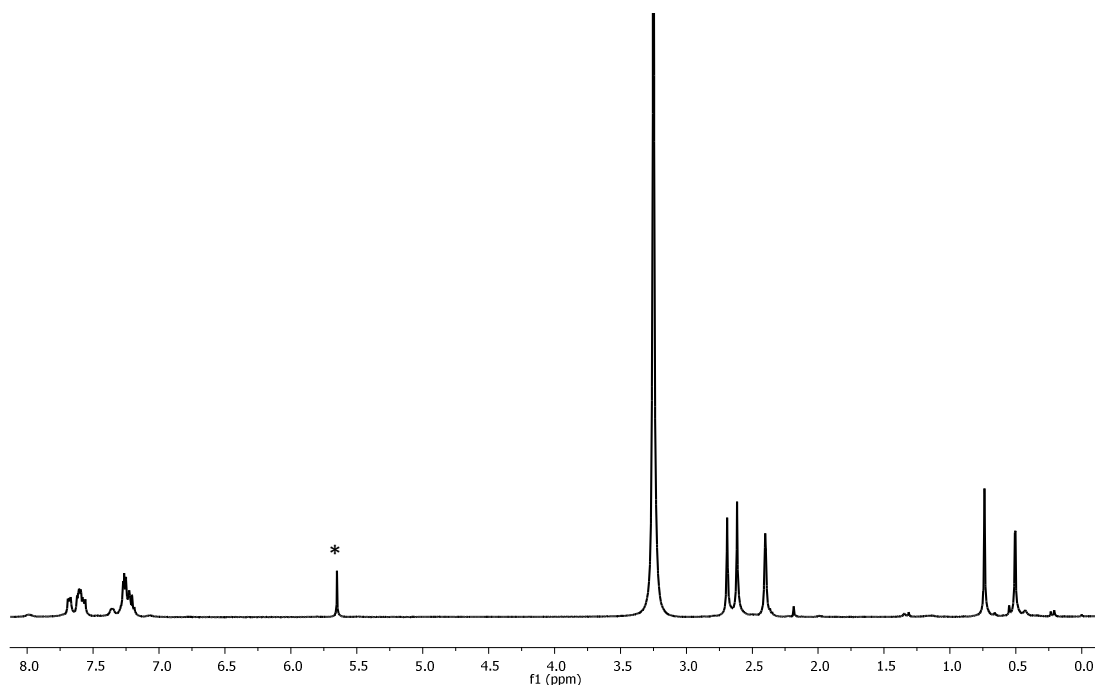
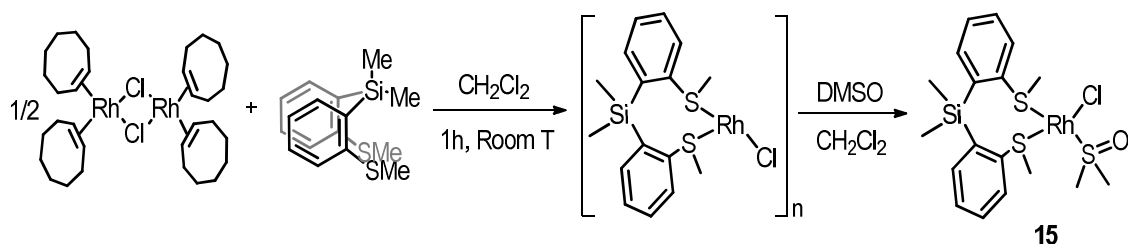


Figure 25. ^1H NMR of compound **15** in DMSO-d_6 (*dichloromethane).

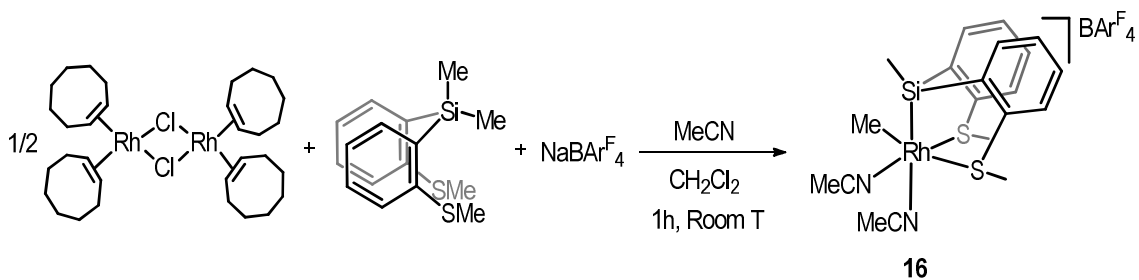
For this reason, the insoluble solid is thought to be an oligomeric compound with a repeated unit of $[\text{RhCl}(\text{Si}(\text{Me})_2(o\text{-C}_6\text{H}_4\text{SMe})_2)]_n$ bonded through a chloride bridge, which is soluble in DMSO most likely due to chloride bridge cleavage by the solvent and formation of compound **15** (Scheme 22).



Scheme 22. Formation of the proposed polymeric compound and compound **15**.

Reaction of preligand **L3** with $[\text{Rh}(\text{coe})_2\text{Cl}]_2$ in the presence of $\text{NaBAR}_4^{\text{F}}$ salt in dichloromethane at room temperature leads to the formation of uncharacterized products, which resulted unstable in solution. However, the presence of acetonitrile in the reaction mixture promoted the unusual⁷⁵⁻⁷⁷ Si- CH_3 bond activation in the silyl-thioether ligand, allowing the coordination of the silicon to the metal centre and the formation of a stable 18 electron product, with cyclooctene displacement. The cationic complex $[\text{Rh}(\text{Me})(\text{Si}(\text{Me})(o\text{-C}_6\text{H}_4\text{SMe})_2)(\text{MeCN})_2]\text{BAR}_4^{\text{F}}$ (**16**) was obtained *via* the C-Si oxidative addition, involving one of the methyl groups bonded to

the silicon atom, and coordination of two molecules of acetonitrile to the metal centre (Scheme 23).



Scheme 23. Formation of compound **16** after the activation of the Si-C bond in **L3**.

Characterisation of **16** in solution was performed by NMR spectroscopy. Moreover, the characterization of **16** in the solid state through X-ray diffraction was possible due to the isolation of a single crystal. In the ^1H NMR spectrum, the methyl group bonded to the rhodium(III) centre shows a broad signal at 0.80 ppm which is correlated to a broad signal at -1.3 ppm in the $^{13}\text{C}\{^1\text{H}\}$ NMR spectrum. The terdentate ligand exhibits a singlet signal at 0.61 ppm for the methyl bonded to the silicon atom, and two 3H relative integral singlets at 2.66 and 2.60 ppm for the non-equivalent SMe groups. A broad signal with a relative integral of 6H at 2.25 ppm is assigned to the coordinated acetonitrile molecules.

Single crystals of **16** were obtained from a dichloromethane solution layered with pentane at room temperature. The structure in the solid state (Figure 26) consists of a Rh(III) centre in a pseudo-octahedral geometry. The terdentate ligand occupies one of the faces of the octahedron, and is bonded to the metal through the silyl fragment (Rh1–Si1 2.2676 Å) and the SMe moieties (Rh1–S1 2.4309 Å and Rh1–S2 2.2782 Å). The acetonitrile molecules are bonded through the nitrogen atom, and are located *trans* to the Si (Rh1–N1 2.2255 Å) and one of the sulphur atoms (Rh1–N2 2.0996 Å). The Rh-N bond distance for the MeCN group *trans* to the silyl fragment is significantly longer, which evidences the *trans* labilizing effect of the silicon atom. The methyl group coordinated to the rhodium centre *via* Si-C activation occupies the last coordination site, *trans* to a thioether moiety (Rh1–C1 2.0882 Å).

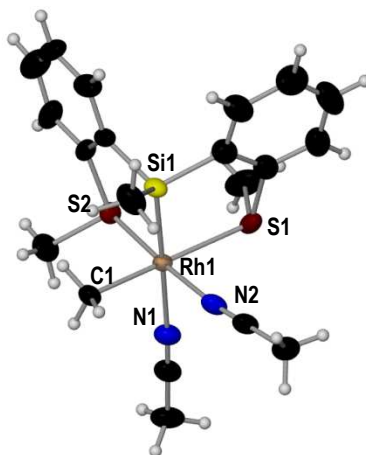


Figure 26. Molecular structure of the cationic unit of compound **16**. Displacement ellipsoids are drawn at 50% probability level. Selected bond lengths (Å) and angles (°): Rh1-Si1 2.2676(), Rh1-S2 2.2782(), Rh1-S1 2.4309(), Rh1-N1 2.2255(), Rh1-N2 2.0996(), Rh1-C1 2.0882(); Si1-Rh1-N1 178.05(), S2-Rh1-N2 176.62(), C1-Rh1-S1 174.09(), S1-Rh1-S2 93.59(), C1-Rh1-N2 91.90(), C1-Rh1-S2 90.74(), S1-Rh1-N2 83.62().

The silicon-carbon bond cleavage to yield compound **16** is remarkable considering the robust nature of a Si-C(sp³) bond, with a dissociation energy of ca. 90 kcal/mol. Further studies on this Si-C(sp³) bond cleavage and the formation of this silyl-(η¹-methyl)-rhodium(III) product are of interest, due to its possible involvement in important reaction mechanisms relevant for Si-C bond catalytic transformations. The activation of the Si-C bond by a direct transition metal insertion under mild temperatures has gained attention recently as an attractive strategy for the functionalization of organosilanes.⁷³ The addition of an external or internal nucleophile to form a hypercoordinate silicon species is an alternate well known method for the silicon-carbon bond cleavage,⁷⁴ although the usual requirement of harsh reaction conditions in these routes has made them less appealing.

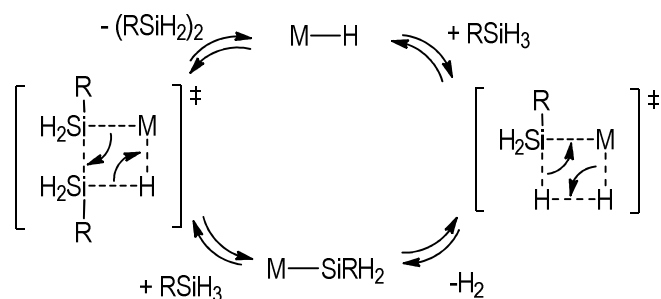
Examples of activation of the Si-C(alkyl) bond within the coordination sphere of a transition metal complex are more limited⁷⁵ due to the low reactivity exhibited by the non-polar unstrained Si-C(sp³) bond when compared to Si-C(sp²) or Si-C(allyl) bonds. Moreover, the usually low stability of the yielded metal-(η¹-alkyl) derivative prevents the isolation of these compounds. Turculet et al. reported a rearrangement of a Cy-PSiP ligand from prepared nickel and palladium [(Cy-PSiP)M(Me)] complexes in solution, involving Si-C(sp³) and Si-C(sp²) bond cleavage processes.⁷⁶ A subsequent publication by Takaya and Iwasawa described a related Si-C(sp³) bond cleavage in Ph-PSiP ligated Pd complexes. In this study, reaction of an allene with

the Pd⁰ complex leads to the reversible transformation between {(Ph₂P)₂-Si}Pd(η¹-allyl) and {(Ph₂P)₂-Si(allyl)}Pd⁰ species.⁷⁷

II. 1. 3. SYNTHESIS AND CATALYTIC APPLICATIONS OF SILYL-HYDRIDE RHODIUM(III) AND IRIIDIUM(III) COMPLEXES DERIVED FROM L1 AND L2

As already mentioned, Si-H bond activation is a key step in both dehydrogenative Si-Si coupling and alkene hydrosilylation reactions. Si-H activation by oxidative addition of a silane to a metal centre results in the formation of hydrido-silyl-metal species, which are present as intermediates in numerous accepted catalytic cycles for these transformations.

In the case of silane dehydrocoupling reactions, which leads to the formation of new Si-Si bonds, the reaction mechanism has been widely studied, and several modes and pathways have been proposed. The first generally accepted mechanism was the σ -bond metathesis, initially proposed by Tilley et al. in 1992 using group 4 metal catalysts.⁷⁸ Successive concerted four-centre transition states are the key steps in this transformation.⁷⁹ Addition of a silane substrate to a metal-hydride catalyst forms a silyl-metal species through a σ -bond metathesis mechanism, with a concomitant loss of a dihydrogen molecule. The second addition of silane leads to another four-centre transition state, with the formation of the Si-Si bond and regeneration of the catalytically active metal-hydride species (Scheme 24).



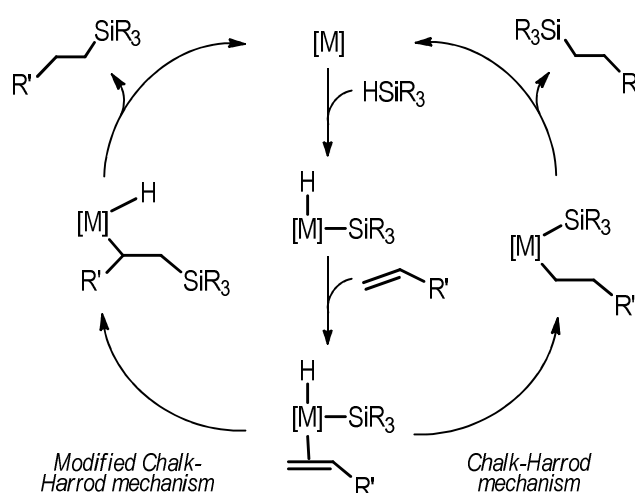
Scheme 24. σ -bond metathesis mechanism proposed by Tilley and co-workers.

The Si-Si bond formation is usually accepted as the rate determining step (RDS) in this type of processes. Therefore steric effects due to bulky substituents in the silane substrate may play an important role in RDS. This is in agreement with the reactivity decrease from primary to secondary silanes, and the preference in linear chain formation over branching in the polymeric products.⁸⁰

While the σ -bond metathesis is accepted mostly for early transition metals,⁸¹ the proposed catalytic pathway for late transition metals is composed of a series of classic oxidative addition and reductive elimination steps.⁸² However, some studies do not exclude the possibility of σ -

bond metathesis steps in the catalytic cycle for late transition metals.⁸³ Most recently, involvement of silylene intermediates in the process involving primary and secondary silanes has also been proposed.⁸⁴

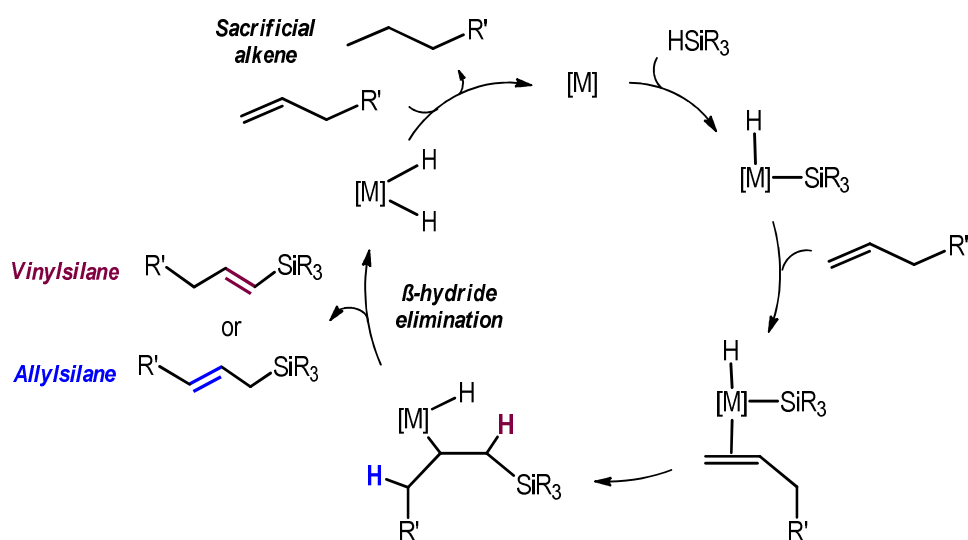
It is well established that metal hydride compounds are also present in the catalytic route of hydrosilylation. Transition metal catalysed alkene hydrosilylation is generally assumed to follow the Chalk-Harrod mechanism.⁸⁵ This route implies oxidative addition of the silane substrate to give a silyl-hydride-metal complex. The π -coordination of the olefin to the metal centre and subsequent olefin insertion into the M-H bond gives a silyl alkyl species. Finally, a Si-C reductive elimination gives the alkylsilane product. In an alternative route, generally referred to as modified Chalk-Harrod mechanism,⁸⁶ the olefin inserts into the M-Si bond. The hydrosilylated product is then formed *via* C-H reductive elimination. Both mechanisms are depicted in Scheme 25.



Scheme 25. The Chalk-Harrod (right) and modified Chalk-Harrod (left) mechanism schemes for alkene hydrosilylation.

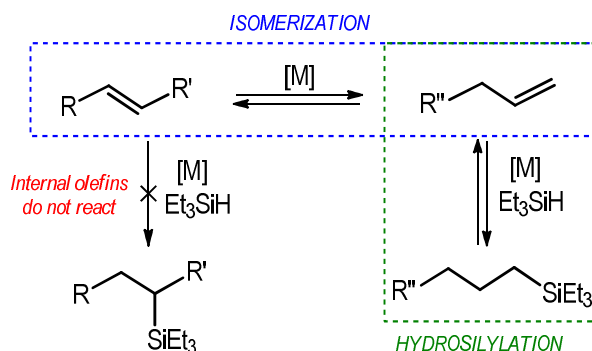
Alkene hydrosilylation can often be accompanied by side reactions such as dehydrogenative silylation, leading to competitive allyl- or vinylsilane products. It was recently suggested that formation of the dehydrogenative silylation product involves a variation of the modified Chalk-Harrod catalytic route, in which a competitive β -hydride elimination step in the hydride-alkyl-metal intermediate would lead to the formation of an unsaturated product (Scheme 26).⁸⁷ These studies also propose the subsequent formation of a dihydride metal complex. The hydrogenation of a sacrificial substrate molecule would lead to the regeneration of the catalyst (Scheme 26). The β -hydride elimination from the hydrido-alkyl-metal intermediate is proposed as the rate determining step of this process. Taken into account the proposed mechanism and

rate determining step, steric and electronic factors of the silanes would contribute to the allyl/vinyl product ratio.⁸⁸ Being a competitive reaction, there are limited examples of selective catalysts to yield vinyl- or allylsilanes by dehydrogenative silylation,⁸⁹ as in most cases these catalytic pathways lead to a mixture of both hydrosilylation and dehydrogenative silylation products.



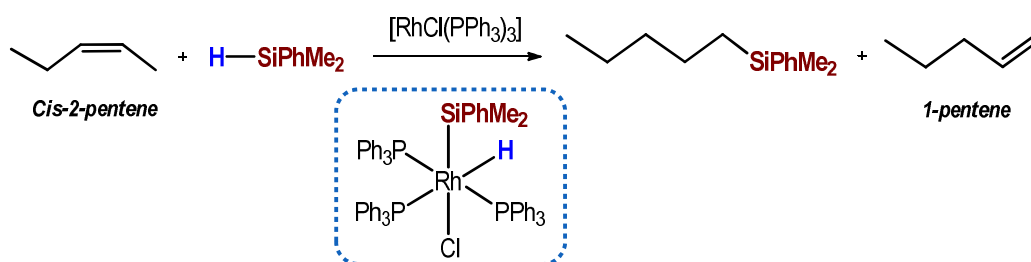
Scheme 26. Proposed catalytic cycle for dehydrogenative silylation.

One important challenge for catalytic systems in alkene hydrosilylation and dehydrogenative silylation is the formation of terminal silylated products from internal olefins or olefin mixtures.⁹⁰ The importance of this reaction is that internal olefin mixtures are more readily accessible and cheaper than pure terminal alkenes. For most common catalysts, the use of a terminal olefin is necessary to obtain a terminal silylated product. Therefore, final conversion of the substrate is reduced whenever there is concomitant α -olefin isomerisation. This limitation could be solved by a catalyst capable of tandem isomerisation-hydrosilylation of an internal alkene (Scheme 27), in which the previous isomerisation from internal to terminal olefins and subsequent α -olefin hydrosilylation is promoted by the same metal complex (Scheme 27).



Scheme 27. Scheme of tandem isomerisation-hydrosilylation pathway.

Examples of efficient tandem isomerization-hydrosilylation of internal alkenes catalysed by first row transition metals such as iron,⁹¹ nickel⁹² or cobalt^{88b,93} complexes, or even nickel nanoparticles⁹⁴ have recently been reported. In most of these cases, large metal loadings or dual catalyst systems were necessary to achieve good results. Moreover, the hydrosilylation of *trans*- or remote internal olefins require in most cases additives or harder reaction conditions. In 1970, Chalk reported the slow isomerisation and subsequent hydrosilylation of *cis*-2-pentene by Wilkinson's catalyst, to give the linear pentylsilane in a low conversion (20 %).⁹⁵ In this context, Chalk and Harrod⁹⁶ proposed the formation of a rhodium(III) hydrido-silyl complex by oxidative addition of the silane to the catalyst (Scheme 28). This silyl-hydride intermediate would be responsible for the isomerisation of the *cis*-2-pentene to 1-pentene, enabling the subsequent hydrosilylation of the terminal species to the pentylsilane product.

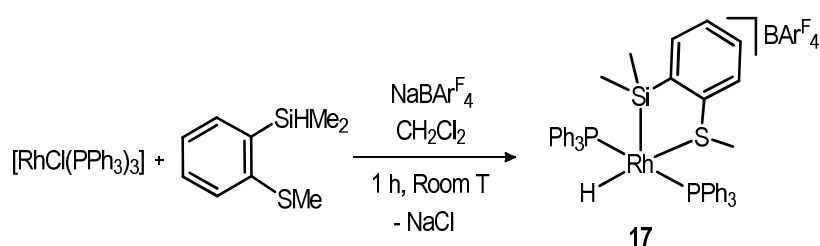


Scheme 28. Hydrosilylation of *cis*-2-pentene catalysed by $\text{RhCl}(\text{PPh}_3)_3$.

Considering these precedents, we thought it interesting to study the activity of Wilkinson's catalyst for dehydrocoupling of our silane ligands and also the catalytic activity of rhodium and iridium complexes derived from **L1** or **L2** and containing triphenylphosphine in dehydrocoupling of silanes and hydrosilylation of alkenes. Therefore various silyl-hydride rhodium and iridium compounds were synthesised from Wilkinson's catalyst $[\text{RhCl}(\text{PPh}_3)_3]$ and iridium dimer $[\text{Ir}(\text{cod})\text{Cl}]_2$, by oxidative addition of the Si-H bond in ligands **L1** and **L2**.

II. 1.3.1. Synthesis of rhodium and iridium catalysts

Earlier in this chapter, the synthesis of silyl-hydride complexes $[\text{RhCl}(\text{SiMe}(\text{o-C}_6\text{H}_4\text{SMe})_2)(\text{PPh}_3)]$ (**5**) and $[\text{RhH}(\text{SiMe}(\text{o-C}_6\text{H}_4\text{SMe})_2)(\text{PPh}_3)]\text{BAR}^{\text{F}}_4$ (**6**), derived from the oxidative addition of tridentate preligand **L2** to Wilkinson's catalyst $[\text{RhCl}(\text{PPh}_3)_3]$, has been described. The same route was followed with the bidentate preligand **L1**. Treatment of $[\text{RhCl}(\text{PPh}_3)_3]$ with one equivalent of **L1** and the equimolar amount of $\text{NaBAR}^{\text{F}}_4$ salt in dichloromethane at room temperature leads to the oxidative addition of the bidentate ligand and extraction of the chlorine, to yield the cationic complex $[\text{RhH}(\text{SiMe}_2(\text{o-C}_6\text{H}_4\text{SMe}))(\text{PPh}_3)_2]\text{BAR}^{\text{F}}_4$ (**17**) (Scheme 29). This unsaturated hydride compound was characterised by NMR spectroscopy and ESI-MS.



Scheme 29. Formation of unsaturated complex **17**.

The presence of the hydride is confirmed with a doublet of triplets at -9.65 ppm in the ^1H NMR spectrum ($J_{\text{Rh-H}} = 22.9$, $J_{\text{P-H}} = 13.5$ Hz) (Figure 27). Other two signals are observed at 2.02 and 0.21 ppm, with a relative integral of 3H and 6H, corresponding to the SMe and SiMe₂ moieties respectively. In the $^{31}\text{P}\{^1\text{H}\}$ spectrum, the two equivalent triphenylphosphine groups show a unique doublet signal at 44.4 ppm ($J_{\text{Rh-P}} = 118$ Hz). A ^1H - ^{29}Si HMQC experiment was also performed, in which a signal at 51.2 ppm proves the coordination of the silicon atom to the metal centre. This formulation is supported by ESI-MS with the presence of a molecular ion at $m/z = 809.15$, corresponding to the $[\text{Rh}(\text{H})(\text{SiMe}_2(\text{o-C}_6\text{H}_4\text{SMe}))(\text{PPh}_3)_2]^+$ fragment. Similarity of these spectroscopic data with the already described related complex $[\text{RhH}(\text{SiMe}(\text{o-C}_6\text{H}_4\text{SMe})_2)(\text{PPh}_3)]\text{BAR}^{\text{F}}_4$ (**6**), with terdentate **L2** ligand, suggests a square-pyramidal structure for **17**, with the strong σ -donor silyl fragment *trans* to the vacant coordination site.

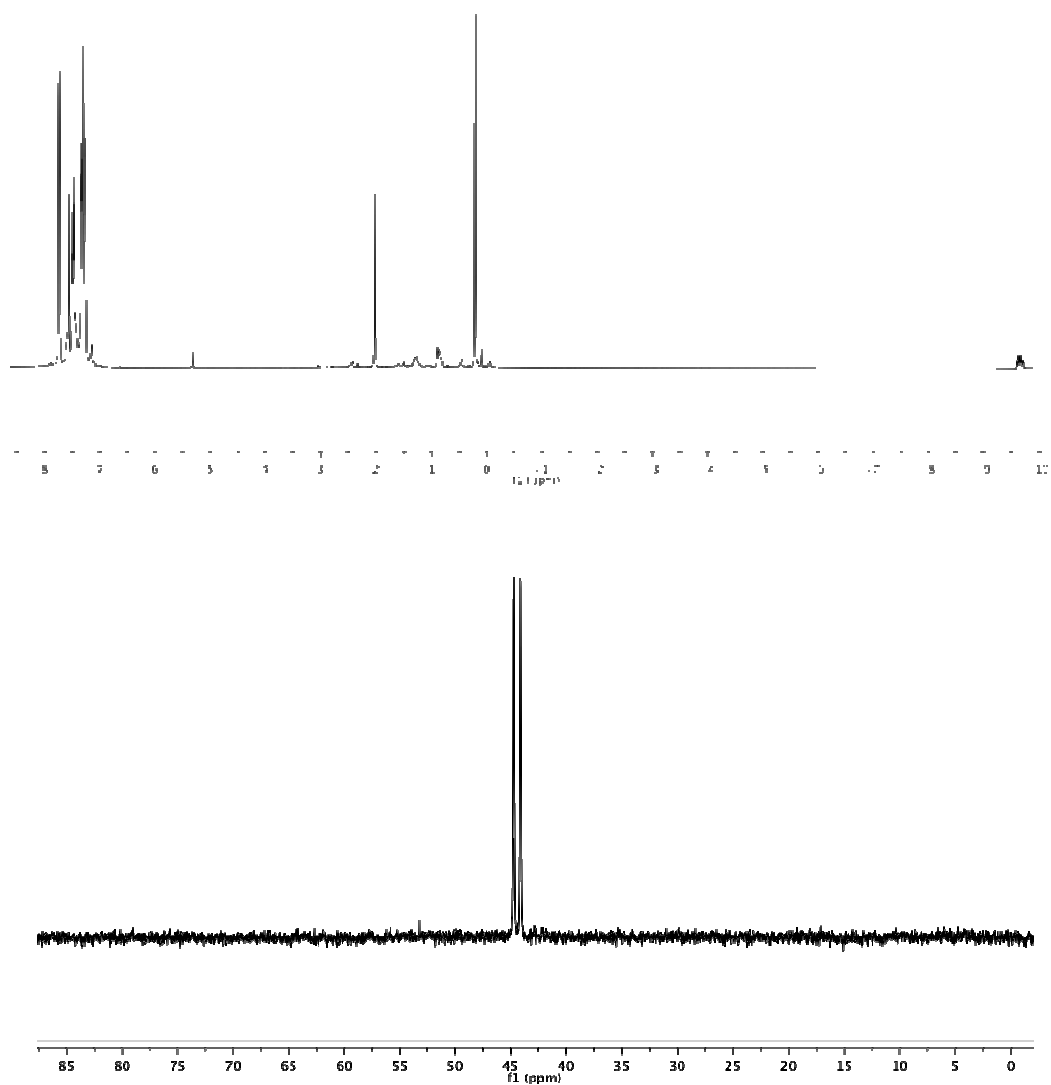
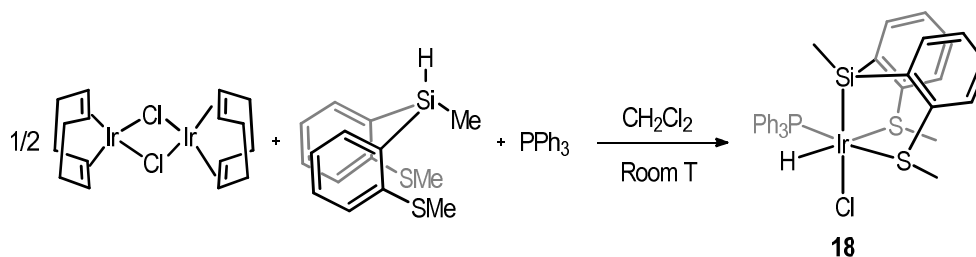


Figure 27. ^1H (top) and $^{31}\text{P}\{^1\text{H}\}$ (bottom) NMR spectra of complex **17** in CD_2Cl_2 .

Preparation of analogous silyl-hydride iridium(III) compounds with tridentate preligand **L2** was also attempted, with the aim of studying the influence of the metal centre in the catalytic processes. Treatment of $[\text{Ir}(\text{cod})\text{Cl}]_2$ dimer with two equivalents of **L2** and two equivalents of triphenylphosphine in dichloromethane allowed the decoordination of the olefin and the formation of the hydride neutral complex $[\text{IrClH}(\text{SiMe}(\text{o-C}_6\text{H}_4\text{SMe})_2)(\text{PPh}_3)]$ (**18**) (Scheme 30), *via* oxidative addition of the Si-H bond to the metal centre.



Scheme 30. Formation of silyl-hydride Ir(III) compound **18**.

The hydride ligand shows a doublet signal at -14.13 ppm in the ¹H NMR, with a coupling constant of 17.6 Hz. The methyl group in the silyl fragment shows a singlet signal at 0.07 ppm, and the presence of two different signals at 2.65 and 3.41 ppm, corresponding to the SMe moieties, indicate the non-equivalence of these units in solution. The coordination of the triphenylphosphine ligand to the Ir(III) centre is evidenced in the ³¹P{¹H} spectrum with a singlet signal at 13.3 ppm. Characterisation by X-Ray diffraction was also possible by isolation of single crystals from a dichloromethane solution layered with pentane. The structure of **18** in the solid state (represented in Figure 28) is in good agreement with the structure deduced from NMR data in solution.

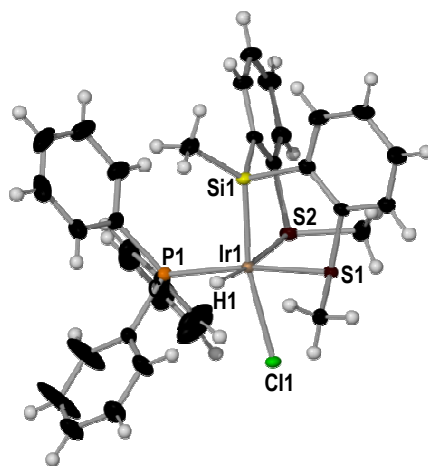
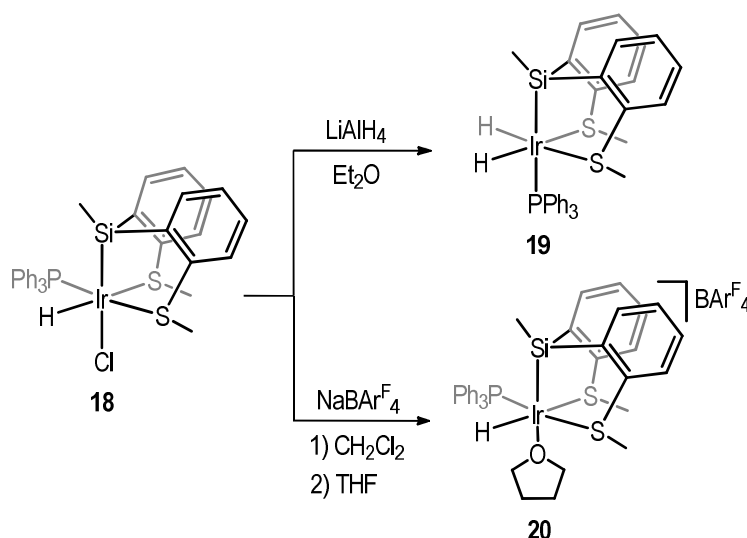


Figure 28. Molecular structure of compound **18** in the solid state. Displacement ellipsoids are drawn at 50% probability level. Selected bond lengths (Å) and angles (°): Ir1-Si1 2.2960(8), Ir1-S1 2.3551(9), Ir1-S2 2.4184(7), Ir1-P1 2.2790(9), Ir1-Cl1 2.5334(7), Ir1-H1 1.59(4), P1-Ir1-Si1 99.04(3), Si1-Ir1-Cl1 168.09(3), Si1-Ir1-S1 86.66(3), Si1-Ir1-S2 86.46(3), P1-Ir1-S2 93.63(3).

The geometry of **18** around the Ir(III) metal centre is pseudo-octahedral. The pincer silyl-thioether ligand occupies one of the octahedron faces, and is bonded to the metal centre through the silicon atom in the silyl fragment (Si1-Ir1 2.2952(11) Å) and the two SMe units (S1-Ir1 2.3547(10) Å and S2-Ir1 2.4188(10) Å). The difference in the Ir-S distances evidences

the stronger *trans* influence of the hydride compared to the phosphorus in the triphenylphosphine ligand, located in the remaining equatorial positions. The chloride ligand is located *trans* to the silyl group, with an Ir(III)-Cl bond distance of 2.5330(10) Å similar to that observed for complex **7**.

With the purpose of exchanging the chloride by another hydride ligand, compound **18** was treated with LiAlH₄, in diethyl ether at room temperature. This reaction yielded neutral dihydride complex [Ir(H)₂(SiMe(*o*-C₆H₄SMe)₂)(PPh₃)] (**19**), represented in Scheme 31. On the other hand, removal of the chlorine ligand by treatment with the NaBAR₄^F salt led to a coordinative vacancy, to yield the cationic compound [IrH(SiMe(*o*-C₆H₄SMe)₂)(PPh₃)]BAR₄^F, equivalent to the unsaturated rhodium(III) complex **6**. However, unlike the Rh(III) analogue, this Ir(III) compound was unstable in solution, and thus was easily degraded. Therefore, saturation of the complex by coordination of a tetrahydrofuran (THF) solvent molecule was attempted. Addition of NaBAR₄^F to compound **18** was done in dichloromethane, and subsequent removal of CH₂Cl₂ and dissolution in THF caused the coordination of a solvent molecule as a labile ligand, and allowed the formation of the cationic compound [IrH(SiMe(*o*-C₆H₄SMe)₂)(PPh₃)(THF)]BAR₄^F (**20**) (Scheme 31), stable in solution.



Scheme 31. Formation of dihydride neutral complex **19** and cationic compound **20** from **18**.

Characterisation of compound **19** was performed in solution by NMR spectroscopy and in solid state by X-ray diffraction. This complex showed a doublet signal at -15.44 ppm in the ¹H NMR spectrum corresponding to the two equivalent hydride ligands, with a coupling constant of J_{P-H} = 14.2 Hz. The SMe moieties, also equivalent in solution, present a singlet signal at 2.15 ppm,

and the SiMe group shows a singlet at 1.09 ppm. The presence of the triphenylphosphine is confirmed by the $^{31}\text{P}\{^1\text{H}\}$ NMR spectrum with a signal at 13.6 ppm.

Isolation of a single crystal of **19** allowed the determination of the structure in the solid state (Figure 29). The geometry disposed around the Ir(III) centre is pseudo octahedral. The $\text{SiMe}(o\text{-C}_6\text{H}_4\text{SMe})_2^-$ unit is located on one of the octahedron faces, coordinated through silicon (Si1–Ir1 2.3156(12) Å) and the two sulphur atoms (S1–Ir1 2.3788(11) Å and S2–Ir1 2.3750(11) Å). The two hydride ligands are located *trans* to the thioether moieties, while the triphenylphosphine is now occupying the *trans* position to the silyl fragment (P1–Ir1 2.3438(11) Å). This disposition could be explained by the strong *trans* influence of the hydride and silyl groups.⁴³

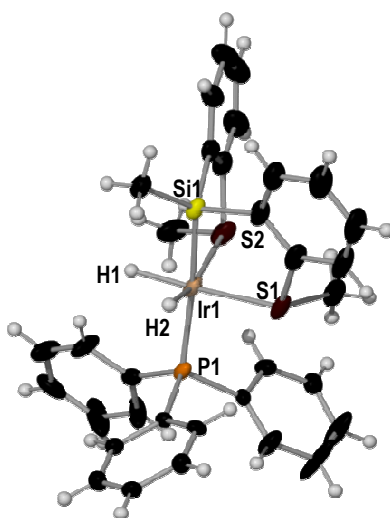


Figure 29. Molecular structure of compound **19** in the solid state. Displacement ellipsoids are drawn at 50% probability level. Selected bond lengths (Å) and angles ($^\circ$): Ir1–Si1 2.3156(12), Ir1–S1 2.3788(11), Ir1–S2 2.3750(11), Ir1–P1 2.3438(12), Ir1–H1 1.59(5), Ir1–H2 1.46(6); Si1–Ir1–P1 172.95(4), Si1–Ir1–S2 86.26(4), S1–Ir1–S2 96.19(4), Si1–Ir1–S1 86.72(4), H1–Ir1–S2 91.0(17).

Characterisation of cationic compound **20** was otherwise done by NMR spectroscopy and ESI-MS. The ^1H NMR spectrum (Figure 30) showed a doublet signal at -14.25 ppm ($J_{\text{P-H}} = 14.8$ Hz) corresponding to the hydride ligand. Singlet signals with relative integrals of 3 H at 3.30, 2.60 and -0.06 ppm correspond to the non-equivalent SMe moieties and the SiMe unit respectively. The two signals at 3.57 and 1.70 ppm in the spectra can be assigned to the coordinated tetrahydrofuran molecule. The proposed structure is supported by ESI-MS with a molecular ion at $m/z = 745.12$, which coincides with the $[\text{IrH}(\text{SiMe}(o\text{-C}_6\text{H}_4\text{SMe})_2)(\text{PPh}_3)]^+$ fragment, after loss of the THF ligand.

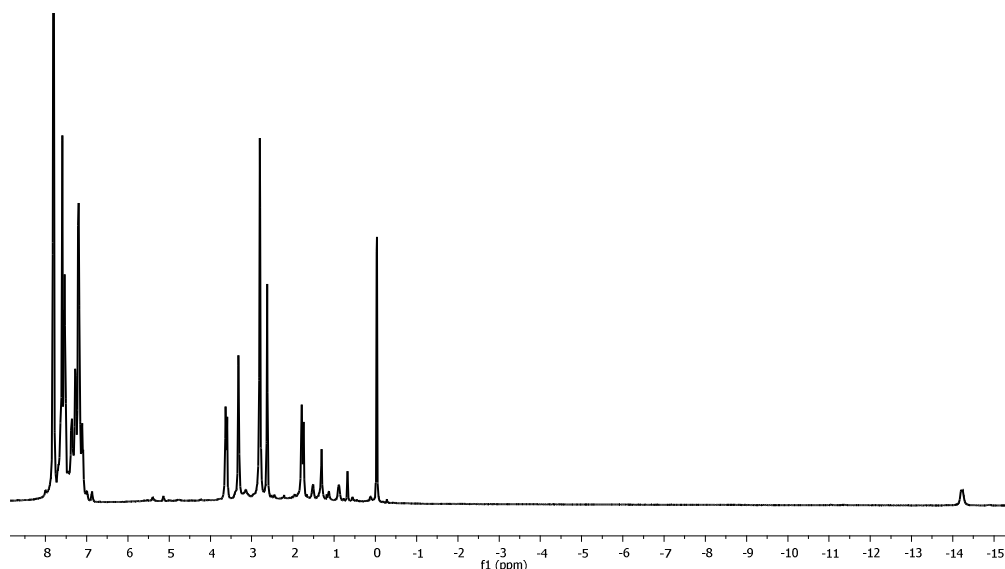
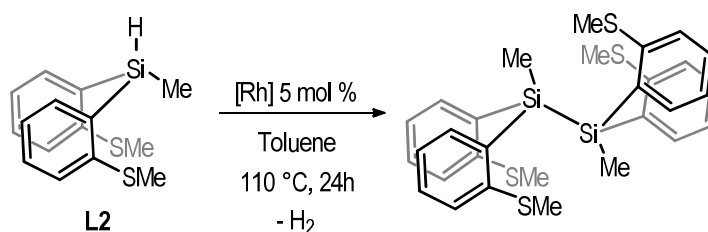


Figure 30. ^1H NMR spectra of complex **20** in THF-d_8 .

II. 1.3.2. Dehydrogenative coupling of **L2** using Wilkinson's catalyst

The tridentate preligand $\text{HSiMe}(o\text{-C}_6\text{H}_4\text{SMe})_2$ (**L2**) was used as a silane substrate for the dehydrogenative coupling reaction. Initially, Wilkinson's complex $[\text{RhCl}(\text{PPh}_3)_3]$ was used as the catalyst for this process. The tertiary silane **L2** was dissolved in 1 mL of toluene at $110\text{ }^\circ\text{C}$ with a catalytic amount of $[\text{RhCl}(\text{PPh}_3)_3]$ (5 mol %). The formation of the dehydrocoupling product, $(o\text{-C}_6\text{H}_4\text{SMe})_2\text{MeSi-SiMe}(o\text{-C}_6\text{H}_4\text{SMe})_2$, was quantitatively determined by NMR spectroscopy after 24 hours of reaction (Scheme 32).



Scheme 32. Formation of the disilane by dehydrogenative coupling catalysed by $[\text{RhCl}(\text{PPh}_3)_3]$.

The formation of the disilane can be confirmed by ^1H NMR. The spectroscopic data show the signals for the two SiMe groups and four SMe moieties at 1.29 and 2.51 ppm respectively. In the ^{19}Si NMR spectrum, the disilane exhibits a multiplet at -31.0 ppm ($J_{\text{H-Si}} = 7\text{ Hz}$), in a similar position to that showed by the **L2** monosilane ($\delta = -31.1\text{ ppm}$, $J_{\text{H-Si}} = 202\text{ Hz}$, $J_{\text{H-Si}} = 7\text{ Hz}$). The lack of a $J_{\text{H-Si}}$ coupling constant in the ^{19}Si NMR spectrum for the disilane product indicates the absence of a Si-H bond (Figure 31). The ESI-MS of the disilane shows a molecular ion at 579.16 m/z , corresponding to the $[\text{Disilane} + \text{-H}^+]^\pm$ fragment. The IR spectrum of the product excludes

the formation of the disiloxane product $(o\text{-C}_6\text{H}_4\text{SMe})_2\text{MeSi-O-SiMe}(o\text{-C}_6\text{H}_4\text{SMe})_2$, as the characteristic $\nu(\text{SiO})$ band around 1000 cm^{-1} is not observed. Observation of disiloxanes as products or side products in dehydrogenative coupling of silanes is relatively common.⁹⁷

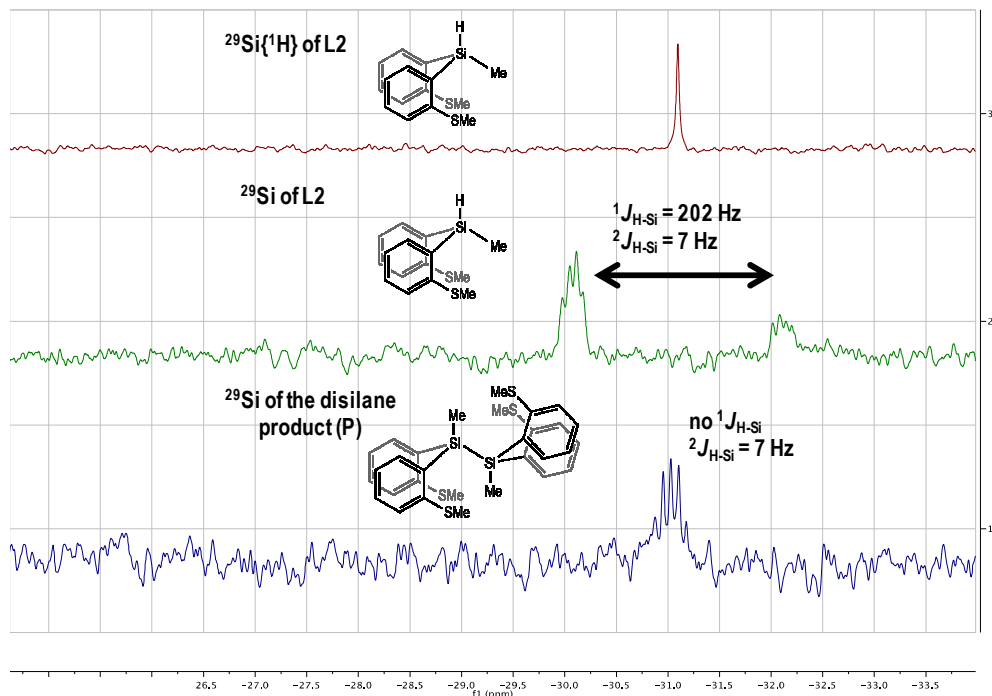


Figure 31. Comparison of ^{29}Si NMR spectra of **L2** and the disilane product.

Monitoring of the catalytic reaction by NMR spectroscopy allowed the identification of intermediate organometallic species. The reaction was stopped after 16 hours in solution, and the organic phase containing the disilane product was separated by extraction with pentane. The ^1H NMR spectrum of the organic phase showed a mixture of the **L2** substrate and the disilane product in a 75 % of conversion. The organometallic phase revealed the presence of the neutral $[\text{RhCl}(\text{SiMe}(o\text{-C}_6\text{H}_4\text{SMe})_2)(\text{PPh}_3)]$ (**5**) complex, already described in this work, along with other unidentified species in a minor proportion (Figure 32). It is known that complex **5** is synthesised by oxidative addition of the tertiary **L2** silane to the rhodium(I) centre of the $[\text{RhCl}(\text{PPh}_3)_3]$ complex. This fact suggests the involvement of a Si-H activation step in the reaction mechanism.

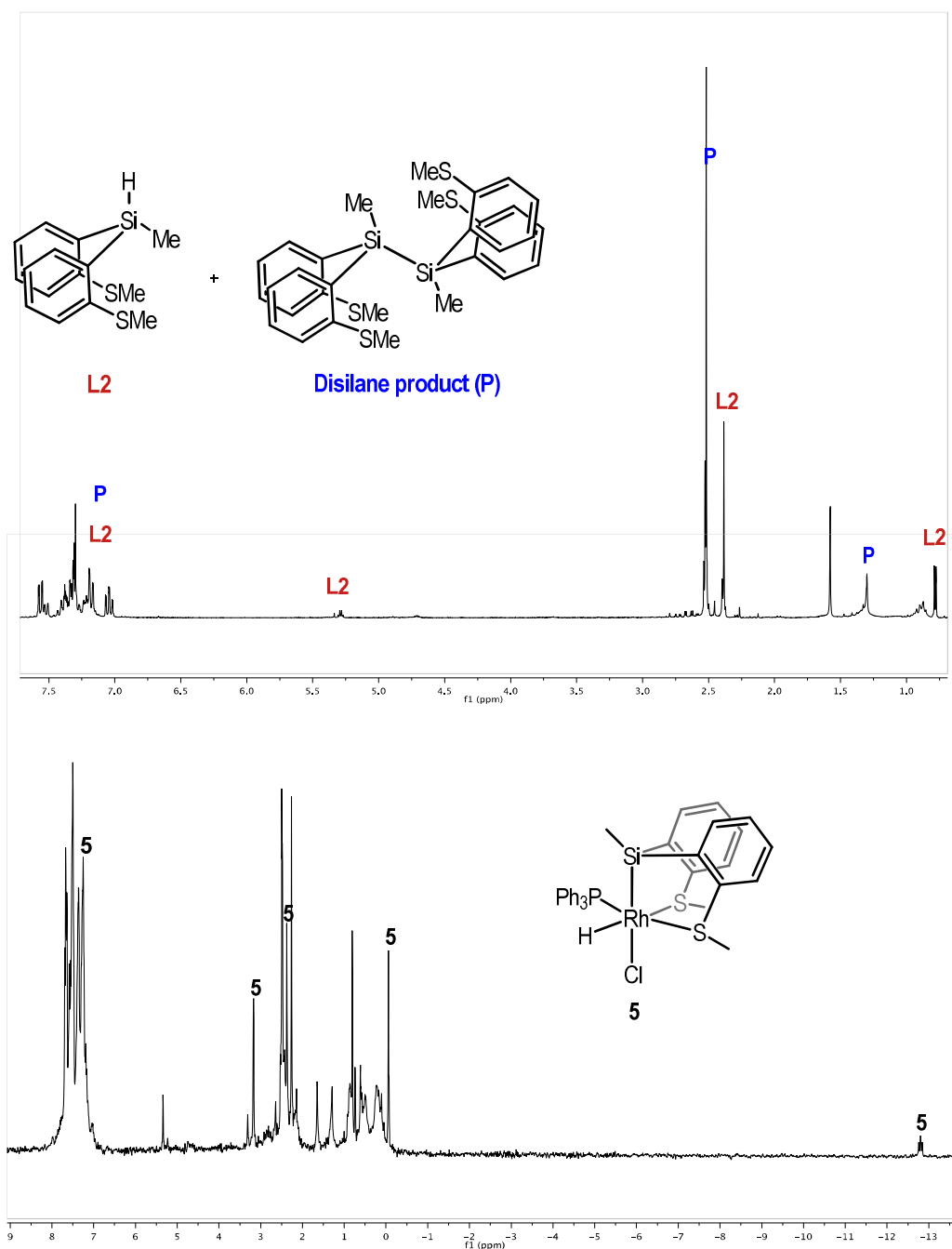
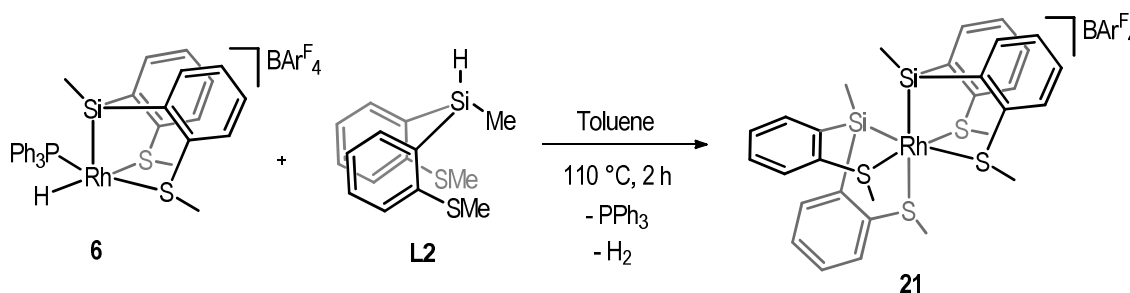


Figure 32. ¹H NMR spectra of the organic (top) and organometallic (bottom) phases after 16 hours of catalysis with [RhCl(PPh₃)₃].

Therefore, we decided to evaluate this silyl-hydride rhodium(III) complex **5** as a catalyst for the dehydrocoupling of tertiary silane **L2**. The performance of the unsaturated rhodium(III) compound [RhH(SiMe(*o*-C₆H₄SMe)₂)(PPh₃)]BAR₄^F (**6**) was also tested, with the purpose of studying the effect of a coordinative vacancy in the catalytic activity of the complex. The results obtained with these two rhodium(III) complexes were compared to the activity exhibited by Wilkinson's catalyst under the same catalytic conditions. Table 1 shows the collection of these results. As a control reaction, a solution of **L2** in toluene was heated at 110 °C in the absence of a catalyst, and silane coupling products were not observed (Table 1, entry 1).

When using Wilkinson's catalyst (Table 1, entry 2), a 95 % of conversion was reached. The use of neutral compound **5** as a catalyst for the dehydrogenative coupling of **L2** afforded similar results, with a conversion of >99 % (Table 1, entry 3). With cationic compound **6**, however, a decrease in the catalytic activity was observed, reaching only a 60 % of conversion (Table 1, entry 4). This reduction could indicate a deactivation of the catalyst when the rhodium complex is unsaturated. To give insight into the possible deactivation mechanism, rhodium(III) complexes **5** and **6** were treated with **L2** in an equimolecular reaction.

Unsaturated compound **6** reacts with an equivalent of **L2** in toluene at 110 °C for 2 hours, to yield the stable rhodium(III) compound $[\text{Rh}(\text{SiMe}(\text{o-C}_6\text{H}_4\text{SMe})_2)_2]\text{BAR}^{\text{F}_4}$ (**21**), with two units of the tertiary silane derived from **L2** coordinated as a tridentate ligand, with the loss of dihydrogen and PPh_3 (Scheme 33). The disilyl-rhodium(III) species **21** showed no activity as a catalyst for the dehydrocoupling of **L2** (Table 1, entry 5). The formation of this inactive species would consequently be the cause of the decrease in the catalytic activity of compound **6**. The reaction of neutral complex **5** with an extra equivalent of **L2** failed to afford **21**.



Scheme 33. Formation of compound **21**.

Cationic complex **21** was characterised in solution by NMR spectroscopy and ESI-MS. The two $[\text{SiMe}(\text{o-C}_6\text{H}_4\text{SMe})_2]^-$ units are equivalent in solution, and showed three singlet signals in the ^1H NMR spectrum at 0.27, 2.46 and 2.90 ppm, with a relative integral of 6H, corresponding to the two SiMe and the four SMe groups. The presence of a molecular ion at $m/z = 681.01$ in the ESI-MS corresponds to the $[\text{Rh}(\text{SiMe}(\text{o-C}_6\text{H}_4\text{SMe})_2)_2]^+$ fragment.

Isolation of single crystals of **21** allowed the determination of the solid state structure by X-Ray diffraction. Although the low quality of the data did not permit the discussion of bond distances and angles, the disposition of the ligands and the geometry adopted around the metal centre can be analysed and confirm the proposed structure (Supporting Information). The geometry around the Rh(III) centre is pseudo octahedral, with the two tridentate ligand

units coordinated through the silicon and sulphur atoms, each with a facial disposition. The two silicon atoms are located mutually *cis*.

To prove the importance of the additional donor functions exhibited by the **L2** hydrosilane in the catalysis, an alkyl tertiary hydrosilane without an additional functional group was also tested as substrate under the same reaction conditions. Entries 6 and 7 in Table 1 show treatment of Et₃SiH with [RhCl(PPh₃)₃] and complex **5** respectively, which resulted in no conversion to the disilane product.

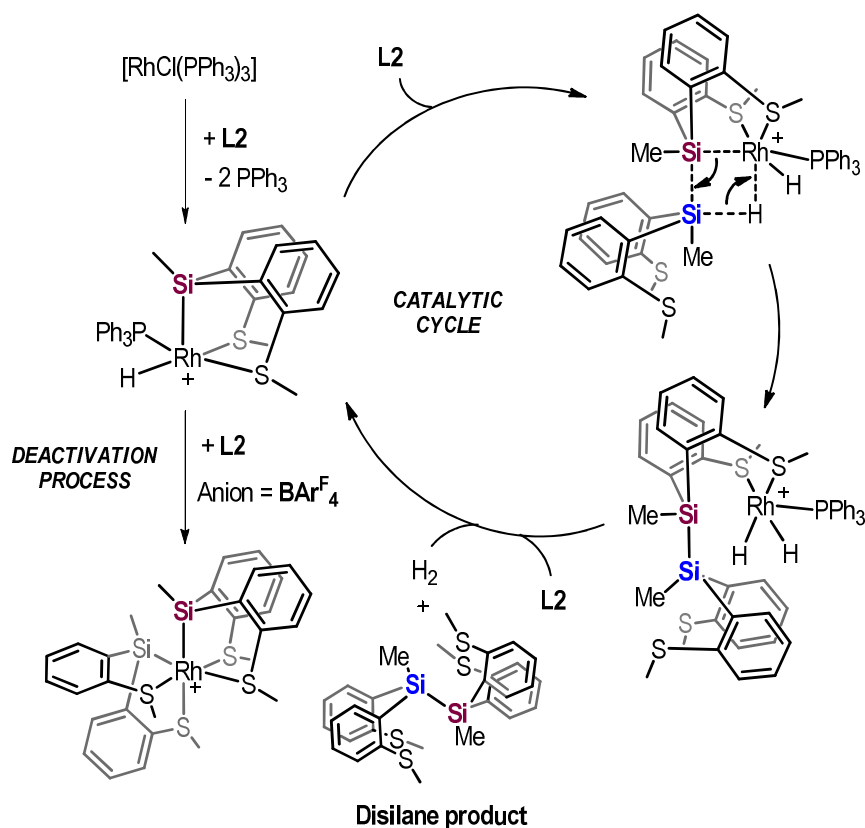
Table 1. Rhodium catalysed dehydrocoupling of silanes.

Entry	[Rh] Catalyst	Substrate ^[a]	Conversion to disilane [%] ^[b]
1	-	L2	0
2	[RhCl(PPh ₃) ₃]	L2	95
3	5	L2	>99
4	6	L2	60
5	21	L2	0
6	[RhCl(PPh ₃) ₃]	Et ₃ SiH	0
7	5	Et ₃ SiH	0

[a] Catalytic conditions: Silane substrate (0.1 mmol), [Rh] catalyst (0.005 mmol) in 1 mL of toluene at 110 °C for 24 h. [b] Conversions were determined by ¹H RMN spectroscopy.

On the basis of these results, a simplified mechanism and a deactivation process for the rhodium catalysed dehydrocoupling of **L2** has been proposed. Addition of the **L2** substrate to [RhCl(PPh₃)₃] allows the Si-H activation of the silane, leading to the formation of silyl-hydride compound **5** by chelate assisted oxidative addition. Compound **5** can be considered to be the active species in the catalysis. In a second step, we propose a σ -bond metathesis route after the formation of **5**, with the involvement of a four-centre transition state that would allow the formation of the Si-Si bond.⁹⁸ The presence of the chloride ligand in the saturated complex would prevent formation of the inactive species **21** *via* a second Si-H activation and the

subsequent inhibition of the disilane product formation by reductive elimination under these catalytic conditions.⁹⁹ Finally, the reaction of a new molecule of **L2** with the dihydride-Rh(III) compound resulting in the previous step would result in the regeneration of the catalytic species **5**. Unsaturated compound **6** would follow the same σ -bond metathesis pathway for the formation of the disilane product, but the reaction of **6** with a second **L2** molecule would result into the inactive species **21** (Scheme 34).



Scheme 34. Proposed mechanism for the disilane product formation and deactivation process.

II. 1.3.3. Tandem isomerisation-hydrosilylation of alkenes

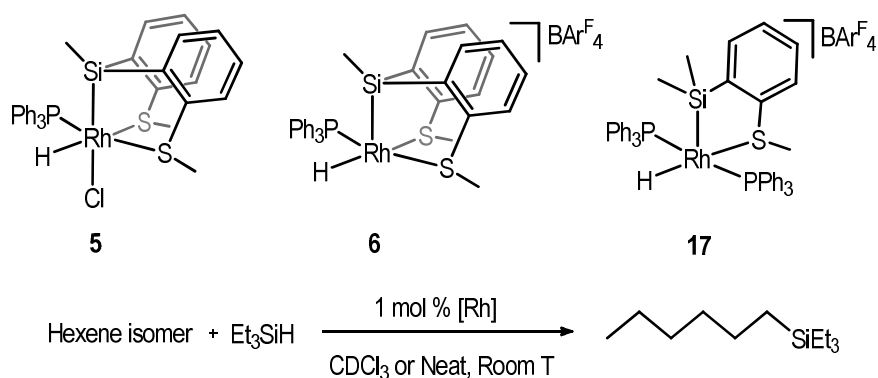
II. 1.3.3a. Rhodium-catalysed alkene tandem isomerisation-hydrosilylation

As it was commented at the beginning of this chapter, in 1970 Chalk reported the tandem isomerisation-hydrosilylation of *cis*-2-pentene to yield the pentylsilane, catalysed by Wilkinson's catalyst.⁹⁵ The formation of a silyl-hydride-rhodium(III) intermediate by oxidative addition of the substrate to the catalyst was also described. In this report, Chalk proposed this intermediate as responsible for the isomerisation of the internal alkene to the terminal species. For this reason, we thought the silyl-hydride rhodium(III) compounds, derived from

the oxidative addition of **L1** or **L2** to $[\text{RhCl}(\text{PPh}_3)_3]$, would serve as active catalysts for the tandem process of isomerisation of an internal olefin to the terminal one, and the subsequent hydrosilylation to form linear alkylsilanes. The compounds tested for this process were $[\text{RhH}(\text{SiMe}_2(o\text{-C}_6\text{H}_4\text{SMe}))(\text{PPh}_3)_2]\text{BAr}^{\text{F}}_4$ (**17**), $[\text{RhH}(\text{SiMe}(o\text{-C}_6\text{H}_4\text{SMe})_2)\text{Cl}(\text{PPh}_3)]$ (**5**) and $[\text{RhH}(\text{SiMe}(o\text{-C}_6\text{H}_4\text{SMe})_2)(\text{PPh}_3)]\text{BAr}^{\text{F}}_4$ (**6**). Their catalytic performance was compared to the activity shown by Wilkinson's catalyst under the same reaction conditions.

A first set of experiments was performed with various pre-dried hexene isomers (1-hexene, *trans*-2-hexene, *trans*-3-hexene and *cis*-2-hexene) and Et_3SiH as substrates, adding 1 mol % of the corresponding rhodium precatalyst. The reactions were carried out in 0.5 mL of CDCl_3 , at room temperature, and under an atmosphere of N_2 . Products were analysed by NMR spectroscopy. The conversion was calculated by ^1H NMR from the reaction crude without any previous treatment. Finally, the mixture was filtered over silica to remove the metal catalyst, and removal of the solvent and the alkene remaining by vacuum allowed the determination of the reaction selectivity. These results are collected in Table 2.

Table 2. Rhodium catalysed tandem isomerisation-hydrosilylation of hexene isomers with Et₃SiH.



Entry ^[a]	Hexene isomer	[Rh] Catalyst	Solvent	Time (h)	Conversion ^[b] (Select.) ^[c] [%]
1	Trans-2-	[RhCl(PPh ₃) ₃]	CDCl ₃	12	0
2	Trans-2-	5	CDCl ₃	12	0
3	Trans-2-	6	CDCl ₃	12	70 (>99)
4	Trans-2-	17	CDCl ₃	12	70 (>99)
5	1-	17	CDCl ₃	4	90 (>99)
6	Cis-2-	17	CDCl ₃	12	70 (>99)
7	Trans-3-	17	CDCl ₃	12	55 (>99)
8	1-	17	Neat	4	99 (>99)
9	Trans-2-	17	Neat	12	97 (>99)
10	Cis-2-	17	Neat	12	98 (>99)
11	Trans-3-	17	Neat	12	92 (>99)

[a] Catalytic conditions: Hexene isomer (0.25 mmol), Et₃SiH (0.25 mmol), 1 % mol [Rh] catalyst (0.002 mmol) in 0.5 mL of CDCl₃, or solvent-free at room temperature. [b] Conversions were determined by ¹H RMN spectroscopy, by alkene remaining. [c] Linear selectivity was determined by ¹H RMN. In all cases, (Et₃Si)₂O appears as a byproduct.

The mixture of *trans*-2-hexene with Et₃SiH in CDCl₃ in the presence of [RhCl(PPh₃)₃], or neutral complex **5**, gave no conversion to the hydrosilylated product (Table 2, entries 1 and 2). By contrast, unsaturated cationic complexes **6** and **17** efficiently catalysed the hydrosilylation of *trans*-2-hexene under the same reaction conditions, to give the anti-Markovnikov hexyltriethylsilane product selectively (Table 2, entries 3 and 4).

Complex **17** was then used to catalyse the hydrosilylation of other hexene isomers with Et₃SiH. In all cases, the hexylsilane product was obtained as the only hydrosilylation product. Entries 4 to 7 in Table 2 show the catalysis of hexene isomers with **17** in CDCl₃ as a solvent. The ¹H NMR spectra of the reaction crude showed a total disappearance of the initial hydrosilane, even though a percentage of remaining alkene was still observed. The fraction of the hydrosilane which was not added to the alkene to form the hydrosilylated product was converted into the disiloxane byproduct (Et₃Si)₂O.¹⁰⁰ A solution of Et₃SiH with 1 mol % of compound **17** in CDCl₃ in absence of alkene was monitored by ¹H NMR in an attempt of explaining the formation of disiloxane in the previous reactions (Figure 33). The spectrum showed the formation of a small amount of the chlorosilane species Et₃SiCl (Scheme 35),¹⁰¹ which increased with longer reaction times. The formed chlorosilane is then transformed into (Et₃Si)₂O by the atmospheric moisture.¹⁰²

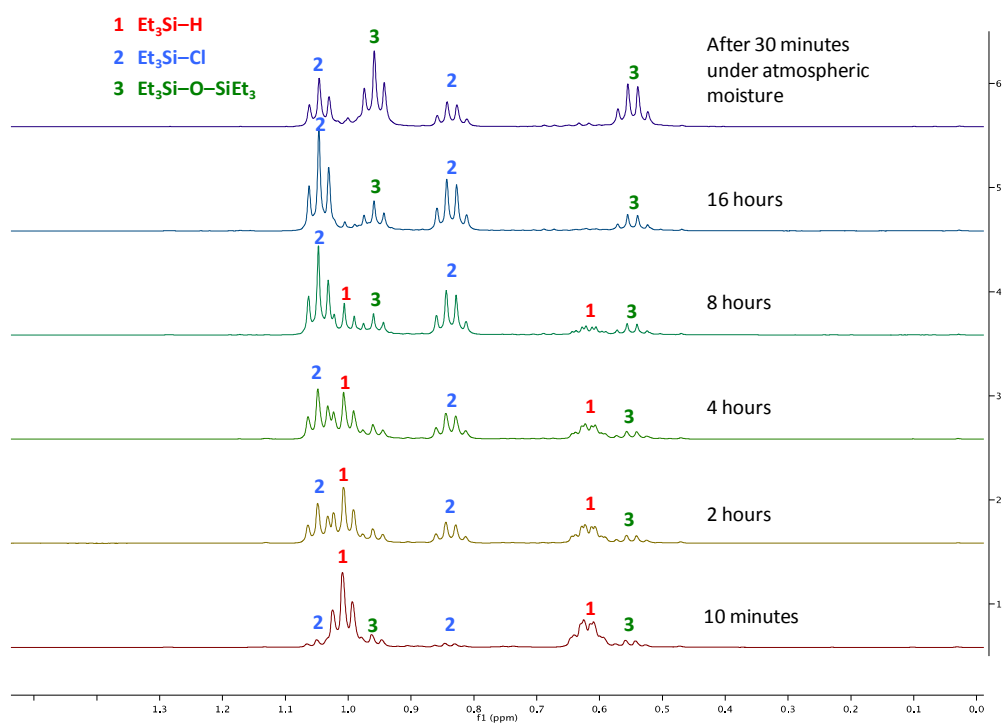
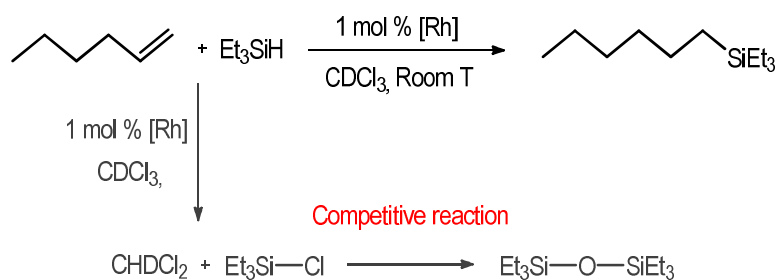


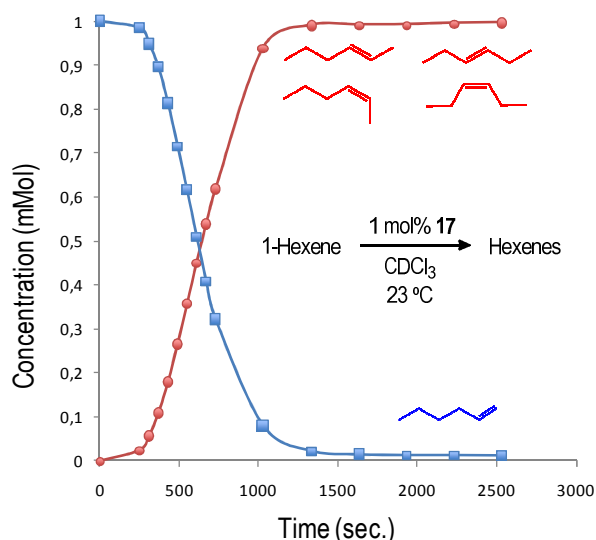
Figure 33. The chlorination reaction of Et₃SiH in CDCl₃ promoted by **17**.



Scheme 35. Hydroosilylation of 1-hexene and competitive formation of the disiloxane.

Conversions of these experiments in CDCl_3 varied from 55 % for the *trans*-3-hexene, to 90 % for the 1-hexene isomer. In the case of 1-hexene (Table 2, entry 5), this conversion was reached in only 4 hours of reaction. Other hexanes required longer reaction times (Table 2, entries 4, 6 and 7), but all reactions were completed in 12 hours. Longer reaction times led to a higher amount of the disiloxane side product, resulting into poorer conversions. In order to avoid this competitive reaction derived from the use of chloroform, experiments catalysed by compound **17** were performed without added solvent (Table, entries 8 to 11). These reactions reached almost complete conversion, and led to the formation of the hexylsilane product selectively.

On the basis of these initial results, the faster hydroosilylation of 1-hexene compared to other internal isomers suggests a tandem process in which an isomerisation reaction is followed by a selective faster hydroosilylation of the terminal alkene. With the purpose of studying the isomerisation process catalysed by the silyl-hydride complex **17**, a solution of 1-hexene in CDCl_3 with 1 mol % of **17** was monitored by ^1H NMR. This solution was prepared in a sealed NMR tube at room temperature. After 45 minutes, the isomerisation reached an equilibrium, in which a mixture of hexene isomers was observed. This isomerisation is shown in Figure 34, along with the alkene ratio in the equilibrium. After completion of the reaction, although the thermodynamically more stable¹⁰³ *trans* species reached a 73 % of the hexene isomer mixture, significant amounts of *cis* species and 1-hexene are also observed.



DISTRIBUTION OF HEXENE ISOMERS

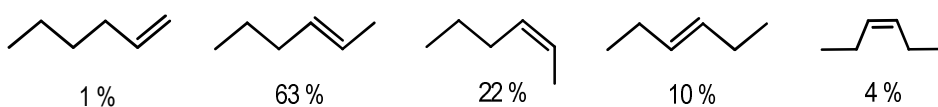


Figure 34. ^1H NMR monitored isomerisation of 1-hexene and distribution of isomers.

The same experiment was carried out with other hexene isomers in the presence of **17**. After 24 hours, the presence of the 1-hexene isomer is observable in all isomer mixtures in equilibrium (Figure 35). This is important considering that 1-hexene is the only active isomer for the hydrosilylation reaction.

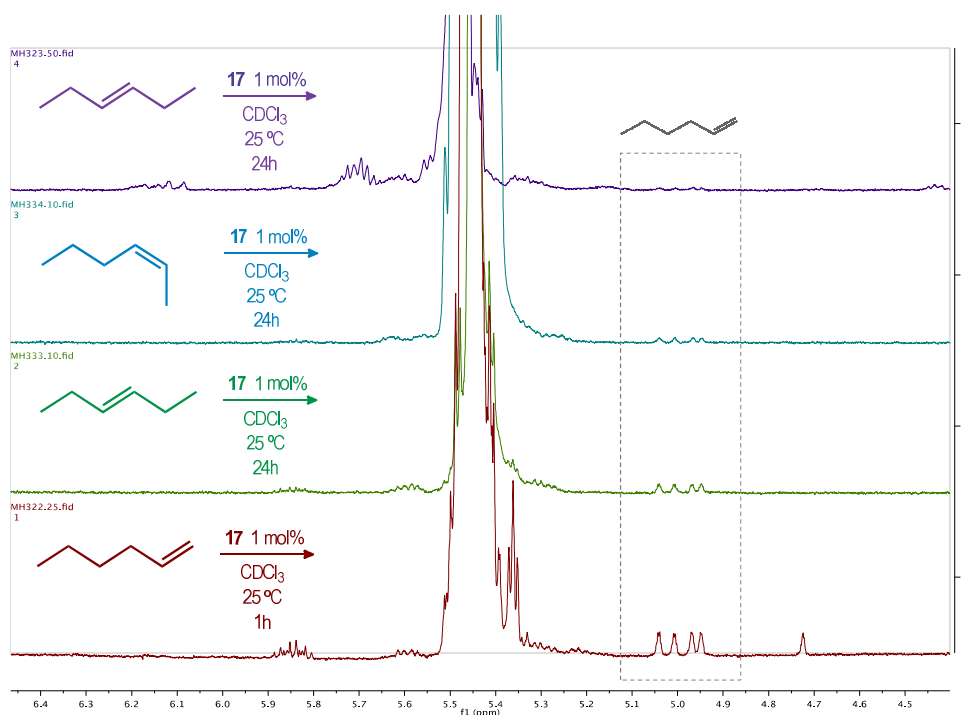
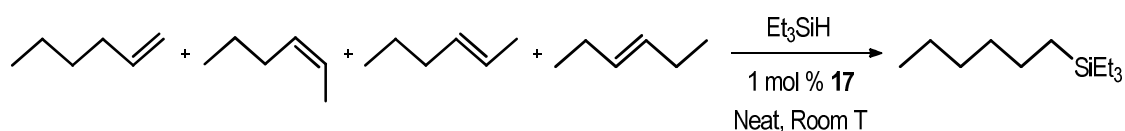


Figure 35. ^1H NMR of the isomerisation of various hexene isomers after 24 hours.

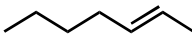

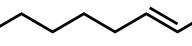
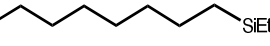
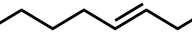
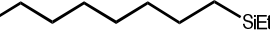
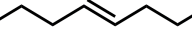
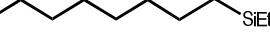
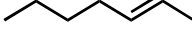

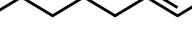
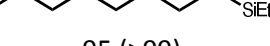
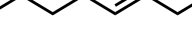
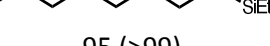

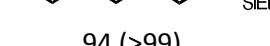
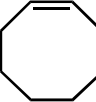
The high activity shown by the silyl-hydrido-Rh(III) compound **17** in the catalysis of the hexene isomerisation and hydrosilylation encouraged the extension of the study to other internal olefins. Table 3 collects the results of the reaction of these olefins with Et₃SiH catalysed by 1 mol % of **17**. The initial isomerisation-hydrosilylation reactions of *trans*-2-heptene (Table 3, entry 1) and *trans*-2, *trans*-3 and *trans*-4-octenes (Table 3, entries 2 to 4) were performed in CDCl₃ as a solvent, yielding the linear anti-Markovnikov product selectively with conversion rates between 44 and 55 %, due to the formation of disiloxane (Et₃Si)₂O as a byproduct. These reactions were repeated in neat olefin (Table 3, entries 5 to 8), based on the good results achieved in the solvent-free experiments with hexene isomers. For *trans*-2-heptene (Table 3, entry 5), this reaction gave the linear heptylsilane as the only hydrosilylation product, with an improved conversion of 94 %. Octene isomers also gave the octyltriethylsilane product selectively with an excellent conversion of 94-95 %, including the remote isomer *trans*-4-octene (Table 3, entry 8). Finally, the reaction of Et₃SiH with a cyclic olefin such as cyclooctene (Table 3, entry 9) gave no reaction, which evidences that internal olefins are not internally hydrosilylated.¹⁰⁴

An additional experiment was carried out to confirm this system being capable of the hydrosilylation of a mixture of various isomers to obtain a single product. This reaction consisted in the addition of 0.3 mmol of 1-hexene, 0.3 mmol of *cis*-2-hexene, 0.3 mmol of *trans*-2-hexene and 0.3 mmol of *trans*-3-hexene to 1.2 mmol of Et₃SiH under the previous catalytic conditions of 1 mol % of **17**, solvent-free and at room temperature, and yielded the linear hexyltriethylsilane product selectively, in an almost complete conversion (Scheme 36).



Scheme 36. Hydrosilylation of a mixture of various hexene isomers with Et₃SiH catalysed by **17**.

Table 3. Tandem isomerisation-hydrosilylation of alkenes with Et₃SiH catalysed by **17**.

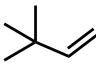
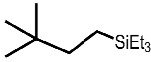
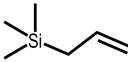
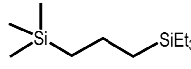
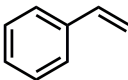
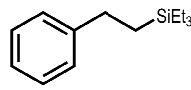
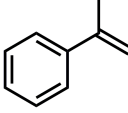
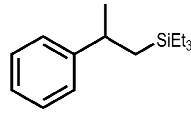
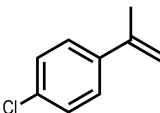
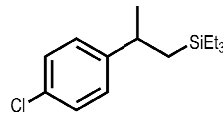
Entry ^[a]	Alkene	Solvent	Time (h)	Conversion ^[b] (Select.) ^[c] [%]
1		CDCl ₃	12	 55 (>99)
2		CDCl ₃	12	 56 (>99)
3		CDCl ₃	12	 45 (>99)
4		CDCl ₃	12	 43 (>99)
5		Neat	12	 94 (>99)
6		Neat	12	 95 (>99)
7		Neat	12	 95 (>99)
8		Neat	12	 94 (>99)
9		Neat or CDCl ₃	12	No reaction

[a] Catalytic conditions: Alkene (0.25 mmol), Et₃SiH (0.25 mmol), 1 % mol catalyst **17** (0.002 mmol) in 0.5 mL of CDCl₃, or solvent-free at room temperature, after 12 hours of reaction. [b] Conversions were determined by ¹H RMN spectroscopy, by alkene remaining. [c] Linear selectivity was determined by ¹H RMN.

To complete this study, the hydrosilylation of other non-linear alkenes was performed with **17** under the same reaction conditions. Table 4 shows these results. The hydrosilylation of *tert*-butylethylene (tbe) and allyltrimethylsilane led to the formation of anti-Markovnikov products (3,3-dimethylbutyl)triethylsilane and triethyl(3-(trimethylsilyl)propyl)silane (table 4, entries 1 and 2), with remarkable yields of 97 and 94 % respectively, after 4 hours of reaction. In the case of styrene (table 4, entry 3), a 48 % conversion of the initial substrate was reached in 4 hours, and a mixture of the hydrosilylated product triethyl(phenethyl)silane and the dehydrogenative silylation product triethyl(styryl)silane was obtained in a 76:24 ratio. The reaction of α -methylstyrene and 4-chloro- α -methylstyrene (Table 4, entries 4 and 5) with

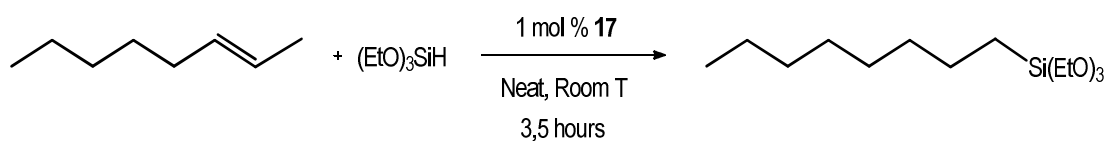
Et₃SiH, however, gave the hydrosilylation products selectively, with a 67 and 62 % of conversion.

Table 4. Tandem isomerisation-hydrosilylation of non-linear alkenes with Et₃SiH catalysed by **17**.

Entry ^[a]	Alkene	Solvent	Time (h)	Conversion ^[b] (Select.) ^[c] [%]
1		Neat	4	 97 (>99)
2		Neat	4	 94 (>99)
3		Neat	4	 48 (76)
4		Neat	4	 67 (>99)
5		Neat	4	 62 (>99)

[a] Catalytic conditions: Alkene (0.25 mmol), Et₃SiH (0.25 mmol), 1 % mol catalyst **17** (0.002 mmol), solvent-free at room temperature, after 4 hours of reaction. [b] Conversions were determined by ¹H RMN spectroscopy, by alkene remaining. [c] Linear selectivity was determined by ¹H RMN

A final experiment was performed to test the activity of silyl-hydrido-rhodium(III) complex **17** in the hydrosilylation of internal olefins using another tertiary silane. A reaction of 0.25 mmol of *trans*-2-octene with the equimolar amount of triethoxysilane (EtO)₃SiH allowed the quantitative formation of the hydrosilylated anti-Markovnikov product triethoxy(octyl)silane selectively, in only 3.5 hours of reaction (Scheme 37).

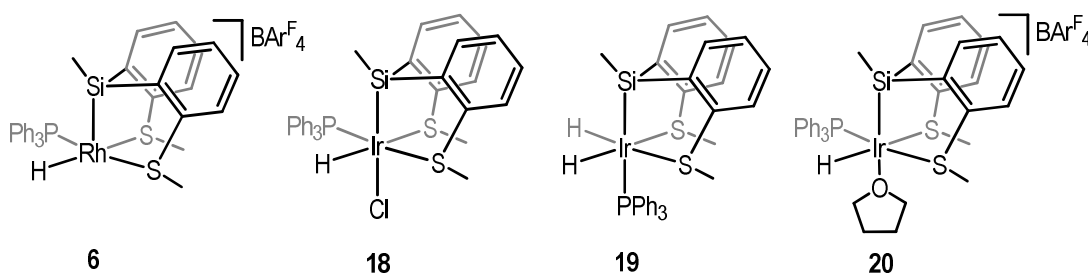


Scheme 37. Hydrosilylation of *trans*-2-octene with triethoxysilane catalysed by **17**.

II. 1.3.3b. Rhodium and iridium catalyzed alkene tandem isomerisation-hydrosilylation or dehydrogenative silylation

The high activity shown by cationic catalyst $[\text{RhH}(\text{SiMe}_2(o\text{-C}_6\text{H}_4\text{SMe}))(\text{PPh}_3)_2]\text{BAR}^{\text{F}}_4$ (**17**) in the tandem isomerisation-hydrosilylation reaction of internal olefins in a solvent-free system at room temperature, prompted the extension of this study using hydrido-silyl rhodium(III) or iridium(III) complexes derived from **L2** as precatalysts. Initial experiments (Table 4) were performed with an equimolar amount of pre-dried *trans*-2-octene and Et_3SiH , with a catalyst load of 1 mol %. The tested precatalysts included the cationic Rh(III) complex $[\text{RhH}(\text{SiMe}(o\text{-C}_6\text{H}_4\text{SMe}_2)(\text{PPh}_3)]\text{BAR}^{\text{F}}_4$ (**6**), the neutral silyl-hydride-chloride Ir(III) complex **18**, the neutral silyl-dihydride Ir(III) complex **19** and the cationic Ir(III) compound **20** (Scheme of Table 4). These experiments were carried out in neat alkene, at room temperature under an atmosphere of N_2 .

Table 4. Tandem isomerisation-hydrosilylation of *trans*-2-octene with Et_3SiH .

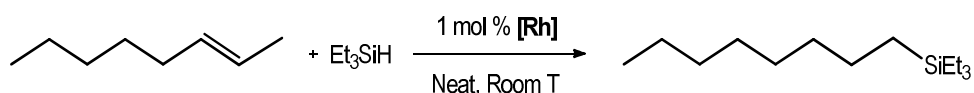


Entry ^[a]	Catalyst	Temperature (°C)	Conversion ^[b] (Select.) ^[c] [%]
1	6	Room T	80 (>99)
2	18	50	30
3	19	50	No reaction
4	20	50	72

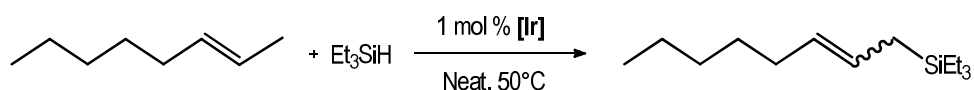
[a] Catalytic conditions: *Trans*-2-octene (0.25 mmol), Et_3SiH (0.25 mmol), 1 % mol [Rh] or [Ir] catalyst (0.002 mmol), solvent-free, after 12 hours of reaction. [b] Conversions were determined by ^1H RMN spectroscopy, by silane remaining. [c] Linear selectivity was determined by ^1H RMN.

Compound **6** was able to catalyse the reaction of *trans*-2-octene with Et₃SiH at room temperature (Table 4, entry 1), yielding an 80 % conversion to the hydrosilylated anti-Markovnikov product triethyl(octyl)silane selectively. However, the low or no activity exhibited by all iridium(III) precatalysts at room temperature led us to perform the hydrosilylation reactions at 50 °C. When heated at this temperature, reaction with analogue cationic Ir(III) compound **20** reached a 72 % conversion (Table 4, entry 4), but the observed main silylated product was the unsaturated allylic triethyl(2-octen-1-yl)silane, present in a 60 % amount. The main occurring process is therefore the catalytic dehydrogenative silylation reaction (Scheme 38). The variation on the nature of the metal centre would be the only factor to favour one of these competitive reactions, as the two catalysts are structurally analogous.

Isomerisation-hydrosilylation



Isomerisation-dehydrogenative silylation



Scheme 38. Tandem isomerisation-hydrosilylation (top) or dehydrogenative silylation (bottom) of *trans*-2-octene with Et₃SiH depending of the catalyst.

While cationic Rh(III) and Ir(III) compounds with the coordinative vacancy catalyse the silylation of *trans*-2-octene efficiently, neutral compounds show a poor catalytic activity in the same process. Chloride-Ir(III) complex **18** led to a 30 % conversion at 50 °C (Table 4, entry 2), yielding a mixture in which the dehydrogenative silylation product prevails. The lower activity of the neutral chloride-Ir(III) compound **18** when compared to the cationic Ir(III) **20** could be due to the difference in the lability of the chloride and the tetrahydrofurane ligands. Finally, dihydride-Ir(III) complex **19** gave no conversion for this process (Table 4, entry 3). The inability of this complex to generate a coordinative vacancy during the reaction due to the presence of a second hydride ligand would explain this lack of activity.

The ability of cationic Rh(III) and Ir(III) complexes to efficiently catalyse the reaction of *trans*-2-octene with Et₃SiH encouraged us to test their activity with a wider olefin scope. These results are collected in table 5. Rhodium catalyst **6** promoted the formation of hydrosilylation products in all cases at room temperature, after 12 hours or reaction. The use of Iridium compound **20**, on the other hand, leads to both hydrosilylation and dehydrogenative silylation

products. The allylic species is the main unsaturated product obtained by dehydrogenative silylation, with a mixture of the E and Z isomers.

Table 5. Tandem isomerisation-hydrosilylation or dehydrogenative silylation of various linear alkenes with Et₃SiH using **6** and **20** as catalysts.^[a]

Cat = [Rh] (6) Conversion ^[b] (Select.) ^[c] [%]	Alkene	Cat = [Ir] (20) Conversion ^[b] (Select.) ^[c] [%]
	ALKENE	
 80 (>99)		 72 (60)
 55 (80)		 73 (59)
 65 (95)		 70 (58)
 90 (93)		 70 (50)
 85 (98)		 75 (36)
 80 (>99)		 66 (50)
 89 (>99)		 67 (47)

[a] Catalytic conditions: Alkene (0.25 mmol), Et₃SiH (0.25 mmol), 1 % mol **6** or **20** (0.002 mmol), solvent-free, after 12 hours of reaction. [b] Conversions were determined by ¹H RMN spectroscopy, by silane remaining. [c] Linear selectivity was determined by ¹H RMN.

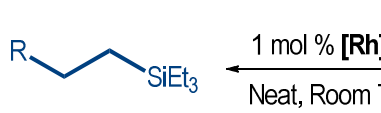
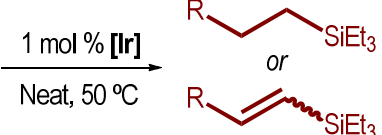
With rhodium complex **6** as a catalyst, the reaction of 1-octene with Et₃SiH gave the linear octylsilane product with a conversion of 90 %, and with a high selectivity. The conversion for internal octene isomers varied from a 55 % for *trans*-3-octene, to an 80 % for *trans*-2-octene,

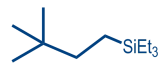
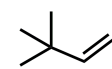
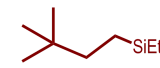
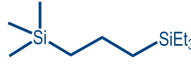
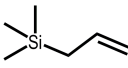
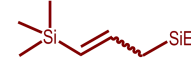
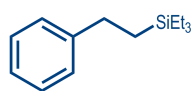
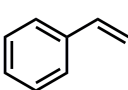
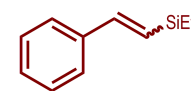
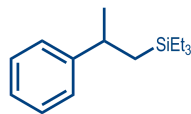
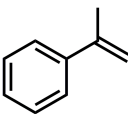
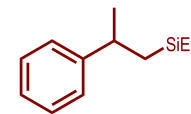
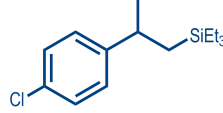
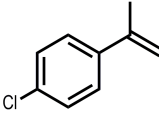
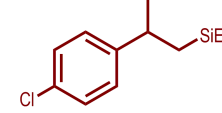
also yielding the octylsilane product with good selectivity. *Trans*-2 and *trans*-3-hexene yielded the linear hexylsilane selectively to reach conversions of 85 % and 80 % respectively, and terminal isomer 1-hexene reached a higher conversion percentage of almost 90 %.

Results of the reactions catalysed by iridium complex **20** are represented on the right side of Table 5. Treatment of all octene isomers with Et₃SiH gave similar conversions of 70-73 %, in which the main product was the allylsilane compound triethyl(2-octenyl)silane. The vinylsilane product, also obtained by dehydrogenative silylation, was present in less than 1 %. Reaction with hexene isomers also reached conversions close to 70 %, with the unsaturated triethyl(2-hexenyl)silane as the main product in all cases. The ratio of the vinylsilane product increases for hexene isomers, to reach 7%, 16% and 14% of the product triethyl(1-hexenyl)silane in *trans*-3-, *trans*-2- and 1-hexene respectively. The variation in the allyl-/vinylsilane product ratio could be attributed to the chain length difference in substrates, as steric factors would lead towards selective β-hydride elimination in the reaction intermediate.¹⁰⁵

Experiments with non-linear alkenes were also performed with rhodium(III) and iridium(III) compounds **6** and **20**. Results of these reactions with Et₃SiH are shown in Table 6.

Table 6. Hydrosilylation or dehydrogenative silylation of various non-linear alkenes with Et₃SiH using **6** and **20** as catalysts.^[a]

Cat = [Rh] (6) Conversion ^[b] (Select.) ^[c] [%]	Alkene	Cat = [Ir] (20) Conversion ^[b] (Select.) ^[c] [%]
 1 mol % [Rh] Neat, Room T	ALKENE	 1 mol % [Ir] Neat, 50 °C

 90 (93)		 90 (>99)
 91 (>99)		 75 (90)
 65 (81)		 31 (69)
 11 (>99)		 56 (>99)
 25 (>99)		 51 (98)

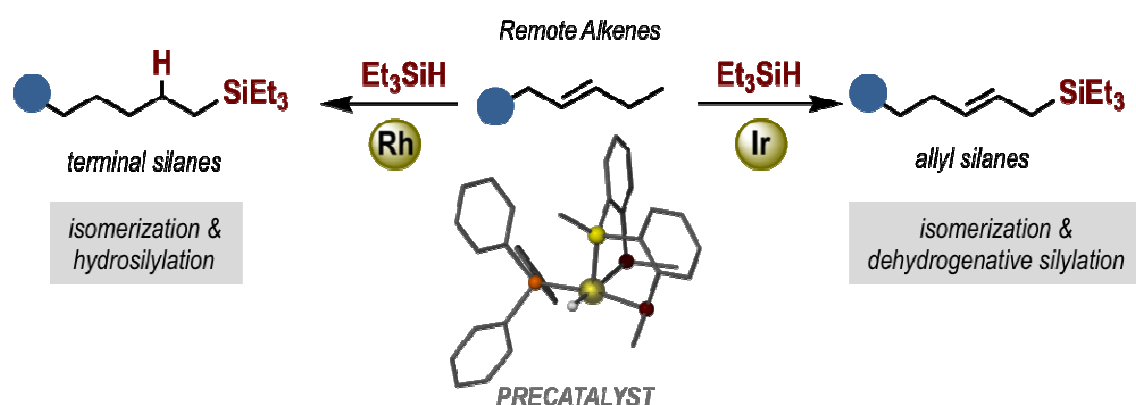
[a] Catalytic conditions: Alkene (0.25 mmol), Et₃SiH (0.25 mmol), 1 % mol **6** or **20** (0.002 mmol), solvent-free, after 12 hours of reaction. [b] Conversions were determined by ¹H RMN spectroscopy, by silane remaining. [c] Linear selectivity was determined by ¹H RMN.

Rhodium catalysed reactions for *tert*-butylethylene and allyltrimethylsilane, both terminal alkenes, led to the selective formation of (3,3-dimethylbutyl)triethylsilane and triethyl(3-(trimethylsilyl)propyl)silane respectively, with almost complete conversion. The reaction with styrene afforded 65% conversion under the same reaction conditions, with 81% selectivity to the linear hydrosilylation product triethyl(styryl)silane, whereas styrene derivatives such as α -

methylstyrene and 4-chloro- α -methylstyrene gave 11% and 25% conversions to the terminal hydrosilylated product, with excellent linear selectivity.

In the case of iridium catalysed reactions, allyltrimethylsilane afforded a selective 75 % conversion to the allylic dehydrogenative silylation product. For styrene, α -methylstyrene, 4-chloro- α -methylstyrene and *tert*-butylethylene (tbe) substrates, the formation of the allylsilane product is not possible, as they can only yield the vinylsilane species or hydrosilylated products. Experiments with these olefins were performed under the same conditions, with the purpose of studying the selectivity of the hydrosilylation reaction with iridium catalyst **20**. These reactions exhibited great selectivity towards the hydrosilylated linear product, except styrene, which afforded a 69 % selectivity for the vinylsilane product in the reaction with Et_3SiH . This could also be explained by steric effects of methyl groups in α -methylstyrene, 4-chloro- α -methylstyrene, and tbe in the β -hydride elimination step, which would favour the elimination away from the bulky substituent.^{89a} Hydrosilylation of tbe successfully yielded linear product to reach 90% of conversion. Notably, α -methylstyrene and 4-chloro- α -methylstyrene yielded hydrosilylation products in a higher conversion (>50%) with iridium(III) catalyst **20** than with the rhodium(III) analogue.

These experiments confirm that the nature of the metal centre in the catalyst influences the silylation reaction pathway. Iridium(III) catalyst **20** promotes the dehydrogenative silylation route in the reaction of these internal olefins with Et_3SiH , yielding the allylsilane as the main product, whereas a rhodium(III) centre leads to hydrosilylation products selectively (Scheme 39).



Scheme 39. General reaction scheme for remote alkenes with Et_3SiH catalysed by analogue Rh(III) and Ir(III) compounds **6** and **20**.

II. 1. 4. BIBLIOGRAPHY

1. M. Tanabe, K. Osakada, *Transition Metal Complexes of Silicon (Excluding Silylene Complexes). Organosilicon Compounds*, **2017**, 31–67.
2. J. K. Hoyano, M. Elder, W. A. G. Graham, *J. Am. Chem. Soc.*, **1969**, *91*, 4568-4569.
3. (a) X. Luo, G. J. Kubas, C. J. Burns, J. C. Bryan, C. J. Unkefer, *J. Am. Chem. Soc.*, **1995**, *117*, 1159-1160; (b) I. Atheaux, F. Delpech, B. Donnadiou, S. Sabo-Etienne, B. Chaudret, K. Hussein, J. Barthelat, T. Braun, S. B. Duckett, R. N. Perutz, *Organometallics*, **2002**, *21*, 5347-5357; (c) S. K. Ignatov, A. Y. Khalimon, N. H. Rees, A. G. Razuvaev, P. Mountford, G. I. Nikonov, *Inorg. Chem.*, **2009**, *48*, 9605-9622.
4. U. Schubert, η^2 Coordination of Si–H σ Bonds to Transition Metals. *Advances in Organometallic Chemistry*, **1990**, 151–187.
5. (a) B. Marciniak, *Silicon Chem.*, **2002**, *1*, 155-175; (b) M. A. Brook, *Silicon in Organic, Organometallic, and Polymer Chemistry*; Wiley: New York, **2000**.
6. X. L. Luo, R. H. Crabtree, *J. Am. Chem. Soc.*, **1989**, *111*, 2527-2535.
7. M. D. Curtis, P. S. Epstein, *Adv. Organomet. Chem.*, **1981**, *19*, 213-255.
8. J. Y. Corey, *Adv. Organomet. Chem.*, **2004**, *51*, 1-52.
9. T. D. Tilley, *The Chemistry of Organic Silicon Compounds, Chapter 24*; John Wiley & Sons: New York, **1989**, 1415.
10. H. Nishiyama, *Transition Metals for Organic Synthesis, Vol 1*, Wiley-VCH, **2004**.
11. I. Fleming, *Comprehensive Organic Chemistry II*, Pergamon Press, Oxford, **1979**, 577.
12. (a) I. Fleming, A. Barbero, D. Walter, *Chem. Rev.*, **1997**, *97*, 2063-2092; (b) S. E. Denmark, C. S. Regens, *Acc. Chem. Res.*, **2008**, *41*, 1486-1499.
13. L. H. Sommer, E. W. Pietrusza, F. C. Whitmore, *J. Am. Chem. Soc.*, **1947**, *69*, 188-188.
14. J. L. Speier, *Adv. Organomet. Chem.*, **1979**, 407-447.
15. P. B. Hitchcock, M. F. Lappert, N. J. W. Warhurst, *Angew. Chem. Int. Ed.*, **1991**, *30*, 438-440.
16. (a) F. Kakiuchi, Y. Tanaka, N. Chatani, S. Murai, *J. Organomet. Chem.*, **1993**, *456*, 45-47; (b) J. C. Mitchener, M. S. Wrighton, *J. Am. Chem. Soc.*, **1981**, *103*, 975-977; (c) M. Brookhart, B. E. Grant, *J. Am. Chem. Soc.*, **1993**, *115*, 2151-2156; (d) Z. Mo, J. Xiao, Y. Gao, L. Deng, *J. Am. Chem. Soc.*, **2014**, *136*, 17414-17417.
17. M. Xue, J. Li, J. Peng, Y. Bai, G. Zhang, W. Xiao, G. Lai, *Appl. Organometal. Chem.*, **2014**, *28*, 120-126.
18. (a) A. J. Chalk, *J. Organomet. Chem.*, **1970**, *21*, 207-213; (b) I. Ojima, T. Kogure, M. Nihonyanagi, Y. Nagai, *J. Chem. Soc., Chem. Commun.*, **1972**, 938a-938a; (c) B. Baruah, K. Osakada, T. Yamamoto, *J. Mol. Catal. A Chem.*, **1995**, *101*, 17-24.
19. J. E. Hill, T. A. Nile, *J. Organometal. Chem.*, **1977**, *137*, 293-300.
20. (a) W. A. Herrmann, C. Köcher, L. J. Gooßen, G. R. J. Artus, *Chem. Eur. J.*, **1996**, *2*, 1627-1636; (b) B. J. Truscott, A. M. Z. Slawin, S. P. Nolan, *Dalton Trans.*, **2013**, *42*, 270-276; (c) S. Díez-González, N.

- Marion, S. P. Nolan, *Chem. Rev.*, **2009**, *109*, 3612-3676; (d) M. V. Jiménez, J. J. Pérez-Torrente, M. I. Bartolomé, V. Gierz, F. J. Lahoz, L. A. Oro, *Organometallics*, **2008**, *27*, 224-234.
21. E. Mas-Marza, M. Sanau, E. Peris, *Organometallics*, **2006**, *25*, 3063-3069.
 22. S. C. Bart, E. Lobkovsky, P. J. Chirik, *J. Am. Chem. Soc.*, **2004**, *126*, 13794-13807.
 23. D. C. Apple, K. A. Brady, J. M. Chance, N. E. Heard, T. A. Nile, *J. Mol. Catal.*, **1985**, *29*, 55-64.
 24. D. Wechsler, A. Myers, R. McDonald, M. J. Ferguson, M. Stradiotto, *Inorg. Chem.* **2006**, *45*, 4562-4570.
 25. E. Calimano, T. D. Tilley, *J. Am. Chem. Soc.*, **2008**, *130*, 9226-9227.
 26. (a) M. A. Fernandez, L. A. Oro, B. R. Manzano, *J. Mol. Catal.*, **1988**, *45*, 7-15; (b) C. Cheng, E. M. Simmons, J. F. Hartwig, *Angew. Chem. Int. Ed.*, **2013**, *52*, 8984-8989.
 27. J. J. Perez-Torrente, D. H. Nguyen, M. V. Jimenez, F. J. Modrego, R. Puerta-Oteo, D. Gomez-Bautista, M. Iglesias, L. A. Oro. *Organometallics*, **2016**, *35*, 2410-2422.
 28. A. Saxena, K. Okoshi, M. Fujiki, M. Naito, G. Guo, T. Hagihara, M. Ishikawa, *Macromolecules*, **2004**, *37*, 367-370.
 29. (a) C. Aitken, J. P. Barry, F. Gauvin, J. F. Harrod, A. Malek, D. Rousseau, *Organometallics*, **1989**, *8*, 1732-1736; (b) T. D. Tilley, *Comments. Inorg. Chem.*, **1990**, *10*, 37-51.
 30. M. D. Curtis, P. S. Epstein, *Adv. Organomet. Chem.*, **1981**, *19*, 213-255.
 31. A. E. Wetherby, N. T. Mucha and R. Waterman, *ACS Catal.*, **2012**, *2*, 1404-1407.
 32. I. Ojima, S. Inaba, T. Kogure, Y. Nagai, *J. Organomet. Chem.*, **1973**, *55*, C7-C8.
 33. (a) K. Brown-Wensley, *Organometallics*, **1987**, *6*, 1591-1593; (b) H. Yamashita, M. Tanaka, *Bull. Chem. Soc. Jpn.*, **1995**, *68*, 403-419.
 34. L. Rosemberg, C. W. Davis, J. Yao, *J. Am. Chem. Soc.*, **2001**, *123*, 5120-5121.
 35. (a) T. Baumgartner, W. Wilk, *Org. Lett.*, **2006**, *8*, 503-505; (b) M. Tanaka, T. Kobayashi, T. Hayashi, T. Sakakura, *Appl. Organomet. Chem.*, **1988**, *2*, 91-92.
 36. (a) M. J. Auburn, S. L. Grundy, S. R. Stobart, M. J. Zaworotko, *J. Am. Chem. Soc.*, **1985**, *107*, 266-274.
 37. (a) W. H. Kwok, G. L. Lu, C. E. F. Rickard, W. R. Roper, L. J. Wright, *J. Organomet. Chem.*, **2004**, *689*, 2511-2522; (b) A. F. Hill, H. Neumann, J. Wagler, *Organometallics*, **2010**, *29*, 1026-1031.
 38. A. Takaoka, N. P. Mankad, J. C. Peters, *J. Am. Chem. Soc.*, **2011**, *133*, 8440-8443.
 39. (a) Yamashita, H.; Tanaka, M. *Bull. Chem. Soc. Jpn.* **1995**, *68*, 403-419; (b) W. Chen, S. Shimada, T. Hayashi, M. Tanaka, *Chem. Lett.*, **2001**, *30*, 1096-1097.
 40. (a) R. A. Gossage, G. D. McLennan, S. R. Stobart, *Inorg. Chem.*, **1996**, *35*, 1729-1732; (b) M. C. MacInnis, D. F. MacLean, R. J. Lundgren, R. McDonald, L. Turculet, *Organometallics*, **2007**, *26*, 6522-6525.
 41. M. Stradiotto, K. L. Furdala, T. D. Tilley, *Chem. Commun.*, **2001**, 1200-1201.
 42. A. J. Ruddy, S. J. Mitton, R. McDonald, L. Turculet, *Chem. Commun.*, **2012**, *48*, 1159-1161.
 43. F. L. Joslin, S. R. Stobart, *J. Chem. Soc., Chem. Commun.*, **1989**, 504-505.
 44. S. J. Mitton, L. Turculet, *Chem. Eur. J.*, **2012**, *18*, 15258-15262.

45. (a) A. F. Hill, H. Neumann, J. Wagler, *Organometallics*, **2010**, *29*, 1026-1031; (b) A. Takaoka, N. P. Mankad, J. C. Peters, *J. Am. Chem. Soc.*, **2011**, *133*, 8440-8443; (c) N. Takeda, D. Watanabe, T. Nakamura, M. Unno, *Organometallics*, **2010**, *29*, 2839-2841.
46. H. B. Kraatz, H. Jacobsen, T. Ziegler, P. M. Boorman, *Organometallics*, **1993**, *12*, 76-80.
47. A. F. Hill, H. Neumann, J. Wagler, *Organometallics*, **2010**, *29*, 1026-1031.
48. N. Takeda, D. Watanabe, T. Nakamura, M. Unno, *Organometallics*, **2010**, *29*, 2839-2841.
49. A. Takaoka, N. P. Mankad, J. C. Peters, *J. Am. Chem. Soc.*, **2011**, *133*, 8440-8443.
50. M. Barquín, M. A. Garralda, L. Ibarlucea, C. Mendicute-Fierro, E. Pinilla, V. San Nacienceno, M. R. Torres, *Organometallics*, **2011**, *30*, 1577-1587.
51. P. I. Djurovich, A. L. Safir, N. L. Keder, R. J. Watts, *Inorg. Chem.*, **1992**, *31*, 3195-3196.
52. R. El Mail, M. A. Garralda, R. Hernández, L. Ibarlucea, E. Pinilla, M. R. Torres, *Helv. Chim. Acta.*, **2002**, *85*, 1485-1495.
53. (a) K. Jonas, *Angew. Chem. Int. Ed. Engl.*, **1985**, *24*, 295-311; (c) F. Gassner, E. Dinjus, H. Görls, W. Leitner, *Organometallics*, **1996**, *15*, 2078-2082.
54. (a) S. Chen, Y. Li, J. Zhao, X. Li, *Inorg. Chem.*, **2009**, *48*, 1198-1206; (b) Y. Yamamoto, Y. Kosaka, Y. Tsutsumi, Y. Sunada, K. Tatsumi, T. Fumie, T. Shigetoshi, *Dalton Trans.*, **2004**, 2969-2978.
55. M. Brookhart, M. L. H. Green, G. Parkin, *PNAS*, **2007**, *104*, 6908-6914.
56. S. Biswas, D. Sarkar, S. Kundu, P. Roy, T. K. Mondal, *Mol. Struct.*, **2015**, *1099*, 297-303.
57. A. J. Ruddy, S. J. Mitton, R. McDonald, L. Turculet, *Chem. Comm.*, **2012**, *48*, 1159-1161.
58. F. Gassner, E. Dinjus, H. Görls, W. Leitner, *Organometallics*, **1996**, *15*, 2078-2082.
59. (a) C. Bianchini, E. Farnetti, M. Graziani, G. Nardin, A. Vacca, F. Zanobini, *J. Am. Chem. Soc.*, **1990**, *112*, 9190-9197; (b) M. J. Fernandez, M. A. Esteruelas, L. A. Oro, M. C. Apreda, C. Foces- Foces, F. H. Cano, *Organometallics*, **1987**, *6*, 1751-1756.
60. L. S. Alekseev, F. M. Dolgushin, I. A. Godovikov, I. T. Chizhevsky, *Organometallics*, **2010**, *29*, 1707-1711.
61. (a) M. Martín, O. Torres, E. Oñate, E. Sola, L. A. Oro, *J. Am. Chem. Soc.*, **2005**, *127*, 18074-18084; (b) B. Raible, V. Gierz, D. Kunz, *Organometallics*, **2015**, *34*, 2018-2027.
62. O. Torres, M. Martín, E. Sola, *Organometallics*, **2010**, *29*, 3201- 3209.
63. (a) D. G. H. Hetterscheid, J. M. M. Smits, B. de Bruin, *Organometallics*, **2004**, *23*, 4236-4246; (b) R. El Mail, M. A. Garralda, R. Hernández, L. Ibarlucea, E. Pinilla, M. R. Torres, M. Zarandona, *Eur. J. Inorg. Chem.*, **2005**, 1671-1677.
64. (a) N. Almenara, L. Ibarlucea, C. Mendicute-Fierro, J. M. Seco, A. Rodriguez-Dieguez, M. A. Garralda, M. A. Huertos, *Dalton Trans.*, **2016**, *45*, 18502-18509; (b) M. Barquín, M. A. Garralda, L. Ibarlucea, C. Mendicute-Fierro, E. Pinilla, V. San Nacienceno, M. R. Torres, *Organometallics*, **2011**, *30*, 1577-1587.
65. M. Brookhart, M. L. H. Green, G. Parkin, *PNAS*, **2007**, *104*, 6908-6914.
66. M. D. Walter, R. A. Moorhouse, S. A. Urbin, P. S. White, M. Brookhart, *J. Am Chem. Soc.*, **2009**, *131*, 9055-9069.

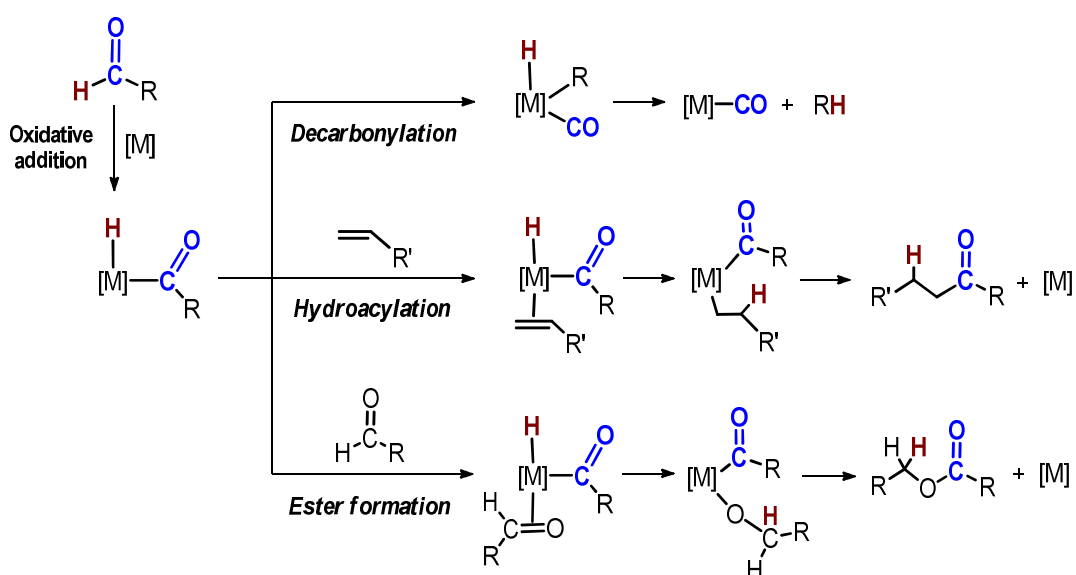
67. P. R. Schleyer, *J. Am. Chem. Soc.*, **1958**, *80*, 1700-1704.
68. S. Wang, M. L. McCrea-Hendrick, C. M. Weinstein, C. A. Caputo, E. Hoppe, J. C. Fetting, M. M. Olmstead, P. P. Power, *J. Am. Chem. Soc.*, **2017**, *139*, 6596-6604.
69. B. Marciniec, *Silicon Chem.* **2002**, *1*, 155-175.
70. (a) T. Onak, *Organoborane Chemistry; Academic: New York*, **1975**; (b) B. M. Mikhailov, Y. N. Bubnov, *Organoboron Compounds in Organic Synthesis; Harwood Academic: Amsterdam*, **1983**.
71. T. E. Müller, K. C. Hultsch, M. Yus, F. Foubelo, M. Tada; *Chem. Rev.*, **2008**, *108*, 3795-3892.
72. G. M. Adams, A. L. Colebatch, J. T. Skornia, A. I. McKay, H. C. Johnson, G. C. Lloyd-Jones, S. A. Macgregor, N. A. Beattie, A. S. Weller, *J. Am. Chem. Soc.*, **2018**, *140*, 1481-1495.
73. L. Li, Y. Zhang, L. Gao, Z. Song, *Tetrahedron Lett.*, **2015**, *56*, 1466-1473.
74. (a) K. Tamao, *Proc. Jpn. Acad., Ser. B*, **2008**, *84*, 123-133; (b) Y. Nakao, T. Hiyama, *Chem. Soc. Rev.*, **2011**, *40*, 4893-4901.
75. (a) I. Ojima, D. A. Fracchiolla, R. J. Donovan, P. Banerji, *J. Org. Chem.*, **1994**, *59*, 7594-7595; (b) C. M. Ong, T. J. Burchell, R. J. Puddephatt, *Organometallics*, **2004**, *23*, 1493-1495; (c) M. Tobisu, M. Onoe, Y. Kita, N. Chatani, *J. Am. Chem. Soc.*, **2009**, *131*, 7506-7507; (d) Y. Liang, S. G. Zhang, Z. F. Xi, *J. Am. Chem. Soc.*, **2011**, *133*, 9204-9207; (e) H. Kameo, S. Ishii, H. Nakazawa, *Dalton Trans.*, **2013**, *42*, 4663-4669; (f) Q. W. Zhang, K. An, W. He, *Angew. Chem., Int. Ed.* **2014**, *53*, 5667-5671.
76. S. J. Mitton, R. McDonald, L. Turculet, *Angew. Chem., Int. Ed.*, **2009**, *48*, 8568-8571.
77. J. Takaya, N. Iwasawa, *Organometallics*, **2009**, *28*, 6636-6638.
78. H. G. Woo, J. F. Walzer, T. D. Tilley, *J. Am. Chem. Soc.* **1992**, *114*, 7047-7055.
79. R. Waterman, *Chem. Soc. Rev.*, **2013**, *42*, 13, 5629-5641.
80. T. D. Tilley, *Acc. Chem. Res.*, **1993**, *26*, 22-29.
81. (a) E. Hengge, M. Weinberger, *J. Organomet. Chem.* **1993**, *443*, 167-173; (b) J. Y. Corey, *Adv. Organomet. Chem.*, **2004**, *51*, 1-52.
82. S. L. Pratt, R. A. Faltynek, *J. Organomet. Chem.*, **1983**, *258*, C5-C8.
83. (a) P. Diversi, F. Marchetti, V. Ermini, S. Matteoni, *J. Organomet. Chem.*, **2000**, *593-594*, 154-160; (b) D. Karshtedt, A. T. Bell, T. D. Tilley, *Organometallics*, **2006**, *25*, 4471-4482; (c) J. Hao, B. Vabre, D. Zargarian, *J. Am. Chem. Soc.*, **2015**, *137*, 15287-15298.
84. M. C. Lipke, F. Neumeyer, T. D. Tilley, *J. Am. Chem. Soc.*, **2014**, *136*, 6092-6102.
85. A. J. Chalk, J. F. Harrod, *J. Am. Chem. Soc.*, **1965**, *87*, 16-21.
86. A. Millan, M. J. Fernandez, P. Bentz, P. M. Maitlis, *J. Mol. Catal.*, **1984**, *26*, 89-104.
87. (a) B. Marciniec, *Coord. Chem. Rev.*, **2005**, *249*, 2374-2390; (b) B. Marciniec, A. Kownacka, I. Kownacki, M. Hoffmann, R. Taylor, *J. Org. Chem.*, **2015**, *791*, 58-65; (c) J. J. Perez-Torrente, D. H. Nguyen, M. V. Jimenez, F. J. Modrego, R. Puerta-Oteo, D. Gomez-Bautista, M. Iglesias, L. A. Oro, *Organometallics*, **2016**, *35*, 2410-2422.
88. (a) J. R. McAtee, G. P. A. Yap, D. A. Watson, *J. Am. Chem. Soc.*, **2014**, *136*, 10166-10172; (b) C. C. H. Atienza, T. Diao, K. J. Weller, S. A. Nye, K. L. Lewis, J. G. P. Delis, J. L. Boyer, A. K. Roy, P. J. Chirik, *J. Am. Chem. Soc.*, **2014**, *136*, 12108-12118.

89. (a) Y. Jiang, O. Blacque, T. Fox, C. M. Frech, H. Berke, *Chem. Eur. J.*, **2009**, *15*, 2121-2128; (b) C. Cheng, E. M. Simmons, J. F. Hartwig, *Angew. Chem. Int. Ed.*, **2013**, *52*, 8984-8989.
90. D. Peng, Y. Zhang, X. Du, L. Zhang, X. Leng, M. D. Walter, Z. Huang, *J. Am. Chem. Soc.*, **2013**, *135*, 19154-19166.
91. X. Jia, Z. Huang, *Nat. Chem.*, **2016**, *8*, 157-161.
92. I. Buslov, J. Becouse, S. Mazza, M. Montandon-Clerc, X. Hu, *Angew. Chem. Int. Ed.*, **2015**, *54*, 14523-14526.
93. D. Noda, A. Tahara, Y. Sunada, H. Nagashima, *J. Am. Chem. Soc.*, **2016**, *138*, 2480-2483.
94. I. Buslov, F. Song, X. Hu, *Angew. Chem. Int. Ed.*, **2016**, *55*, 12295-12299.
95. A. J. Chalk, *J. Organomet. Chem.*, **1970**, *21*, 207-213.
96. J. F. Harrod, A. H. Chalk, *J. Am. Chem. Soc.*, **1965**, *87*, 1133-1135.
97. (a) H. K. Sharma, K. H. Pannell, *Angew. Chem. Int. Ed.*, **2009**, *48*, 7052-7054; (b) H. K. Sharma, K. Pannell, *Angew. Chem.*, **2009**, *121*, 7186-7188.
98. R. Waterman, *Chem. Soc. Rev.*, **2013**, *42*, 5629-5641.
99. (a) G. Nerthon-Gelloz, B. de Bruin, B. Tinant, I. E. Marko, *Angew. Chem. Int. Ed.*, **2009**, *48*, 3161-3164; (b) G. Berthon-Gelloz, B. de Bruin, B. Tinant, I. E. Markó, *Angew. Chem.*, **2009**, *121*, 3207-3210.
100. H. K. Sharma, K. H. Pannell, *Angew. Chem. Int. Ed.*, **2009**, *48*, 7052-7054.
101. M. A. Esteruelas, J. Herrero, M. Oliván, *Organometallics*, **2004**, *23*, 3891-3897.
102. K. Jurkschat, A. Tzschach, J. Meunier-Piret, M. J. van Meerssche, *Organomet. Chem.*, **1986**, *317*, 145-151.
103. W. V. Steele, R. D. Chirico, *J. Phys. Chem. Ref. Data*, **1993**, *22*, 377-430.
104. R. N. Haszeldine, R. V. Parish, D. J. Parry, *J. Chem. Soc. A*, **1969**, 683-690.
105. J. R. McAtee, G. P. A. Yap, D. A. Watson, *J. Am. Chem. Soc.*, **2014**, *136*, 10166-10172.

II. 2. ACTIVATION OF THE CARBON-HYDROGEN BOND IN ALDEHYDES

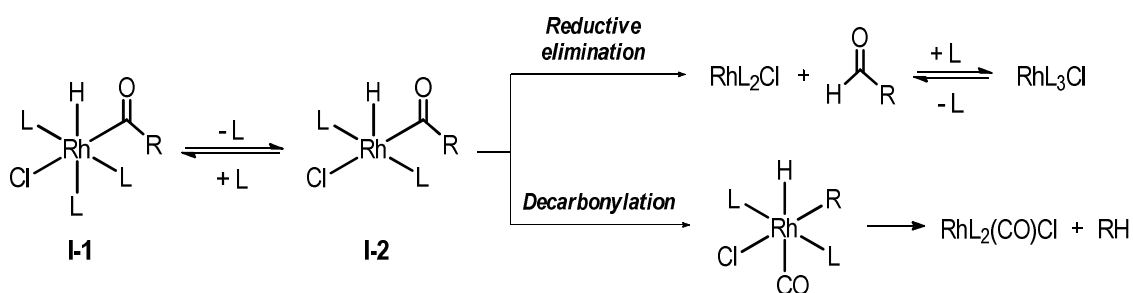
II.2.1. INTRODUCTION

The transition-metal promoted activation and functionalization of C-H bonds has been the subject of extensive research for years.¹ Although C-H bonds exhibit a generally low reactivity, associated to the non-polar nature of the bond,² aldehydes are versatile substrates and can undergo a variety of transformations. Activation of the OC-H bond in aldehydes by a transition metal complex in a low oxidation state is accepted to occur *via* oxidative addition, leading to the formation of acyl hydrido derivatives. These species are considered intermediates in reactions involving the construction of new C-C and C-O bonds, as in hydroacylation³ or ester formation⁴ reactions respectively (Scheme 40). They also participate in decarbonylation⁵ reactions, with a subsequent C-C bond cleavage and removal of the CO group in the aldehyde, without affecting other functionalities in the molecule (Scheme 40). Subsequent reductive elimination from the alkyl-hydride species leads to the formation of an alkane and a metal carbonyl compound as the final products. Transition metal decarbonylation of aldehydes represents an important synthetic route in organic chemistry, and it has recently proved to be a safe source of CO for other reactions.⁶



Scheme 40. Examples of reaction pathways involving acyl hydride metal intermediates.

Aldehyde decarbonylation represents an important competing side reaction of the hydroacylation process⁷ and most likely is a consequence of the lower stability showed by the acyl hydride complex, in contrast to metal carbonyl derivatives. However, there are some examples of stable complexes with phosphine ligands derived from the addition of simple aldehydes.⁸ The first reported rhodium examples were compounds $[\text{RhClH}(\text{COR})(\text{PMe}_3)_3]$ ($\text{R} = \text{Me}, \text{Ph}, p\text{-FC}_6\text{H}_4, p\text{-MeOC}_6\text{H}_4$) (**I-1**), which were synthesised from the oxidative addition of the aldehyde (RCHO) to $[\text{RhCl}(\text{PMe}_3)_3]$.⁹ These complexes were stable at room temperature, but experienced competitive decarbonylation or intramolecular reductive elimination reactions when heated above 60 °C (Scheme 41). Abstraction of a ligand accelerated these reactions by formation of a common unsaturated intermediate (**I-2**), and an excess of phosphine resulted in retardation of the process.



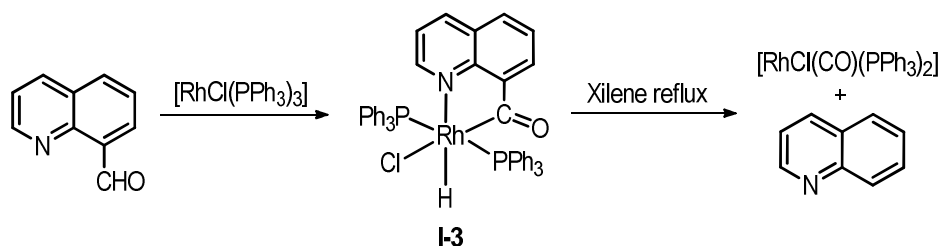
Scheme 41. Competitive reductive elimination and decarbonylation reactions from an unsaturated hydride-acyl intermediate.

The formation of a five or six membered chelate by the use of tethered aldehydes has been established as a useful method for the stabilisation of acyl-hydrido metal intermediates, as the metallacycle arrangement would be kinetically or thermodynamically favoured, and the chelating group blocks the free coordination site necessary for the carbonyl deinsertion to occur. Furthermore, decarbonylation would lead to a strained four-membered metallacycle that contributes to a higher barrier for the decarbonylation pathway.¹⁰ Aldehydes featuring *P*-, *N*-, *O*-, and *S*-based chelating groups have been employed as substrates in transition-metal catalysed intermolecular hydroacylation reactions.^{10a-d} First isolation of stable cyclometalated acyl-metal complexes were derived from 8-quinolinecarboxaldehyde¹¹ ($\text{C}_9\text{H}_6\text{NCHO}$) and 2-(diphenylphosphino)benzaldehyde¹² ($\text{PPh}_2(o\text{-C}_6\text{H}_4\text{CHO})$) (Figure 33), and made an important breakthrough in chelation-assisted hydroacylation.



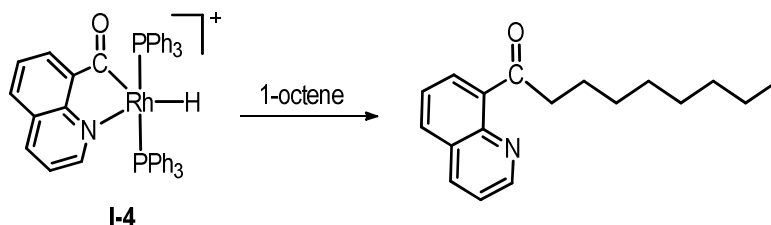
Figure 33. Structures of chelating aldehydes C_9H_6NCHO and $PPh_2(o-C_6H_4CHO)$.

In the mentioned work with the 8-quinolinecarboxaldehyde,¹¹ Suggs reported the reaction of C_9H_6NCHO with Wilkinson's catalyst $[RhCl(PPh_3)_3]$, which allowed the isolation of the stable $[RhH(\kappa^2-C_9H_6NCO)Cl(PPh_3)_2]$ (**I-3**) complex. In this compound, the aldehyde leads to a coordinated bidentate ligand with the formation of a five-membered chelate. Heating this **I-3** complex at 130 °C caused the decarbonylation reaction, leading to the quinoline product (Scheme 42).



Scheme 42. Decarbonylation reaction involving rhodium complex **I-3** derived from 8-quinolinecarboxaldehyde.

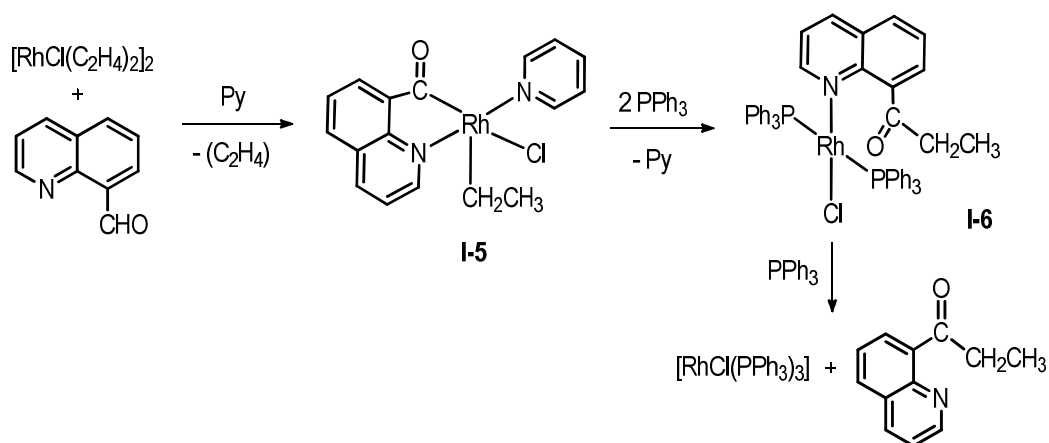
Chloride extraction in complex **I-3** gave the unsaturated species $[RhH(\kappa^2-C_9H_6NCO)(PPh_3)_2]^+$ (**I-4**), which promoted the hydroacylation reaction of 1-octene with C_9H_6NCHO with the formation of the 8-quinolinyl(octyl)ketone (Scheme 43). Isolation of this cationic compound **I-4** confirmed the presence of acyl hydride metal intermediates in olefin hydroacylation reactions.



Scheme 43. Hydroacylation of 1-octene with 8-quinolinecarboxaldehyde, promoted by unsaturated compound **I-4**.

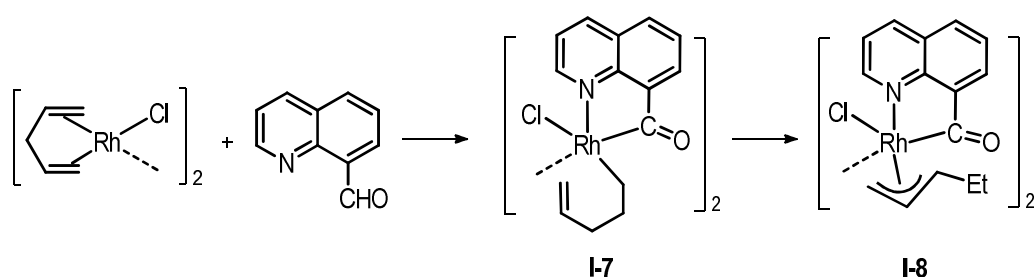
A mechanism for the olefin hydroacylation was later proposed by Suggs et al.¹³ based on the intermediates isolated from reaction of 8-quinolinecarboxaldehyde with $[RhCl(C_2H_4)_2]_2$ in the

presence of pyridine (Scheme 44). This reaction leads to compound $[\text{RhCl}(\kappa^2\text{-C}_9\text{H}_6\text{NCO})(\text{CH}_2\text{CH}_3)(\text{Py})]$ (**I-5**), formed by oxidative addition of the aldehyde to the rhodium centre, and the subsequent insertion of the olefin ligand into the Rh-H bond. The hydroacylation product 8-quinoliny(ethyl)ketone was obtained by addition of two equivalents of triphenylphosphine, which stabilised the rhodium(I) centre and favoured the ketone formation *via* reductive elimination to afford **I-6**. Coordination of another PPh_3 molecule allowed the dissociation of the ethylene hydroacylation product.



Scheme 44. Hydroacylation of ethylene with $\text{C}_9\text{H}_6\text{NCHO}$ reported by Suggs and co-workers.

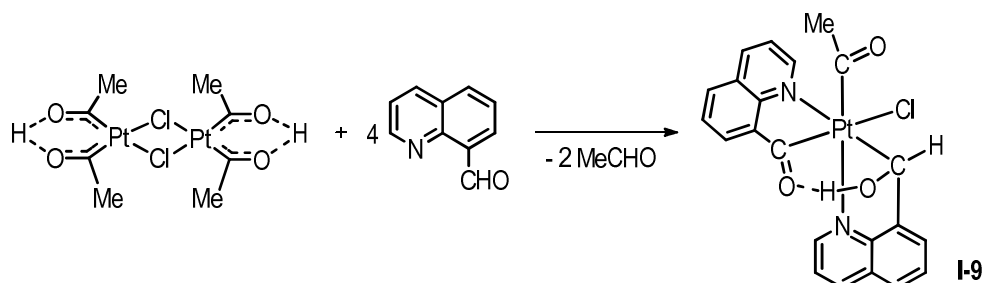
Reaction of the quinoline $\text{C}_9\text{H}_6\text{NCHO}$ with various dimeric rhodium $[\text{RhCl}(\text{diolefin})]_2$ complexes allowed the formation of acyl- η^3 -allyl rhodium(III) derivatives.¹⁴ The reactions were performed with 1,4-pentadiene (Scheme 45) and 1,5-hexadiene as coordinated diolefins. Activation of the aldehyde C-H bond by the metal centre and insertion of the diolefin into the Rh-H bond led to an acyl-(η^1 -alkylolefin) species (**I-7**), and the allyl fragment was formed by migration of the double bond, to give $[\text{Rh}(\text{C}_9\text{H}_6\text{NCO})(\eta^3\text{-allyl})(\mu\text{-Cl})]_2$ (**I-8**) complexes.



Scheme 45. Formation of η^3 -allyl derivatives with $\text{C}_9\text{H}_6\text{NCHO}$.

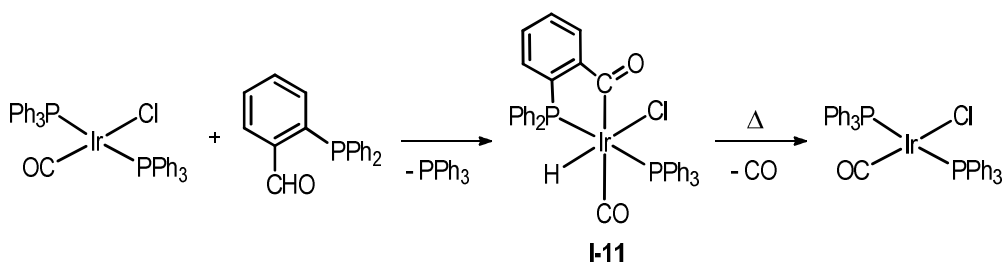
Hydroxyalkyl complexes derived from $\text{C}_9\text{H}_6\text{NCHO}$ have been obtained by reaction with a platina- β -diketone, which contains an acyl-hydroxycarbene fragment stabilized by an

intramolecular O–H···O hydrogen bond.¹⁵ This reaction leads to the water-assisted carbon to oxygen proton transfer, formally between the two aldehyde fragments, yielding an acyl(hydroxyalkyl)platinum(IV) species [Pt(COMe)Cl(κ^2 -C₉H₆NCO)(κ^2 -C₉H₆NCHOH)] (**I-9**) that also shows a strong O···H-O hydrogen bond (Scheme 46).



Scheme 46. Synthesis of the acyl(hydroxyalkyl)platinum(IV) complex **I-9** from a platinum- β -diketone.

Reactions with *o*-(diphenylphosphino)benzaldehyde also involve the stabilisation of the acyl hydride intermediate by formation of a metallacycle. First reported reaction of this ligand with iridium complex [Ir(cod)Cl]₂ led to the saturated compound [IrClH(κ^2 -PPh₂(*o*-C₆H₄CO))(Cod)] (**I-10**) (Figure 34) through oxidative addition of the aldehyde to the metal.¹² The same paper described the reaction of *trans*-[IrCl(CO)(PPh₃)₂] with PPh₂(*o*-C₆H₄CHO) to give the acyl hydride product [IrClH(κ^2 -PPh₂(*o*-C₆H₄CO))(CO)(PPh₃)] (**I-11**). Heating this **I-11** complex at 130 °C promoted the decarbonylation of the bidentate PPh₂(*o*-C₆H₄CO) ligand, which affords PPh₃ and CO, leading to the starting complex *trans*-[IrCl(CO)(PPh₃)₂] (Scheme 47).



Scheme 47. First reported reaction of [IrCl(CO)(PPh₃)₂] with PPh₂(*o*-C₆H₄CHO).

Treatment of the iridium(I) complex [IrCl(CO)₂(*p*-NH₂C₆H₄CH₃)] with two equivalents of PPh₂(*o*-C₆H₄CHO) allows the coordination of the phosphine as a bidentate and a monodentate ligand.¹⁶ In the resulting compound [IrH(PPh₂(*o*-C₆H₄CO)- κ P, κ C)Cl(CO)(PPh₂(*o*-C₆H₄CHO)- κ P)] (**I-12**), the second PPh₂(*o*-C₆H₄CHO) unit is coordinated through the phosphorus atom, maintaining a pendant aldehyde group. Other reported examples of this phosphine-aldehyde as a bidentate ligand include P,O coordination, as in the ruthenium compound [RuCl(η^6 -

arene)(κ^2 -PPh₂(*o*-C₆H₄CHO))]SbF₆ (**I-13**),¹⁷ and P, π -aldehyde coordination as in cobalt and tungsten compounds [Co(Cp*)(PPh₂(*o*-C₆H₄CHO)- κ P, η^2 -CO)]¹⁸ (**I-14**) and [W(CO)₂(PPh₂(*o*-C₆H₄CHO)- κ P, η^2 -CO)₂] (**I-15**).¹⁹ Examples of the coordination modes of this tethered aldehyde are shown in Figure 34.

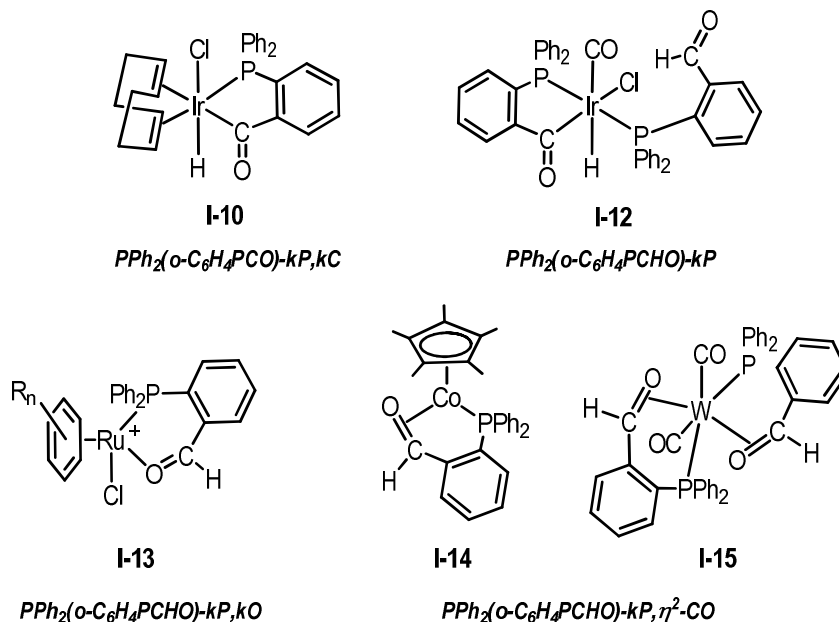


Figure 34. Examples of PPh₂(*o*-C₆H₄CHO) coordination modes reported by Rauchfuss et al.,^{13,16} Gimeno et al.,¹⁷ White et al.¹⁸ and Lee et al.¹⁹

Additionally, *o*-(diphenylphosphino)benzaldehyde has been widely used as a precursor in the synthesis of hemilabile ligands by reaction with amines.²⁰ Condensation of the aldehyde with a primary amine forms an imine group, leading to potentially bidentate PN,²¹ terdentate PNN,²² or tetradentate PNNP²³ ligands. The mixture of a soft donor atom such as phosphorus and hard nitrogen donor atoms confers unique properties to the ligand. While one coordinating group is firmly bound to the metal centre, the other can easily dissociate to create a vacant site for the binding of a potential substrate. Thus, the behaviour of these ligands has proved to increase catalytic activity. The reaction of PPh₂(*o*-C₆H₄CHO) with rhodium complexes containing chelating amino ligands, such as 8-aminoquinoline and *o*-phenylenediamine, would allow the formation of tridentate hemilabile PNN ligands in [RhH(PPh₂(*o*-C₆H₄CO))(PNN)]Cl (**I-16**, **I-17**) compounds (Figure 35).²⁴ The reaction with coordinated biacetyldihydrazone would lead to the formation of the PNN terdentate ligand with an hemiaminal group (**I-18**) (Figure 35),²⁵ which is an intermediate in the imination reaction.

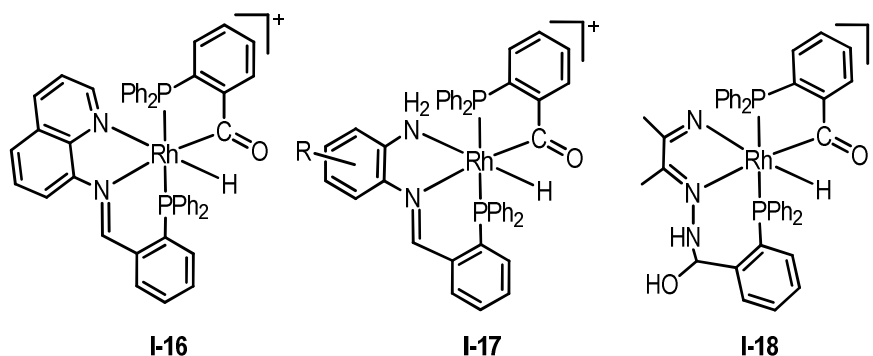
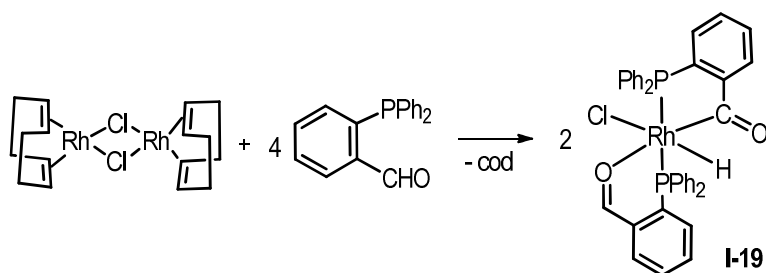


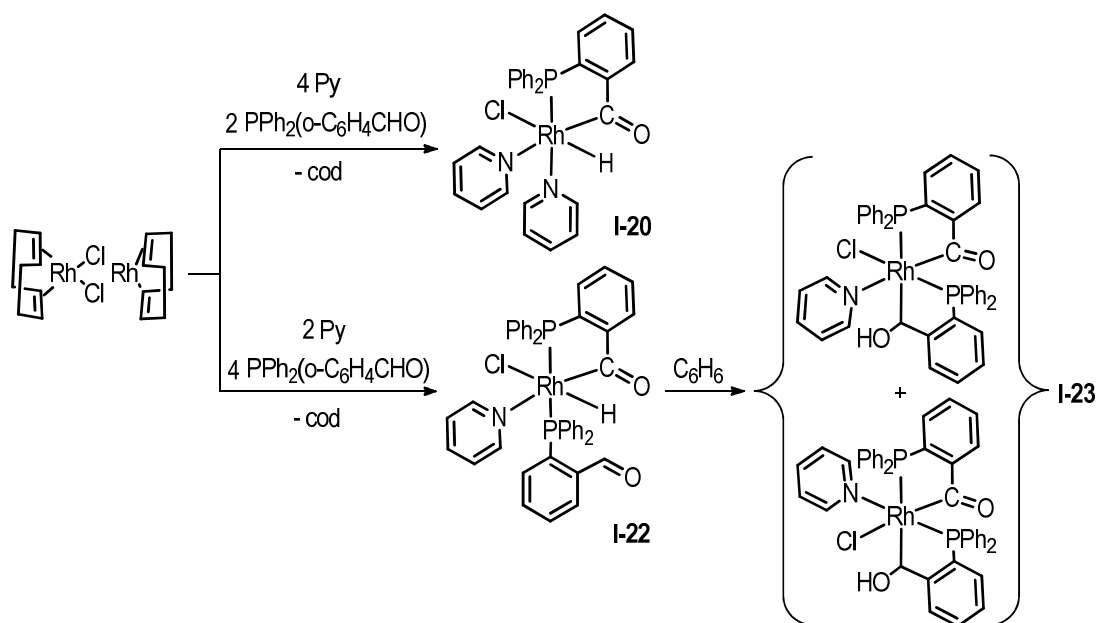
Figure 35. Examples of PNN ligands formed by reaction of $\text{PPh}_2(o\text{-C}_6\text{H}_4\text{CHO})$ with coordinated 8-aminoquinoline (**I-16**), *o*-phenylenediamine (**I-17**) and biacetyldihydrazone (**I-18**).

Reaction of the rhodium diolefinic dimer $[\text{Rh}(\text{cod})\text{Cl}]_2$ with four equivalents of $\text{PPh}_2(o\text{-C}_6\text{H}_4\text{CHO})$ gives the neutral acyl hydride complex $[\text{RhClH}(\kappa^2\text{-PPh}_2(o\text{-C}_6\text{H}_4\text{CO}))(\kappa^2\text{-PPh}_2(o\text{-C}_6\text{H}_4\text{CHO}))]$ (**I-19**), with olefin displacement and the phosphine ligands coordinated as a P,C- and a P,O-chelate (Scheme 48).²⁶



Scheme 48. Formation of the acyl hydrido compound $\text{RhClH}(\kappa^2\text{-PPh}_2(o\text{-C}_6\text{H}_4\text{CO}))(\kappa^2\text{-PPh}_2(o\text{-C}_6\text{H}_4\text{CHO}))$ (**I-19**).

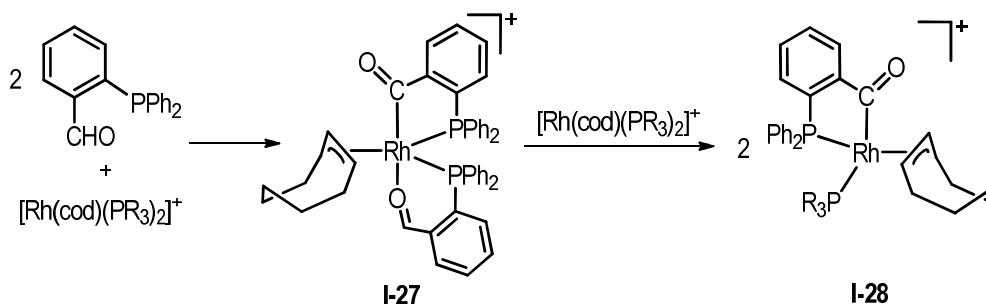
When the reaction of $[\text{Rh}(\text{cod})\text{Cl}]_2$ with $\text{PPh}_2(o\text{-C}_6\text{H}_4\text{CHO})$ is performed in the presence of a monomeric N-donor ligand such as pyridine, complex $[\text{RhClH}(\text{PPh}_2(o\text{-C}_6\text{H}_4\text{CO}))(\text{py})_2]$ (**I-20**) is formed (Scheme 49). This compound was found to undergo hydride exchange in chlorinated solvents to reach the dichloride neutral compound $[\text{Rh}(\text{PPh}_2(o\text{-C}_6\text{H}_4\text{CO}))\text{Cl}_2(\text{py})_2]$ (**I-21**).²⁷ The reaction of $[\text{Rh}(\text{cod})\text{Cl}]_2$ with two equivalents of $\text{PPh}_2(o\text{-C}_6\text{H}_4\text{CHO})$ and pyridine would lead to neutral complex $[\text{RhClH}(\text{PPh}_2(o\text{-C}_6\text{H}_4\text{CO}))(\kappa^1\text{-PPh}_2(o\text{-C}_6\text{H}_4\text{CHO}))(\text{py})]$ (**I-22**) (Scheme 49), which has only been characterised in solution due to its high reactivity. In a benzene solution, **I-22** reacts readily to afford the hydroxyalkyl derivative $[\text{RhCl}(\text{PPh}_2(o\text{-C}_6\text{H}_4\text{CO}))(\kappa^1\text{-PPh}_2(o\text{-C}_6\text{H}_4\text{CHOH}))(\text{py})]$ (**I-23**) as a mixture of two geometric isomers. **I-23** is formed by insertion of the aldehyde group into the Rh-H bond and coordination of the hydroxyalkyl moiety by an sp^3 carbon, to give a five-membered metallacycle.²⁷



Scheme 49. Synthesis of acyl hydride- and acyl hydroxyalkyl- rhodium(III) complexes with 2-(diphenylphosphino)benzaldehyde and pyridine.

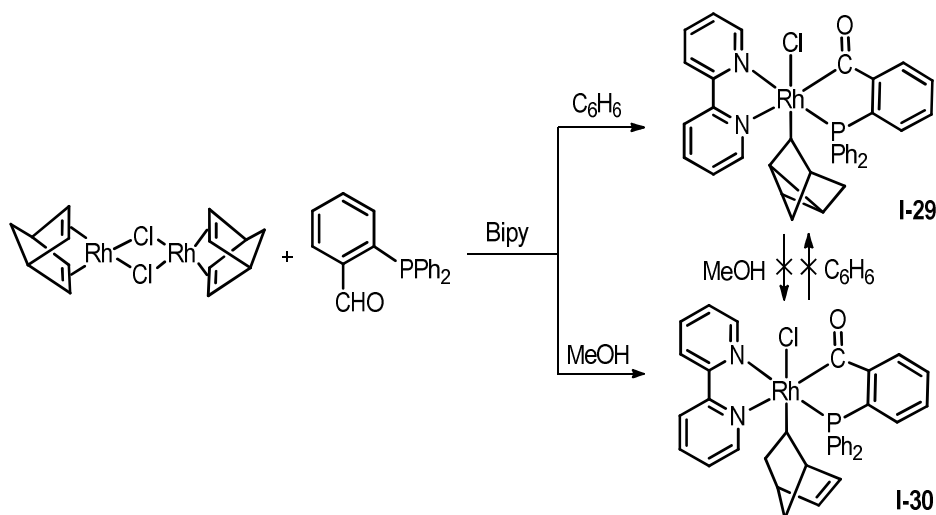
The same kind of complexes can be formed in the presence of diimines, such as 2,2'-bipyridine (bipy). Treatment with one or two equivalents of the phosphine leads to neutral $[\text{RhClH}(\kappa^2\text{-PPh}_2(o\text{-C}_6\text{H}_4\text{CO}))(\text{bipy})]$ (**I-24**) or cationic $[\text{RhH}(\kappa^2\text{-PPh}_2(o\text{-C}_6\text{H}_4\text{CO}))(\text{bipy})(\kappa^1\text{-PPh}_2(o\text{-C}_6\text{H}_4\text{CHO}))]^+$ (**I-25**) compounds respectively. In the latter cationic compound **I-25**, the pendant aldehyde group undergoes insertion into the Rh-H bond to give the acyl hydroxyalkyl species $[\text{Rh}(\kappa^2\text{-PPh}_2(o\text{-C}_6\text{H}_4\text{CO}))(\text{bipy})(\kappa^2\text{-PPh}_2(o\text{-C}_6\text{H}_4\text{CHO}))]^+$ (**I-26**).²⁸

Formation of the mentioned acyl hydride rhodium(III) neutral complexes with *o*-(diphenylphosphino)benzaldehyde occurs with displacement of the olefin. However, cationic rhodium(I) compounds $[\text{Rh}(\text{cod})_2]\text{ClO}_4$ or $[\text{Rh}(\text{cod})(\text{PR}_3)_2]\text{ClO}_4$ ($\text{R} = \text{C}_6\text{H}_5$, *p*- FC_6H_4 , *p*- ClC_6H_4 , *p*- MeOC_6H_4) afford cyclooctenyl derivatives by reaction with the phosphine.²⁹ Treatment of these complexes with two equivalents of $\text{PPh}_2(o\text{-C}_6\text{H}_4\text{CHO})$ led to $[\text{Rh}(\eta^3\text{-cyclooctenyl})(\kappa^2\text{-PPh}_2(o\text{-C}_6\text{H}_4\text{CO}))(\kappa^2\text{-PPh}_2(o\text{-C}_6\text{H}_4\text{CHO}))]\text{ClO}_4$ (**I-27**) complexes *via* oxidative addition of one of the aldehydes, followed by insertion of the 1,5-cyclooctadiene into the Rh-H bond and rearrangement to give the η^3 -allyl species. Cyclooctenyl **I-27** complex reacts with another unit of $[\text{Rh}(\text{cod})(\text{PR}_3)_2]\text{ClO}_4$, with the P,O-chelate opening and oxidative addition of the aldehyde to the Rh(I) centre (Scheme 50), to form two units of compound $[\text{Rh}(\eta^3\text{-cyclooctenyl})(\kappa^2\text{-PPh}_2(o\text{-C}_6\text{H}_4\text{CO}))(\text{PR}_3)]\text{ClO}_4$ (**I-28**).



Scheme 50. Synthesis of η^3 -cyclooctenyl complexes derived from $\text{PPh}_2(o\text{-C}_6\text{H}_4\text{CHO})$.

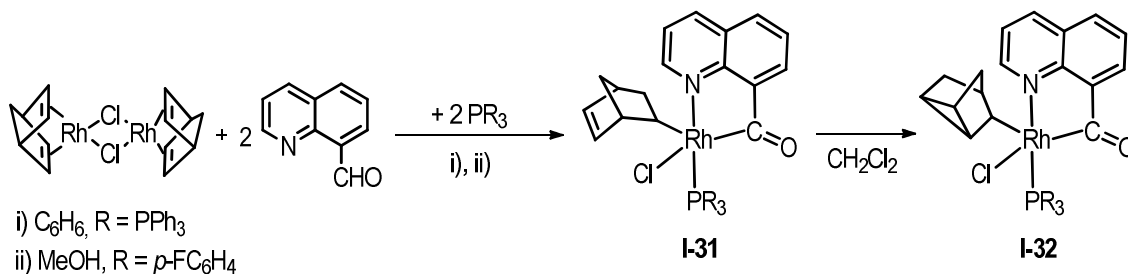
The diolefinic $[\text{Rh}(\text{nbd})\text{Cl}]_2$ complex also reacts with $\text{PPh}_2(o\text{-C}_6\text{H}_4\text{CHO})$ in the presence of N-donor ligands, such as pyridine or 2,2'-bipyridine, to give σ -nortricyclyl (**I-29**) or σ -norbornenyl (**I-30**) derivatives selectively, depending on the solvent.³⁰ These derivatives are formed by activation of the aldehydic C-H bond and insertion of norbornadiene into the formed Rh-H bond. The use of an ionising solvent such as methanol would favour the σ -norbornenyl formation in **I-30**, *via* a proposed cationic $[\text{Rh}(\eta^2\text{-C}_7\text{H}_8)\text{H}(\kappa^2\text{-PPh}_2(o\text{-C}_6\text{H}_4\text{CO}))(\text{bipy})]\text{Cl}$ intermediate, while the use of benzene leads to the σ -nortricyclyl species in **I-29** *via* a proposed neutral $[\text{Rh}(\eta^4\text{-C}_7\text{H}_8)\text{H}(\kappa^2\text{-PPh}_2(o\text{-C}_6\text{H}_4\text{CO}))\text{Cl}]$ intermediate that would allow the required rearrangement (Scheme 51).



Scheme 51. Synthesis of σ -nortricyclyl and σ -norbornenyl complexes with $\text{PPh}_2(o\text{-C}_6\text{H}_4\text{CHO})$.

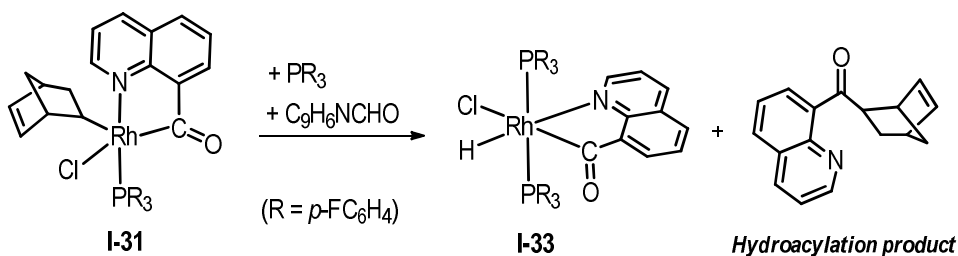
Recent examples of σ -norbornenyl transformation into σ -nortricyclyl involves the reaction of the $[\text{Rh}(\text{nbd})\text{Cl}]_2$ complex with $\text{C}_9\text{H}_6\text{NCHO}$, in the presence of P-donor PR_3 ($\text{R} = \text{C}_6\text{H}_5, p\text{-FC}_6\text{H}_4$) co-ligands.^{31,32} These reactions led to the σ -norbornenyl unsaturated complexes $[\text{RhCl}(\text{C}_9\text{H}_6\text{NCO})(\text{nbyl})(\text{PR}_3)]$ (**I-31**) by chelate-assisted oxidative addition of the aldehyde, and subsequent insertion of the norbornadiene into the Rh-H bond. Complexes **I-31** showed low

stability in solution due to the coordinative vacancy, and underwent rapid isomerisation to the thermodynamically favoured σ -norbornenyl species (**I-32**) by a double bond shift and a ring closure reaction (Scheme 52).



Scheme 52. Formation of σ -norbornenyl compounds and isomerisation into the σ -norbornenyl species in dichloromethane solution.

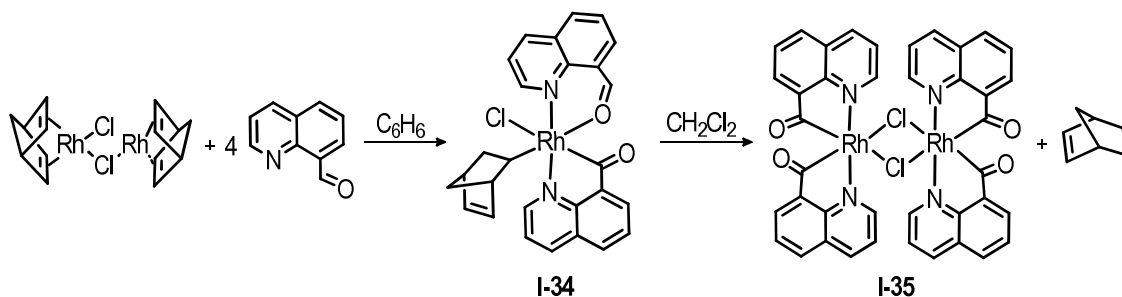
Norbornenyl-acyl complex **I-31** with $P(p\text{-}FC_6H_4)_3$ as a co-ligand also promoted the formation of the quinolinylnorbornenyl-ketone, in the presence of an additional equivalent of both C_9H_6NCHO and phosphine (Scheme 53). The reductive elimination of the ketone is promoted by the phosphine and allows the liberation of the diolefin hydroacylation product, and the oxidative addition of another C_9H_6NCHO molecule gave the hydrido-acyl complex $[RhClH(C_9H_6NCO)(P(p\text{-}FC_6H_4)_3)_2]$ (**I-33**). Both norbornenyl-acyl **I-31** and hydrido-acyl **I-33** Rh(III) species were found active in the catalytic hydroacylation of norbornadiene with C_9H_6NCHO .³²



Scheme 53. Formation of the hydroacylation product of norbornadiene with C_9H_6NCHO promoted by a norbornenyl-acyl-Rh(III) complex.

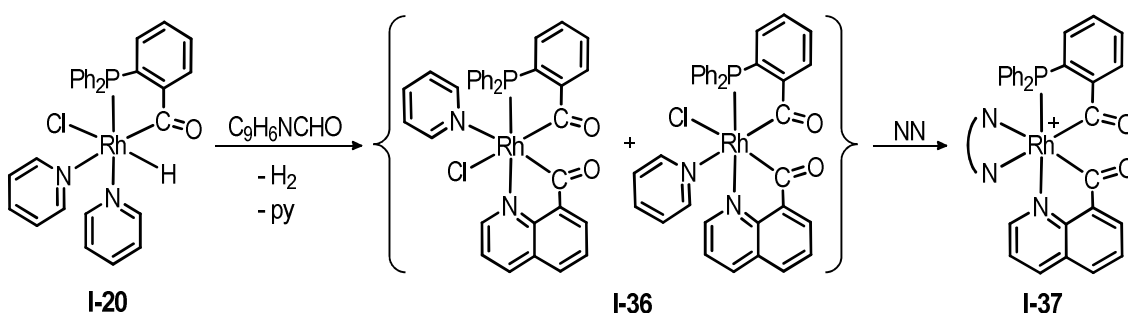
When the reaction of the chloronorbornadienerhodium(I) dimer with C_9H_6NCHO is performed in benzene, using $Rh:C_9H_6NCHO = 1/2$ stoichiometric ratios, the chelate-assisted oxidative addition of one aldehyde-quinoline is produced, with the subsequent Rh-H insertion of the norbornadiene, while a second quinoline-aldehyde is $\kappa^2\text{-N,O}$ coordinated to form a six-membered metallacycle (Scheme 54).³¹ The resulting mononuclear $[RhCl(C_9H_6NCO)(nbyl)(\kappa^2\text{-}C_9H_6NCHO)]$ (**I-34**) compound is unstable in dichloromethane, and undergoes C-H activation of

the coordinated quinoline-aldehyde to form dimeric $[\text{Rh}(\mu\text{-Cl})(\text{C}_9\text{H}_6\text{NCO})]_2$ (**I-35**) complex, and the liberation of norbornene by transfer of hydrogen from the aldehyde (Scheme 54).



Scheme 54. Formation of $[\text{Rh}(\mu\text{-Cl})(\text{C}_9\text{H}_6\text{NCO})]_2$ and liberation of norbornene.

The reaction of the aforementioned hydrido-acyl complex $[\text{RhClH}(\text{PPh}_2(o\text{-C}_6\text{H}_4\text{CO}))(\text{py})_2]$ (**I-20**), derived from *o*-(diphenylphosphino)benzaldehyde, with 8-quinolinecarboxaldehyde affords a mixed diacyl neutral species, *via* C-H activation of the aldehyde. Displacement of a pyridine and proton transfer from the coordinated $\text{C}_9\text{H}_6\text{NCHO}$ to the hydride allows the formation of complex $[\text{RhCl}(\text{py})(\text{C}_9\text{H}_6\text{NCO})(\text{PPh}_2(o\text{-C}_6\text{H}_4\text{CO}))]$ (**I-36**) as a mixture of two geometric isomers, and hydrogen release (Scheme 55).³³ Treatment of **I-36** with bidentate N-donor ligands (NN) such as 2,2'-bipyridine and 2-(aminomethyl)pyridine leads to cationic diacyl mixed $[\text{Rh}(\text{NN})(\text{C}_9\text{H}_6\text{NCO})(\text{PPh}_2(o\text{-C}_6\text{H}_4\text{CO}))]$ (**I-37**) derivatives, by displacement of chloride and pyridine (Scheme 55).³³



Scheme 55. Formation of mixed neutral and cationic diacyl compounds **I-36** and **I-37**.

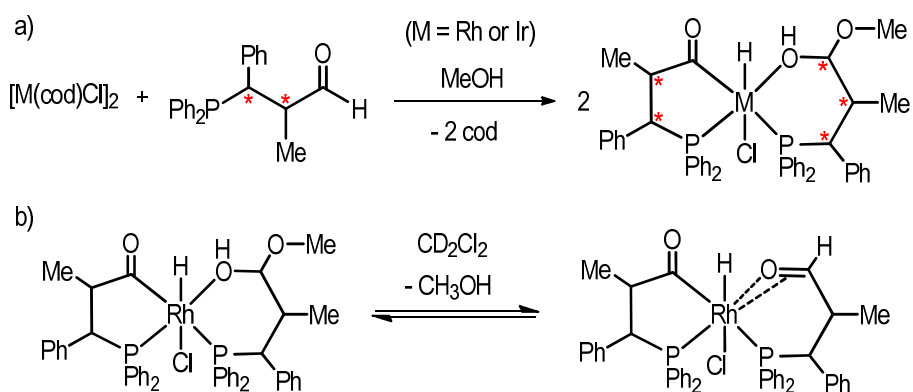
This chapter describes a study on the aldehydic carbon-hydrogen activation in tethered phosphine-alkyl-aldehyde $\text{PPh}_2\text{CH}(\text{Ph})\text{CH}_2\text{CHO}$ promoted by rhodium(I) diolefinic $[\text{Rh}(\text{cod})\text{Cl}]_2$ and $[\text{Rh}(\text{nbd})\text{Cl}]_2$ complexes, in the presence of N-donor monodentate and bidentate ligands. Most of these studies have been devoted to aryl aldehydes, while reports on tethered alkylaldehydes are scarce. The reactivity of the formed species to undergo a variety of reactions such as insertions, iminations or dehydrogenations is also presented. The use of a

racemic mixture of the phosphinoalkylaldehyde, allows a discussion on the diastereoselectivity of the reactions performed. The aldehydic carbon-hydrogen activation in quinoline-8-carbaldehyde in the presence of pyrazole allows the synthesis of efficient homogeneous catalysts for the hydrolysis of ammonia-borane in air for the release of hydrogen, and these results are also discussed.

II.2.2. REACTIVITY OF PHOSPHINE-ALDEHYDE $\text{PPh}_2\text{CH(Ph)CH}_2\text{CHO}$ WITH DIOLEFINIC RHODIUM(I) COMPLEXES

The extensive use of *o*-(diphenylphosphino)benzaldehyde when compared to other phosphine-aldehydes is due to the high stability exhibited by this ligand, conferred by an aryl structure. An alkyl chain to bond the aldehyde group to the phosphorus would lead to more flexible metal-ligand structures. However, examples of chelating phosphine-alkylaldehydes remain scarce, as a result of difficult preparation methods and low yields. Such phosphines containing electrophilic aldehyde groups are highly reactive, as they can easily undergo unselective polymerisation with the formation of carbon-phosphorus bonds.³⁴

The reaction of phosphinopropionaldehyde ($\text{PPh}_2\text{CH}_2\text{CH}_2\text{CHO}$) with $(\text{CO})_5\text{MnH}$ was reported,³⁵ but at variance with related $\text{PPh}_2(o\text{-C}_6\text{H}_4\text{CHO})$, it fails to undergo any C-H activation and only leads to the $\kappa^1\text{-P}$ -coordinated complex with a pendant aldehyde group, without the formation of a metallacycle. A recent publication by James et al.³⁶ described the reaction of [3-(diphenylphosphino)-3-phenyl-2-methyl]propionaldehyde ($\text{PPh}_2\text{CH(Ph)CH(Me)CHO}$) with Rh(I) and Ir(I) complexes. Treatment of $[\text{Rh}(\text{cod})\text{Cl}]_2$ and $[\text{Ir}(\text{cod})\text{Cl}]_2$ with this ligand in MeOH afforded acyl hydride complexes *via* the oxidative addition of an aldehyde to form a five membered $\kappa^2\text{-P,C}$ chelate. A second phosphino-aldehyde undergoes conversion into the hemiacetal species to form a six membered $\kappa^2\text{-P,OH}$ chelate (Scheme 56a). In dichloromethane solution, the rhodium complex shows a slow rearrangement of the hemiacetal group to form the aldehyde species, reaching an equilibrium (Scheme 56b). This phosphine-aldehyde contains two chiral centres in the two carbon atoms of the aliphatic chain, and a new chiral centre is generated with the hemiacetal formation. Although these metal complexes contain five chiral carbons located in ligands, along with a newly formed stereogenic metal centre, only three preferred diastereomers are observed in solution by NMR spectroscopy.

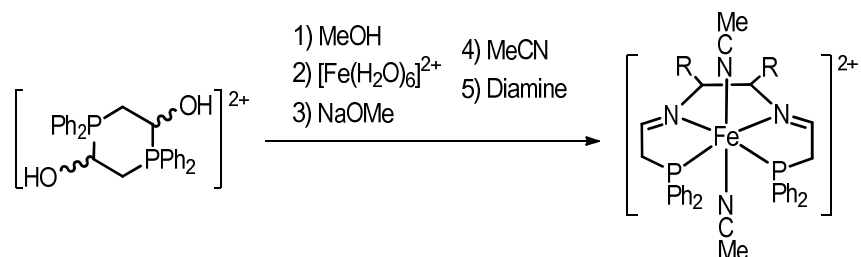


Scheme 56. a) Synthesis of Rh(I) and Ir(I) acyl hydride complexes with $\text{PPh}_2\text{CH}(\text{Ph})\text{CH}(\text{Me})\text{CHO}$. b) Equilibrium between the hemiacetal and aldehyde rhodium species in CD_2Cl_2 .

The coordination of a ligand with a chiral centre to an octahedral complex allows the formation of diastereomeric species, by generation of a metal stereocentre. By all means, chiral metal complexes synthesised from racemic or achiral ligands would be formed as racemates. However, the chirality of a metal complex may be predetermined, when a certain absolute configuration at the ligand chiral centre (S or R) corresponds to a determined absolute configuration at the metal (A or C).³⁷ In this manner, predetermination of the metal chirality yields products of one absolute configuration preferentially. This ensures a diastereoselective synthesis of chiral metal compounds by the use of enantiopure chiral ligands. Interest in such diastereopure complexes has escalated greatly in recent years due to their potential in asymmetric catalysis. Relevant examples include half-sandwich compounds with the formula $[(\eta^n\text{-ring})\text{M}(\text{LL}^*)\text{L}]^{n+}$ (where LL^* represents a chiral bidentate ligand).³⁸ However, the use of bidentate chiral ligands for the diastereoselective synthesis of octahedral complexes with non-half-sandwich metal precursors has received less attention.³⁹ Also, many compounds containing tetradentate N_4 , N_2O_2 or N_2P_2 ligands, useful as catalysts for enantioselective reactions, have been prepared.⁴⁰

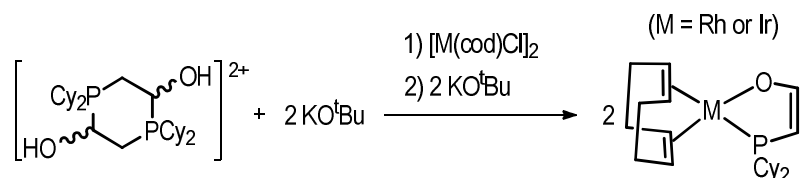
Due to the low stability of phosphine-alkyl aldehyde ligands, a successful strategy for the preparation of complexes of chiral PNN or PNNP ligands has been the use of phosphonium dimers as precursors of the required phosphine-alkylaldehyde.⁴¹ Scheme 57 shows the one-pot synthesis of a Fe(II) complex containing a tetradentate PNNP ligand, starting from an air-stable dimeric phosphonium compound, *via* a multicomponent template reaction. The phosphine-alkylaldehyde is first generated *in situ* by deprotonation of the phosphonium dimer under basic conditions, and in conjunction with a diamine and a metal precursor, the tetradentate PNNP Fe(II) complex is then formed. The role of the metal is to facilitate the condensation

reaction between the diamine and the aldehyde by coordination of the chelating ligand. In the absence of the Fe(II) complex, the direct reaction of the phosphine-aldehyde with amines did not lead to isolated PNNP ligands.^{41a}



Scheme 57. Formation of a PNNP tetradentate complex from a phosphonium dimer in a multicomponent template synthesis.

In the absence of diimine this strategy may afford phosphine-enolate complexes. Morris and co-workers described the syntheses of Rh(I) and Ir(I) chelating κ^2 -*P,O* enolate complexes derived from the phosphine-alkylaldehyde $\text{PCy}_2\text{CH}_2\text{CHO}$ (Cy = cyclohexyl), also formed by treatment of the correspondent phosphonium dimer with base.⁴² The addition of the $[\text{M}(\text{cod})\text{Cl}]_2$ complex to the reaction mixture and the subsequent treatment with additional base allowed the enolization of the aldehyde functionality, to give neutral Rh(I) and Ir(I) compounds.



Scheme 58. Formation of Rh(I) and Ir(I) phosphino-enolate complexes from reaction with phosphonium dimer and base.

In this work, we decided to study the reactivity of the chiral bidentate phosphine-alkylaldehyde $\text{PPh}_2\text{CH}(\text{Ph})\text{CH}_2\text{CHO}$ with diolefinic rhodium(I) compounds. The reaction of diphenylphosphine with cinnamaldehyde affords a racemic mixture of the *R* and *S* enantiomers of the phosphine (Figure 36).⁴³ The formation of a chelate by treatment of rhodium compounds with the enantiomeric mixture of this ligand would generate metal centrochirality, leading to two diastomeric forms.

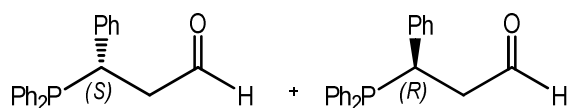


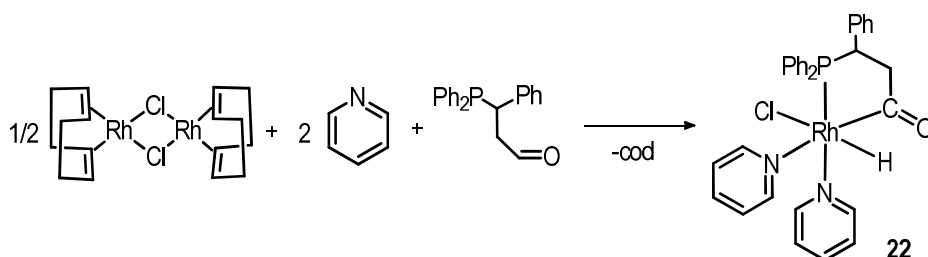
Figure 36. Representation of the enantiomers **S** (left) and **R** (right) of the phosphine-alkyl-aldehyde $\text{PPh}_2\text{CH}(\text{Ph})\text{CH}_2\text{CHO}$.

This chapter will also describe the reactivity of rhodium complexes derived from $\text{PPh}_2\text{CH}(\text{Ph})\text{CH}_2\text{CHO}$ with the above mentioned tethered phosphine-arylaldehyde $\text{PPh}_2(o\text{-C}_6\text{H}_4\text{CHO})$, or with 8-quinolinecarboxaldehyde $\text{C}_9\text{H}_6\text{NCHO}$. Reactions will be also performed in the presence of various N-donor bidentate ligands, such as aromatic diimines (1,10-phenantroline and 2,2'-bipyridine) or amino-imines (8-aminoquinoline and 2-aminomethylpyridine) that can afford new PNN coordinated ligands. DFT calculations have also been employed in collaboration with Dr. Eider San Sebastián, to predict the diastereoselectivity of the reactions involving the chiral phosphine ligand. Results of these calculations are compared to the experimental diastereoselectivity determined by solution NMR spectroscopy.

II. 2.2.1. Reactivity with $[\text{Rh}(\text{cod})\text{Cl}]_2$

II. 2.2.1a. Synthesis, characterization and reactivity of neutral acylhydridorhodium(III) complexes.

The reaction of $[\text{Rh}(\text{cod})\text{Cl}]_2$ with the racemic mixture of the phosphine $\text{PPh}_2\text{CH}(\text{Ph})\text{CH}_2\text{CHO}$ and pyridine in a Rh:P:py = 1:1:2 ratio in dichloromethane at room temperature gives the acylhydride complex $[\text{RhClH}(\text{PPh}_2\text{CH}(\text{Ph})\text{CH}_2\text{CO})(\text{py})_2]$ (**22**). The displacement of the diolefin and the chelate assisted oxidative addition of the phosphine-aldehyde to the rhodium centre allow the formation of this complex (Scheme 59).



Scheme 59. Chelate-assisted formation of complex **22**.

Complex **22** was characterised in solution by ESI-MS and NMR spectroscopy. The ESI-MS spectroscopy shows a molecular ion at $m/z = 534.02$, which is in accordance with the $[M - \text{py} - \text{H}]^+$ ion, $[\text{RhCl}(\text{PPh}_2\text{CH}(\text{Ph})\text{CH}_2\text{CO})(\text{py})]^+$. NMR spectra show high diastereoselectivity for this reaction. The ^1H NMR spectrum (Figure 37) shows the presence of two hydride signals at -16.00 and -16.20 ppm, indicating the existence of two isomers of **22** in solution, in a 95:5 ratio respectively. The chemical shift is consistent with a hydride *trans* to an electronegative atom, such as chloride.⁴⁴ However, the possibility of the hydride being *trans* to pyridine cannot be excluded, as both exhibit a similar *trans* influence.⁴⁵ A two-dimensional COSY experiment allows the assignment of the multiplet signals at 3.86 and 3.06 ppm to the CHPh and CH_2 moieties in the aliphatic chain of the phosphine. The $^{31}\text{P}\{^1\text{H}\}$ NMR spectrum (Figure 37) shows two doublet signals ($J_{\text{Rh-P}} = 170$ Hz) at 97.9 and 93.9 ppm, the characteristic low field due to the formation of a five-membered ring.⁴⁶

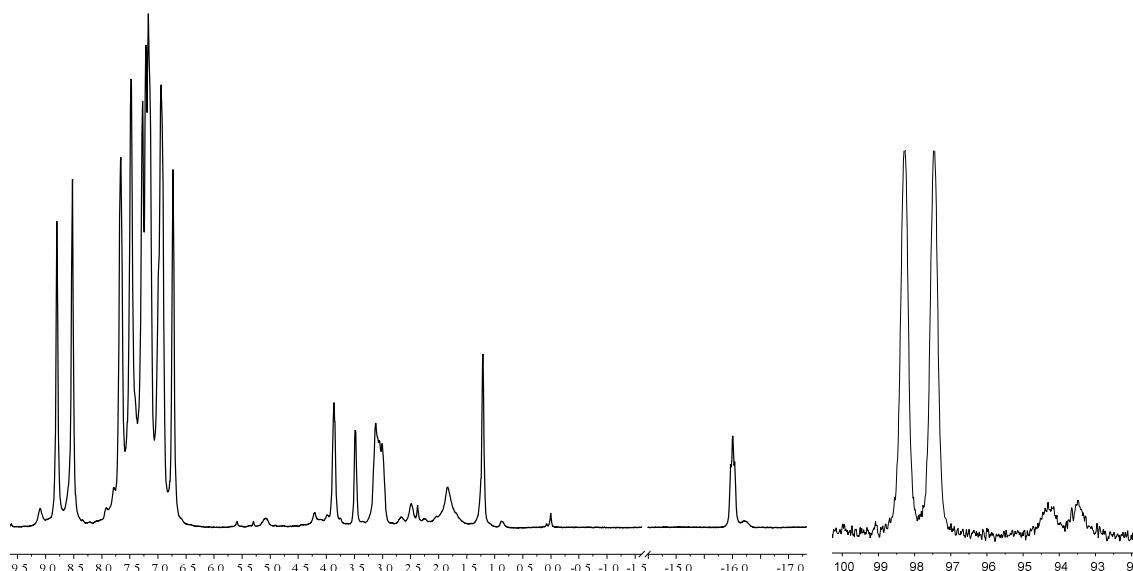


Figure 37. ^1H (left) and $^{31}\text{P}\{^1\text{H}\}$ (right) NMR of complex **22** in CDCl_3 .

The spectroscopic data agree with three possible geometric isomers of **22**, in which the hydride is located *trans* to chloride or pyridine (Figure 38). In addition, the oxidative addition of the phosphine leads to a chiral rhodium centre, which allows the formation of two diastereomers for each geometric isomer. Each diastereomer also includes a pair of enantiomeric species, named $\text{C}_{\text{Rh}}\text{R}_{\text{C}} / \text{A}_{\text{Rh}}\text{S}_{\text{C}}$ and $\text{C}_{\text{Rh}}\text{S}_{\text{C}} / \text{A}_{\text{Rh}}\text{R}_{\text{C}}$.

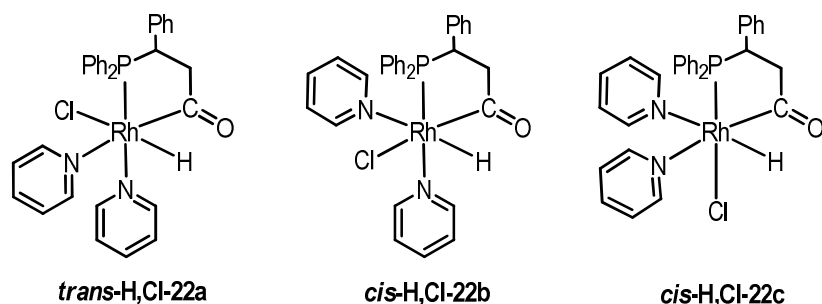


Figure 38. Possible geometric isomers for **22** in agreement with experimental data.

DFT calculations indicate the presence in solution of the diastereomeric pair of the geometric isomer with hydride *trans* to chloride (***trans*-H,Cl-22a** and ***trans*-H,Cl-22a'**), with the $C_{Rh}R_C / A_{Rh}S_C$ species (***trans*-H,Cl-22a**) as the major species in solution (Figure 39). The calculated diastereomeric ratio is in excellent agreement with the experimentally determined proportion.

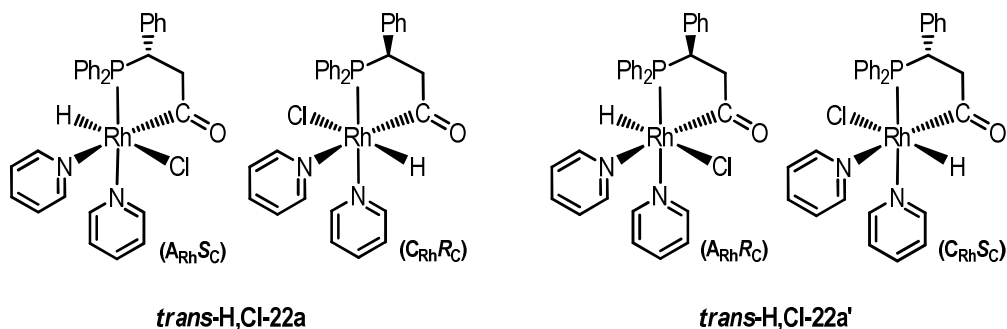
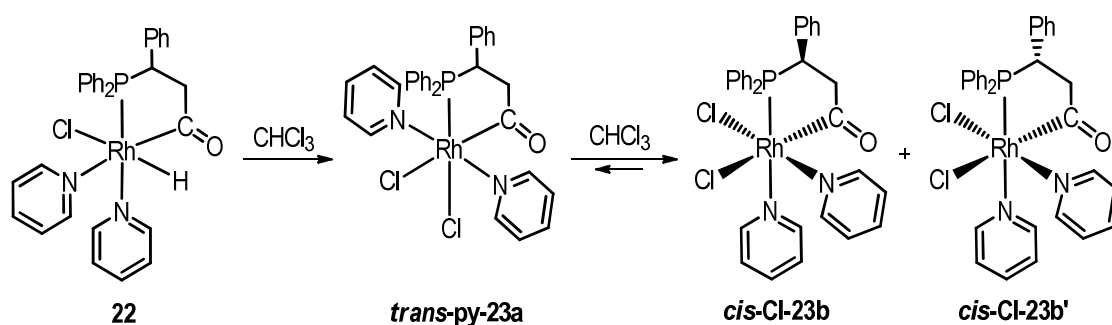


Figure 39. Enantiomeric species for diastereomers ***trans*-H,Cl-22a** and ***trans*-H,Cl-22a'**.

A NOE experiment confirmed ***trans*-H,Cl-22a** as the major species in solution (Supporting Information). Upon irradiation of the resonance at -16.00 ppm, no enhancement of the proton at the stereogenic centre was observed, while enhancement of the signal due to CH_2 was certainly observed.

As observed in similar hydride-rhodium(III) complexes with tethered phosphine $PPh_2(o-C_6H_4CO)$,²⁷ mentioned in the introduction of this chapter, complex **22** shows low stability in chlorinated solvents, and in chloroform solution exchange of hydride ligand by chloride is produced. This allows the formation of compound $[RhCl_2(PPh_2CH(Ph)CH_2CO)(py)_2]$ (**23**) as a mixture of three isomeric species with a higher proportion of one of them (***cis*-Cl-23b**), as shown in Scheme 60.



Scheme 60. Formation of **23** by chlorination in CHCl_3 solution, as a mixture of geometric isomers *trans*-py-**23a** and *cis*-Cl-**23** as a mixture of two diastereoisomers (*cis*-Cl-**23b** and *cis*-Cl-**23b'**).

This proposal is supported by ESI-MS spectroscopy, with the presence of a molecular ion at $m/z = 534.02$ corresponding to the $[\text{M} - \text{py} - \text{Cl}]^+$ ion $[\text{RhCl}(\text{PPh}_2\text{CH}(\text{Ph})\text{CH}_2\text{CO})(\text{py})]^+$. The ^1H NMR spectrum of **23** shows the presence of three groups of signals due to the aliphatic chain in the phosphine ligand, corresponding to three species in solution, in the 3-5.5 ppm range. The absence of a hydride signal confirms the chlorination of the compound. The $^{31}\text{P}\{^1\text{H}\}$ NMR spectrum shows two doublet signals at 74.4 and 72.5 ppm, assigned to two diastereoisomers of the species with both chloride and pyridine ligands mutually *cis* (*cis*-Cl-**23b** and *cis*-Cl-**23b'**). A third doublet signal at 66.4 ppm is assigned to a geometric isomer in which pyridines are located in a *trans* position (*trans*-py-**23a**), and therefore achiral at metal. This assignment was supported by DFT calculations, which indicate that these three isomers may coexist in solution, which would contain *cis*-Cl-**23b** as the major species and similar amounts of minor *cis*-Cl-**23b'** and *trans*-py-**23a**. Both *cis*-Cl-**23b** and *cis*-Cl-**23b'** exist as a mixture of two enantiomeric species (Figure 40).

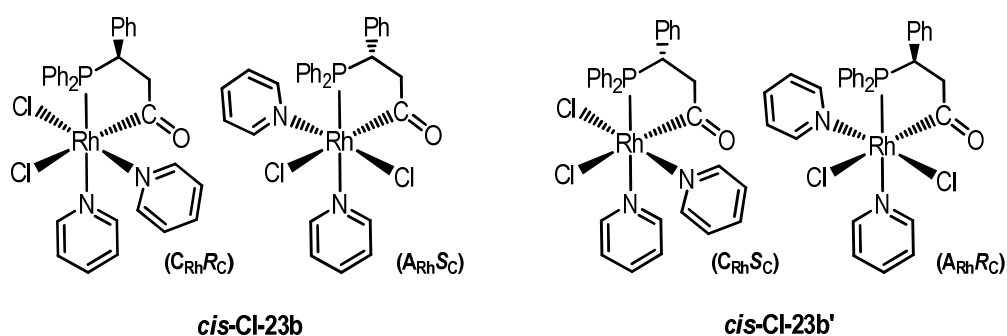


Figure 40. Enantiomeric species for diastereomers *cis*-Cl-**23b** and *cis*-Cl-**23b'**.

Formation of **23** in CDCl_3 was monitored by NMR (Figure 41). The fast formation of a kinetically favoured species (*trans*-py-**23a**) is observed in the first steps of the reaction. A slow concomitant isomerisation affords the geometric isomer *cis*-Cl, *cis*-py with chloride *trans* to

acyl as a mixture of two diastereomers (*cis*-Cl-**23b** and *cis*-Cl-**23b'**). Equilibrium between these three species is reached after 24 hours of reaction, with the total disappearance of the starting material **22** and a *cis*-Cl-**23b**/*cis*-Cl-**23b'**/*trans*-py-**23a** ratio of 48:24:28. The ^1H NMR spectra show the appearance of a signal due to CH_2Cl_2 .

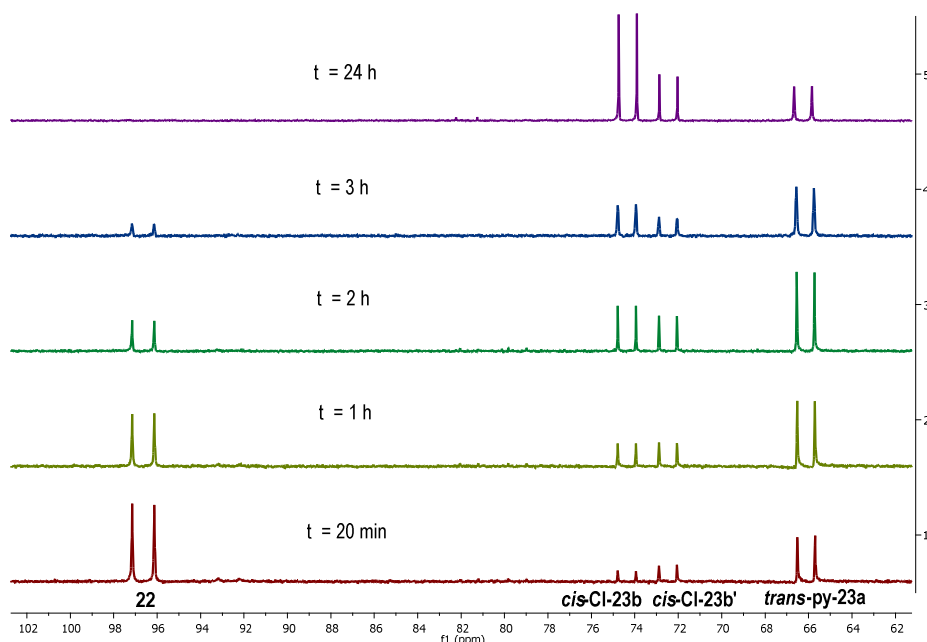


Figure 41. Monitoring of the formation of **23** by $^{31}\text{P}\{^1\text{H}\}$ NMR.

Repeated crystallisation of **23** allowed the formation of single crystals identified by NMR as the major species *cis*-Cl-**23b**, which was also characterised by X-ray diffraction (Figure 42). The crystal consists of pairs of $A_{\text{Rh}}S_{\text{C}}$ and $C_{\text{Rh}}R_{\text{C}}$ enantiomers. The geometry around the Rh(III) centre is pseudo octahedral, with the phosphorus atom (Rh1-P1 2.2776(9) Å) and the nitrogen of one pyridine ligand (Rh1-N1 2.151(3) Å) in the apical positions. The equatorial plane is occupied by the two chlorides (Rh1-Cl1 2.3528(8) Å and Rh1-Cl2 2.5673(6) Å) mutually *cis*, a second pyridine molecule (Rh1-N2 2.084(2) Å) and the carbon atom of the acyl-phosphine ligand (Rh1-C1 1.993(2) Å). The Rh-Cl and Rh-N distances evidence the acyl > phosphine > chloride \approx pyridine *trans* influence order of the ligands.⁴⁷

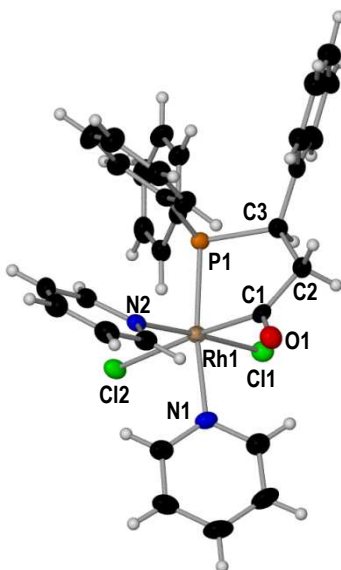
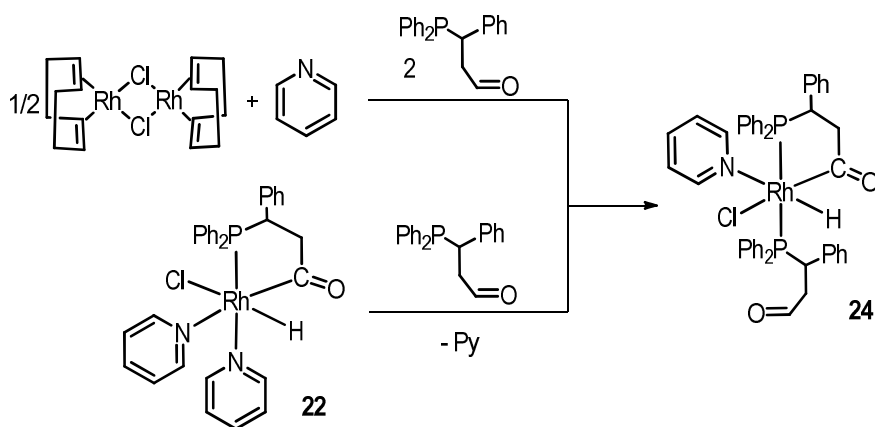


Figure 42. Molecular structure of compound *cis*-Cl-**23b**. Displacement ellipsoids are drawn at 50% probability level. Selected bond lengths (Å) and angles (°): Rh1–Cl1, 2.3528(8); Rh1–Cl2, 2.5673(6); Rh1–N1, 2.151(3); Rh1–N2, 2.084(2); Rh1–P1, 2.2776(9); Rh1–C1, 1.993(2); C1–O1, 1.195(4); Cl1–Rh1–N2, 177.37(6); P1–Rh1–N1, 170.42(6); C1–Rh1–Cl2, 175.76(8).

Reaction of the mixture of isomers of complex **22** with an additional molecule of the acylphosphine $\text{PPh}_2\text{CH}(\text{Ph})\text{CH}_2\text{CHO}$ in dichloromethane leads to the formation of compound $[\text{RhClH}(\text{PPh}_2\text{CH}(\text{Ph})\text{CH}_2\text{CO})(\text{PPh}_2\text{CH}(\text{Ph})\text{CH}_2\text{CHO})(\text{py})]$ (**24**) by displacement of one pyridine ligand. The second phosphine coordinates as P-monodentate and maintains a pendant aldehyde group, which neither undergoes insertion into the Rh–H bond nor promotes a second oxidative addition. Complex **24** can also be reached by direct reaction of $[\text{Rh}(\text{cod})\text{Cl}]_2$ with the racemic phosphine $\text{PPh}_2\text{CH}(\text{Ph})\text{CH}_2\text{CHO}$ and pyridine in a Rh:P:py = 1:2:1 ratio in dichloromethane at room temperature (Scheme 61), which affords a mixture of two isomers in a **24a**/**24a'** = 80:20 mixture.



Scheme 61. Formation of **24** from $[\text{Rh}(\text{cod})\text{Cl}]_2$ or from compound **22**.

The reaction of **22** with $\text{PPh}_2\text{CH}(\text{Ph})\text{CH}_2\text{CHO}$ was monitored by NMR (Figure 43), in which the appearance of two isomeric species (**24a** and **24a'**) in a 50:50 ratio can be observed at the first stages of the reaction. Subsequent transformation of **24a'** into **24a** occurs and the equilibrium is reached after 1 hour, with a **24a/24a'** = 80:20 mixture.

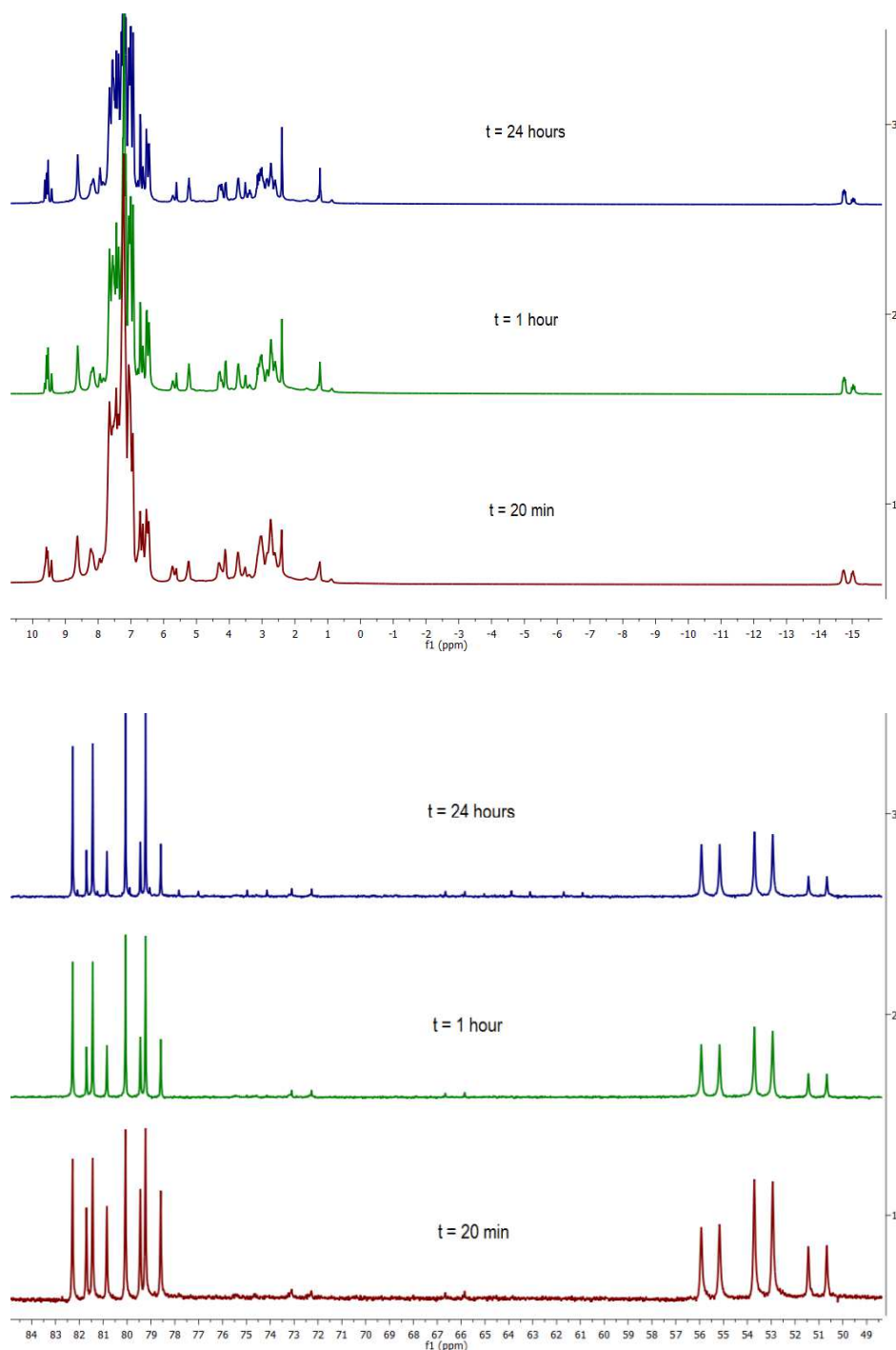


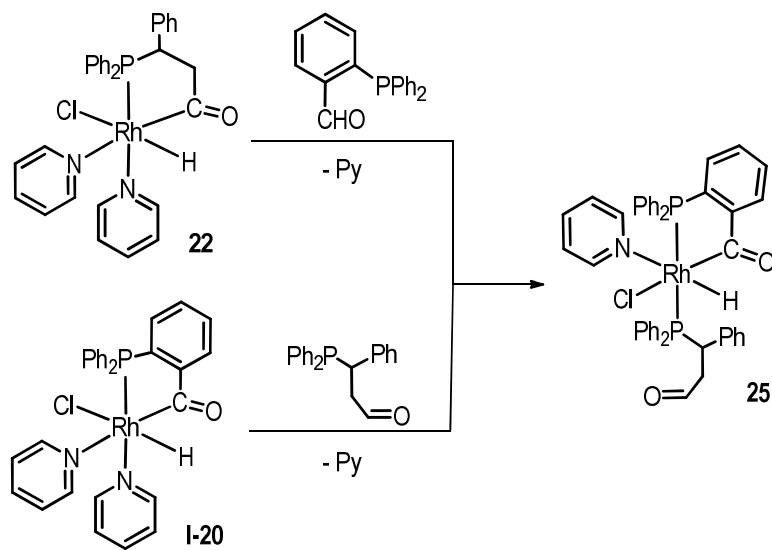
Figure 43. Monitoring of the reaction of **22** with $\text{PPh}_2\text{CH}(\text{Ph})\text{CH}_2\text{CHO}$ to afford **24** by ^1H (top) and $^{31}\text{P}\{^1\text{H}\}$ (bottom) NMR in CDCl_3 .

Formation of **24** is supported by ESI-MS, which shows a molecular ion at $m/z = 739.14$ corresponding to the $[M - py - Cl]^+$ ion $[RhH(PPh_2CH(Ph)CH_2CO)(PPh_2CH(Ph)CH_2CHO)]^+$. The $^{31}P\{^1H\}$ NMR spectrum shows an AMX spin system with two doublets of doublets for each isomer, which confirm the coordination of the two phosphine ligands. Each phosphine couples with the rhodium centre and with the other phosphorus atom. Resonances in the 80.5-79.5 ppm range correspond to the chelating acyl-phosphine, and signals in a lower range of 55.0-52.0 ppm are due to the P-monodentate phosphine. The J_{P-P} coupling constants (360 and 370 Hz) are characteristic of two phosphorus atoms mutually *trans*. The $^{13}C\{^1H\}$ NMR spectrum also shows the expected two doublets at 242.5 and 242.6 ppm ($J_{Rh-C} = 32-30$ Hz) corresponding to the coordinated acyl groups in the chelating ligand.

In the 1H NMR spectrum, doublet signals corresponding to the free aldehyde HC=O group can also be observed at 9.54 (**24a**) and 9.43 ppm (**24a'**), with J_{P-H} coupling constants of 5 and 3 Hz. A 2D HSQC experiment correlates these signals with doublets at 203 and 202 ppm in the $^{13}C\{^1H\}$ NMR spectrum, with J_{P-C} constants of 21 and 11 Hz respectively. Two hydride signals at -14.75 and -15.02 ppm, corresponding respectively to the two isomeric species **24a** and **24a'** in solution are also observed. The chemical shift values for hydride ligands suggest an electronegative atom in a *trans* position. The two isomeric species could therefore be geometric, due to exchange of the chloride and nitrogen relative position *trans* to hydride, or they could be diastereomers. A related complex derived from *o*-(diphenylphosphino)benzaldehyde with coordinated pyrazole was reported as only one isomer, with the chloride ligand *trans* to the acyl moiety and the N-donor ligand *trans* to the hydride.⁴⁸ Similarities with this compound and spectroscopic data enables us to propose compound **24** as a mixture of two diastereomers of the species shown in Scheme 61, with the hydride *trans* to pyridine and the two phosphine ligands mutually *trans*.

A remarkable diastereoselectivity is thus observed in the formation of complex **24**, containing three stereogenic centres, which leads to only two diastereomers in an 80:20 ratio. Consecutive reductive elimination and oxidative addition steps of the phosphine-aldehyde may allow the transformation of **24a'** into **24a** to reach the final proportion of the mixture. At variance with phosphino-arylaldehyde examples **I-22** and **I-25** mentioned in the introduction of this chapter,²⁷⁻²⁸ the formation of a hydroxyalkyl species by insertion of the pendant aldehyde into the Rh-H appears to be inhibited. This behaviour was previously observed in the reaction of $(CO)_5MnH$ with alkylaldehyde $PPh_2CH_2CH_2CHO$, in which the phosphine ligand remains κ^1 -P-coordinated without the formation of a five-membered metallacycle.³⁵

The reaction of the hydrido complex **22** with an arylaldehyde was then performed, with the aim of preparing a hydroxyalkyl derivative. However, treatment of complex **22** with an equivalent of $\text{PPh}_2(o\text{-C}_6\text{H}_4\text{CHO})$ in dichloromethane affords compound $[\text{RhClH}(\text{PPh}_2(o\text{-C}_6\text{H}_4\text{CO}))(\kappa^1\text{-PPh}_2(\text{CH}(\text{Ph})\text{CH}_2\text{CHO}))(\text{py})]$ (**25**), in which the insertion into the Rh-H bond neither occurs. Instead, an exchange between the alkylacyl and the arylaldehyde occurs (Scheme 62). The reductive elimination of the alkyl aldehyde and subsequent oxidative addition of the aryl aldehyde C-H to the Rh(I) centre would lead to the formation of **25**, with displacement of one pyridine ligand. Alternatively, the C-H activation of $\text{PPh}_2(o\text{-C}_6\text{H}_4\text{CHO})$ by oxidative addition or σ -bond metathesis promoted by rhodium(III) can precede the reductive elimination of the alkylaldehyde.⁴⁹ The lower steric hindrance in the metallacycle formed by aryl phosphines would explain the preferred oxidative addition of *o*-(diphenylphosphino)benzaldehyde.⁵⁰ Product **25** can also be formed by reaction of complex $[\text{RhH}(\text{PPh}_2(o\text{-C}_6\text{H}_4\text{CO}))\text{Cl}(\text{py})_2]$ ²⁷ (**I-20**) with one equivalent of alkyl phosphine $\text{PPh}_2\text{CH}(\text{Ph})\text{CH}_2\text{CHO}$, which displaces a pyridine ligand (Scheme 62).



Scheme 62. Formation of **25** from compounds **22** or $[\text{RhH}(\text{PPh}_2(o\text{-C}_6\text{H}_4\text{CO}))\text{Cl}(\text{py})_2]$, in dichloromethane at room temperature.

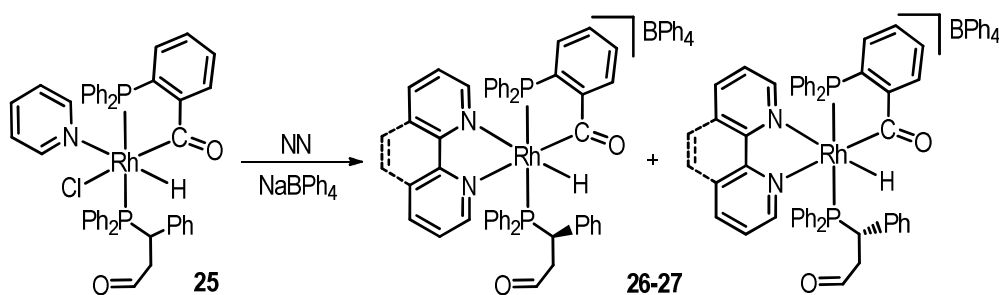
The ESI-MS spectroscopy of **25** shows a molecular ion at $m/z = 711.11$, which is in accordance with the $[\text{M} - \text{py} - \text{Cl}]^+$ ion, $[\text{RhH}(\text{PPh}_2(o\text{-C}_6\text{H}_4\text{CO}))(\kappa^1\text{-PPh}_2(\text{CH}(\text{Ph})\text{CH}_2\text{CHO}))]^+$. The ^1H NMR spectrum shows the presence of two isomers in an equimolar amount, with two hydride signals at -14.70 and -15.06 ppm as doublet of doublets of doublets (ddd), due to coupling to the rhodium centre and to the two coordinated phosphorus atoms. Two doublet signals at 9.44 and 9.56 ppm corresponding to the pendant aldehyde fragment are also observed, which

correlate to doublets at 202.0 and 203.0 ppm in the $^{13}\text{C}\{^1\text{H}\}$ NMR in a 2D HSQC experiment. In the $^{31}\text{P}\{^1\text{H}\}$ NMR spectrum, two doublet of doublets are observed for each isomer. The chelating aryl phosphine shows signals in the 63.5-63.0 ppm range while, as in **24**, the P-monodentate alkyl phosphine shows signals in the 55.0-52.0 ppm range. The $J_{\text{P-P}}$ coupling constants of 360 and 370 Hz agree with two phosphorus atoms in a *trans* disposition. A mixture of two diastereomeric species **25a** and **25a'** is therefore proposed, based on similarities with compound **24** and on spectroscopic data.

DFT calculations are in agreement with our proposal of **25** as shown in Scheme 62. Nevertheless, according to theoretical calculations a diastereomeric **25a/25a'** = 89:11 ratio is to be expected, with the major species **25a** corresponding to the $\text{C}_{\text{Rh}}\text{S}_{\text{C}}$ and $\text{A}_{\text{Rh}}\text{R}_{\text{C}}$ diastereomer. Our experimental **25a/25a'** = 50:50 ratio represents most likely a kinetic product that requires an isomerisation from **25a'** to **25a** to reach the estimated proportions, which could entail the reductive elimination of the arylaldehyde. The existence of kinetic barriers that hamper the transformation could explain the observed behaviour. The difference in diastereomeric ratios observed for **24** (80:20) and **25** (50:50) suggests a lower activation barrier for the diastereoisomerisation reaction to take place when involving alkylaldehydes (**24**) than when involving arylaldehydes (**25**).

II. 2.2.1b. Synthesis and characterization of cationic acylhydridorhodium(III) complexes with NN bidentate or PNN-terdentate ligands.

The reaction of compound **25** with aromatic diimines such as 1,10-phenantroline (phen) and 2,2'-bipyridine (bipy) afforded acylhydride cationic compounds in which N-donor ligands are coordinated in a bidentate fashion, by displacement of chloride and pyridine. These compounds were isolated in methanol as tetraphenylborate salts $[\text{RhH}(\text{NN})(\text{PPh}_2(o\text{-C}_6\text{H}_4\text{CO}))(\kappa^1\text{-PPh}_2(\text{CH}(\text{Ph})\text{CH}_2\text{CHO}))]\text{BPh}_4$ (NN = phen, **26**; bipy, **27**) (Scheme 63), in which the two phosphine ligands maintain a *trans* position. Spectroscopic data show the presence of two isomeric species in solution for **26** and **27** in a 50:50 and a 60:40 ratio respectively. As there are no possible geometric isomers with two phosphines mutually *trans*, these species can only be diastereomers. This confirms the proposal of complex **25** as a mixture of two diastereomeric species of a unique geometric isomer.



Scheme 63. Formation of compounds $[\text{RhH}(\text{NN})(\text{PPh}_2(o\text{-C}_6\text{H}_4\text{CO}))(\kappa^1\text{-PPh}_2(\text{CH}(\text{Ph})\text{CH}_2\text{CHO}))]\text{BPh}_4$ **26** (NN = phen) and **27** (NN = bipy).

Isolation of these compounds with tetraphenylborate as a counter anion allowed the separation of diastereomers due to their difference of solubility in chloroform. From the **26/26a'** equimolar mixture, **26a'** was isolated by precipitation, while **26a** remained in solution (Figure 44). Characterisation of the isomer **26a'** was carried out in dimethylsulfoxide. The ^1H NMR spectra showed signals corresponding to the pendant aldehyde and hydride at 9.56 and -12.85 ppm for species **26a**, and at 9.50 and -13.25 ppm for isomer **26a'**. From the solution of **27a/27a'** = 60:40 in chloroform, the precipitation of an equimolar mixture enabled the isolation of pure isomer **27a** in a low yield in the remaining solution. The ^1H NMR spectrum of **27a** showed a doublet for the pendant aldehyde at 9.52 ppm and a hydride signal at -13.21 ppm. For isomer **27a'**, the aldehyde shows a doublet at 9.47 ppm and the hydride appears at -13.53 ppm.

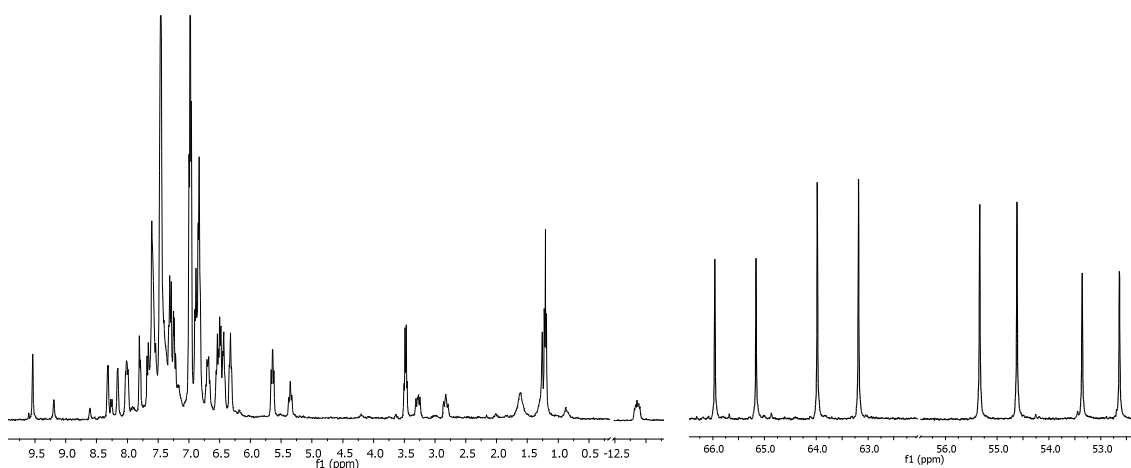


Figure 44. ^1H (left) and $^{31}\text{P}\{^1\text{H}\}$ (right) NMR of isolated complex **26a** in CDCl_3 .

The $^{31}\text{P}\{^1\text{H}\}$ NMR spectra of compounds **26** and **27** shows a set of two doublet of doublets, with signals corresponding to the chelating acylphosphine in the 64-66 ppm range and in the 51-54

ppm range for the monodentate alkylphosphine. The J_{p-p} coupling constants of 320-330 Hz confirm the *trans* position of the two phosphine ligands in the molecule.

Single crystals of **26a** suitable for X-ray diffraction were isolated from a chloroform solution of **26**. This complex crystallises as a mixture of $C_{Rh}R_C$ and $A_{Rh}S_C$ enantiomers. The structure of **26a** in the solid state (Figure 45) consists of a Rh(III) centre in a pseudo-octahedral geometry. The two phosphorus atoms occupy the apical positions *trans* to each other, with a P1–Rh1–P2 angle of 168.40(3)°. The Rh1–P1 bond distance (2.2721(8) Å) is shorter than the Rh1–P2 bond distance (2.3592(9) Å) due to P1 being part of a five-membered chelate, while P2 belongs to a monodentate phosphine.^{36,48} The equatorial plane includes the two nitrogen atoms of the phenantroline ligand *trans* to the hydride and the coordinated acyl moiety in the arylphosphine. The longer Rh1–N1 bond distance (2.193(3) Å) than the Rh1–N2 bond distance (2.157(3) Å) evidences a slightly larger *trans* effect of the acyl group than that of the hydride. The C20–O2 bond distance (1.199(6) Å) in the pendant aldehyde is slightly shorter than the C1–O1 bond distance of the acyl moiety bonded to the rhodium centre (1.235(4) Å), which may be due to the π -acceptor ability of the coordinated acyl group.

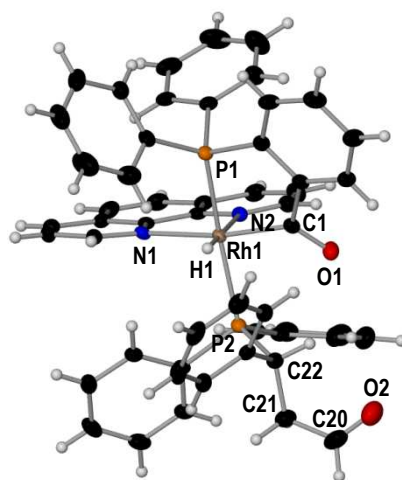
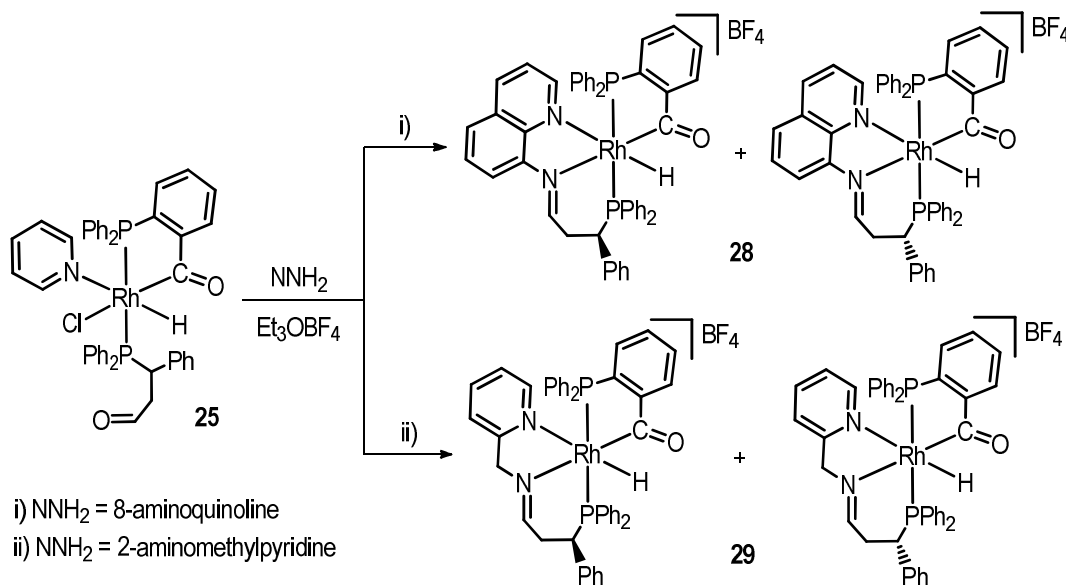


Figure 45. Molecular structure of the cationic unit of compound **26a**. Displacement ellipsoids are drawn at 50% probability level. Selected bond lengths (Å) and angles (°): Rh1–H1, 1.22(6); Rh1–C1, 1.993(4); Rh1–N1, 2.193(3); Rh1–N2, 2.157(3); Rh1–P1, 2.2721(8); Rh1–P2, 2.3592(9); C1–O1, 1.235(4); C20–O2, 1.199(6); P1–Rh1–P2, 168.40(3); C1–Rh1–N1, 169.6(1); N2–Rh1–H1, 179(2).

Reaction of compound **25** with bidentate aromatic and aliphatic amino-imines such as 8-aminoquinoline (aqui) and 2-aminomethylpyridine (ampy) yielded imination products by condensation of the free aldehyde and amine groups. Condensation reactions led to the formation of terdentate PNN hemilabile ligands that generate a six-membered metallacycle by

displacement of chloride and pyridine (Scheme 64). The resulting cationic compounds were isolated as tetrafluoroborate salts $[\text{RhH}(\text{PPh}_2(o\text{-C}_6\text{H}_4\text{CO}))(\text{PNN})]\text{BF}_4$ ($\text{PNN} = \kappa^3\text{-PPh}_2(\text{CH}(\text{Ph})\text{CH}_2\text{CNC}_9\text{H}_6\text{N}, \mathbf{28}; \kappa^3\text{-PPh}_2(\text{CH}(\text{Ph})\text{CH}_2\text{CNCH}_2\text{C}_5\text{H}_4\text{N}, \mathbf{29})$).



Scheme 64. Formation of compounds $[\text{RhH}(\text{PPh}_2(o\text{-C}_6\text{H}_4\text{CO}))(\text{PNN})]\text{BF}_4$ **28** ($\text{NNH}_2 = \text{aqui}$) and **29** ($\text{NNH}_2 = \text{ampy}$) in dichloromethane.

Final products are a mixture of two diastereomers in a **28a/28a'** = 55:45 and **29a/29a'** = 60:40 ratio. Attempts to separate these isomeric species proved to be unsuccessful. The ^1H NMR spectra (Figure 46) of these compounds show two hydride signals as doublet of doublets of doublets (ddd) due to coupling to rhodium and to both phosphorus atoms in each phosphine ligand. Singlet signals observed in the 8.7-9.4 ppm range correspond to the newly formed imine $\text{HC}=\text{N}$ group. 2D HSQC experiments correlate these singlets to signals in the 173-177 ppm range in the $^{13}\text{C}\{^1\text{H}\}$ NMR spectra. Coordinated acyl groups show doublet signals in the 239-242 ppm range in the $^{13}\text{C}\{^1\text{H}\}$ NMR, with a $J_{\text{Rh-C}}$ coupling constant of 30 Hz. The $^{31}\text{P}\{^1\text{H}\}$ NMR spectra (Figure 46) show resonances in the 56-62 ppm range corresponding to the chelating acyl phosphine, while the phosphorus atom in the PNN ligand shows signals at lower frequency, varying from 55 to 45 ppm.

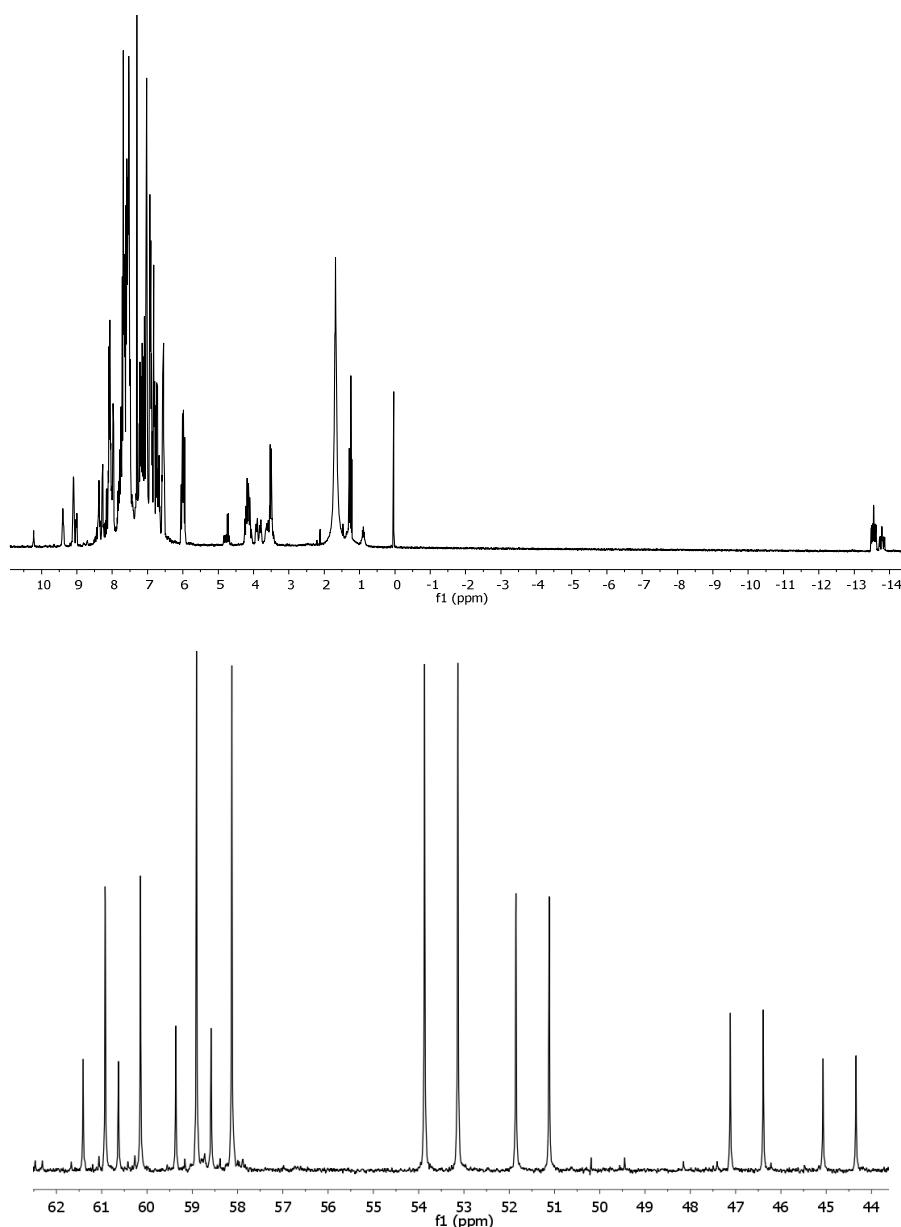


Figure 46. ^1H (top) and $^{31}\text{P}\{^1\text{H}\}$ (bottom) NMR of the mixture of **28a** and **28a'** in CDCl_3 .

Isolation of single crystals of **28a** allowed the characterisation of this compound by X-ray diffraction (Figure 47). The crystals contain a mixture of $A_{\text{Rh}}S_{\text{C}}$ and $C_{\text{Rh}}R_{\text{C}}$ enantiomers. The solid state structure shows the rhodium(III) centre in a distorted octahedron, where the terdentate PNN ligand adopts a facial disposition, with the formation of a six-membered metallacycle. The P2 phosphorus atom of the hemilabile PNN ligand and the P1 atom of the arylphosphine are located mutually *trans* in the apical positions, with a P1–Rh1–P2 angle of $164.13(5)^\circ$. The P1–Rh1 bond distance of $2.2802(12) \text{ \AA}$ is shorter than the P2–Rh1 bond distance ($2.3213(12) \text{ \AA}$), which could be due to P1 being part of a five-membered metallacycle.²⁵ The acyl group *trans* to the nitrogen N1 atom of the new C=N imino moiety, and the hydride ligand *trans* to the heterocyclic N2 atom form the equatorial plane. The formation of the imine is confirmed by

the N1–C20 bond distance of 1.294(6) Å and the N1–C20–C21 angle of 120.3(4)°. Both Rh–N distances are equal, indicating a similar *trans* influence for the hydride and the acyl fragment in the arylphosphine. A similar structure was reported for a complex derived from *o*-(diphenylphosphino)benzaldehyde and 8-aminoquinoline,²⁴ mentioned in the introduction of this chapter (**I-16**), in which the terdentate PNN ligand was generated by condensation of the aldehyde group in PPh₂(*o*-C₆H₄CHO) with the amino-imine.

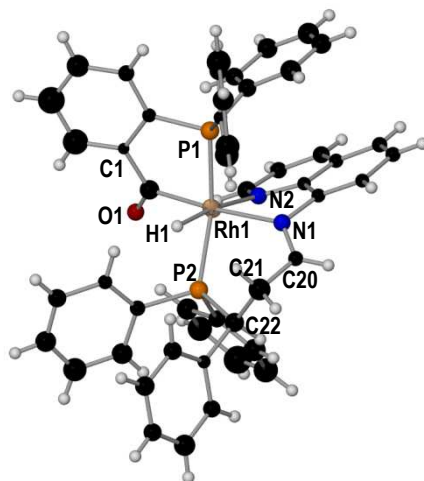
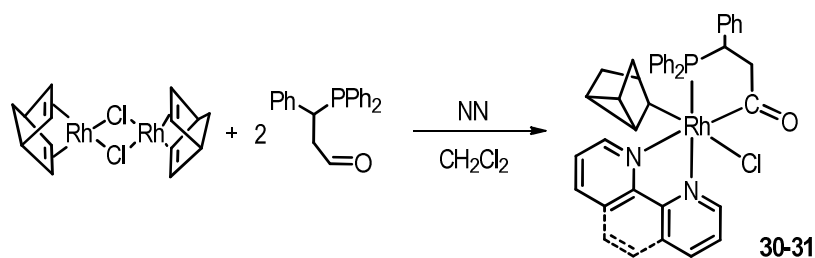


Figure 47. Molecular structure of the cationic unit of compound **28a**. Displacement ellipsoids are drawn at 50% probability level. Selected bond lengths (Å) and angles (°): Rh1–H1, 1.4392; Rh1–C1, 2.006(4); Rh1–N1, 2.163(4); Rh1–N2, 2.166(4); Rh1–P1, 2.2802(12); Rh1–P2, 2.3213(12); C1–O1, 1.201(5); C20–N1, 1.294(6); P1–Rh1–P2, 164.13(5); C1–Rh1–N1, 172.05(16); N2–Rh1–H1, 175.8; N1–C20–C21, 120.3(4).

A previous publication described the reaction of a complex related to **25**, derived from *o*-(diphenylphosphino)benzaldehyde, and 2-aminomethylpyridine leading to a complex related to **29** but containing a stable hemiaminal -CH(OH)NH- fragment. Hemiaminals are intermediates in the imination reactions that usually lose water readily to afford the imine.⁵¹ However, this result is not repeated in the presence of the alkyl-phosphine PPh₂(CH(Ph)CH₂CHO), where the condensation reaction leads to the final imine product **29**. The higher flexibility of the aliphatic chain in the present phosphine could explain this behaviour, as it would facilitate the final step in the condensation between the pendant aldehyde and the amine groups.

II.2.2.2. Reactivity with $[\text{Rh}(\text{nbd})\text{Cl}]_2$. Alkyl(phosphinoacyl)- and alkyl(phosphinoester)- rhodium(III) complexes

As previously reported for *o*-(diphenylphosphino)benzaldehyde,²⁶⁻²⁸ the results discussed in this chapter showed that the oxidative addition of $\text{PPh}_2\text{CH}(\text{Ph})\text{CH}_2\text{CHO}$ to neutral $[\text{Rh}(\text{cod})\text{Cl}]_2$ complex also led to the displacement of the cyclooctadiene. The reaction of tethered aldehydes with (norbornadiene)rhodium derivatives, on the other hand, can yield σ -norbornenyl or nortricyclyl derivatives by oxidative addition of the aldehyde, followed by the insertion of the olefin into the Rh-H bond.³⁰⁻³² Treatment of complex $[\text{Rh}(\text{nbd})\text{Cl}]_2$ with alkylphosphine $\text{PPh}_2\text{CH}(\text{Ph})\text{CH}_2\text{CHO}$ led to the same outcome. Subsequent addition of N-donor diimines such as 1,10-phenanthroline and 2,2'-bipyridine, in dichloromethane at room temperature, yielded σ -nortricyclyl derivatives $[\text{RhCl}(\text{NN})(\text{ntr})](\text{PPh}_2\text{CH}(\text{Ph})\text{CH}_2\text{CO})$ (NN = phen, **30**; bipy, **31**) (Scheme 65). The σ -nortricyclyl ligand is formed by a ring closure reaction from the σ -norbornenyl species.



Scheme 65. Formation of compounds $[\text{RhCl}(\text{NN})(\text{ntr})](\text{PPh}_2\text{CH}(\text{Ph})\text{CH}_2\text{CO})$ (NN = phen, **30**; bipy, **31**).

Spectroscopic NMR data of **30** and **31** in solution show two isomers in a 75:25 mixture. We propose the presence of two diastereomers of a single geometric isomer, with a preference for one particular species. In reported complexes synthesised from the reaction of $[\text{Rh}(\text{nbd})\text{Cl}]_2$ with *o*-(diphenylphosphino)benzaldehyde,³⁰ (**I-29** and **I-30**) a single geometric isomer is also described. Computational DFT calculations confirm the proposal in Scheme 65, but reveal a complete selectivity for one diastereomer. Our experimental results show a kinetic ratio and lack of isomerisation to obtain the thermodynamic ratio.

In the $^{31}\text{P}\{^1\text{H}\}$ NMR spectra two doublets can be observed at 77.2 and 80.9 ppm for **30a** and **30a'**, and at 78.9 and 80.6 ppm for **31a** and **31a'** respectively. ^1H NMR spectra confirm the presence of the coordinated σ -nortricyclyl with a group of signals in the 1.77 to -1.17 ppm range. These include multiplets at 1.10 and 1.25 ppm corresponding to the proton of the carbon atom coordinated to the rhodium centre, which correlate with doublets at 39.0 and

40.0 ppm respectively in the $^{13}\text{C}\{^1\text{H}\}$ NMR spectra. Multiplets from 0.3 to -1.2 ppm correspond to the cyclopropyl moiety in the ligand. The coordinated acyl group shows resonances in the 244-247 ppm range in the $^{13}\text{C}\{^1\text{H}\}$ NMR spectrum. Figure 48 shows the ^1H and $^{31}\text{P}\{^1\text{H}\}$ NMR spectra of compound **30**.

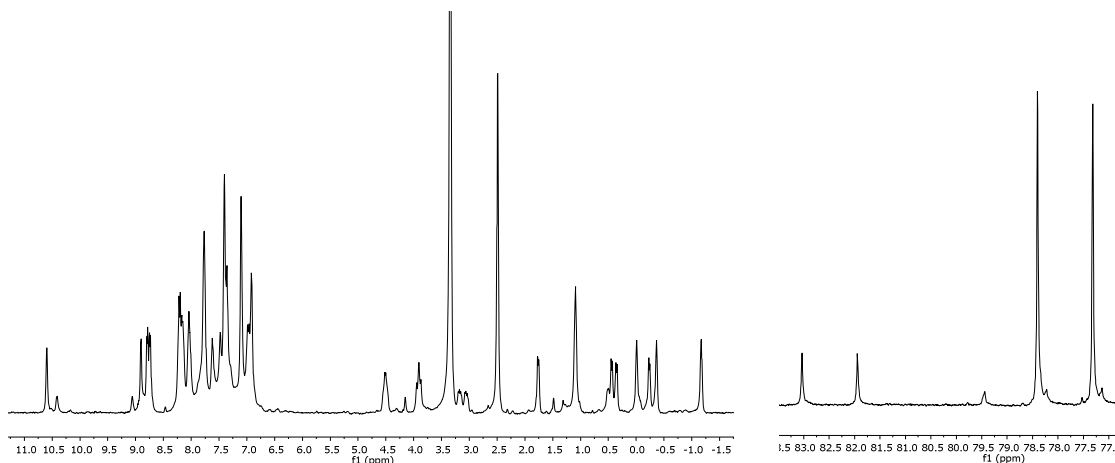


Figure 48. ^1H (left) and $^{31}\text{P}\{^1\text{H}\}$ (right) NMR of the mixture of **30a** and **30a'** in CDCl_3 .

Compound **31** was also characterised by X-ray diffraction analysis (Figure 49). Isolated single crystals correspond to diastereomer **31a**, and are formed by the pair of $A_{\text{Rh}}S_{\text{C}}$ and $C_{\text{Rh}}R_{\text{C}}$ enantiomers, predicted as the most stable by DFT calculations. The structure in the solid state is in good agreement with the structure deduced from spectroscopic data in solution. The rhodium(III) centre is in a pseudo octahedron, in which axial positions are occupied by the phosphorus atom and one of the nitrogen atoms of the bipyridine ligand, with a P1-Rh-N1 angle of $179.06(9)^\circ$. The equatorial plane is formed by nortricyclyl *trans* to the chloride ligand, and the acyl moiety of the phosphine *trans* to the other N atom of the bipyridine. The larger *trans* influence of the acyl group is again evidenced in the slightly larger Rh-N2 distance ($2.193(3) \text{ \AA}$) compared to the Rh-N1 bond distance ($2.146(3) \text{ \AA}$), which is located *trans* to phosphorus. The Rh1-C1 (nortricyclyl) bond distance ($2.103(5) \text{ \AA}$) is significantly longer than the distance observed for the Rh1-C8 (acyl) distance ($1.997(4) \text{ \AA}$). This could be due to the different hybridization of $\text{C1}(\text{sp}^3)$ and $\text{C8}(\text{sp}^2)$ carbon atoms, and to C8 being part of a five-membered metallacycle. All carbon-carbon distances in the nortricyclyl moiety agree with single bond distances.

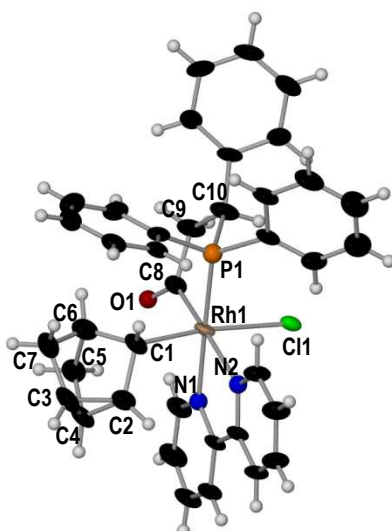
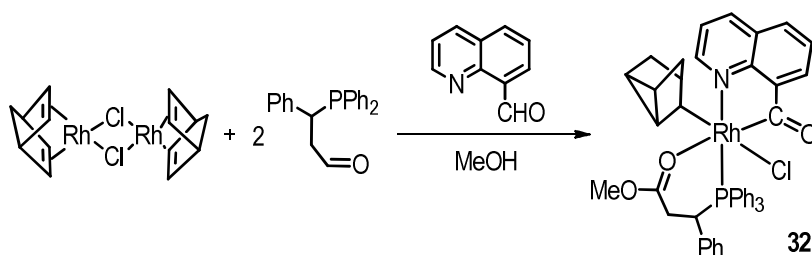


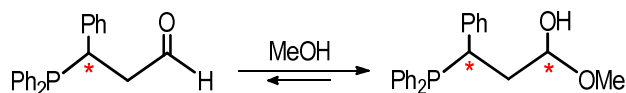
Figure 49. Molecular structure of compound **31a**. Displacement ellipsoids are drawn at 50% probability level. Selected bond lengths (Å) and angles (°): Rh1–P1, 2.270(1); Rh1–Cl1, 2.520(1); Rh1–C1, 2.103(5); Rh1–N1, 2.146(3); Rh1–N2, 2.193(3); Rh1–C8, 1.997(4); C8–O1, 1.218(5); C1–C2, 1.538(6); C2–C3, 1.515(7); C2–C4, 1.518(7); C3–C4, 1.506(8); C4–C5, 1.518(8); C1–Rh1–P1, 90.5(1); C8–Rh1–C1, 97.4(1); C8–Rh1–N1, 98.4(1); C1–Rh1–N1, 90.4(1); N1–Rh1–N2, 76.0(1); C8–Rh1–N2, 174.0(1); C1–Rh1–Cl1, 172.4(1); P1–Rh1–N1, 179.06(9).

The reaction of the (norbornadiene)rhodium(I) dimer with the phosphine-alkylaldehyde and other tethered aldehydes was also attempted. Treatment of $[\text{Rh}(\text{nbdc})\text{Cl}]_2$ with two equivalents of $\text{PPh}_2\text{CH}(\text{Ph})\text{CH}_2\text{CHO}$ and 8-quinolinecarboxaldehyde in methanol led to the formation of the neutral compound $[\text{RhCl}(\text{nty})](\text{C}_9\text{H}_6\text{NCO})(\text{k}^2\text{-PPh}_2\text{CH}(\text{Ph})\text{CH}_2\text{CO}(\text{OCH}_3))$ (**32**), as a single diastereomer. In this complex, the quinoline ligand forms a five-membered metallacycle by aldehyde C-H oxidative addition to the rhodium centre. The insertion of norbornadiene into the Rh-H bond and subsequent rearrangement leads to the σ -nortricyclyl species. Interestingly, the phosphine coordinates as a chelate via the phosphorus and oxygen atoms by formation of an ester (Scheme 66). When the reaction was performed in an aprotic solvent such as dichloromethane, a complex product mixture was obtained.



Scheme 66. Formation of compound $[\text{RhCl}(\text{nty})](\text{C}_9\text{H}_6\text{NCO})(\text{k}^2\text{-PPh}_2\text{CH}(\text{Ph})\text{CH}_2\text{CO}(\text{OCH}_3))$ (**32**).

The formation of **32** was monitored by $^{31}\text{P}\{^1\text{H}\}$ NMR in CD_3OD (Figure 50). Dissolution of $\text{PPh}_2\text{CH}(\text{Ph})\text{CH}_2\text{CHO}$ in methanol promotes the transformation into the hemiacetal species, with the generation of two diastereomers by formation of a second chiral carbon (Scheme 67). This behaviour was also observed in reported examples with phosphino-aldehyde $\text{PPh}_2\text{CH}(\text{Ph})\text{CH}(\text{Me})\text{CHO}$ in methanol solution.³⁶



Scheme 67. Hemiactal formation in a methanol solution of $\text{PPh}_2\text{CH}(\text{Ph})\text{CH}_2\text{CHO}$.

Upon addition of $[\text{Rh}(\text{nbd})\text{Cl}]_2$ to the mixture, the phosphine-hemiacetal coordinates to the rhodium centre to give a mixture of two isomers of an intermediate $[\text{RhCl}(\text{nbd})(\text{PPh}_2(\text{CH}(\text{Ph})\text{CH}_2\text{CH}(\text{OMe})(\text{OH})))]$, which exhibit doublet signals at 37.1 ($J_{\text{Rh,P}} = 173$ Hz) and at 35.7 ppm ($J_{\text{Rh,P}} = 173$ Hz) in the $^{31}\text{P}\{^1\text{H}\}$ NMR spectrum. Evidences of a metallacycle formation by oxidative addition of the phosphine are not observed. When 8-quinolinecarboxaldehyde is added, it coordinates to rhodium by chelate-assisted oxidative addition, with the subsequent Rh-H insertion and rearrangement of the olefin to yield the σ -nortricycyl ligand. Dehydrogenation of the hemiacetal to form the ester fragment allows the coordination of the oxygen atom to form a six-membered metallacycle. Dehydrogenation of hemiacetals to give ester derivatives is proposed as an intermediate step in the transition metal catalysed esterification of alcohols.⁵² Hydrogen gas is released in these transformations, which in some cases is accepted by a sacrificial molecule. The high yield (91%) obtained for **32** implies this to be an acceptorless dehydrogenation.

As shown in Figure 50, **32** is originally formed as a mixture of two diastereomers that evolves into a single species. The transformation of one isomeric species to another may occur through a pentacoordinated intermediate formed by opening of the ester-phosphine chelate. Metal inversion in five-coordinated complexes has been reported.⁵³

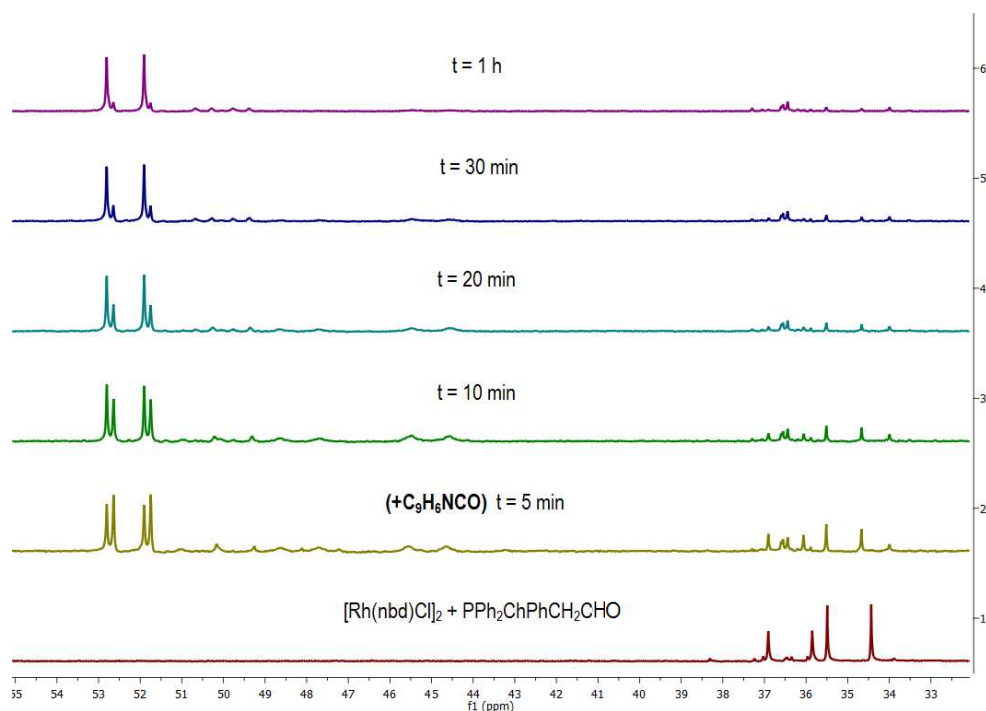


Figure 50. Monitoring of the formation of **32** by $^{31}\text{P}\{^1\text{H}\}$ NMR in CD_3OD .

The $^{31}\text{P}\{^1\text{H}\}$ NMR spectrum of **32** shows a doublet at 52.4 ppm, with a $J_{\text{Rh-P}}$ coupling constant of 184 Hz. Coordination of the nortricycyl ligand can be observed by ^1H NMR, with a group of multiplet signals from 2.11 to -0.49 ppm. The resonance at 1.05 ppm corresponds to the carbon atom coordinated to the rhodium centre, which correlates to a doublet signal at 42.6 ppm ($J_{\text{Rh-C}} = 28$ Hz) in the $^{13}\text{C}\{^1\text{H}\}$ NMR spectrum, and multiplets at -0.49, 0.06 and 0.35 ppm in the ^1H NMR spectrum correspond to the cyclopropyl fragment. The methyl group in the ester moiety shows a signal at 4.01 ppm, which correlates to a singlet signal at 53.6 ppm in the $^{13}\text{C}\{^1\text{H}\}$ NMR. The acyl group in the ester fragment shows a singlet at 180.2 ppm, whereas the coordinated acyl on the quinoline can be observed at 222.9 ppm in the $^{13}\text{C}\{^1\text{H}\}$ NMR spectrum, with a $J_{\text{Rh-C}}$ coupling constant of 39 Hz. The ESI-MS of **32** shows a molecular ion at $m/z = 700.15$, in accordance with the $[\text{M} - \text{Cl}]^+$ ion $[\text{Rh}(\text{ntyl})(\text{C}_9\text{H}_6\text{NCO})(\text{k}^2\text{-PPh}_2\text{CH}(\text{Ph})\text{CH}_2\text{CO}(\text{OCH}_3))]^+$.

Compound **32** was also characterised by X-ray diffraction. Single crystals consist of a mixture of $A_{\text{Rh}}S_{\text{C}}$ and $C_{\text{Rh}}R_{\text{C}}$ enantiomers, with the phenyl group of the chiral carbon atom furthest away from the nortricycyl ligand, as expected on DFT calculations. The structure of **32** in the solid state is in good agreement with the one proposed from spectroscopic data (Figure 51). The geometry adopted around the rhodium(III) centre is pseudo-octahedral, with the phosphorus atom *trans* to the nitrogen in the quinoline ligand with a N1-Rh1-P1 angle of $178.63(6)^\circ$. The equatorial plane is formed by the chloride *trans* to the nortricycyl moiety, and the acyl group in the quinoline *trans* to the coordinated oxygen in the newly formed ester fragment. The

solid-state structure confirms the bidentate coordination of the phosphino-ester ligand to the metal through the phosphorus atom and the oxygen of the carbonyl group. This coordination leads to a six-membered metallacycle in a distorted chair conformation, whereas the five-membered ring formed by the quinoline adopts a quasi-planar geometry. The carbonyl moieties in both chelating ligands show equal bond distances (C8–O1 1.219(3) Å and C38–O2 1.224(3) Å). All carbon-carbon distances in the nortricycyl ligand are equal and agree with single bond distances.

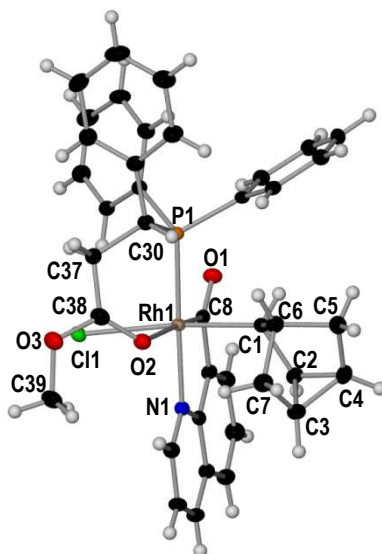
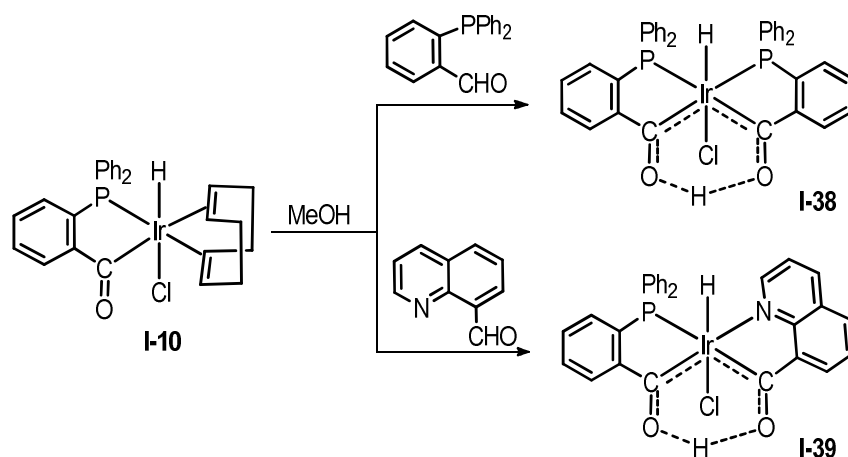


Figure 51. Molecular structure of compound **32** (50% probability ellipsoids). Selected bond lengths (Å) and angles ($^{\circ}$): Rh1–Cl1, 2.5371(6); Rh–C1, 2.105(2); Rh–C8, 1.941(2); Rh–N1, 2.105(2); Rh–O2, 2.365(2); Rh–P1, 2.2929(7); C8–O1, 1.219(3); C38–O2, 1.224(3); C38–O3, 1.334(3); C1–C2, 1.527(63); C2–C3, 1.519(3); C2–C4, 1.518(4); C3–C4, 1.521(4); C4–C5, 1.516(4); C5–C6, 1.545(4); C6–C7, 1.536(3); Cl1–Rh1–C1, 173.96(6); C8–Rh1–O2, 173.59(7); N1–Rh1–P1, 178.63(6).

II.2.3. THE REACTION OF $[\text{Rh}(\text{nbd})\text{Cl}]_2$ WITH 8-QUINOLINECARBOXALDEHYDE AND PYRAZOLE. REACTIVITY AND CATALYTIC APPLICATIONS.

In the previous section we have described the C-H activation of the alkylaldehyde in $\text{PPh}_2\text{CH}(\text{Ph})\text{CH}_2\text{CHO}$ by diolefinic rhodium complexes that leads to the chelate-assisted formation of hydrido- or alkyl-acyl rhodium(III) derivatives. We have also observed that the C-H activation of potentially chelating arylaldehydes such as $\text{PPh}_2(o\text{-C}_6\text{H}_4\text{CHO})$ or $\text{C}_9\text{H}_6\text{CHO}$ is competitive with that of the alkylaldehyde, so that the C-H activation of the former is usually preferred.

It is known that the reaction of $[\text{Ir}(\text{cod})\text{Cl}]_2$ with $\text{PPh}_2(o\text{-C}_6\text{H}_4\text{CHO})$ allows the formation of the acyl-hydride-diolefin iridium(III) chelate complex $[\text{IrClH}(\kappa^2\text{-PPh}_2(o\text{-C}_6\text{H}_4\text{CO}))(\text{cod})]$ (**I-10**).¹² The addition of a second molecule of the phosphine $\text{PPh}_2(o\text{-C}_6\text{H}_4\text{CHO})$ to this complex in a polar solvent leads to the displacement of the diolefin, to afford the hydrido-irida- β -diketone derivative $[\text{IrClH}((\kappa^2\text{-PPh}_2(o\text{-C}_6\text{H}_4\text{CO}))_2\text{H})]$ (**I-38**).⁵⁴ A mixed $[\text{IrClH}((\kappa^2\text{-PPh}_2(o\text{-C}_6\text{H}_4\text{CO}))(\kappa^2\text{-C}_9\text{H}_6\text{NCO})\text{H})]$ (**I-39**) species has also been prepared by reaction of **I-10** with the quinoline $\text{C}_9\text{H}_6\text{NCHO}$ (Scheme 68).⁵⁵

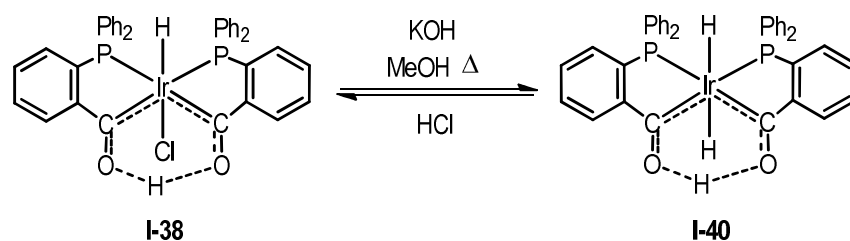


Scheme 68. Formation of hydrido-irida- β -diketone complexes with $\text{PPh}_2(o\text{-C}_6\text{H}_4\text{CHO})$ and $\text{C}_9\text{H}_6\text{NCHO}$ chelating aldehydes.

Metalla- β -diketones are species that contain an acyl and a hydroxycarbene group, which are stabilised by the presence of a strong intramolecular $\text{O}\cdots\text{H}\cdots\text{O}$ hydrogen bond. They were first synthesised by Lukehart et al. by protonation of diacylmetalate anions $[\text{L}_x\text{M}(\text{COR})(\text{COR}')]$ ($\text{M} = \text{Mo}, \text{W}, \text{Mn}, \text{Re}, \text{Fe}, \text{Os}$).⁵⁶ It has been proposed that the formation of the hydrido-irida- β -

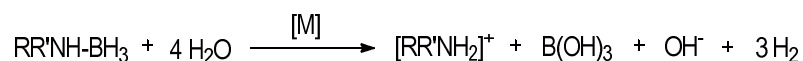
diketone species **I-38-39** would be preceded by chelate-assisted oxidative addition of aldehyde leading to a cationic diacyl-dihydride iridium(V) $[\text{Ir}(\text{H})_2(\kappa^2\text{-PPh}_2(o\text{-C}_6\text{H}_4\text{CO}))_2]\text{Cl}$ intermediate, which would undergo Ir-to-O hydrogen transfer to generate the final product.^{54,55}

The reaction of neutral complex **I-38** with KOH in refluxing methanol leads to a new dihydrido-irida- β -diketone $[\text{IrH}_2((\kappa^2\text{-PPh}_2(o\text{-C}_6\text{H}_4\text{CO}))_2\text{H})]$ (**I-40**) by formal exchange of chloride by hydride (Scheme 69).⁵⁷ Dehydrodechlorination of **I-38** by base to afford a pentacoordinated Ir(III) intermediate that would allow the coordination of methoxide is proposed in the formation of this compound. Subsequent β -H transfer would give a dihydride, with liberation of formaldehyde, and protonation of the diacyl fragment could lead to the β -diketone **I-40** species.⁵⁸ Treatment of **I-40** with HCl gas affords the **I-38** starting product.



Scheme 69. Formation of neutral dihydrido-irida- β -diketone.

Hydrido-irida- β -diketone species proved to be efficient homogeneous catalysts for the hydrolysis of amine- or ammonia-boranes to release hydrogen gas, at room temperature, in the presence of air and in THF- H_2O mixtures, according to scheme 70.⁵⁹ Complex **I-38** was reported as the first metal-based homogeneous catalyst for this reaction.

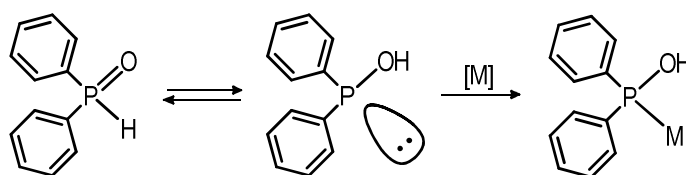


Scheme 70. Hydrolysis reaction of amine-boranes to generate hydrogen gas.

The search for a clean and available source of energy as an alternative for fossil fuels encourages the study of these reactions. Hydrogen is considered a feasible emission-free alternative. However, safe handling and storage of hydrogen gas are still unsolved problems.⁶⁰ Hydrogen storage materials, such as amine-boranes, allow a controlled evolution of hydrogen gas through a chemical reaction and can be used as a hydrogen source for portable cells.⁶¹ A large number of heterogeneous systems are known to efficiently catalyse the hydrogen release from amine-borane substrates, in anhydrous systems and by hydrolysis.^{62,63} In contrast, homogeneous systems for the hydrolysis reaction have been less studied, and examples are

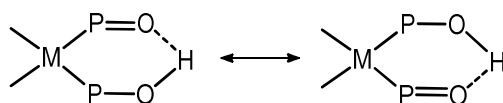
scarce. A few efficient catalysts based on iridium^{64,65} or ruthenium⁶⁶⁻⁶⁸ have been reported. Efficient rhodium-based homogeneous catalytic systems have also been recently developed in our laboratory.^{69,70} These rhodium catalysts present a common feature with hydrido-irida- β -diketones. They consist of hydrido-acyl rhodium(III) complexes with ligands capable of intramolecular hydrogen bond interactions, such as diphenylphosphinous acid (O-H \cdots O) or pyrazoles (N-H \cdots O).

Secondary phosphine oxides (SPOs), such as $\text{PPh}_2(\text{O})\text{H}$, are capable of intra- and intermolecular hydrogen bond interactions when they are κ^1 -*P*-coordinated to a metal centre. These ligands exist as two tautomeric isomers in equilibrium, the pentavalent oxide form $\text{RR}'\text{P}(\text{O})\text{H}$, and the phosphinous acid form $\text{RR}'\text{P}-\text{OH}$ (Scheme 71).⁷¹ Aromatic and aliphatic R substituents favour the pentavalent form, which is not capable of *P*-coordination. However, transition metals promote tautomerisation and stabilise the trivalent form by *P*-coordination (Scheme 71).⁷²



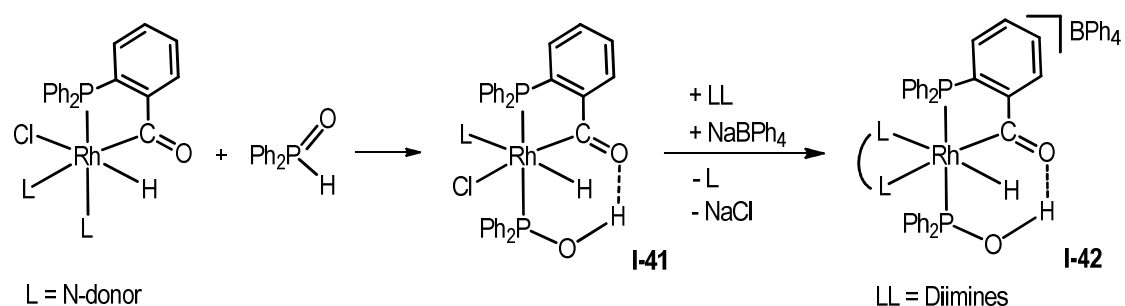
Scheme 71. Tautomerisation of diphenylphosphine oxide and stabilisation by coordination of the trivalent form.

The coordination of SPO ligands to transition metals enables the formation of $[\text{L}_n\text{M}((\text{R}_2\text{PO})_2\text{H})]$ complexes, in which one of the SPO fragments is deprotonated. In these complexes, a strong $\text{R}_2\text{PO}-\text{H}\cdots\text{OPR}_2$ intramolecular hydrogen bond between the *cis* located diphenylphosphinite and hydroxydiphenylphosphine ligands leads to a quasi-six-membered chelate (Scheme 72).⁷³ In reported examples of acetyl-diphenylphosphinous platinum complexes, the formation of an intramolecular hydrogen bond between the acyl and the phosphinous acid moieties is observed.⁷⁴ Intermolecular O-H \cdots Cl or O-H \cdots O hydrogen interactions have also been described in platinum $[\text{Pt}(\text{C}\equiv\text{C}-t\text{Bu})((\text{PPh}_2\text{O})_2\text{H})(\text{PPh}_2\text{OH})]$ complexes to form infinite one-dimensional chains.⁷⁵



Scheme 72. Canonical forms of the hydrogen bond between diphenylphosphinite and hydroxydiphenylphosphine coordinated ligands.

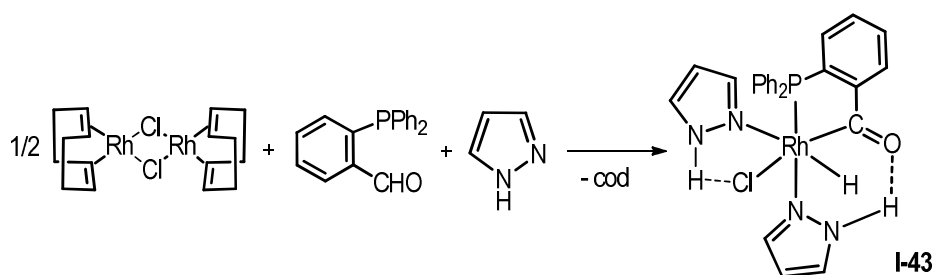
The reaction of diphenylphosphine oxide $\text{PPh}_2(\text{O})\text{H}$ with acyl-hydride rhodium(III) complexes derived from *o*-(diphenylphosphino)benzaldehyde affords neutral (acyl-diphenylphosphinous acid)rhodium(III) $[\text{RhClH}((\text{PPh}_2(o\text{-C}_6\text{H}_4\text{CO}))(\text{PPh}_2\text{O})\text{H})(\text{L})]$ (**I-41**) ($\text{L} = \text{N-donor ligand}$) derivatives containing intramolecular $\text{O}\cdots\text{H}\cdots\text{O}$ hydrogen bonds between the oxygen atoms in the diphenylphosphinous acid and the acyl moieties (Scheme 73).⁶⁹ The presence of these hydrogen interactions generates a new PCP pincer ligand with trans phosphorus atoms. The reaction of neutral **I-41** complexes with N-donor bidentate ligands leads to the displacement of the chloride and N-ligands, to give cationic $[\text{RhH}((\text{PPh}_2(o\text{-C}_6\text{H}_4\text{CO}))(\text{PPh}_2\text{O})\text{H})(\text{LL})]^+$ (**I-42**) compounds (Scheme 73).



Scheme 73. Formation of neutral and cationic [(acyl)(diphenylphosphinous acid)]-rhodium(III) complexes with a $\text{O}\cdots\text{H}\cdots\text{O}$ hydrogen bond.

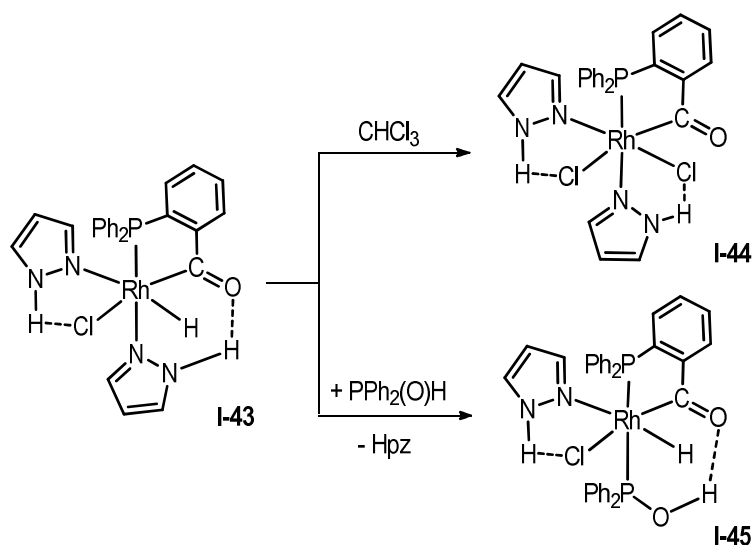
Pyrazoles (Hpz), with the formula $\text{C}_3\text{HR}_3\text{N}_2$, have planar five-membered heterocyclic structures with two adjacent nitrogen atoms. A pyridine-type nitrogen has a non-bonding electron pair, and is able to coordinate to a metal centre. This lone electron pair confers weak base and nucleophilic properties to the ligand. The adjacent N-H group has a rather acidic character.⁷⁶ The acid-base functionality of pyrazoles promotes the formation of both inter- and intramolecular hydrogen bonding between the N-H moiety and another electronegative group. Intermolecular interactions are responsible for the formation of diverse supramolecular structures containing pyrazole ligands.⁷⁷ Intramolecular bonds between pyrazole N-H groups and halide, acyl or other pyrazolate moieties in transition metal complexes are also known.⁷⁸ Pyrazoles exhibit diverse chemical and biological properties, and are found in numerous compounds in agricultural and pharmaceutical industries, or polymer chemistry.⁷⁹

The reaction of diolefinic $[\text{Rh}(\text{cod})\text{Cl}]_2$ with *o*-(diphenylphosphino)benzaldehyde and pyrazole leads to a neutral acylhydride compound $[\text{RhClH}(\text{PPh}_2(o\text{-C}_6\text{H}_4\text{CO}))(\text{Hpz})_2]$ (**I-43**) (Scheme 74). In these complexes, the formation of hydrogen $\text{N-H}\cdots\text{O}$ and $\text{N-H}\cdots\text{Cl}$ bonds between pyrazole and acyl or chloride moieties is observed.⁷⁰



Scheme 74. Synthesis of acylhydride rhodium(III) complex with pyrazoles containing intramolecular hydrogen bonds.

Upon dissolution in chloroform compound **I-43** undergoes exchange of hydride by chloride to afford dichloride acyl [RhCl₂(PPh₂(*o*-C₆H₄CO))(Hpz)₂] (**I-44**) complex, which also exhibits intramolecular hydrogen bonds between pyrazole and chloride ligands (Scheme 75). In this case, N-H...Cl hydrogen bonding is preferred to N-H...O involving the oxygen atom of the acyl group. Treatment of **I-43** with diphenylphosphine oxide PPh₂(O)H leads to the formation of [RhCl(PPh₂(*o*-C₆H₄CO))((PPh₂O)H)(Hpz)] (**I-45**) complex by displacement of one pyrazole molecule (Scheme 75). This compound displays a hydrogen bond between the oxygen atom of the diphenylphosphinous acid and the oxygen atom of the coordinated acyl group.

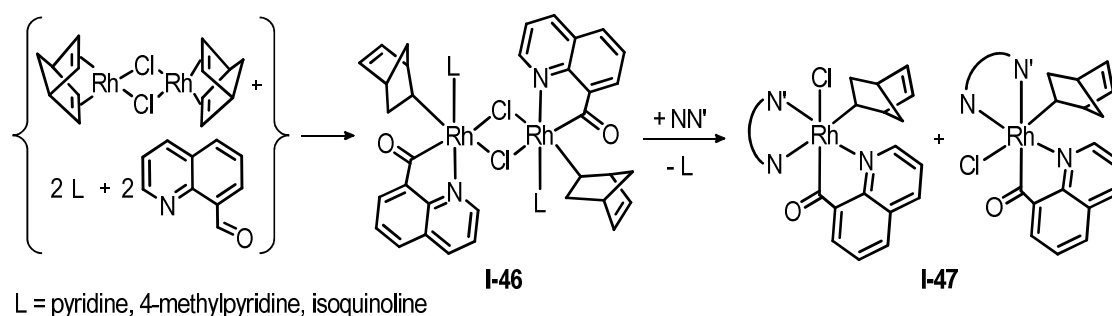


Scheme 75. Formation of dichloride-acylrhodium(III) **I-44** and acylhydride rhodium(III) **I-45** complexes.

The high activity showed by acylrhodium(III) compounds with diphenylphosphinous acid and pyrazole ligands in ammonia-borane hydrolysis encouraged the study of new rhodium complexes containing intramolecular hydrogen interactions as catalysts for this reaction. It was considered interesting to prepare acylrhodium compounds by reacting norbornadiene derivatives with 8-quinolinecarboxaldehyde in the presence of pyrazole or PPh₂(O)H, with the

aim of preparing various acyl chelate complexes containing N-H...O or N-H...Cl hydrogen bond intramolecular interactions.

It is known that the reaction of norbornadienerhodium(I) dimer with C_9H_6NCHO in the presence of other monodentate N-donors, such as pyridine or isoquinoline, leads to the chelate-assisted oxidative addition of the quinoline-aldehyde followed by the insertion of the norbornadiene into the Rh-H bond to afford dimeric σ -norbornenyl $[Rh(\mu-Cl)(C_9H_6NCO)(nbyl)L]_2$ (**I-46**) derivatives (Scheme 76).³¹ Treatment with bidentate N-donor ligands leads to the cleavage of the chloride bridge and allows the formation of mononuclear σ -norbornenyl $[RhCl(C_9H_6NCO)(nbyl)(NN')]$ (**I-47**) compounds (NN' = 8-aminoquinoline, 2-aminomethylpyridine, 2,2'-bipyridine, biacetyldihydrazone), as a mixture of two geometric isomers (Scheme 76).



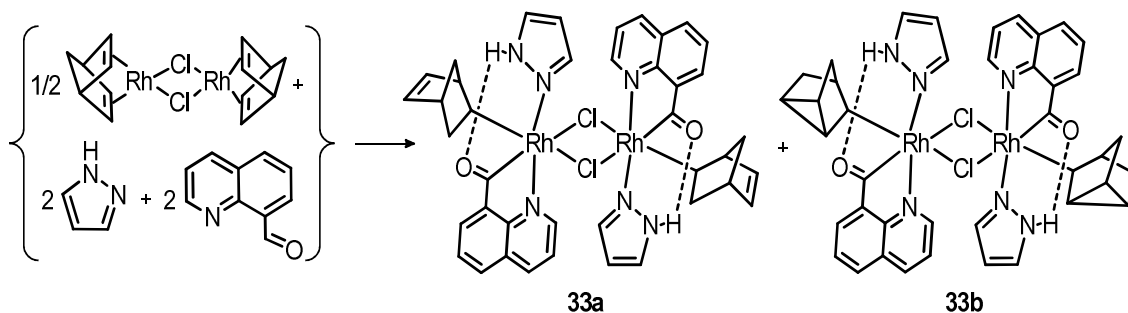
Scheme 76. Formation of acylrhodium $[Rh(\mu-Cl)(C_9H_6NCO)(Nbyl)L]_2$ and $[RhCl(C_9H_6NCO)(Nbyl)(NN')]$ compounds.

As mentioned above, the reaction of $[Rh(nbd)Cl]_2$ with 8-quinolinecarboxaldehyde and pyrazole are described in this work. The reactivity of the obtained alkyl-acylrhodium derivatives with monodentate ligands such as the N-donor pyrazole or the P-donors triphenylphosphine and diphenylphosphine oxide was also studied. These compounds have been tested as catalysts for the hydrolysis of ammonia-borane in air for hydrogen generation.

II. 2.3.1. Synthesis of alkyl-quinolineacyl-pyrazole rhodium(III) complexes

Compound $[Rh(nbd)Cl]_2$ reacted with 8-quinolinecarboxaldehyde and pyrazole in methanol at room temperature, to afford the immediate precipitation of the dimer complex $[RhCl(C_9H_6NCO)](Hpz)(C_7H_9)]_2$. A major species $[RhCl(C_9H_6NCO)](Hpz)(nbyl)]_2$ (nbyl = σ -norbornenyl) (**33a**) is formed *via* a chelate-assisted C-H activation of the aldehyde, with a subsequent insertion of the norbornadiene into the Rh-H bond to give the norbornenyl species (Scheme 77). A minor species $[RhCl(C_9H_6NCO)](Hpz)(ntyl)]_2$ (ntyl = σ -nortricyclyl) (**33b**) was

also observed in solution in a **33a/33b** = 85:15 ratio. This species would be formed by rearrangement of the norbornenyl ligand, which undergoes a double bond shift with a ring closure to give the nortricyclyl derivative.



Scheme 77. Chelate-assisted formation of a mixture of dimeric complexes **33a** and **33b**.

Complex **33** was characterised in solution by NMR spectroscopy. The low solubility of this product mixture in several deuterated solvents led to a characterisation in dimethylsulfoxide. NMR spectra showed compound **33a** as the main species in solution (Figure 52). A singlet signal at 14.12 ppm in the ^1H NMR corresponds to the N-H group in the pyrazole ligand. The low field position of this signal can be attributed to the presence of an intramolecular N-H \cdots O hydrogen bond between the nitrogen in the pyrazole and the oxygen atom of the coordinated acyl group. The pyrazole CH groups exhibit three sharp signals at 8.47, 8.13 and 6.55 ppm, indicating the absence of metallotropic tautomerization with the pyrazole firmly bonded to the rhodium centre.⁸⁰ Two doublet of doublets at 5.27 and 4.13 ppm would correspond to the uncoordinated olefinic fragment of a norbornenyl ligand. A two-dimensional HSQC experiment correlates these signals with peaks at 134.2 and 133.1 ppm respectively in the $^{13}\text{C}\{^1\text{H}\}$ NMR spectrum. The signal corresponding to the norbornenyl CH group bonded to the rhodium atom appears at 3.30 ppm in the ^1H NMR spectrum, which is correlated to a doublet at 36.6 ppm ($J_{\text{Rh-C}} = 28$ Hz) in the $^{13}\text{C}\{^1\text{H}\}$ NMR. The coordinated acyl group in the quinoline shows a doublet in the $^{13}\text{C}\{^1\text{H}\}$ NMR at 232.6 ppm ($J_{\text{Rh-C}} = 39$ Hz).

The presence of the minor **33b** species can be observed with signals at -0.40 and 1.10 ppm that could correspond to the C-H moieties located in the cyclopropyl ring of the nortricyclyl. A singlet at 14.31 ppm corresponds to the N-H moiety in the pyrazole, which could be also involved in a N-H \cdots O intramolecular interaction with the acyl group coordinated to the metal centre.

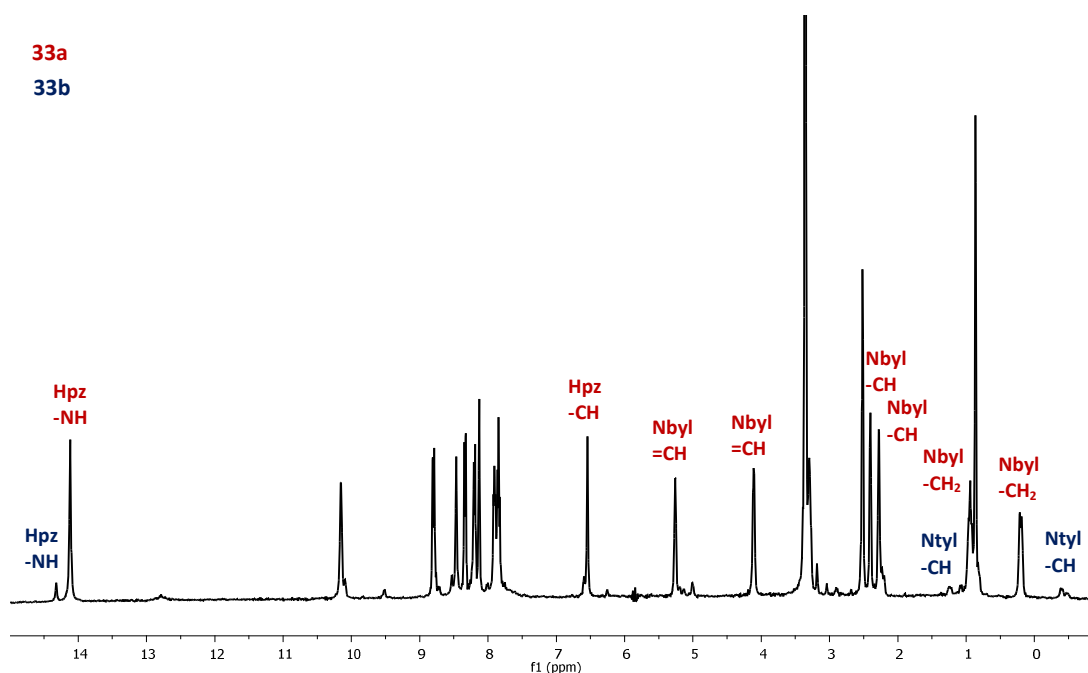


Figure 52. ^1H NMR spectrum of the mixture of **33a** (red) and **33b** (blue) species in DMSO-d_6 .

The ^1H NMR spectrum of very dilute solutions of **33** in CDCl_3 also shows a mixture of **33a** and **33b**. The latter is identified by the signals at -0.28 and 0.22 ppm that could correspond to the cyclopropyl ring. After 48h in solution, further isomerisation of the coordinated σ -norbornenyl into the nortricycyl derivative is not observed. Instead, decomposition of **33** occurs.

Isolation of single crystals from a chloroform solution allowed the determination of the structure of this product by X-ray diffraction. The structure in the solid state of the obtained crystals corresponds to the minor nortricycyl species **33b** (Figure 53).

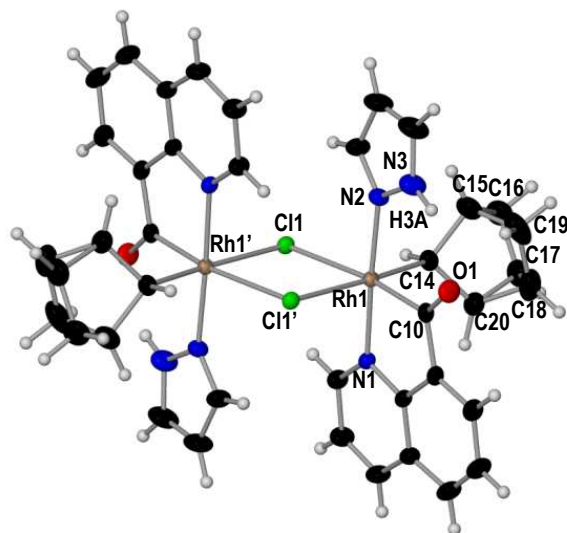


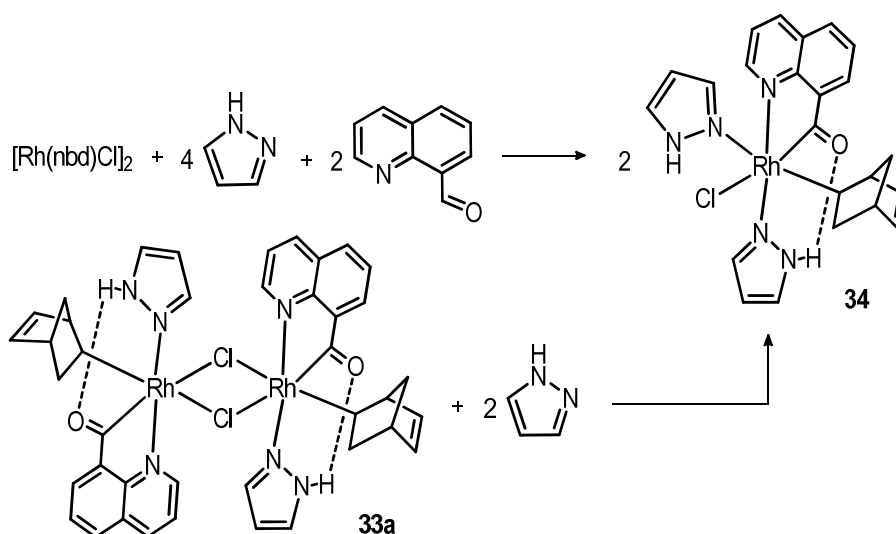
Figure 53. Molecular structure of the nortricyclyl species **33b**. Displacement ellipsoids are drawn at 50% probability level. Selected bond lengths (Å) and angles (°): Rh1–Cl1, 2.562(1); Rh1–Cl1', 2.611(8); Rh1–N1, 2.051(4); Rh1–N2, 2.062(4); Rh1–C10, 1.929(3); C10–O1, 1.231(4); Rh1–C14, 2.074(4); Rh1–Rh1', 3.860(5); N3–O1, 2.649(5); N3–H3A, 0.860; O1–H3A, 1.936; N1–Rh1–N2, 177.6(1); Cl1–Rh1–C10, 173.9(1); Cl1'–Rh1–C14, 171.2(1); N3–H3A–O1, 139.4.

This compound consists of a centrosymmetric dinuclear $C_{40}H_{38}N_6O_2Cl_2Rh_2$ molecule with two chloride bridges between the two rhodium(III) centers. The geometry around the metal atoms is distorted octahedral, in which the pyrazole and quinoline ligands occupy apical positions. The equatorial plane is formed by bridging chloride ligands, in *trans* position to the η^1 -coordinated nortricyclyl and acyl groups. The Rh–N bond distances are equal (Rh1–N1 2.051(4) Å and Rh1–N2 2.062(4) Å), but the nortricyclyl-rhodium (Rh1–C14) distance of 2.074(4) Å is longer than the acyl-rhodium (Rh1–C10) distance of 1.929(3) Å. As in complexes **31a** and **32** previously discussed, this can be a consequence of the different hybridization of C14 (sp^3) and C10 (sp^2), and to the latter being part of a five-membered metallacycle.⁸¹ All the carbon-carbon distances in the nortricyclyl group are equal, and agree with single bond distances. The Rh1–Rh1' distance of 3.860(5) Å excludes any metal-metal interaction.

The pyrazole ligand forms a moderately strong intramolecular N–H...O hydrogen bond interaction with the oxygen atom in the acyl moiety.⁸² The H3A...O1 distance of 1.936 Å, the N3–H3A distance of 0.860 Å and the donor-acceptor N3–O1 bond distance of 2.649(5) Å are in agreement with the established values for a hydrogen bond.⁸² The small N3–H3A...O1 angle of 139.4° is similar to the observed angles for other reported complexes with these hydrogen interactions involving pyrazoles.⁸³ The dihedral angle between two planes can also be indicative of a hydrogen bond. The plane including the pyrazole ligand with the N–H group and

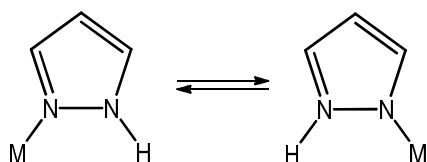
the plane formed by the coordinated acyl atoms C10 and O1, the metal centre Rh1 and the coordinated atoms N1, N2 and Cl1' should be close to 0°, indicating that the N-H group in the pyrazole would be oriented towards the acyl moiety.^{78c} The measured angle between those planes is 8.4°, which is consistent with the existence of an intramolecular hydrogen bond.

The reaction of compound **33** with pyrazole in dichloromethane allowed the cleavage of the chloride bridge and led to the neutral complex $[\text{RhCl}(\text{C}_9\text{H}_6\text{NCO})(\text{Hpz})_2(\text{nbyl})]$ (**34**). The formation of **34** was also possible by a chelate-assisted oxidative addition of 8-quinolinecarboxaldehyde to $[\text{Rh}(\text{nbd})\text{Cl}]_2$, in the presence of two equivalents of pyrazole per rhodium, in dichloromethane at room temperature (Scheme 78).



Scheme 78. Formation of **34** from complex **33a** and from $[\text{Rh}(\text{nbd})\text{Cl}]_2$.

Characterisation of compound **34** in solution was done by NMR spectroscopy. A sharp singlet in the ^1H NMR at 14.50 ppm would indicate the presence of a $\text{N-H}\cdots\text{O}$ hydrogen bond between a pyrazole and the acyl moiety. The CH signals for this pyrazole are observed at 7.62, 6.28 ppm and 6.00 ppm. A broad signal at 12.80 ppm corresponds to the N-H group of the second pyrazole ligand, which could be involved in a $\text{N-H}\cdots\text{Cl}$ hydrogen bond with the *cis* located chloride.^{30,78c-d} Two of the CH groups of this second pyrazole ligand also appear as notably broad signals at 7.20 and 8.40 ppm. The broadness of the signals corresponding to the second pyrazole ligand suggests a metallotropic tautomerism of the pyrazole (Scheme 79). The ligand would exist in two identical tautomeric forms at room temperature, by fast exchange of the metal and the proton bonded to the nitrogen atoms.^{77b,84}



Scheme 79. Metallotropic tautomerism of pyrazole ligands.

The temperature was lowered in an attempt to slow down the tautomeric exchange. As shown in figure 54, signals corresponding to the pyrazole in this equilibrium become sharper at 233 K, and three singlets can be observed for the CH groups at 8.50, 7.20 and 6.80 ppm. Singlets at 12.80 and 10.25 ppm also sharpen, which correspond to the N-H moiety in the pyrazole and to the CH group in the quinoline adjacent to the nitrogen atom, respectively. The lack of tautomerism in one of the pyrazole ligands could be due to the presence of the intramolecular N-H...O bond that would hamper the pyrazole dissociation. This could also indicate the absence, at room temperature, of an N-H...Cl interaction in the pyrazole involved in the equilibrium.

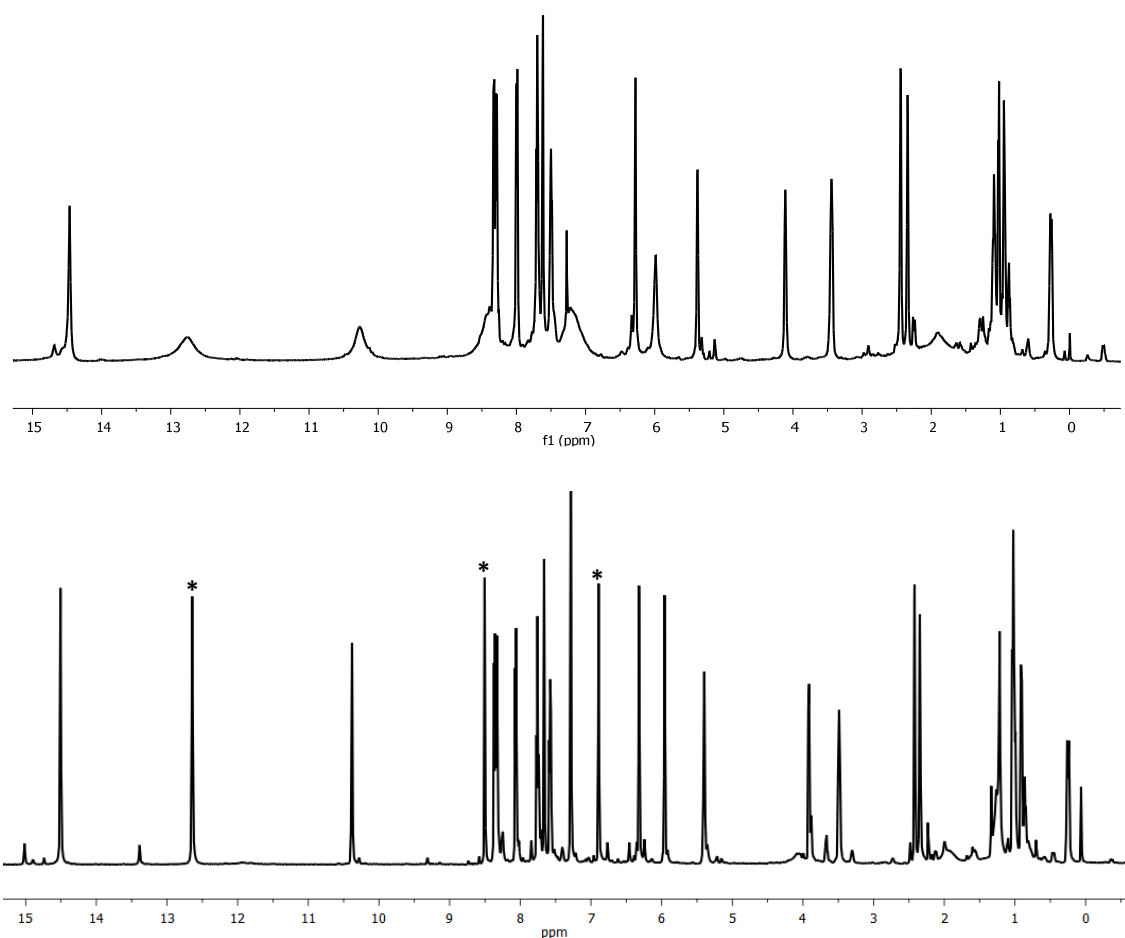
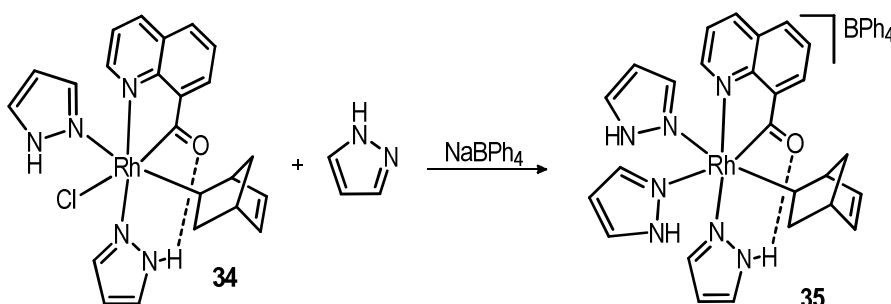


Figure 54. ^1H NMR spectra of **34** at room temperature (top) and at 233 K (bottom) in CDCl_3 , (*) denotes the signals due to the pyrazole ligand undergoing metallotropic tautomerism at room temperature.

Signals corresponding to the norbornenyl fragment can also be observed in the ^1H NMR spectrum. The uncoordinated olefinic fragment exhibits two doublets of doublets at 5.40 and 4.11 ppm, which are correlated to signals at 135.3 and 133.6 ppm in the $^{13}\text{C}\{^1\text{H}\}$ NMR spectrum, respectively. The CH group bonded to the rhodium centre shows a resonance at 3.44 ppm in the ^1H NMR spectrum, and correlates to a doublet carbon signal at 32.2 ppm ($J_{\text{Rh-C}} = 27$ Hz). A doublet in the $^{13}\text{C}\{^1\text{H}\}$ NMR spectrum at 237.8 ppm ($J_{\text{Rh-C}} = 27$ Hz) confirms the coordination of the quinoline ligand by the acyl moiety.

Finally, addition of the NaBPh_4 salt to complex **34** in the presence of pyrazole promoted the chloride extraction and formation of the cationic compound $[\text{Rh}(\text{C}_9\text{H}_6\text{NCO})(\text{Hpz})_3(\text{nbyl})]\text{BPh}_4$ (**35**), which contains three coordinated pyrazole molecules (Scheme 80).

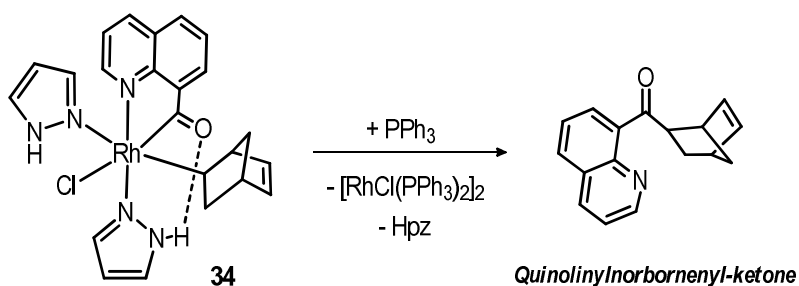


Scheme 80. Formation of cationic compound **35**.

Compound **35** was characterised in solution by NMR spectroscopy. The norbornenyl olefinic fragment exhibits signals in the ^1H NMR spectrum at 5.45 and 3.90 ppm, which are correlated to resonances at 136.1 and 133.5 ppm in the $^{13}\text{C}\{^1\text{H}\}$ NMR spectrum. The CH group coordinated to the rhodium centre shows a singlet at 2.98 ppm in the ^1H NMR, and is correlated to a doublet signal at 33.4 ppm ($J_{\text{Rh-C}} = 26$ Hz) in the $^{13}\text{C}\{^1\text{H}\}$ NMR. A doublet signal at 238.5 ppm ($J_{\text{Rh-C}} = 30$ Hz) in the $^{13}\text{C}\{^1\text{H}\}$ NMR spectrum confirms the coordination of the quinoline *via* the acyl fragment. At room temperature, a broad signal at 15.00 ppm in the ^1H NMR spectrum corresponds to the N-H bond of pyrazole. The low field position of the signal suggests a N-H \cdots O hydrogen bond between pyrazole and the quinoline acyl moiety. A singlet at 6.38 ppm can also be ascribed to a CH group of pyrazole, but other signals also corresponding to pyrazole molecules cannot be found. This could be due to the metallotropic tautomerism experimented by these ligands, in which the rapid exchange between tautomeric forms in solution results into broadness or inexistence of signals in the NMR spectrum. Unfortunately, the low solubility of this compound did not allow the performance of a low temperature ^1H NMR experiment.

II. 2.3.2. Reactivity of alkyl-quinolineacyl-pyrazole rhodium(III) complexes with monodentate P-donor ligands, PPh₃ or PPh₂OH

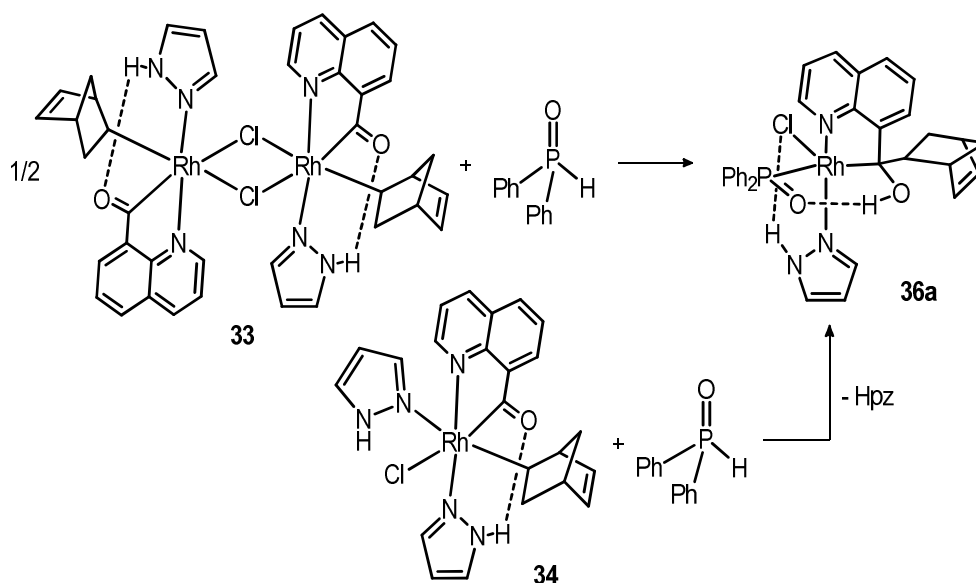
It is known that reactions of [Rh(nbd)Cl]₂ with C₉H₆NCHO and triarylphosphines lead to the formation of stable pentacoordinated (alkyl)(acyl)-rhodium(III) compounds or to the reductive elimination of the hydroacylation product, depending on the stoichiometric ratios employed.^{30,31} On the other hand, the addition of phosphine ligands to (alkyl)(acyl)-rhodium complexes containing N-donor ligands also results in the formation of ketone.^{13,14,31,32} The addition of triphenylphosphine to complex **34** in dichloromethane led to the latter outcome, causing the reductive elimination of the quinolinylnorbornenyl-ketone C₉H₆NC(O)nbyl (Scheme 81). The formation of a triphenylphosphine-rhodium compound can also be observed, which exhibits a doublet at 42.2 ppm, with a coupling constant of J_{Rh-P} = 184 Hz in the ³¹P{¹H} NMR. These resonance values are similar to those reported for rhodium-phosphine dimer complexes such as [RhCl(P(*p*-tolyl)₃)₂]₂,⁸⁵ which exhibits a doublet at 49.5 ppm (J_{Rh-P} = 196 Hz), and this enables us to propose [RhCl(PPh₃)₂]₂ as an additional reaction product.



Scheme 81. Formation of the quinolinylnorbornenyl-ketone from compound **34**.

Alternatively, treatment of complex **34** with one equivalent of diphenylphosphine oxide in dichloromethane gives the unsaturated compound [RhCl(C₉H₆NC(nbyl)OH)(Hpz)(Ph₂PO)] (**36a**) after the decoordination of one pyrazole molecule (Scheme 82). The coordination of the trivalent hydroxydiphenylphosphine form promotes the migration of the σ -norbornenyl to the carbon atom in the quinoline acyl moiety. This migration leads to the formation of a new C-C bond, with a consequent hybridization change of the acyl carbon atom from sp² to sp³. A ligand-assisted outer-sphere hydrogen transfer from the hydroxydiphenylphosphine to the oxygen atom in the quinoline allows the formation of the phosphinito and a stable quinolinylnorbornenylhydroxyalkyl moiety, connected by a hydrogen bond, which prevents the release of the ketone product observed in the reaction of **34** with triphenylphosphine.

Complex **36a** can be also formed by reaction of the dinuclear compound **33** with diphenylphosphine oxide in a Rh:P = 1:1 ratio, in dichloromethane and at room temperature (Scheme 82). The cleavage of the chloride bridge would generate a coordinative vacancy, allowing the coordination of the hydroxydiphenylphosphine ligand. The subsequent nucleophilic attack of the alkyl fragment to the quinolineacyl group, and the hydrogen migration from the phosphine hydroxyl group generates the final product. This transformation has been observed previously in our laboratory upon reaction of the related $[\text{Rh}(\mu\text{-Cl})(\text{C}_9\text{H}_6\text{NCO})(\text{nbyl})\text{L}]_2$ (L = picoline, isoquinoline) (**I-35**) with $\text{PPh}_2(\text{O})\text{H}$.⁸⁶



Scheme 82. Formation of complex **36a** from reaction of compounds **33** or **34** with diphenylphosphine oxide.

This unsaturated complex was characterised in solution by NMR spectroscopy, which confirmed the formation of a quinolinyl-(norbornenylhydroxyalkyl) ligand, and by ESI-MS. In the $^{13}\text{C}\{^1\text{H}\}$ NMR spectrum (Figure 55), a doublet at 92.6 ppm with a coupling constant of 26 Hz suggests the presence of a hydroxyalkyl C-OH fragment coordinated to the rhodium atom. This feature, along with the absence of a signal for the acyl group in the 220-230 ppm region of the $^{13}\text{C}\{^1\text{H}\}$ NMR spectrum confirms the transformation of sp^2 into sp^3 for the carbon atom. Accordingly, the norbornenyl CH group, whose migration is responsible for the hybridization change, shows a signal at 3.10 ppm in the ^1H NMR spectrum (Figure 56), which is correlated to a singlet signal at 49.8 ppm in the $^{13}\text{C}\{^1\text{H}\}$ NMR spectrum. This indicates that the norbornenyl is no longer coordinated to the metal centre. The protons in the olefinic fragment of the norbornenyl show two signals at 5.88 and 5.19 ppm. The displacement of these values to a lower field when compared to complexes **33**, **34** and **35**, in the range of 5.45-5.27 and 4.13-

3.90 ppm, also suggests the migration of the norbornenyl from the rhodium to the quinoline substituent. The olefinic ^1H NMR signals correlate to resonances at 139.0 and 130.4 ppm in the $^{13}\text{C}\{^1\text{H}\}$ NMR spectrum. The pyrazole ligand shows a broad signal at 13.14 ppm in the ^1H NMR spectrum that corresponds to the N-H group in the pyrazole. The low field position of this resonance would indicate the formation of a N-H \cdots Cl hydrogen bond with the chloride ligand. The three CH groups in the pyrazole exhibit sharp signals at 8.41, 7.41 and 6.02 ppm. The $^{31}\text{P}\{^1\text{H}\}$ NMR spectrum (Figure 56) shows a doublet at 80.3 ppm ($J_{\text{Rh-P}} = 150$ Hz) due to the coordination of the phosphinito ligand to the rhodium. The presence of a molecular ion at $m/z = 622.11$ in the ESI-MS corresponds to the fragment $[\text{Rh}(\text{C}_9\text{H}_6\text{NC}(\text{nbyl})\text{OH})(\text{Hpz})(\text{Ph}_2\text{PO})]^+$ or $\{\text{M} - \text{Cl}\}^+$, and confirms the proposed formulation for **36a**. The IR spectrum shows a band at 1100 cm^{-1} due to $\nu(\text{P}=\text{O})$.⁸⁷

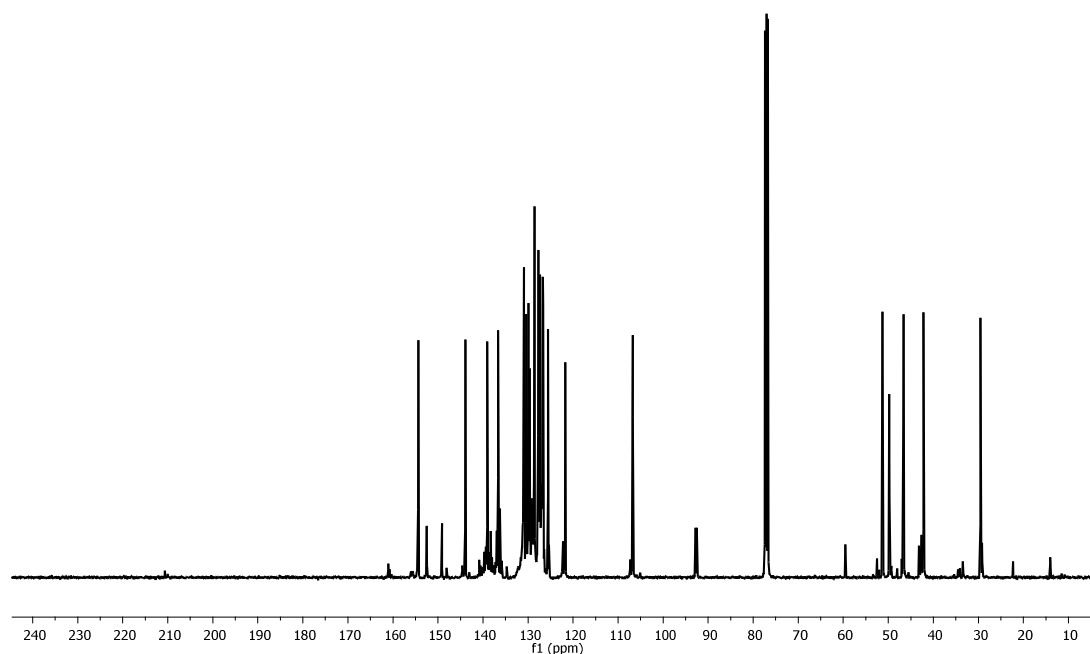


Figure 55. $^{13}\text{C}\{^1\text{H}\}$ NMR spectrum of **36** in CDCl_3 at room temperature.

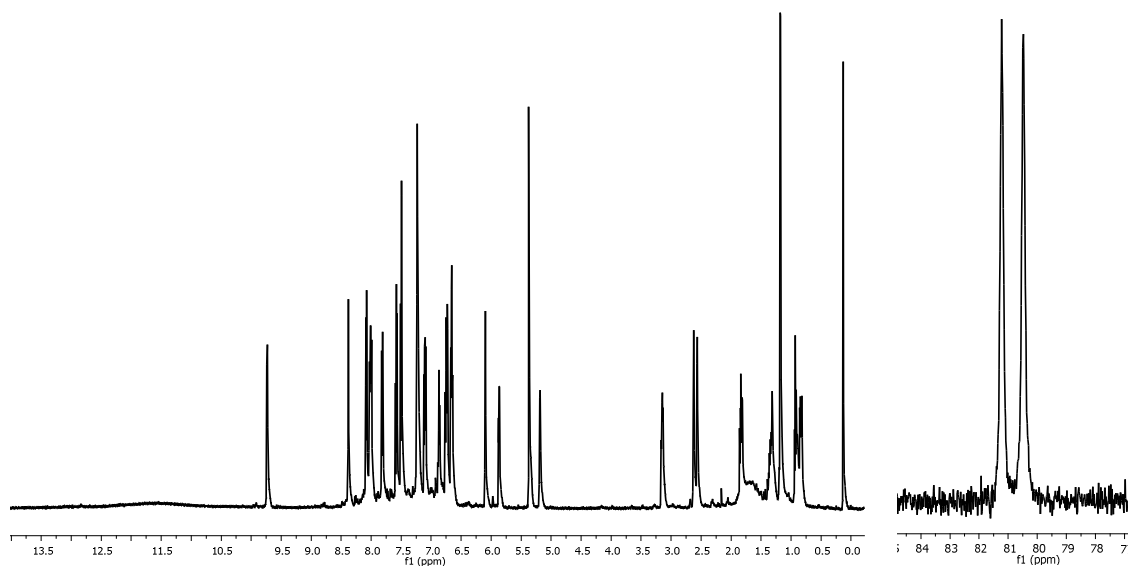


Figure 56. ^1H NMR (left) and ^{31}P NMR (right) spectra of **36** in CD_2Cl_2 at room temperature.

The determination of the structure of compound **36a** by single-crystal X-ray diffraction was also possible (Figure 57). The resulting structure of **36a** in the solid state is in good agreement with the structure deduced from spectroscopic data in solution. The geometry adopted around the rhodium(III) centre is a distorted trigonal bipyramid. The pyrazole and quinoline ligands are located in the apical positions of the bipyramid, bonded to the rhodium centre *via* N2 and N1 nitrogen atoms respectively. The equatorial positions are occupied by the chloride, diphenylphosphinito and the sp^3 carbon C10 atom of the C-OH moiety in the quinoline ligand. Both Rh-N bond distances are equal (Rh1–N1 2.039(7) Å and Rh1–N2 2.041(7) Å). The Rh1–C10 bond distance is 2.090(7) Å, which is longer than the Rh-C bond distance found in the coordinated quinoline-acyl group in compound **33** (1.929(3) Å), confirms the hybridization variation from sp^2 to sp^3 produced in C10 by migration of the norbornenyl group. The C10–C11 and C10–O1 bond distances of 1.56(1) and 1.397(9) Å respectively correspond to single bonds, and confirm the formation of a new C-C bond and a hydroxy group after the nucleophilic attack of the alkyl fragment. However, the C10–O1 bond distance is slightly shorter than the C-O distances in the range of 1.440 to 1.411 Å observed in complexes with hydroxy groups involved in intramolecular hydrogen interactions.^{15,25,88}

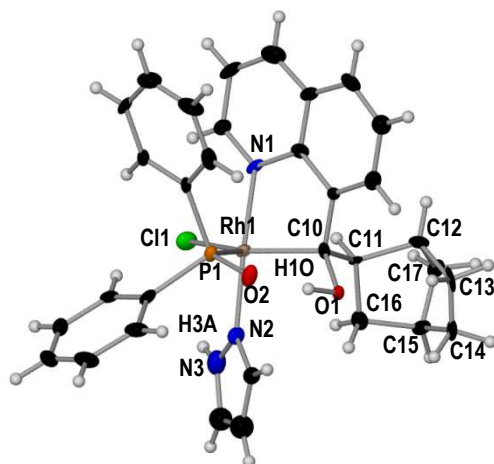


Figure 57. Molecular structure of complex **36a**. Displacement ellipsoids are drawn at 50% probability level. Selected bond lengths (Å) and angles (°): Rh1–Cl1, 2.464(2); Rh1–N1, 2.039(7); Rh1–N2, 2.041(7); Rh1–C10, 2.090(7); Rh1–P1, 2.213(2); P1–O2, 1.516(6); C10–O1, 1.397(9); O1–H10, 1.045; O2–H10, 1.596; O1–O2, 2.599(7); C10–C11, 1.56(1); N3–H3A, 0.859; N2–Cl1, 3.121(7); Cl1–H3A, 2.572; N1–Rh1–N2, 176.7(3); Cl1–Rh1–C10, 145.6(2); Cl1–Rh1–P1, 125.66(7); P1–Rh1–C10, 88.3(2); O1–H10–O2, 158.9; N3–H3A–Cl1, 122.7.

The formation of an O–H \cdots O hydrogen bond can be observed between the diphenylphosphinito and the quinoline-hydroxyalkyl group, resulting in the formation of a pseudo-pincer PCN ligand. The O1–H10 (1.045 Å) and O2 \cdots H10 (1.596 Å) distances, and the donor-acceptor O1–O2 distance of 2.599(7) Å agree with the formation of this hydrogen bond interaction. The O1–H10–O2 bridge is almost linear, with an angle of 158.9°. The Rh1–P1 bond distance (2.213(2) Å) is shorter than Rh–P distances measured in reported diphenylphosphinous acid-rhodium complexes with O–H \cdots O intramolecular bonds,⁶⁹ and closer to those observed for diaryl-phosphinous acid ligands with electron-withdrawing properties.⁸⁹ The P1–O2 bond distance (1.516(6) Å) agrees with the formation of a P=O double bond.⁹⁰

The formation of an intramolecular N–H \cdots Cl hydrogen bond is also observed, with a donor-acceptor N3–Cl1 bond distance of 3.121(7) Å, a H3A \cdots Cl1 distance of 2.572 Å and an N3–H3A–Cl1 angle of 122.7°, similar to those found in other metal complexes containing these pyrazole-chloride hydrogen bond interactions.⁹¹ The dihedral angle between the plane including the pyrazole N–H group and the plane containing the chloride Cl1, the rhodium centre and the nitrogen N2 and N1 atoms is 12.12°, which indicates that the N–H group is oriented towards the chloride ligand.^{78c,91d}

The presence of a broad signal for the N-H bond in the ^1H NMR spectrum, and the absence of a resonance for the newly formed hydroxyl group in the quinolinyl-(norbornenylhydroxyalkyl) ligand at room temperature motivated a low temperature multinuclear NMR study (Figures 58 and 59). At 263 K, the appearance of a new signal at 9.85 ppm can be noticed in the ^1H NMR spectrum (Figure 58). This signal is attributed to the proton in the hydroxyl moiety, which would be involved in an O-H \cdots O hydrogen bond with the adjacent phosphinito ligand. By 243 K, this resonance and the signal corresponding to the N-H \cdots Cl group at 13.14 ppm are sharp. At this temperature, the sharp doublet observed at 80.3 ppm in the $^{31}\text{P}\{^1\text{H}\}$ NMR spectrum at room temperature (Figure 59) is displaced towards lower field and becomes broader, indicating the existence of an additional equilibrium. After coalescence, the signal is resolved by 193 K into two doublets revealing the presence of a major species **36a** (84.6 ppm, $J_{\text{RH-P}} = 150$ Hz) and a minor species **36b** (83.0 ppm, $J_{\text{RH-P}} = 152$ Hz) in solution.

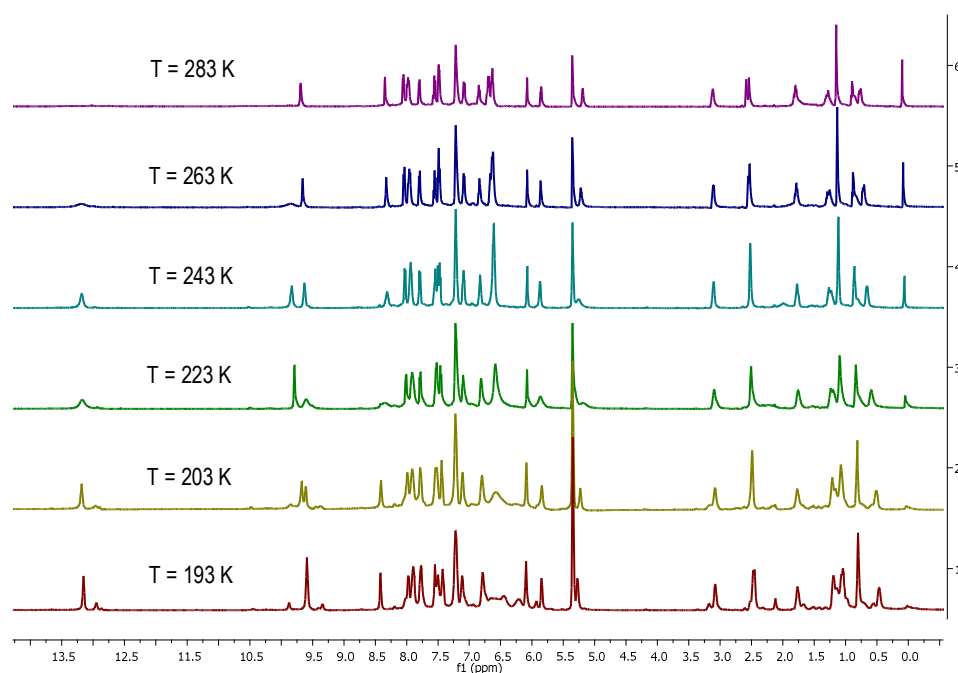


Figure 58. ^1H NMR spectra of **36** in CD_2Cl_2 in the 193K to 283K range.

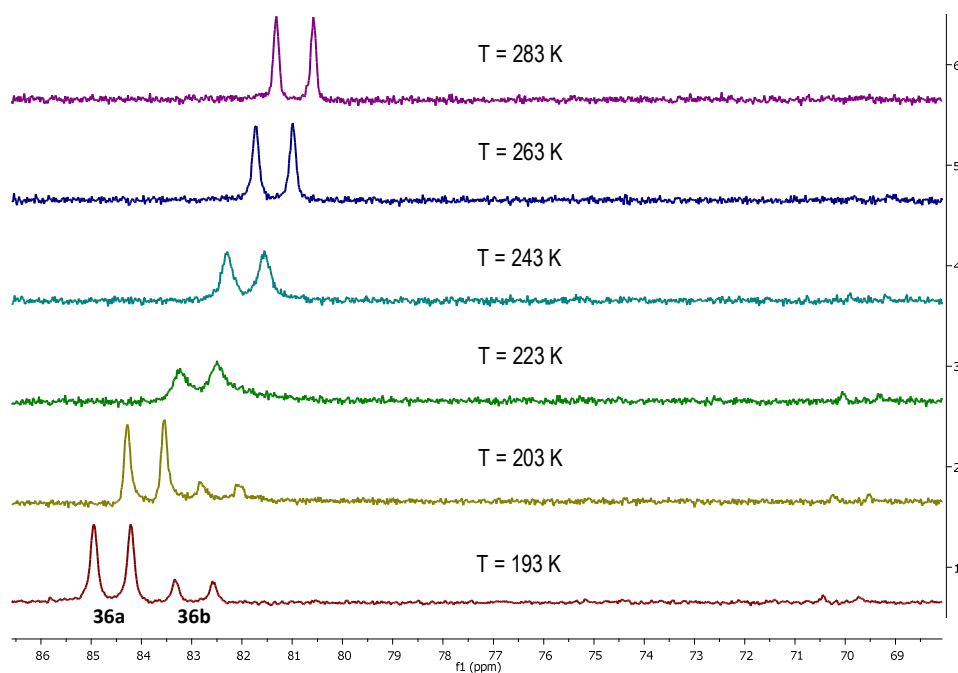
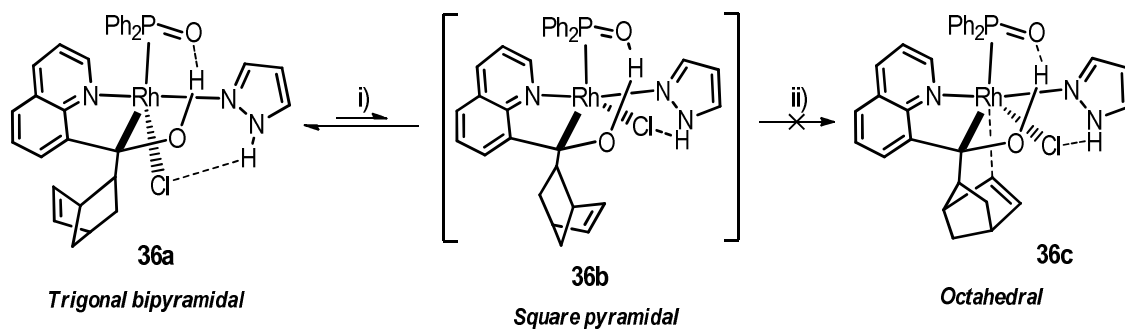


Figure 59. $^{31}\text{P}\{^1\text{H}\}$ NMR spectra of **36** in CD_2Cl_2 in the 193K to 283K range.

The spectroscopic data of **36a** are similar to those of our recently reported related pentacoordinated (norbornenylhydroxyalkyl)rhodium(III) complex containing 4-picoline (pic) as a N-donor ligand, with formula $[\text{RhCl}((\text{C}_9\text{H}_6\text{NC}(\text{nbyl})\text{OH})(\text{Ph}_2\text{PO})(\text{pic}))]$ (**a-pic**). This compound was obtained as a kinetic product of the reaction between $\text{Ph}_2\text{P}(\text{O})\text{H}$ and a dinuclear (acylquinoliny)(norbornenyl)(pic)-rhodium(III) complex $[\text{Rh}(\mu\text{-Cl})(\text{C}_9\text{H}_6\text{NCO})(\text{nbyl})(\text{pic})_2]$ and transformed into a thermodynamic pseudo-octahedral isomer (**c-pic**) containing a weak $\eta^1\text{-C}$ anagostic interaction between the Rh(III) centre and the norbornenyl ligand. DFT calculations allowed the proposal of a distorted trigonal bipyramidal structure for compound **a-pic** and a very small energy difference ($2.5 \text{ kcal}\cdot\text{mol}^{-1}$) between **a-pic** and **c-pic**. These calculations also proposed that the transformation of **a-pic** into **c-pic** may occur by isomerisation of the trigonal bipyramid to attain a distorted square-planar pyramidal structure with apical phosphinito (**b-pic**), lower in energy than **a-pic** by only $0.7 \text{ kcal}\cdot\text{mol}^{-1}$.⁸⁶

The present results confirm the trigonal bipyramidal structure (**a**) for the (norbornenylhydroxyalkyl)rhodium(III) complex first formed in these reactions. Furthermore, we believe that the minor species **36b**, found at 193 K in the $^{31}\text{P}\{^1\text{H}\}$ NMR spectrum, could also correspond to the unsaturated 16e species with a square pyramidal arrangement (Scheme 83). Examples of both trigonal bipyramid and square pyramidal geometries are known for rhodium(III) pentacoordinated complexes,^{30,31,92} and it is established that the trigonal

bipyramid structure is generally favoured when the ligand *trans* to the acute angle in the equatorial plane is a π -donor, such as chloride.⁹³



Scheme 83. (i) Equilibrium between pentacoordinated trigonal bipyramidal **36a** and square-pyramidal **36b**. (ii) Inhibited transformation into octahedral **36c**.

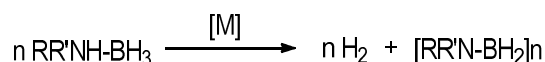
In the present case a final transformation of **36b** into pseudo-octahedral species **36c** appears inhibited, and this may be due to the presence of a N-H...Cl hydrogen bond involving the pyrazole.

II. 2.3.3. Catalytic activity of alkyl-quinolineacyl-pyrazole rhodium(III) complexes in the hydrolysis of ammonia-borane for hydrogen liberation

Hydrogen is considered a feasible alternative to fossil fuels in the near future. Although hydrogen gas does not naturally exist on earth in large quantities, it is widely distributed in numerous compounds, and it could be produced on an industrial scale with the appropriate technology. It is also viewed as a clean energy source, with water and heat as the only products of its combustion. However, the safe storage and delivery of hydrogen gas remains an issue that needs to be solved for its consolidation as a capable option. This has encouraged the research on chemical 'hydrogen storage' materials, which exhibit high hydrogen weight percentage and allow its controlled generation by a chemical reaction.⁶⁰ Ammonia or amine-borane N-B compounds are among these materials. Ammonia-borane ($\text{H}_3\text{N-BH}_3$) contains a 19.6 wt % of hydrogen and shows high thermal and water stability at room temperature. It provides a stable source of transportable hydrogen for subsequent consumption.⁶¹ Main uses of these materials include vehicles powered by fuel cells, which convert chemical energy from a fuel into electricity.

Hydrogen liberation from ammonia-borane (AB) by thermolysis has been widely studied, both in solid state and in solution. Nevertheless, release of one hydrogen equivalent per mole of

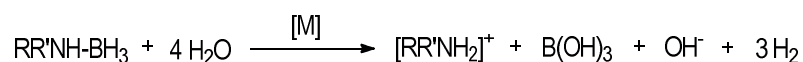
substrate by thermolysis requires relative high temperatures.⁹⁴ The use of homogeneous transition-metal based catalyst to produce the dehydrogenation of ammonia- or amine-boranes has gained attention in recent years.⁹⁵ A large number of transition metals are known to promote hydrogen release from amine-boranes, such as Ti, Zr, Ru, Rh, Pd or Pt.⁹⁶ The dehydrogenation reaction catalysed by these metal complexes affords up to one equivalent of hydrogen gas under mild conditions, and requires an inert atmosphere (Scheme 84).



Scheme 84. Dehydrogenation reaction of amine-boranes to generate hydrogen gas.

There are examples of catalysts for ammonia-borane dehydrogenation capable of liberating up to two hydrogen equivalents per mole of substrate. These examples include Pd complexes,⁹⁷ Ni-carbenes⁹⁸, Ru-PN⁹⁹ species and tripodal polyphosphine-Co compounds.¹⁰⁰ More recent examples describe the use of air stable Ru compounds that afford the production of more than two equivalents of hydrogen gas per mole of ammonia-borane,¹⁰¹ without loss of catalytic activity under air and water exposure.

Hydrolysis reactions, on the other hand, provide an additional method for hydrogen liberation from ammonia- and amine-borane compounds, and can afford up to three equivalents of hydrogen per mole of substrate (Scheme 85).



Scheme 85. Hydrolysis reaction of amine-boranes to generate hydrogen gas.

Various reported transition-metal heterogeneous systems are known to efficiently catalyse hydrogen release by hydrolysis at room temperature,⁶² although they often require an inert atmosphere. Rhodium nanoparticles are among the most active heterogeneous catalysts for this hydrolysis reaction to date.⁶³ Efficient water and air-stable Ni, Pd, or Au nanoparticles have also been described,¹⁰² and more recently nanoparticles involving other non-noble transition metals such as Fe, Co or Cu have been reported to catalyse these hydrolytic reactions, though with lower activity.¹⁰³ The efficient homogeneous version of this ammonia-borane hydrolysis reaction was first reported in 2010 using the afore-mentioned hydrido-irida- β -diketones,^{59a} and more recently using acyl-hydride rhodium(III) compounds containing diphenylphosphinous acid (**I-48**) and pyrazole (**I-49**) ligands.⁶⁹⁻⁷⁰ Both these rhodium catalysts contain intramolecular

hydrogen bonds, and are capable of liberating up to three equivalents of hydrogen gas in air under mild conditions (Figure 60).

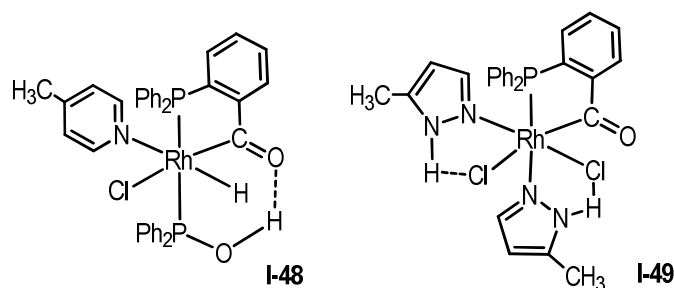


Figure 60. Acyl-hydride rhodium(III) catalysts for amine-borane hydrolysis containing diphenylphosphinous acid (left) or pyrazole (right).

Other reported homogeneous catalysts for the amine-borane hydrolysis include highly active 14e, 16e or saturated iridium(III)-carbene species,⁶⁴ and pincer type iridium(III)-PNP compounds⁶⁵ (Figure 61).

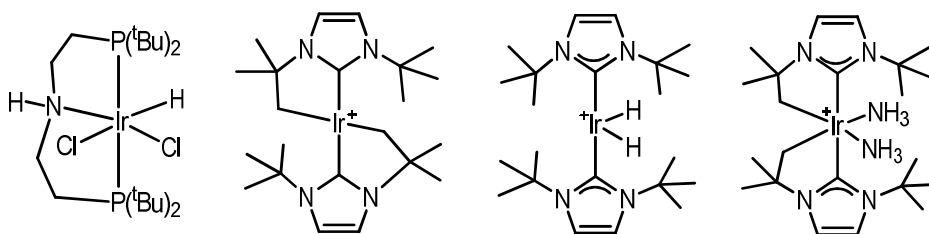


Figure 61. Reported homogeneous iridium(III) catalysts for the hydrolysis of ammonia-borane.

Ruthenium *p*-cymene^{66,68} and dicarbonyl⁶⁷ complexes have also been studied. A mechanistic study on the hydrolysis of AB catalysed by ruthenium *p*-cymene complexes points to B-H coordination of AB to Ru and formation of a solvent-stabilized borenium cation formulated as $[H_3N-BH_2(S)]^+$ ($S = THF$ or H_2O) as key intermediate, common to dehydrogenation and hydrolytic competitive reactions. In the hydrolytic path, interaction of $[H_3N-BH_2(OH_2)]^+$ with Ru leads to the release of amine-hydroxyborane that undergoes a fast hydrolysis.⁶⁸ Dicarbonylruthenacyclic compounds also promote the anhydrous release of hydrogen, though at a much lower rate. These catalysts are represented in Figure 62.

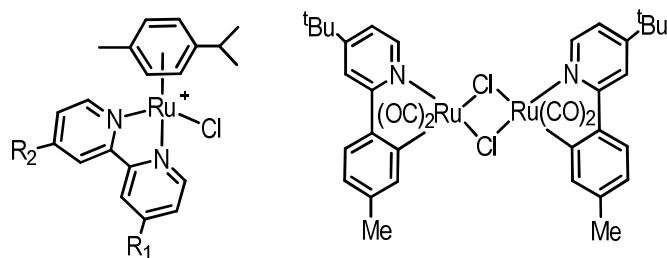


Figure 62. Reported homogeneous ruthenium catalysts for the hydrolysis of ammonia-borane.

The efficiency of reported rhodium-based homogeneous systems containing strong intramolecular hydrogen bonds for the hydrolysis of ammonia-borane led us to study the catalytic activity of the previously described compounds **33-36**, which also exhibit hydrogen bond interactions.

II. 2.3.3a. Optimization of reaction conditions

The optimization of the hydrolysis reaction conditions was performed with 1.38 mmol of ammonia-borane (AB) $\text{NH}_3\text{-BH}_3$ as a substrate (0.46 M) and 0.1 mol % of compound $[\text{RhCl}(\text{C}_9\text{H}_6\text{NCO})(\text{Hpz})(\text{nbyl})]_2$ (**33**) as a catalyst, at 30°C. This reaction was carried out in a THF/ H_2O mixture, as the insolubility of rhodium complexes in H_2O inhibits their catalytic activity. Figure 63 shows ammonia-borane hydrolysis experiments using different proportions of THF/ H_2O .

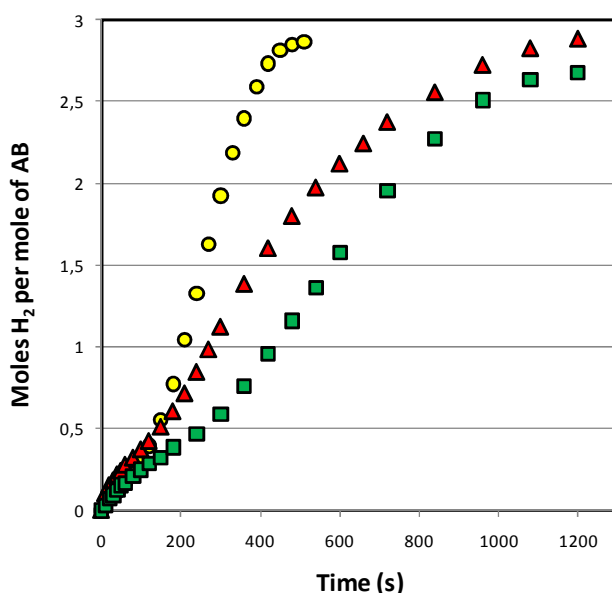


Figure 63. Hydrogen liberation from 0.46 M of AB at 30°C with 0.1 mol % of catalyst **33** in different THF/ H_2O mixtures: 50/50 (o), 90/10 (Δ) and 25/75 (\square).

The THF/H₂O mixture of 50/50 was found optimal, as it allowed the liberation of almost 3 equivalents of hydrogen gas in the minimum amount of time. Performance of this hydrolysis with higher amounts of water led to the precipitation of the catalyst, and the efficiency of the reaction is therefore reduced. A higher amount of tetrahydrofurane also leads to a lower hydrogen release rate.

The hydrolysis reaction was performed in a THF/H₂O mixture of 50/50 under the same conditions (with an AB concentration of 0.46 M and a 0.1 mol % of **33** catalyst loading at 30°C) in the presence of Hg. A decrease in the hydrogen release rate would imply a heterogeneous catalytic process, as Hg is a well-known heterogeneous catalyst poison.¹⁰⁴ Similar results afforded by this experiment confirm the homogeneous nature of the catalytic reaction.

II. 2.3.3b. Hydrolysis of ammonia-borane catalysed by $[RhCl(C_9H_6NCO)](Hpz)(nbyl)]_2$ (33**), $[RhCl(C_9H_6NCO)](Hpz)_2(nbyl)]$ (**34**), $[Rh(C_9H_6NCO)](Hpz)_3(nbyl)]BPh_4$ (**35**) or $[RhCl(C_9H_6NC(nbyl)OH)](Hpz)(Ph_2PO)]$ (**36**).**

The catalytic activity of complexes **33-36** was studied for the homogeneous hydrolysis of ammonia-borane in a THF/H₂O mixture of 50/50 in the presence of air. Hydrolysis experiments for these complexes were carried out at 30°C with 1.38 mmol of AB (0.46 M) and 0.2 mol % of compounds **34**, **35** and **36**, and 0.1 mol % of compound **33**, to compare equal rhodium concentrations in solution. A blank test under the same reaction conditions was also performed in absence of catalyst. Figure 64 shows collected data of the hydrogen release from AB in the presence of these complexes.

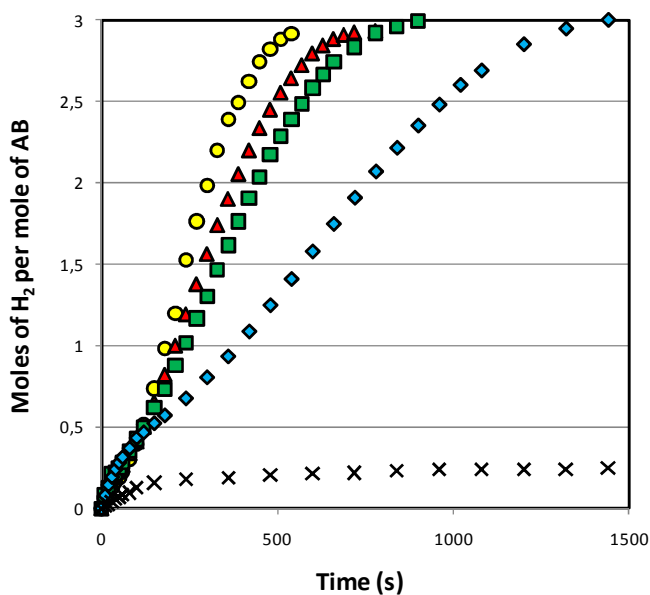


Figure 64. Hydrogen liberation from THF/H₂O mixtures of 50/50 at 30°C, with 0.46 M of AB and 0.1 mol % of catalyst **33** (o), or 0.2 % mol of catalysts **34** (Δ), **35** (□), **36** (◇) and a blank test in absence of a catalyst (×).

Experimental data show similar reaction rates in hydrolysis catalysed by alkyl-acyl rhodium complexes **33**, **34** and **35**, which proved to be efficient homogeneous catalysts for this reaction. These compounds afforded the generation of almost three hydrogen equivalents per mole of AB. The highest reaction rate corresponds to dimeric complex [RhCl(C₉H₆NCO))(Hpz)(nbyl)]₂ (**33**), affording the release of 97% of the maximum hydrogen content within 9 minutes. Neutral and cationic compounds [RhCl(C₉H₆NCO))(Hpz)₂(nbyl)] (**34**) and [Rh(C₉H₆NCO))(Hpz)₃(nbyl)]BPh₄ (**35**) showed slightly lower reaction rates, affording the liberation of 98-99% of the hydrogen content within 13 and 15 minutes respectively. Complex [RhCl(C₉H₆NC(nbyl)OH))(Hpz)(Ph₂PO)] (**36**) also leads to the generation of all three hydrogen equivalents per mole of substrate, but exhibits a lower activity, affording the complete hydrolysis of ammonia-borane within 24 minutes. A blank test, performed under the same reaction conditions, shows a poor uncatalysed hydrolysis of AB, leading to the liberation of an 8 % of the total amount of hydrogen content after 25 minutes.

Due to the higher efficiency showed by complex **33**, it was chosen to perform a kinetic study. A simple first-order kinetic model would not properly explain the behavior of the catalytic system. The experimental data of hydrogen gas evolution catalysed by **33** includes the hydrogen liberation of catalysed and uncatalysed hydrolysis processes. The uncatalysed reaction is significant during the first stages of reaction, until equilibrium is reached (Figure

64), whereas the catalyzed reaction practically allows the maximum hydrogen evolution in the presence of all tested catalysts. Attempts of obtaining a suitable rate law to explain the global process as a sum of catalysed and uncatalysed reactions were unsuccessful. Nevertheless, a first-order approach can be applied for comparison purposes to the AB hydrolysis catalysed by **33**, leading to fairly good results.

The dependence of the hydrogen release rate with the catalyst loading was studied. Figure 65 collects results obtained from hydrolysis of 1.38 mmol of ammonia-borane in THF/H₂O mixtures of 50/50 at 30 °C, in the presence of various concentrations of **33**. Catalyst loadings vary from 0.05 to 0.025 mol %, due to the insolubility exhibited by the rhodium compound in the solvent mixture at concentrations higher than 0.1 mol %. Experimental data show the increase of the hydrogen liberation rate with the catalyst concentration.

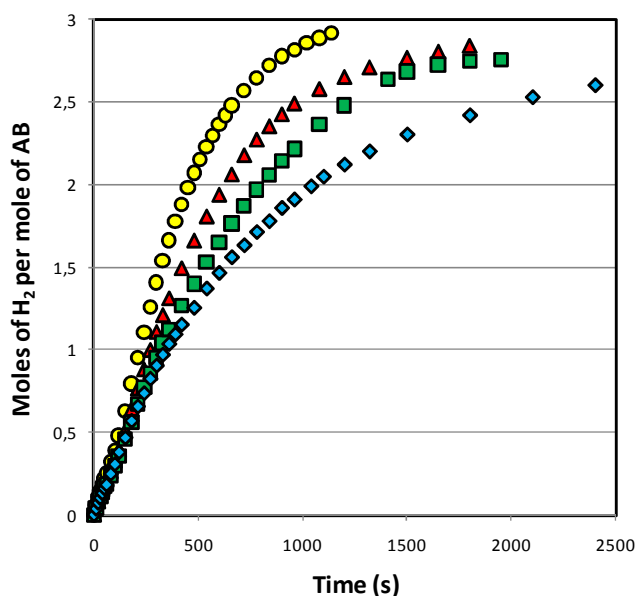


Figure 65. Hydrogen liberation from THF/H₂O mixtures of 50/50 at 30°C, with 0.46 M of AB and various concentrations of catalyst **33**: 0.05 % (○), 0.04 % (Δ), 0.032 % (□) and 0.025 mol % (◇).

Assuming first-order dependence with respect to AB, the reaction rate would be given by equation 1. The observed reaction rate (v_{exp}) collects both catalysed (v_{cat}) and uncatalysed (v_{uncat}) reaction rates.

$$v_{\text{exp}} = (k_{\text{uncat}} + k_{\text{cat}}[\text{catalyst}]_0)[\text{substrate}] \quad \text{Eq 1}$$

$$\text{where: } (k_{\text{uncat}} + k_{\text{cat}}[\text{catalyst}]_0) = k_{\text{obs}}$$

Table 7 collects maximum conversion data, time required and rate constants (k_{obs}) calculated for each concentration of catalyst **33** in the hydrolysis of ammonia-borane. The k_{obs} values for each catalyst loading were calculated from lineal representation of the hydrolysis reactions. Figure 66 shows first order linear representation of hydrogen liberation experimental data up to 3 half-lives catalysed by compound **33**.

Table 7. Influence of catalyst $[\text{RhCl}(\text{C}_9\text{H}_6\text{NCO})(\text{Hpz})(\text{nbyl})_2]$ (**33**) loading in the AB hydrolysis reaction rate at 30°C.

% Cat	% Conversion	Time (s)	$10^3 k_{\text{obs}} (\text{s}^{-1})$
0.05	98	1300	2.65 ± 0.05
0.04	95	1800	1.83 ± 0.03
0.032	92	1950	1.39 ± 0.01
0.025	95	4500	0.98 ± 0.01

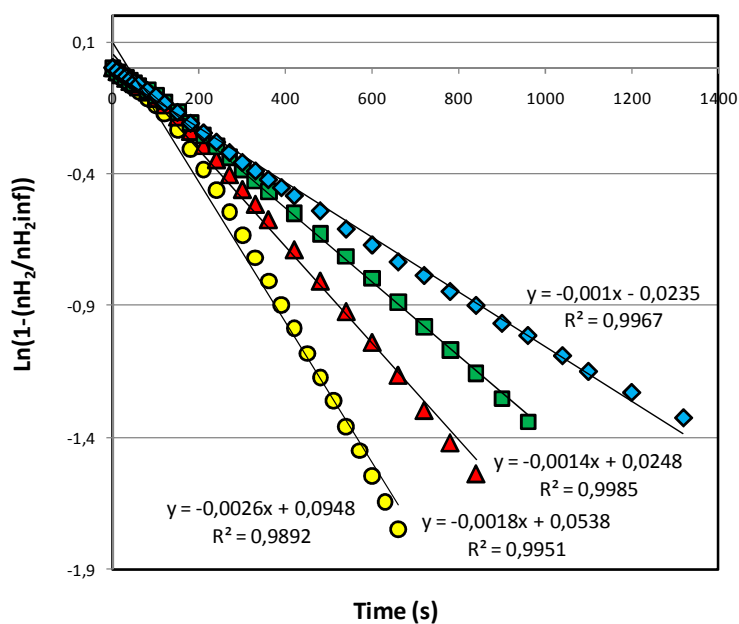


Figure 66. Lineal representation of the generated hydrogen from THF/H₂O mixtures of 50/50 at 30°C, with 0.46 M of AB and various concentrations of catalyst **33**: 0.05 % (○), 0.04 % (Δ), 0.032 % (□) and 0.025 (◇) mol %.

Representation of the rate constant (k_{obs}) versus the corresponding catalyst loading ($[\text{catalyst}]_0$) allows the determination of k_{cat} and k_{uncat} values as the slope and the intercept of the resultant plot, according to equation 1. Figure 67 shows the plot of k_{obs} versus $[\text{catalyst}]_0$ in the range of 0.69×10^{-3} to 0.345×10^{-3} range (0.05 to 0.025 mol %) for compound **33**. From this plot, values of $k_{\text{cat}} = 4.63 \pm 0.34 \text{ M}^{-1} \text{ s}^{-1}$ and $k_{\text{uncat}} = 0.65 \pm 0.18 \text{ M}^{-1} \text{ s}^{-1}$ were obtained.

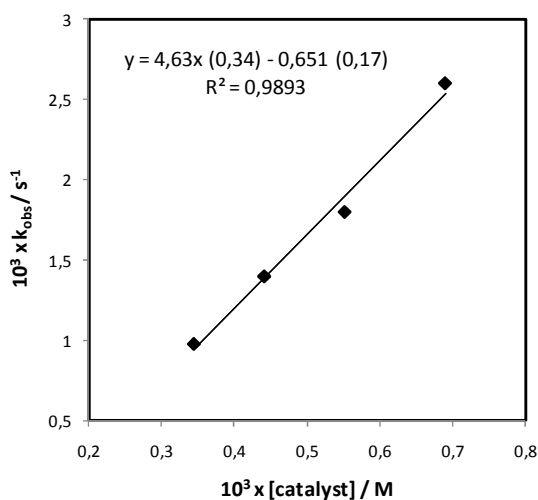


Figure 67. Influence of $[\text{catalyst}]_0$ on k_{obs} for the hydrogen release from AB catalysed by **33**.

The behaviour of catalyst **33** was compared with that of previously mentioned acylrhodium(III) complexes $[\text{RhClH}(\text{PPh}_2(o\text{-C}_6\text{H}_4\text{CO}))(\text{PPh}_2\text{O})\text{H}](4\text{-pic})$ (**I-48**) or $[\text{RhClH}(\text{PPh}_2(o\text{-C}_6\text{H}_4\text{CO}))(\text{Hmpz})_2]$ (**I-49**) containing diphenylphosphinous acid or pyrazole ligands respectively, which were developed in our laboratory. These data are collected in table 8.

Table 8. Comparison of the behaviour of catalysts $[\text{RhClH}(\text{PPh}_2(o\text{-C}_6\text{H}_4\text{CO}))(\text{PPh}_2\text{O})\text{H}](4\text{-pic})$ (**I-48**), $[\text{RhClH}(\text{PPh}_2(o\text{-C}_6\text{H}_4\text{CO}))(\text{Hmpz})_2]$ (**I-49**) and $[\text{RhCl}(\text{C}_9\text{H}_6\text{NCO})(\text{Hpz})(\text{nbyl})_2]$ (**33**) in the AB hydrolysis reaction in THF/ H_2O mixtures of 50/50.

CATALYST	% Cat	% Rh	T (°C)	% Conversion	$10^3 k_{\text{obs}} (\text{s}^{-1})$
I-48	0.5	0.5	25	89.5	1.54 ± 0.07
I-49	0.5	0.5	25	90.0	1.89 ± 0.06
33	0.05	0.1	25	86.7	1.57 ± 0.09
I-48	0.5	0.5	30	91.2	2.6 ± 0.10
33	0.05	0.1	30	98.0	2.65 ± 0.05

With a rhodium loading as low as 0.1 mol %, compound **33** displays a rate constant of $2.65 \times 10^{-3} \text{ s}^{-1}$ at 30 °C, with an almost total conversion, while catalysts **I-48** and **I-49** require a 0.5 mol % catalyst loading, reaching a maximum of a 91 % of the total hydrogen release. At 25 °C, the performance of **33** is also similar to that showed by **I-48** and **I-49** but with a five times lower rhodium concentration.

II.2.4. BIBLIOGRAPHY

1. (a) A. E. Shilov, G. B. Shul'pin, *Chem. Rev.*, **1997**, *97*, 2879–2932; (b) Ritleng, C. Sirlin, M. Pfeffer, *Chem. Rev.*, **2002**, *102*, 1731-1770; (c) Y. J. Park, J. W. Park, C. H. Jun, *Acc. Chem. Res.*, **2008**, *41*, 222-234.
2. G. Dyker, *Handbook of C-H Transformations: Applications in Organic Synthesis*, Wiley-VCH, Weinheim, **2005**.
3. (a) A. H. Roy, C. P. Lenges, M. J. Brookhart, *Am. Chem. Soc.*, **2007**, *129*, 2082–2093; (b) M. C. Willis, *Chem. Rev.*, **2010**, *110*, 725-748.
4. (a) G. E. Dobereiner, R.H. Crabtree, *Chem. Rev.*, **2010**, *110*, 681-703; (b) A. M. Whittaker, V. M. Dong, *Angew. Chem. Int. Ed.* **2015**, *54*, 1312-1315.
5. (a) D. Necas, M. Kotora, *Curr. Org. Chem.*, **2007**, *11*, 1566-1591; (b) M. A. Esteruelas, Y. A. Hernández, A. M. López, M. Oliván, L. Rubio, *Organometallics*, **2008**, *27*, 799-802; (c) F. Chen, T. Wang, N. Jiao, *Chem. Rev.*, **2014**, *114*, 8613–8661.
6. T. Morimoto, M. Fujioka, K. Fujii, K. Tsutsumi, K. Kakiuchi, *Pure Appl. Chem.*, **2008**, *80*, 1079-1087.
7. D. Milstein, *Acc. Chem. Res.*, **1984**, *17*, 221-26.
8. (a) D. Milstein, W. C. Fultz, J. C. Calabrese, *J. Am. Chem. Soc.*, **1986**, *108*, 1336-1338; (b) K. Wang, T. J. Emge, A. S. Goldman, C. Li, S. P. Nolan, *Organometallics*, **1995**, *14*, 4929-4936; (c) R. Goikhman, D. Milstein, *Angew. Chem. Int. Ed.*, **2001**, *40*, 1119-1122; (d) V. Circu, M. A. Fernandes, L. Carlton, *Inorg. Chem.*, **2002**, *41*, 3859-3865.
9. D. Milstein, *Organometallics*, **1982**, *1*, 1549-1551.
10. (a) C. H. Jun, C. W. Moon, D. Y. Lee, *Chem. Eur. J.*, **2002**, *8*, 2422-2428; (b) M. C. Willis, S. J. McNally, P. J. Beswick, *Angew. Chem. Int. Ed.*, **2004**, *43*, 340-343; (c) C.-H. Jun, E.-A. Jo, J.-W. Park, *Eur. J. Org. Chem.*, **2007**, 1869-1881; (d) M. M. Coulter, K. G. M. Kou, B. Galligan, V. M. Dong, *J. Am. Chem. Soc.*, **2010**, *132*, 16330-16333; (e) K. Tanaka, *Rhodium Catalysis in Organic Synthesis: Methods and Reactions*, Wiley-VCH, Weinheim, **2019**.
11. J. W. Suggs, *J. Am. Chem. Soc.*, **1978**, *100*, 640-641.
12. T. B. Rauchfuss, *J. Am. Chem. Soc.*, **1979**, *101*, 1045-1047.
13. J. W. Suggs, M. J. Wovkulich, S. D. Cox, *Organometallics*, **1985**, *4*, 1101-1107.
14. (a) C. H. Jun, *J. Organomet. Chem.*, **1990**, *390*, 361-370; (b) C. H. Jun, *Organometallics*, **1996**, *15*, 895-897.
15. I. Zumeta, T. Kluge, C. Mendicute-Fierro, C. Wagner, L. Ibarlucea, T. Ruffer, V. San Nacienceno, D. Steinborn, M. A. Garralda, *Organometallics*, **2014**, *33*, 788-795.
16. E. F. Landvatter, T. B. Rauchfuss, *Organometallics*, **1982**, *1*, 506-513.
17. P. Crochet, M. A. Fernández-Zumel, C. Beauquis, J. Gimeno, *Inorg. Chim. Acta*, **2003**, *352*, 114-120.
18. C. P. Lenges, M. Brookhart, P. S. White, *Angew. Chem. Int. Ed. Engl.*, **1999**, *38*, 552-555.
19. W. Y. Yeh, C. S. Lin, S. M. Peng, G. H. Lee, *Organometallics*, **2004**, *23*, 917-920.
20. M. A. Garralda, *C. R. Chimie*, **2005**, *8*, 1413-1420.

21. (a) C. A. Ghilardi, S. Midollini, S. Moneti, A. Orlandini, G. J. Scapacci, *J. Chem. Soc., Dalton Trans.*, **1992**, 3371-3376; (b) S. Antonaroli, B. Crociani, *J. Organomet. Chem.*, **1998**, *560*, 137-146; (c) G. Sánchez, J. L. Serrano, M. A. Moral, J. Pérez, E. Molins, G. López, *Polyhedron*, **1999**, *18*, 3057-3064.
22. (a) R. E. Rülke, V. E. Kaasjager, P. Wehman, C. J. Elsevier, P. W. N. M. Van Leeuwen, K. Vrieze, J. Fraanje, K. Goubitz, A. L. Spek, *Organometallics*, **1996**, *15*, 3022-3031; (b) W. Yeh, C. Yang, S. Peng, G. Lee, *J. Chem. Soc., Dalton Trans.*, **2000**, 1649-1654.
23. (a) J. C. Jeffery, T. B. Rauchfuss, P. A. Tucker, *Inorg. Chem.*, **1980**, *19*, 3306-3315; (b) T. L. Marxen, B. J. Johnson, P. V. Nilsson, L. H. Pignolet, *Inorg. Chem.*, **1984**, *23*, 4663-4670.
24. M. A. Garralda, R. Hernandez, L. Ibarlucea, E. Pinilla, M. R. Torres, M. Zarandona, *Inorg. Chim. Acta*, **2004**, *357*, 2818-2826.
25. R. El Mail, M. A. Garralda, R. Hernandez, L. Ibarlucea, E. Pinilla, M. R. Torres, *Organometallics*, **2000**, *19*, 5310-5317.
26. R. El Mail, M. A. Garralda, R. Hernández, L. Ibarlucea, *J. Organomet. Chem.*, **1994**, *648*, 149-154.
27. M. A. Garralda, R. Hernández, L. Ibarlucea, E. Pinilla, M. R. Torres, M. Zarandona, *Organometallics*, **2007**, *26*, 1031-1038.
28. G. Brockaart, R. El Mail, M. A. Garralda, R. Hernandez, L. Ibarlucea, J. I. Santos, *Inorg. Chim. Acta*, **2002**, *338*, 249-254.
29. R. El Mail, M. A. Garralda, R. Hernández, L. Ibarlucea, E. Pinilla, M. R. Torres, *Helv. Chim. Acta*, **2002**, *85*, 1485-1495.
30. R. El Mail, M. A. Garralda, R. Hernández, L. Ibarlucea, E. Pinilla, M. R. Torres, M. Zarandona, *Eur. J. Inorg. Chem.*, **2005**, 1671-1677.
31. M. Barquín, M. A. Garralda, L. Ibarlucea, C. Mendicute-Fierro, E. Pinilla, V. San Nacienceno, M. R. Torres, *Organometallics*, **2011**, *30*, 1577-1587.
32. N. Almenara, L. Ibarlucea, C. Mendicute-Fierro, J. M. Seco, A. Rodríguez-Diéguez, M. A. Garralda, M. A. Huertos, *Dalton Trans.*, **2016**, *45*, 18502-18509.
33. M. Barquín, M. A. Garralda, R. Hernández, L. Ibarlucea, C. Mendicute-Fierro, M. C. Torralba, M. R. Torres, V. San Nacienceno, I. Zumeta, *Eur. J. Inorg. Chem.*, **2012**, 1445-1452.
34. (a) H. Brisset, Y. Gourdel, P. Pellon, M. Le Corre, *Tetrahedron Lett.*, **1993**, *34*, 4523-4526; (b) D. Matt, R. Ziesel, A. D. Cian, J. Fischer, *New J. Chem.*, **1996**, *20*, 1257-1263; (c) D. V. Moiseev, P. Marcazzan, B. R. James, *Can. J. Chem.*, **2009**, *87*, 582-590; (d) A. A. Mikhailine, P. O. Lagaditis, P. E. Sues, A. J. Lough, R. H. Morris, *J. Organomet. Chem.*, **2010**, *695*, 1824-1830.
35. G. D. Vaughn, J. A. Gladysz, *J. Am. Chem. Soc.*, **1986**, *108*, 1473-1480.
36. F. Lorenzini, D. Moiseev, B. O. Patrick, B. R. James, *Inorg. Chem.*, **2010**, *49*, 2111-2122.
37. (a) U. Knof, A. von Zelewsky, *Angew. Chem. Int. Ed.*, **1999**, *38*, 302-322; (b) M. Carmona, R. Rodríguez, I. Méndez, V. Passarelli, F. J. Lahoz, P. García-Orduña, D. Carmona, *Dalton Trans.*, **2017**, *46*, 7332-7350.
38. (a) H. Brunner, *Angew. Chem. Int. Ed.*, **1999**, *38*, 1194-1208; (b) E. B. Bauer, *Chem. Soc. Rev.*, **2012**, *41*, 3153-3167.

39. (a) L. Gong, L. A. Chen, E. Meggers, *Angew. Chem. Int. Ed.*, **2014**, *53*, 10868–10874; (b) N. Hubert, C. Mazet, *Chem. Commun.*, **2016**, *52*, 10629–10631.
40. (a) P. D. Knight, P. Scott, *Coord. Chem. Rev.*, **2003**, *242*, 125–143; (b) K. Matsumoto, B. Saito, T. Katsuki, *Chem. Commun.*, **2007**, 3619–3627; (c) O. Cussó, X. Ribas, M. Costas, *Chem. Commun.*, **2015**, *51*, 14285–14298; (d) R. H. Morris, *Acc. Chem. Res.*, **2015**, *48*, 1494–1502.
41. (a) A. A. Mikhailine, E. Kim, C. Dingels, A. J. Lough, R. H. Morris, *Inorg. Chem.*, **2008**, *47*, 6587–6589; (b) P. O. Lagaditis, A. A. Mikhailine, A. J. Lough, R. H. Morris, *Inorg. Chem.*, **2010**, *49*, 1094–1102.
42. K. Park, P. O. Lagaditis, A. J. Lough, R. H. Morris, *Inorg. Chem.*, **2013**, *52*, 5448–5456.
43. D. V. Moiseev, B. O. Patrick, B. R. James, *Inorg. Chem.*, **2007**, *46*, 11467–11474.
44. (a) G. K. Anderson, R. Kumar, *Inorg. Chim. Acta*, **1988**, *146*, 89–92; (b) M. A. Garralda, R. Hernández, L. Ibarlucea, E. Pinilla, M. R. Torres, M. Zarandona, *Inorg. Chim. Acta*, **2004**, *357*, 2818–2826.
45. T. G. Appleton, H. C. Clark, L. I. Manzer, *Coord. Chem. Rev.*, **1973**, *10*, 335–422.
46. P. E. Garrou, *Chem. Rev.*, **1981**, *81*, 229–266.
47. (a) B. de Bruin, J. A. Brands, J. J. J. Donners, M. P. J. Donners, R. de Gelder, J. M. M. Smits, A. W. Gal, A. L. Spek, *Chem. Eur. J.*, **1999**, *5*, 2921–2936; (b) B. J. Coe, S. J. Glenwright, *Coord. Chem. Rev.*, **2000**, *203*, 5–80.
48. V. San Nacienceno, S. Azpeitia, L. Ibarlucea, C. Mendicutie-Fierro, A. Rodríguez-Diéguez, J. M. Seco, E. San Sebastian, M. A. Garralda, *Dalton Trans.*, **2015**, *44*, 13141–13155.
49. (a) B. K. Corkey, F. L. Taw, R. G. Bergman, M. Brookhart, *Polyhedron*, **2004**, *23*, 2943–2954; (b) K. S. Chan, C. M. Lau, *Organometallics*, **2006**, *25*, 260–265.
50. C. Bianchini, A. Meli, M. Peruzzini, J. A. Ramírez, A. Vacca, F. Vizza, F. Zanobini, *Organometallics*, **1989**, *8*, 337–345.
51. M. A. Garralda, R. Hernández, L. Ibarlucea, E. Pinilla, M. R. Torres, M. Zarandona, *Organometallics*, **2007**, *26*, 5369–5376.
52. (a) C. Gunanathan, D. Milstein, *Science*, **2013**, *341*, 1229712; (b) S. Chakraborty, P. O. Lagaditis, M. Förster, E. A. Bielinski, N. Hazari, M. C. Holthausen, W. D. Jones, S. Schneider, *ACS Catal.*, **2014**, *4*, 3994–4003; (c) J. Cheng, M. Zhu, C. Wang, J. Li, X. Jiang, Y. Wei, W. Tang, D. Xue, J. Xiao, *Chem. Sci.*, **2016**, *7*, 4428–4434; (d) C. Vicent, D. G. Gusev, *ACS Catal.*, **2016**, *6*, 3301–3309.
53. (a) I. De Castro, M. V. Galakhov, M. Gómez, P. Gómez-Sal. A. Martín, P. Royo, *J. Organomet. Chem.*, **1996**, *514*, 51–58; (b) V. Alezra, G. Bernardinelli, C. Corminboeuf, U. Frey, E. P. Kundig, A. E. Merbach, C. M. Saudan, F. Viton, J. Weber, *J. Am. Chem. Soc.*, **2004**, *126*, 4843–4853; (c) S. C. Marinescu, R. R. Schrock, M. Li, A. H. Hoveyda, *J. Am. Chem. Soc.*, **2009**, *131*, 58–59; (d) E. P. A. Couzjin, J. C. Slootweg, A. W. Ehlers, K. Lammertsma, *J. Am. Chem. Soc.*, **2010**, *132*, 18127–18140; (e) J. Takaya, N. Kirai, N. Iwasawa, *Organometallics*, **2014**, *33*, 1499–1502.
54. M. A. Garralda, R. Hernández, L. Ibarlucea, E. Pinilla, M. R. Torres, *Organometallics*, **2003**, *22*, 3600–3006.
55. R. Ciganda, M. A. Garralda, L. Ibarlucea, E. Pinilla, M. R. Torres, *Dalton Trans.*, **2009**, 4227–4235.

56. (a) C. M. Lukehart, *Acc. Chem. Res.*, **1981**, *14*, 116-122; (b) C. M. Lukehart, *Adv. Organomet. Chem.*, **1986**, *25*, 45-71.
57. F. Acha, R. Ciganda, M. A. Garralda, R. Hernandez, L. Ibarlucea, E. Pinilla, M. R. Torres, *Dalton Trans.*, **2008**, 4602-4611.
58. J. G. Cordaro, R. G. Bergman, *J. Am. Chem. Soc.*, **2004**, *126*, 16912-16929.
59. (a) R. Ciganda, M. A. Garralda, L. Ibarlucea, E. Pinilla, M. R. Torres, *Dalton Trans.*, **2010**, *39*, 7226-7229; (b) M. A. Garralda, C. Mendicute-Fierro, A. Rodríguez-Diéguez, J. M. Seco, C. Ubide, I. Zumeta, *Dalton Trans.*, **2013**, *42*, 11652-11660.
60. (a) G. W. Crabtree, M. S. Dresselhaus, M. V. Buchanan, *Phys. Today*, **2004**, *57*, 39-44; (b) U. Eberle, M. Felderhoff, F. Schüth, *Angew. Chem., Int. Ed.*, **2009**, *48*, 6608-6630; (c) A. F. Dalebrook, W. Gan, M. Grasemann, S. Moret, G. Laurenczy, *Chem. Commun.*, **2013**, *49*, 8735-8751.
61. (a) H. W. Langmi, G. S. McGrady, *Coord. Chem. Rev.*, **2007**, *251*, 925-935; (b) T. Umegaki, J. M. Yan, X. B. Zhang, H. Shioyama, N. Kuriyama, Q. Xu, *Int. J. Hydrogen Energy*, **2009**, *34*, 2303-2311; (c) A. Staubitz, A. P. M. Robertson, I. Manners, *Chem. Rev.*, **2010**, *110*, 4079-4124.
62. (a) H. L. Jjiang, Q. Xu, *Catal. Today*, **2011**, *170*, 56-63; (b) P. Z. Li, A. Aijaz, Q. Xu, *Angew. Chem., Int. Ed.*, **2012**, *51*, 6753-6756; (c) S. Caliskan, M. Zahmakiran, F. Durap, S. Özkar, *Dalton Trans.*, **2012**, *41*, 4976-4984; (d) Y. Du, N. Cao, L. Yang, W. Luo, G. Cheng, *New J. Chem.*, **2013**, *37*, 3035-3042; (e) S. Akbayrak, S. Ozkar, *Dalton Trans.*, **2014**, *43*, 1797-1805; (f) F. Qiu, G. Liu, L. Li, Y. Wang, C. Xu, C. An, C. Chen, Y. Xu, Y. Huang, Y. Wang, L. Jiao, H. Yuan, *Chem. – Eur. J.*, **2014**, *20*, 505-509; (g) H. Cheng, T. Kamegawa, K. Mori, H. Yamashita, *Angew. Chem., Int. Ed.*, **2014**, *53*, 2910-2914.
63. (a) M. Chandra, Q. Xu, *J. Power Sources*, **2007**, *168*, 135-142; (b) T. J. Clark, G. R. Whittell, I. Manners, *Inorg. Chem.*, **2007**, *46*, 7522-7527; (c) M. Fetz, R. Gerber, O. Blacque, C. M. Frech, *Chem. Eur. J.*, **2011**, *17*, 4732-4736; (d) C. Xu, M. Hu, Q. Wang, G. Fan, Y. Wang, Y. Zhang, D. Gao, J. Bi, *Dalton Trans.*, **2018**, *47*, 2561-2567.
64. (a) G. C. Fortman, A. M. Z. Slawin, S. P. Nolan, *Organometallics*, **2011**, *30*, 5487-5492; (b) D. J. Nelson, B. J. Truscott, J. D. Egbert, S. P. Nolan, *Organometallics*, **2013**, *32*, 3769-3772.
65. T. W. Graham, C. W. Tsang, X. Chen, R. Guo, W. Jia, S. M. Lu, C. Sui-Seng, C. B. Ewart, A. Lough, D. Amoroso, K. Abdur-Rashid, *Angew. Chem., Int. Ed.*, **2010**, *49*, 8708-8711.
66. M. Muñoz-Olasagasti, A. Telleria, J. Pérez-Miqueo, M. A. Garralda, Z. Freixa, *Dalton Trans.*, **2014**, *42*, 11652-11660.
67. C. Boulho, J. P. Djukic, *Dalton Trans.*, **2010**, *39*, 8893-8905.
68. A. Tellería, C. Vicent, V. San Nacienceno, M. A. Garralda, Z. Freixa, *ACS Catal.*, **2017**, *7*, 8394-8405.
69. V. San Nacienceno, L. Ibarlucea, C. Mendicute-Fierro, A. Rodríguez-Diéguez, J. M. Seco, I. Zumeta, C. Ubide, M. A. Garralda, *Organometallics*, **2014**, *33*, 6044-6052.
70. V. San Nacienceno, S. Azpeitia, L. Ibarlucea, C. Mendicute-Fierro, A. Rodríguez-Diéguez, J. M. Seco, E. San Sebastian, M. A. Garralda, *Dalton Trans.*, **2015**, *44*, 13141-13155.
71. D. M. Roundhill, R. F. Sperline, W. B. Beaulieu, *Coord. Chem. Rev.*, **1978**, *26*, 263-279.

72. (a) D. M. Roudhill, R. P. Sperline, W. B. Beaulieu, *Coord. Chem. Rev.*, **1978**, *26*, 263-279; (b) B. Walther, *Coord. Chem. Rev.*, **1984**, *60*, 67-105; (c) A. Christiansen, L. Chuanzhao, M. Garland, D. Selent, R. Ludwig, A. Spannenberg, W. Baumann, R. Franke, *Eur. J. Org. Chem.*, **2010**, 2733-2741.
73. K. R. Dixon, A. D. Rattray, *Can. J. Chem.*, **1971**, *49*, 3997-4004.
74. P. W. N. M. van Leeuwen, C. F. Roobeek, R. L. Wife, J. H. G. J. Frijns, *J. Chem. Soc., Chem. Commun.*, **1986**, 31-33.
75. A. Díez, J. Forniés, J. Gómez, E. Lalinde, A. Martín, M. T. Moreno, S. Sánchez, *Dalton Trans.*, **2007**, 3653-3660.
76. (a) P. J. Brothers, *Prog. Inorg. Chem.*, **1981**, *28*; (b) J. Elguero. *Comprehensive Heterocyclic Chemistry, Volume 5. Pergamon Press, Oxford*, **1984**, 167-303.
77. (a) D. H. Choi, J. H. Yoon, J. H. Lim, H. C. Kim, C. S. Hong, *Inorg. Chem.*, **2006**, *45*, 5947-5952; (b) J. Pérez, L. Riera, *Eur. J. Inorg. Chem.*, **2009**, 4913-4925.
78. (a) D. Carmona, L. A. Oro, M. P. Lamata, J. Elguero, M. C. Apreda, C. Foces-Foces, F. H. Cano, *Angew. Chem., Int. Ed. Engl.*, **1986**, *25*, 1114-1115; (b) P. Paredes, M. Arroyo, D. Miguel, F. Villafañe, *J. Organomet. Chem.*, **2003**, *667*, 120-125; (c) D. B. Grotjahn, S. Van, D. Combs, D. A. Lev, C. Schneider, C. D. Incarvito, K. C. Lam, G. Rossi, A. L. Rheingold, M. Rideout, C. Meyer, G. Hernández, L. Mejorado, *Inorg. Chem.*, **2003**, *42*, 3347-3355; (d) A. V. Khripun, S. I. Selivanov, V. Y. Kukushkin, M. Haukkalnorg, *Inorg. Chim. Acta*, **2006**, *359*, 320-326; (e) I. Ara, J. Forniés, R. Lasheras, A. Martín, V. Sicilia, *Eur. J. Inorg. Chem.*, **2006**, 948-957; (f) G. Albertin, S. Antoniutti, J. Castro, S. García-Fontán, *Eur. J. Inorg. Chem.*, **2011**, 510-520.
79. (a) A. Tanitame, Y. Oyamada, K. Ofuji, M. Fujimoto, K. Suzuki, T. Ueda, H. Terauchi, M. Kawasaki, K. Nagai, M. Wachi, J. I. Yamagishi, *Bioorg. Med. Chem.*, **2004**, *12*, 5515-5524; (b) C. B. Vicentini, C. Romagnoli, E. Andreotti, D. J. Mares, *Agric. Food Chem.*, **2007**, *55*, 10331-10338; (c) S. Fustero, R. Roman, J. F. Sanz-Cervera, A. Simon-Fuentes, J. Bueno, S. J. Villanova, *Org. Chem.*, **2008**, *73*, 8545-8552; (d) S. Fustero, M. Sánchez-Roselló, P. Barrio, A. Simón-Fuentes, *Chem. Rev.*, **2011**, *111*, 6984-7034; (e) V. Mukundam, A. Kumar, K. Dhanunjayarao, A. Ravi, S. Peruncheralathana, K. Venkatasubbaiah, *Polym. Chem.*, **2015**, *6*, 7764-7770; (f) M. J. Naim, O. Alam, F. Nawaz, M. J. Alam, P. Alam, *J. Pharm. Bioallied Sci.*, **2016**, *8*, 2-17.
80. G. A. Ardizzioia, G. LaMonica, A. Maspero, M. Moret, N. Massiocchi, *Eur. J. Inorg. Chem.*, **1998**, 1503-1512.
81. (a) G. R. Clark, T. R. Greene, W. R. Roper, *J. Organomet. Chem.*, **1985**, *293*, C25-C28; (b) C. Hahn, M. Spiegler, E. Herdtweck, R. Taube, *Eur. J. Inorg. Chem.*, **1999**, 435-440; (c) R. El Mail, M. A. Garralda, R. Hernández, L. Ibarlucea, E. Pinilla, M. R. Torres, M. Zarandona, *Eur. J. Inorg. Chem.*, **2005**, 1671-1677.
82. T. Steiner, *Angew. Chem., Int. Ed.*, **2002**, *41*, 48-76.
83. (a) F. P. Pruchnik, P. Jakimowicz, Z. Ciunik, J. Zakrzewska-Czerwinska, A. Opolski, J. Wietrzyk, E. Wojdat, *Inorg. Chim. Acta.*, **2002**, *334*, 59-66; (b) R. Q. Zou, C. S. Liu, X. S. Shi, X. H. Bu, J. Ribas, *CrystEngComm*, **2005**, *7*, 722-727; (c) M. Arroyo, M. T. García-de-Prada, C. García-Martín, V. García-

- Pacios, R. García-Rodríguez, P. Gómez-Iglesias, F. Lorenzo, I. Martín-Moreno, D. Miguel, F. Villafañe, *J. Organomet. Chem.*, **2009**, *694*, 3190–3199; (d) M. R. Healy, J. W. Roebuck, E. D. Doidge, L. C. Emeleus, P. J. Bailey, J. Campbell, A. J. Fischmann, J. B. Love, C. A. Morrison, T. Sassi, D. J. White, P. A. Tasker, *Dalton Trans.*, **2016**, *45*, 3055-3062.
84. (a) M. Cano, J. V. Heras, M. Maeso, M. Alvaro, R. Fernández, E. Pinilla, J. A. Campo, A. Monge, *J. Organomet. Chem.*, **1997**, *534*, 159–172; (b) E. D. Raczynska, W. Kosinska, B. Osmialowski, R. Gawinecki, *Chem. Rev.*, **2005**, *105*, 3561–3612.
85. C. A. Tolman, P. Z. Meakin, D. L. Lindner, J. P. Jesson, *J. Am. Chem. Soc.*, **1974**, *96*, 2762-2774.
86. V. San Nacianceno, L. Ibarlucea, C. Mendicute-Fierro, A. Rodríguez-Diéguez, J. M. Seco, A. J. Mota, M. A. Garralda, *Inorg. Chem.*, **2018**, *57*, 5307-5319.
87. P. Larkin, *Infrared and Raman Spectroscopy: Principles and Spectral Interpretation*, Elsevier, **2011**.
88. I. Zumeta, C. Mendicute-Fierro, A. Rodríguez-Diéguez, J. M. Seco, M. A. Garralda, *Organometallics*, **2015**, *34*, 348-354.
89. A. Christiansen, D. Selent, A. Spannenberg, W. Baumann, R. Franke, A. Börner, *Organometallics*, **2010**, *29*, 3139–3145.
90. (a) S. Pavlik, K. Mereiter, M. Puchberger, K. Kirchner, *Organometallics*, **2005**, *24*, 3561–3575; (b) S. D. Hastings, H. Byrd, L. N. Gray, M. J. Jablonsky, J. L. Freeman, G. M. Gray, *Eur. J. Inorg. Chem.*, **2013**, *16*, 2900–2911; (c) L. V. Graux, M. Giorgi, G. Buono, H. Clavier, *Organometallics*, **2015**, *34*, 1864–1871.
91. (a) D. B. Grotjahn, D. V. S. Combs, G. Aguirre, F. Ortega, *Inorg. Chem.*, **2000**, *39*, 2080-2086; (b) H. Jude, F. N. Rein, W. Chen, B. L. Scott, D. M. Dattelbaum, R. C. Rocha, *Eur. J. Inorg. Chem.*, **2009**, 683–690; (c) I. A. Guzei, L. C. Spencer, M. K. Ainooson, J. Darkwa, *Acta Cryst.*, **2010**, *C66*, m336–m338; (d) J. Díez, J. Gimeno, I. Merino, E. Rubio, F. J. Suarez, *Inorg. Chem.*, **2011**, *50*, 4868–4881.
92. (a) J. W. Suggs, *J. Am. Chem. Soc.*, **1978**, *100*, 640–641; (b) J. A. Cabeza, V. Riera, M. A. Villa García, L. Ouahab, S. Triki, *J. Organomet. Chem.*, *441*, **1992**, 323-331; (c) M. Murakami, K. Itami, Y. Ito, *J. Am. Chem. Soc.*, **1996**, *118*, 46, 11672-11673.
93. (a) I. El-Idrissi, O. Eisenstein, Y. Jean, *New J. Chem.*, **1990**, *14*, 671–677; (b) J. F. Riehl, Y. Jean, O. Eisenstein, M. Péliissier, *Organometallics*, **1992**, *11*, 729–737; (c) A. Baroudi, A. El-Hellani, A. A. Bengali, A. S. Goldman, F. Hasanayn, *Inorg. Chem.*, **2014**, *53*, 12348–12359.
94. (a) M. G. Hu, R. A. Geanangel, W. W. Wendlandt, *Thermochim. Acta*, **1978**, *23*, 249–255; (b) F. H. Stephens, R. T. Baker, M. H. Matus, D. J. Grant, D. A. Dixon, *Angew. Chem., Int. Ed.*, **2007**, *46*, 746–749.
95. A. Staubitz, A. P. M. Robertson, M. E. Sloan, I. Manners, *Chem. Rev.*, **2010**, *110*, 4023-4078.
96. (a) T. Beweries, S. Hansen, M. Kessler, M. Klahn, U. Rosenthal, *Dalton Trans.*, **2011**, *40*, 7689-7692; (b) D. F. Schreiber, C. O'Connor, C. Grave, Y. Ortin, H. Müller-Bunz, A. D. Phillips, *ACS Catalysis*, **2012**, *2*, 2505-2511; (c) L. J. Sewell, G. C. Lloyd-Jones, A. S. Weller, *J. Am. Chem. Soc.*, **2012**, *134*, 3598-3610; (d) L. J. Sewell, M. A. Huertos, M. E. Dickinson y A. S. Weller, *Inorg. Chem.*, **2013**, *52*, 4509-4516; (e) A. Rossin, G. Bottari, A. M. Lozano-Vila, M. Paneque, M. Peruzzini, A. Rossi, F. Zanobini,

- Dalton Trans.*, **2013**, 42, 3533-3541; (f) M. Roselló-Merino, J. López-Serrano, S. Conejero, *J. Am. Chem. Soc.*, **2013**, 135, 10910-10913.
97. S. K. Kim, W. S. Han, T. J. Kim, T. Y. Kim, S. W. Nam, M. Mitoraj, L. Piekos, A. Michalak, S. J. Hwang, S. O. Kang, *J. Am. Chem. Soc.*, **2010**, 132, 9954-9955.
98. R. J. Keaton, J. M. Blacquiere, R. T. Baker, *J. Am. Chem. Soc.*, **2007**, 129, 1844-1845.
99. N. Blaquiere, S. Diallo-Garcia, S. I. Gorelsky, D. A. Black, K. Fagnou, *J. Am. Chem. Soc.*, **2008**, 130, 14034-14035.
100. S. Todisco, L. Luconi, G. Giambastiani, A. Rossin, M. Peruzzini, I. E. Golub, O. A. Filippov, N. V. Belkova, E. S. Shubina, *Inorg. Chem.*, **2017**, 56, 4296-4307.
101. (a) B. L. Conley, D. Guess, T. J. Williams, *J. Am. Chem. Soc.*, **2011**, 133, 14212-14215. (b) X. Zhang, L. Kam, R. Trerise, T. J. Williams, *Acc. Chem. Res.*, **2017**, 50, 86-95.
102. (a) J. M. Yan, X. B. Zhang, S. Han, H. Shioyama, Q. Xu, *Inorg. Chem.*, **2009**, 48, 7389-7393; (b) J. M. Yan, X. B. Zhang, T. Akita, M. Haruta, Q. Xu, *J. Am. Chem. Soc.*, **2010**, 132, 5326-5327; (c) B. Kilic, S. Sencanli, O. Metin, *J. Mol. Catal.*, **2012**, 361-362, 104-110.
103. (a) Z. Fu, Y. Xu, S. L. Chan, W. Wang, F. Li, F. Liang, Y. Chen, Z. Lin, W. Fu, C. Che, *Chem. Commun.*, **2017**, 53, 705-708; (b) C. Wang, J. Tuninetti, Z. Wang, C. Zhang, R. Ciganda, L. Salmon S. Moya J. Ruiz, D. Astruc, *J. Am. Chem. Soc.*, **2017**, 139, 11610-11615; (c) I. B. Baguc, I. Efecan Ertas, M. Yurderi, A. Bulut, M. Zahmakiran, M. Kaya, *Inorg. Chim. Acta*, **2018**, 483, 431-439.
104. (a) G. M. Whitesides, M. Hackett, R. L. Brainard, J. P. P. M. Lavalleye, A. F. Sowinski, A. N. Izumi, S. S. Moore, D. W. Brown, E. M. Staudt, *Organometallics*, **1985**, 4, 1819-1830; (b) J. A. Widegren, R. G. Finke, *J. Mol. Catal. A.: Chem.*, **2003**, 198, 317-341.

III. CONCLUSIONS

1.- Three new silyl-thioether multidentate preligands formulated as $\text{SiMe}_2\text{H}(o\text{-C}_6\text{H}_4\text{SMe})$ (**L1**), $\text{SiMeH}(o\text{-C}_6\text{H}_4\text{SMe})_2$ (**L2**) and $\text{SiMe}_2(o\text{-C}_6\text{H}_4\text{SMe})_2$ (**L3**) have been synthesised by reaction of $2\text{-MeS}(C_6H_4Br)$ with *n*-butyllithium, and subsequent treatment with the corresponding chlorosilane. These silanes are suitable to study Si-X (X = H or C) activation reactions promoted by rhodium(I) and iridium(I) compounds.

2.- The reaction of $[\text{Rh}(\text{cod})\text{Cl}]_2$ with four equivalents of **L1** yields the dinuclear neutral Rh(III)/Rh(III) complex $[\text{Rh}(\text{SiMe}_2(o\text{-C}_6\text{H}_4\text{SMe}))_2\text{Cl}]_2$ (**1**). The mechanism proposed for the formation of **1** starts with a first Si-H activation of **L1** by a Rh(I) centre, which would lead to an unobservable rhodium-hydrido-cyclooctadiene complex, followed by the insertion of the cyclooctadiene into the Rh-H bond to give a Rh(I)cyclooctadiene/Rh(III)cyclooctenyl dimer. A second Si-H activation of **L1** allows the formation of the Rh(I)cyclooctadiene/Rh(III)bis(silane) intermediate $[(\text{cod})\text{Rh}(\mu\text{-Cl})_2\text{Rh}(\text{SiMe}_2(o\text{-C}_6\text{H}_4\text{SMe}))_2]$ (**2**). The second Rh(I) atom would follow the same process with the addition of another unit of **L1**, leading to a Rh(III)cyclooctenyl/Rh(III)bis(silane) compound, and a fourth Si-H activation of **L1** to form the final product **1**. This mechanism is supported by the isolation of a mononuclear Rh(III)cyclooctenyl complex $[\text{Rh}(\eta^3\text{-cyclooctenyl})(\text{SiMe}(o\text{-C}_6\text{H}_4\text{SMe})_2\text{Cl})]$ (**3**) by reaction of $[\text{Rh}(\text{cod})\text{Cl}]_2$ with terdentate preligand **L2**.

3.- The removal of chlorine from complex **3** with $\text{NaBAR}_4^{\text{F}}$ yields the cationic cyclooctenyl 16e compound $[\text{Rh}(\eta^3\text{-cyclooctenyl})(\text{SiMe}(o\text{-C}_6\text{H}_4\text{SMe})_2)\text{BAR}_4^{\text{F}}]$ (**4**), which can also be synthesised by coordination and insertion of 1,5-cyclooctadiene into the Rh-H bond of the unsaturated Rh(III) compound $[\text{Rh}(\text{H})(\text{SiMe}(o\text{-C}_6\text{H}_4\text{SMe})_2)(\text{PPh}_3)]\text{BAR}_4^{\text{F}}$ (**6**), with a subsequent rearrangement. This reaction, unobserved for saturated $[\text{RhCl}(\text{H})(\text{SiMe}(o\text{-C}_6\text{H}_4\text{SMe})_2)(\text{PPh}_3)]$ (**5**) is possible for unsaturated complex **6** because of its vacant coordination site. The analogous 16e Ir(III) compound $[\text{Ir}(\eta^3\text{-cyclooctenyl})(\text{SiMe}(o\text{-C}_6\text{H}_4\text{SMe})_2)\text{BAR}_4^{\text{F}}]$ (**8**), obtained as **4**, is unstable and transforms into the hydrido species $[\text{Ir}(\text{H})(\eta^4\text{-cod})(\text{SiMe}_2(o\text{-C}_6\text{H}_4\text{SMe})_2)]\text{BAR}_4^{\text{F}}$ (**9**), thus attaining coordinative saturation. According to DFT calculations the transformation of **8** into **9** occurs by consecutive β -hydride elimination and olefin insertion steps involving Ir(III) intermediates.

4.- The reaction of **L2** with $[\text{Rh}(\text{nbd})\text{Cl}]_2$ allows the formation of 16e complex $[\text{RhCl}(\text{ntyl})(\text{SiMe}_2(o\text{-C}_6\text{H}_4\text{SMe})_2)]$ (**10**) by the chelate-assisted oxidative addition of the Si-H bond. The insertion of the norbornadiene into the Rh-H bond yields the σ -norbornenyl species, and the subsequent rearrangement leads to the formation of the thermodynamically favoured σ -nortricyclyl derivative. The abstraction of chloride fails to afford a 14e species. Instead, it

promotes a reverse rearrangement with cleavage of the cyclopropyl fragment to allow the novel isomerisation from the σ -nortricycyl to the σ,π -norbornenyl ligand in a 16e $[\text{Rh}(\sigma,\pi\text{-nbyl})(\text{SiMe}_2(o\text{-C}_6\text{H}_4\text{SMe})_2)]\text{BAR}^{\text{F}_4}$ (**11**) complex, *via* successive β -hydride elimination and olefin insertion processes proposed by theoretical calculation.

5.- The treatment of $[\text{Rh}(\text{cod})\text{Cl}]_2$, $[\text{Rh}(\text{nbd})\text{Cl}]_2$ and $[\text{Ir}(\text{cod})\text{Cl}]_2$ with the preligand $\text{SiMe}_2(o\text{-C}_6\text{H}_4\text{SMe})_2$ (**L3**) and $\text{NaBAR}^{\text{F}_4}$ leads to the formation of cationic M(I) 16 electron $[\text{M}(\text{diolefin})\text{SiMe}_2(o\text{-C}_6\text{H}_4\text{SMe})_2]\text{BAR}^{\text{F}_4}$ compounds by coordination of the two thioether moieties. However, the reaction of **L3** with $[\text{Rh}(\text{coe})_2\text{Cl}]_2$ and $\text{NaBAR}^{\text{F}_4}$ in the presence of acetonitrile results into the unusual activation of the Si-CH₃ bond to form the Rh(III) 18e compound $[\text{Rh}(\text{Me})(\text{Si}(\text{Me})(o\text{-C}_6\text{H}_4\text{SMe})_2)(\text{MeCN})_2]\text{BAR}^{\text{F}_4}$ (**16**).

6.- The dehydrogenative coupling of the tertiary silane $\text{SiMeH}(o\text{-C}_6\text{H}_4\text{SMe})_2$ (**L2**) is catalysed by $[\text{RhCl}(\text{PPh}_3)_3]$ to give the disilane $(o\text{-C}_6\text{H}_4\text{SMe})_2\text{MeSi-SiMe}(o\text{-C}_6\text{H}_4\text{SMe})_2$ product. We propose a simplified mechanism involving the formation of complex $[\text{RhClH}(\text{SiMe}(o\text{-C}_6\text{H}_4\text{SMe})_2)(\text{PPh}_3)]$ (**5**) as the active species in the catalytic cycle, followed by σ -bond metathesis and reductive elimination of the disilane product. The formation of an inactive species $[\text{Rh}(\text{SiMe}(o\text{-C}_6\text{H}_4\text{SMe})_2)_2]\text{BAR}^{\text{F}_4}$ (**21**) is observed and explains the lower activity as catalyst of the cationic compound $[\text{Rh}(\text{H})[\text{SiMe}(o\text{-C}_6\text{H}_4\text{SMe})_2](\text{PPh}_3)]\text{BAR}^{\text{F}_4}$ (**6**), which forms readily **21** in the presence of **L2**.

7.- Complex $[\text{RhH}(\text{SiMe}_2(o\text{-C}_6\text{H}_4\text{SMe}))(\text{PPh}_3)_2]\text{BAR}^{\text{F}_4}$ (**17**) has proved to be an efficient pre-catalyst in the solvent-free tandem isomerisation-hydrosilylation reaction of internal olefins with Et_3SiH at room temperature, showing a complete selectivity to linear alkylsilanes. This complex is also able to catalyse the dehalogenation of CDCl_3 in the presence of Et_3SiH to form the chlorosilane species Et_3SiCl and CHDCl_2 .

8.- Analogous compounds $[\text{RhH}(\text{SiMe}(o\text{-C}_6\text{H}_4\text{SMe})_2)(\text{PPh}_3)]\text{BAR}^{\text{F}_4}$ (**6**) and $[\text{IrH}(\text{SiMe}(o\text{-C}_6\text{H}_4\text{SMe})_2)(\text{PPh}_3)(\text{THF})]\text{BAR}^{\text{F}_4}$ (**20**) are precatalysts for solvent-free tandem reactions of internal olefins with Et_3SiH . While Rh(III) complex **6** selectively promotes the tandem isomerisation-hydrosilylation reaction to yield linear hydrosilylation products at room temperature, Ir(III) compound **20** promotes the tandem isomerisation-dehydrogenative silylation of internal olefins to give the allylsilane as the main product.

9.- Activation of the C-H aldehyde bond in a racemic mixture of phosphinoalkylaldehyde $\text{PPh}_2\text{CH}(\text{Ph})\text{CH}_2\text{CHO}$ by $[\text{Rh}(\text{cod})\text{Cl}]_2$ in the presence of pyridine led to the chelate-assisted oxidative addition and formation of a unique hydrido(diphenylphosphino)alkylacyl $[\text{RhClH}(\text{PPh}_2\text{CH}(\text{Ph})\text{CH}_2\text{CO})(\text{py})_2]$ (**22**) species with high diastereoselectivity. At variance with related phosphinoarylaldehydes, insertion of alkylaldehyde into the Rh-H bond to afford hydroxyalkyl derivatives fails to occur. Reaction of **22** with an additional molecule of $\text{PPh}_2\text{CH}(\text{Ph})\text{CH}_2\text{CHO}$ does not promote a second oxidative addition, leading to the formation of compound $[\text{RhClH}(\text{PPh}_2\text{CH}(\text{Ph})\text{CH}_2\text{CO})(\text{PPh}_2\text{CH}(\text{Ph})\text{CH}_2\text{CHO})(\text{py})]$ (**24**) with remarkable diastereoselectivity, which maintains a pendant aldehyde group. On the other hand, the addition of the arylaldehyde $\text{PPh}_2(o\text{-C}_6\text{H}_4\text{CHO})$ to **22** promoted the reductive elimination of the alkylaldehyde and led to the formation of a preferred arylacyl metallacycle, in complex $[\text{RhClH}(\text{PPh}_2(o\text{-C}_6\text{H}_4\text{CO}))(\kappa^1\text{-PPh}_2(\text{CH}(\text{Ph})\text{CH}_2\text{CHO}))(\text{py})]$ (**25**) as an equimolar mixture of two diastereomers. These results suggest a lower activation barrier for the diastereoisomerisation reaction to take place when involving alkylaldehydes (**24**) than when involving arylaldehydes (**25**).

10.- The reaction of the (acylhydrido)rhodium(III) compound $[\text{RhClH}(\text{PPh}_2(o\text{-C}_6\text{H}_4\text{CO}))(\kappa^1\text{-PPh}_2(\text{CH}(\text{Ph})\text{CH}_2\text{CHO}))(\text{py})]$ (**25**) with aromatic diimines such as 1,10-phenanthroline and 2,2'-bipyridine afforded cationic $[\text{RhH}(\text{NN})(\text{PPh}_2(o\text{-C}_6\text{H}_4\text{CO}))(\kappa^1\text{-PPh}_2(\text{CH}(\text{Ph})\text{CH}_2\text{CHO}))]\text{BPh}_4$ compounds, with trans phosphorus atoms, as a mixture of two diastereomers, whose physical separation was possible due to their different solubility in chloroform. The P-monodentate alkylaldehyde in **25** undergoes complete imination in the presence of both amino imines 8-aminoquinoline and 2-aminomethylpyridine to afford PNN terdentate hemilabile ligands in $[\text{RhH}(\text{PPh}_2(o\text{-C}_6\text{H}_4\text{CO}))(\text{PNN})]\text{BF}_4$ compounds. This reaction with 2-aminomethylpyridine is in contrast with that observed for the related complex derived from arylaldehyde $\text{PPh}_2(o\text{-C}_6\text{H}_4\text{CHO})$, which led to a stable hemiaminal $-\text{CH}(\text{OH})\text{NH}-$ fragment. This could be explained by the higher flexibility of the aliphatic chain in the phosphinoalkylaldehyde, as it would facilitate the final condensation step in the reaction between the pendant aldehyde and the amine groups.

11.- The oxidative addition of $\text{PPh}_2\text{CH}(\text{Ph})\text{CH}_2\text{CHO}$ to $[\text{Rh}(\text{nbd})\text{Cl}]_2$ yielded σ -norticycyl derivatives $[\text{RhCl}(\text{NN})(\text{Ntyl})(\text{PPh}_2\text{CH}(\text{Ph})\text{CH}_2\text{CO})]$ in the presence of N-donor diimines, by insertion of the norbornadiene into the Rh-H bond and subsequent rearrangement. In all cases, kinetic 75:25 mixtures of diastereomers of a single geometric isomer were obtained. Performing the reaction in methanol in the presence of 8-quinolinecarboxaldehyde allowed

the transformation of the alkylaldehyde into an alkylester and the oxidative addition of the arylaldehyde to afford complex $[\text{RhCl}(\text{Ntyl})(\text{C}_9\text{H}_6\text{NCO})(\text{k}^2\text{-PPh}_2\text{CH}(\text{Ph})\text{CH}_2\text{CO}(\text{OCH}_3))]$ (**32**), via a P-coordinated (diphenylphosphine)hemiacetal intermediate. The hemilabile P,O ligand allows an isomerisation reaction leading to complete diastereoselectivity.

12.- Treatment of $[\text{Rh}(\text{nbd})\text{Cl}]_2$ with 8-quinolinecarboxaldehyde and pyrazole led to the formation of coordinatively saturated 18e dinuclear neutral, and mononuclear neutral or cationic alkyl-quinolineacyl-pyrazole rhodium(III) complexes with one and two or three coordinated pyrazole molecules, by insertion of the norbornadiene into the Rh-H bond to form preferably σ -norbornenyl species or low amounts of σ -norticycyl species. These compounds are stabilised by the formation of hydrogen N-H...O and N-H...Cl bonds between the pyrazole and the acyl or the chloride moieties.

13.- The addition of triphenylphosphine to complex $[\text{RhCl}(\text{C}_9\text{H}_6\text{NCO})(\text{Hpz})(\text{nbyl})]_2$ (**33**) led to the reductive elimination of the quinolinylnorbornenyl-ketone $\text{C}_9\text{H}_6\text{NC}(\text{O})\text{Nbyl}$ product. However, the reaction with diphenylphosphine oxide allowed the formation of a stable quinolinylnorbornenylhydroxyalkyl moiety in the unsaturated compound $[\text{RhCl}(\text{C}_9\text{H}_6\text{NC}(\text{nbyl})\text{OH})(\text{Hpz})(\text{Ph}_2\text{PO})]$ (**36a**), with a trigonal bipyramidal structure, by migration of the σ -norbornenyl to the carbon atom in the quinoline acyl moiety and formation of a new C-C bond and an O-to-O outer sphere hydrogen transfer from coordinated phosphinous acid to coordinated carboxy. Lowering the temperature reveals an equilibrium between the unsaturated species with trigonal bipyramidal and square pyramidal structure.

14.- The four alkyl-quinolineacyl-pyrazole rhodium(III) complexes were tested as homogeneous catalysts for the hydrolysis of ammonia-borane in THF/H₂O, at 30 °C and in the presence of air. All compounds showed high activity in this reaction and afforded the generation of almost three hydrogen equivalents per mole of substrate, with the highest reaction rate corresponding to the dimeric complex $[\text{RhCl}(\text{C}_9\text{H}_6\text{NCO})(\text{Hpz})(\text{nbyl})]_2$ (**33**).

IV. EXPERIMENTAL SECTION

IV. 1. INSTRUMENTAL TECHNIQUES

General working conditions

All manipulations, unless otherwise stated, were performed under an atmosphere of nitrogen, using standard Schlenk techniques. Glassware was oven dried at 120°C overnight. Solvents were previously distilled under nitrogen, degassed by successive freeze-pump-thaw cycles¹ and stored over 3 Å molecular sieves.

Hydrogenation reactions

Hydrogenation reactions were performed in a high pressure NMR tube equipped with a J. Young's valve. The dissolved compound of interest was cooled to 77K. The tube was evacuated and H₂ admitted (1 atm). The tube was then sealed and warmed to 298K, resulting in a pressure of approximately 4atm ($298/77 \approx 4$).

Elemental analysis

Mass percentages of carbon, nitrogen, sulphur and hydrogen in the synthesised complexes were determined by elemental microanalysis. The analysis was carried out with a LECO Truspec Micro CHNS microanalyser.

Conductivity

Conductivity measures were performed at room temperature with a Metrohm-Herisau 712 electrical conductivity meter. The system was equipped with a 0.8 cm⁻¹ constant Metrohm 00450920 conductivity cell. Measures were carried out in 2.5x10⁻⁴ M acetone solutions.

Infrared spectroscopy

IR spectra were obtained between a wavenumber range of 4000-500 cm⁻¹ with a Nicolet FTIR 510 spectrometer. Measures were performed in a KBr disc.

Nuclear magnetic resonance spectroscopy

¹H, ¹³C{¹H}, ³¹P{¹H} and ²⁹Si{¹H} RMN spectra were recorded on Bruker AVD 500, 400 or 300 MHz spectrometers at room temperature unless otherwise stated. ¹H and ¹³C{¹H} NMR spectra were referenced to the solvent residual signal, or with TMS as internal standard. ²⁹Si NMR spectra were referenced with TMS as internal standard. In ³¹P{¹H} NMR spectra H₃PO₄ (85%) was used as an external standard.

Electrospray ionization mass spectrometry (ESI-MS)

ESI-MS were recorded on a Bruker MicrOTOF-Q instrument. For complexes **12** and **13**, spectra were carried out using a Bruker MicrOTOF instrument directly connected to a modified Innovative Technology glovebox. In all ESI-MS spectra there was a good fit to both the principal molecular ion and the overall isotopic distribution.

X-Ray diffraction

Obtained crystals were mounted on a glass fibre and used for data collection on a Bruker D8 Venture with Photon detector equipped with graphite monochromated MoK α radiation ($\lambda=0.71073$ Å). Lorentz-polarisation and empirical absorption corrections were applied. The structures were solved by direct methods and refined with full-matrix least-squares calculations on F2 using the program SHELXS-97 and SHELXS-2013. Crystallographic data are collected in Supporting Information.

IV. 2. SYNTHESIS OF STARTING MATERIAL

Synthesis of $[\text{Rh}(\text{cod})\text{Cl}]_2$

Compound $[\text{Rh}(\text{cod})\text{Cl}]_2$ was synthesised as previously described by Chatt and Venazi,¹ by reaction of $\text{RhCl}_3 \cdot x\text{H}_2\text{O}$ with 1,5-cyclooctadiene in an ethanol reflux.

Synthesis of $[\text{Rh}(\text{nbd})\text{Cl}]_2$

Compound $[\text{Rh}(\text{nbd})\text{Cl}]_2$ was synthesised as previously described by Abel et al.² by reaction of $\text{RhCl}_3 \cdot x\text{H}_2\text{O}$ with 2,5-norbornadiene in ethanol at room temperature.

Synthesis of $[\text{Ir}(\text{cod})\text{Cl}]_2$

Compound $[\text{Ir}(\text{cod})\text{Cl}]_2$ was synthesised as previously described by Cushing et al.³ by reaction of $\text{IrCl}_3 \cdot x\text{H}_2\text{O}$ with 1,5-cyclooctadiene in a 2-propanol and H_2O mixture at 120°C.

Synthesis of $[\text{Rh}(\text{coe})_2\text{Cl}]_2$

Compound $[\text{Rh}(\text{coe})_2\text{Cl}]_2$ was synthesised by reaction of 2 g of $\text{RhCl}_3 \cdot x\text{H}_2\text{O}$ with 6 mL of cyclooctene in a 2-propanol (40 mL) and H_2O (10 mL) mixture at room temperature for 5 days.⁴

Synthesis of $\text{C}_9\text{H}_6\text{NCHO}$

8-quinolinecarboxaldehyde was prepared by the method reported by Anklin and Pregosin.⁵

Synthesis of $\text{PPh}_2(o\text{-C}_6\text{H}_4\text{CHO})$

Diphenylphosphine(*o*-benzaldehyde) was prepared by the method reported by Liese and co-workers.⁶

Synthesis of $\text{PPh}_2\text{CHPhCH}_2\text{CHO}$

The alkylphosphine-aldehyde $\text{PPh}_2\text{CHPhCH}_2\text{CHO}$ was prepared by the method reported by Moiseev, Patrick and James.⁷

Synthesis of $[\text{RhHCl}(\text{PPh}_2(o\text{-C}_6\text{H}_4\text{CO}))(\text{py})_2]$

Compound $[\text{RhHCl}(\text{PPh}_2(o\text{-C}_6\text{H}_4\text{CO}))(\text{py})_2]$ was synthesised by reaction of $[\text{Rh}(\text{cod})\text{Cl}]_2$ with pyridine and diphenylphosphine(*o*-benzaldehyde) in benzene at room temperature.⁸

Synthesis of $\text{SiHMe}_2(o\text{-C}_6\text{H}_4\text{SMe})$

Compound $\text{SiHMe}_2(o\text{-C}_6\text{H}_4\text{SMe})$ was prepared by an adaptation of the published route by using *n*BuLi.⁹

To a Schlenk charged with 2-Bromothioanisole (0.47 mL, 0.0035 mol) in Et₂O (10 ml) an excess of 1.1 of nBuLi (2.4 mL of a 1.6 M solution in hexane, 0.0038 mol) was added slowly, at a temperature of 0°C. The mixture was stirred for 1 hour and an equivalent of ClSiMe₂ was added dropwise (0.39 mL, 0.0035 mol). After being stirred at room temperature overnight, the reaction mixture was quenched with water and extracted with diethyl ether. The solvent was removed under vacuum to give the product as a colorless oil. Yield 71 %.

¹H NMR (500 MHz, CDCl₃): δ 7.53-7.17 (m, 8 H_{aromatic}), 4.60 (hpt, J_{H-H} = 3.9, with satellites J_{Si-H} = 192.1 Hz, Si-H), 2.52 (s, 3 H, S-CH₃), 0.45 (d, J_{H,H} = 3.9, 6 H, Si-CH₃).

¹³C{¹H} NMR (125 MHz, CDCl₃): δ 144.9 (s, C_{aromatic}), 138.2 (s, C_{aromatic}), 135.3 (s, HC_{aromatic}), 130.2 (s, HC_{aromatic}), 127.6 (s, HC_{aromatic}), 125.2 (s, HC_{aromatic}), 17.7 (s, S-CH₃), -3.4 (s, 2 Si-CH₃).

²⁹Si{¹H} NMR (99 MHz, CDCl₃): δ -18.7 (s).

Synthesis of SiHMe(*o*-C₆H₄SMe)₂

To a Schlenk flask charged with a solution of 2-bromothioanisole (0.47 mL, 0.0035 mol) in diethyl ether (10 mL) an excess of 1.1 of nBuLi (2.4 mL of a 1.6 M solution in hexane, 0.0038 mol) was added at 0 °C. The reaction mixture was stirred for 1 hour, and half an equivalent of Cl₂SiMeH was added dropwise (0.18 mL, 0.0018 mol). After being stirred at room temperature overnight, the reaction mixture was quenched with water and extracted with diethyl ether. The solvent was removed under vacuum to give the product as a colorless oil. Yield 76 %.

¹H NMR (500 MHz, CDCl₃): δ 7.55-7.18 (m, 8 H_{aromatic}), 5.29 (q, J_{H-H} = 3.8, with satellites J_{Si-H} = 191.4 Hz, Si-H), 2.38 (s, 6 H, S-CH₃), 0.78 (d, J_{H-H} = 3.8, 3 H, Si-CH₃).

¹³C{¹H} NMR (125 MHz, CDCl₃): δ 145.1 (s, C_{aromatic}), 136.7 (s, C_{aromatic}), 136.5 (s, HC_{aromatic}), 130.4 (s, HC_{aromatic}), 127.9 (s, HC_{aromatic}), 125.3 (s, HC_{aromatic}), 18.0 (s, 2 S-CH₃), -4.2 (s, Si-CH₃).

²⁹Si{¹H} NMR (99 MHz, CDCl₃): δ -31.1 (s).

Synthesis of SiMe₂(*o*-C₆H₄SMe)₂

To a Schlenk charged with 2-Bromothioanisole (0.50 mL, 0.0037 mol) in Et₂O (10 ml) an excess of 1.1 of nBuLi (2.6 mL of a 1.6 M solution in hexane, 0.0041 mol) was added slowly, at a temperature of 0°C (ice bath). The mixture was stirred for 1 hour. After that time half an equivalent of dichlorodimethylsilane (Cl₂Me₂Si) was added dropwise (0.23 mL, 0.0019 mol) and was left to stir overnight at room temperature. The mixture was then quenched with water

and the product was extracted with diethyl ether. Evaporation of the solvent under vacuum gave product $[\text{Si}(\text{Me})_2(o\text{-C}_6\text{H}_4\text{SMe})_2]$ as a crystalline white solid. Yield 62 %.

^1H NMR (500 MHz, CD_2Cl_2): δ 7.60-7.40 (m, 8 $\text{H}_{\text{aromatic}}$), 2.18 (s, 6 H, S- CH_3), 0.65 (s, 6 H, Si- CH_3).

IV. 3. SYNTHESIS AND CHARACTERISATION OF COMPLEXES

Synthesis of $[\text{RhCl}(\text{SiMe}_2(o\text{-C}_6\text{H}_4\text{SMe}))_2]_2$ (**1**)

To a Schlenk flask charged with $[\text{Rh}(\text{cod})\text{Cl}]_2$ (50 mg, 0.10 mmol) and 4.4 equivalents of $\text{SiMe}_2\text{H}(o\text{-C}_6\text{H}_4\text{SMe})$ (81 mg, 0.44 mmol,) 10 mL of CH_2Cl_2 were added. The solution was stirred overnight (16 h.) at room temperature. The mixture was concentrated under vacuum, pentane (20 mL) was added, and it was stored at $-20\text{ }^\circ\text{C}$ overnight to complete the crystallization of the product. Yield 73 %.

^1H NMR (500 MHz, CDCl_3): δ 7.63 (d, $J_{\text{H-H}} = 7.4$ Hz, 4 $\text{H}_{\text{aromatic}}$), 7.45 (d, $J_{\text{H-H}} = 6.6$ Hz, 4 $\text{H}_{\text{aromatic}}$), 7.36 (m, 8 $\text{H}_{\text{aromatic}}$), 2.97 (s, 12 H, S- CH_3), 0.62 (s, 12 H, Si- CH_3^{a}), -0.24 (s, 12 H, Si- CH_3^{b}).

$^{13}\text{C}\{^1\text{H}\}$ NMR (125 MHz, CDCl_3): δ 150.5 (s, $\text{C}_{\text{aromatic}}$), 141.9 (s, $\text{C}_{\text{aromatic}}$), 132.8 (s, $\text{HC}_{\text{aromatic}}$), 129.7 (s, $\text{HC}_{\text{aromatic}}$), 129.5 (s, $\text{HC}_{\text{aromatic}}$), 128.4 (s, $\text{HC}_{\text{aromatic}}$), 27.8 (s, S- CH_3), 7.3 (s, Si- CH_3), 0.1 (s, Si- CH_3).

$^{29}\text{Si}\{^1\text{H}\}$ NMR (99 MHz, CDCl_3): δ 44.2 (d, $J_{\text{Si-Rh}} = 28$ Hz).

ESI-MS (CH_3CN): calculated for $\{\text{M} - \text{Cl}\}^+$ or $\{\text{C}_{18}\text{H}_{26}\text{RhS}_2\text{Si}_2\}^+$ 465.01; found 465.01.

Elemental Analysis: $\text{C}_{36}\text{H}_{52}\text{Cl}_2\text{Rh}_2\text{S}_4\text{Si}_4 \cdot 0.25(\text{CH}_2\text{Cl}_2)$ Calculated C 42.54, H 5.17, S 12.53. Found C 42.55, H 5.97, S 12.23.

Synthesis of $[(\text{cod})\text{Rh}(\mu\text{-Cl})_2\text{Rh}(\text{SiMe}_2(o\text{-C}_6\text{H}_4\text{SMe}))_2]_2$ (**2**)

To a Schlenk flask charged with $[\text{Rh}(\text{cod})\text{Cl}]_2$ (50 mg, 0.10 mmol) and 4.4 equivalents of $\text{SiMe}_2\text{H}(o\text{-C}_6\text{H}_4\text{SMe})$ (81 mg, 0.44 mmol,) 10 mL of CH_2Cl_2 were added. The solution was stirred at room temperature for 8 h. The mixture was concentrated under vacuum, layered with pentane (20 mL), and stored at $-20\text{ }^\circ\text{C}$ overnight. A small amount of compound **2** crystallized from the reaction mixture.

^1H NMR (500 MHz, CDCl_3): δ 7.75-7.42 (8 $\text{H}_{\text{aromatics}}$), 4.24 (m, 4 H, cod), 3.39 (s_{broad} , 3 H, S- CH_3), 2.97 (s_{broad} , 3 H, S- CH_3), 2.47 (m, 4 H, cod), 1.77 (m, 4 H, cod), 0.58 (s_{broad} , 6 H, Si- CH_3), -0.18 (s_{broad} , 6 H, Si- CH_3).

Synthesis of [RhCl(η^3 -cyclooctenyl)(SiMe(*o*-C₆H₄SMe)₂)] (3)

To a Schlenk flask charged with [Rh(cod)Cl]₂ (25 mg, 0.05 mmol) and 2 equivalents of SiMeH(*o*-C₆H₄SMe)₂ (30 mg, 0.10 mmol) 10 mL of CH₂Cl₂ were added. The solution was stirred at room temperature for 30 min. The mixture was concentrated under vacuum, pentane (20 mL) was added, and it was stored at -20 °C overnight to complete the crystallization of the product. Yield 72 %.

¹H NMR (500 MHz, CDCl₃): δ 7.50 (dd, J_{H-H} = 7.0, 4J_{H-H} = 1.8 Hz, H_{aromatic}), 7.45 (dd, J_{H-H} = 6.6, J_{H-H} = 2.4 Hz, H_{aromatic}), 7.24 (m, 2 H, aromatics), 5.14 (dt, J_{Rh-H} = 7.9, J_{H-H} = 3.4 Hz, 1 H, η^3 -cyclooctenyl), 3.78 (q, J_{Rh-H} = 8.5, J_{H-H} = 8.5 Hz, 2 H, η^3 -cyclooctenyl), 2.90 (s, 6 H, S-CH₃), 2.74 (m, 2 H, cyclooctenyl), 2.05 (m, 2 H, cyclooctenyl), 1.71 (m, 2 H, cyclooctenyl), 1.41 (m, 4 H, cyclooctenyl), 0.70 (s, Si-CH₃).

¹³C{¹H} NMR (125 MHz, CDCl₃): δ 147.5 (s, C_{aromatic}), 142.9 (s, C_{aromatic}), 132.8 (s, HC_{aromatic}), 129.9 (s, HC_{aromatic}), 129.5 (s, HC_{aromatic}), 128.5 (s, HC_{aromatic}), 96.7 (d, J_{Rh-C} = 6Hz, η^3 -cyclooctenyl), 66.8 (d, J_{Rh-C} = 9Hz, 2 C, η^3 -cyclooctenyl), 30.2 (s, cyclooctenyl), 28.1 (s, 2 C, S-CH₃), 27.4 (s, 2 C, cyclooctenyl), 23.9 (s, 2 C, cyclooctenyl), 1.3 (s, Si-CH₃).

²⁹Si{¹H} NMR (99 MHz, CDCl₃): δ 47.0 (d, J_{Si-Rh} = 24 Hz).

ESI-MS (CH₃CN): calculated for {M - Cl}⁺ or {C₂₃H₃₀RhS₂Si}⁺ 501.06; found 501.06.

Elemental Analysis: C₂₃H₃₀ClRhS₂Si Calculated C 51.44, H 5.63, S 11.94. Found C 50.76, H 4.95, S 11.94.

Synthesis of [Rh(η^3 -cyclooctenyl)(SiMe(*o*-C₆H₄SMe)₂)]BAR^F₄ (4)

Method a: To a Schlenk charged with complex [RhCl(η^3 -cyclooctenyl)(SiMe(*o*-C₆H₄SMe)₂)] (3) (30 mg, 0.06 mmol) and 1.1 equivalents of NaBAR^F₄ (55 mg, 0.06 mmol) 2 mL of CH₂Cl₂ were added. The solution was stirred for 30 minutes at room temperature and filtered off to another schlenk. The mixture was concentrated under vacuum, 20 mL of pentane were added and the mixture was stored at -20 °C overnight to complete the crystallization of the product. Yield 89 %.

Method b: To a Schlenk charged with compound {Rh(H)[SiMe(*o*-C₆H₄SMe)₂](PPh₃)}[BAR^F₄] (6) (50 mg, 0.03 mmol) and 1.2 equivalents of 1,5-cyclooctadiene (5 μ l, 0.04 mmol) 5 mL of toluene were added. The solution was refluxed for 2 h. The mixture was concentrated under vacuum. Addition of 20 mL of pentane gave a white precipitate that was washed with pentane and dried under vacuum. Yield 75 %.

^1H NMR (500 MHz, CDCl_3): δ 7.73 (s, 8H, BAR_4^{F}), 7.56 (s, 4H, BAR_4^{F}), 7.70-7.41 (m, 8 $\text{H}_{\text{aromatic}}$), 5.26 (dt, $J_{\text{H-H}} = 7.8$ Hz, 2.6 Hz, 1 H, CH, cyclooctenyl), 4.40 (dt, $J_{\text{H-H}} = 4.4$ Hz, 2 H, CH, cyclooctenyl), 2.58 (s, 6 H, S- CH_3), 2.40 (m, 2 H, CH_2 , cyclooctenyl), 1.70 (m, 4 H, CH_2 , cyclooctenyl), 1.45 (m, 2 H, CH_2 , cyclooctenyl), 1.33 (m, 2 H, CH_2 , cyclooctenyl) 0.78 (s, 3 H, Si- CH_3).

$^{13}\text{C}\{^1\text{H}\}$ NMR (125 MHz, CDCl_3): δ 162.1 (q, $J_{\text{F-C}} = 50$ Hz, BAR_4^{F}), 134.9 (s, BAR_4^{F}), 129.3 (q, $J_{\text{F-C}} = 12$ Hz, BAR_4^{F}), 125.9 (q, $J_{\text{F-C}} = 273$ Hz, CF_3), 117.5 (s, BAR_4^{F}), 130.0-135.0 (s, $\text{C}_{\text{aromatic}}$), 105.6 (d, $J_{\text{Rh-C}} = 6.0$ Hz, HC, cyclooctenyl), 75.6 (d, $J_{\text{Rh-C}} = 8.0$ Hz, HC, cyclooctenyl), 31.4 (s, H_2C , cyclooctenyl), 28.5 (s, H_2C , cyclooctenyl), 28.5 (s, S- CH_3), 22.4 (s, H_2C , cyclooctenyl), 0.8 (s, Si- CH_3).

ESI-MS (CH_3CN): calculated for $\{\text{C}_{23}\text{H}_{30}\text{RhS}_2\text{Si}\}^+$ 501.06; found m/z 501.06.

Elemental Analysis: $\text{C}_{55}\text{H}_{42}\text{RhS}_2\text{SiBF}_{24}$ Calculated: C 48.40, H 3.10, S 4.70. Found: C 49.15, H 3.18, S 4.36.

Synthesis of $[\text{RhClH}(\text{SiMe}(\text{o-C}_6\text{H}_4\text{SMe})_2)(\text{PPh}_3)]$ (5)

To a Schlenk charged with $[\text{RhCl}(\text{PPh}_3)_3]$ (100 mg, 0.11 mmol) in CH_2Cl_2 (5 mL) and excess of 1.5 equivalents of ligand $\text{SiMeH}(\text{o-C}_6\text{H}_4\text{SMe})_2$ (**L1**) (50 mg, 0.17 mmol) was added. The mixture was stirred for 60 min and concentrated under vacuum. Addition of 20 mL of pentane gave a white precipitate that was washed with pentane and dried under vacuum. Yield 84 %.

^1H NMR (500 MHz, CDCl_3): δ 7.80-7.10 (m, 23 $\text{H}_{\text{aromatic}}$), 3.13 (s, 3 H, S- CH_3^{a}), 2.46 (s, 3 H, S- CH_3^{b}), -0.09 (s, 3 H, Si- CH_3), -12.83 (t, $J_{\text{H-Rh}} = 16.0$, $J_{\text{H,P}} = 18.3$ Hz, H-Rh).

$^{13}\text{C}\{^1\text{H}\}$ NMR (125 MHz, CDCl_3): δ 151.7-125.9 ($\text{C}_{\text{aromatic}}$), 32.2 (s, S- CH_3^{a}), 22.1 (s, S- CH_3^{b}), -0.3 (s, Si- CH_3).

$^{31}\text{P}\{^1\text{H}\}$ NMR (202 MHz, CDCl_3): δ 46.8 (d, $J_{\text{P-Rh}} = 138.3$ Hz).

ESI-MS (CH_3CN): calculated for $\{\text{M} - \text{Cl}\}^+$ or $\{\text{C}_{33}\text{H}_{33}\text{PRhS}_2\text{Si}\}^+$: 655.06; found m/z 655.06.

Elemental Analysis: $\text{C}_{33}\text{H}_{33}\text{ClPRhS}_2\text{Si}$ Calculated C 57.26, H 4.95, S 9.26. Found C 57.18, H 4.79, S 9.13.

Synthesis of $[\text{RhH}(\text{SiMe}(\text{o-C}_6\text{H}_4\text{SMe})_2)(\text{PPh}_3)]\text{BAR}_4^{\text{F}}$ (6)

To a Schlenk charged with complex $[\text{RhClH}(\text{SiMe}(\text{o-C}_6\text{H}_4\text{SMe})_2)(\text{PPh}_3)]$ (**5**) (60 mg, 0.09 mmol) in CH_2Cl_2 (5 mL) an equivalent of $\text{NaBAR}_4^{\text{F}}$ (77 mg, 0.09 mmol) was added. The mixture was stirred

for 30 min, filtered off to another Schlenk and concentrated under vacuum. Addition of 20 mL of pentane gave a pale yellow precipitate that was washed with pentane and dried under vacuum. Yield 61 %.

$^1\text{H NMR}$ (500 MHz, CDCl_3): δ 7.85-6.95 (m, 35 $\text{H}_{\text{aromatics}}$), 2.97 (s, 3 H, S- CH_3^{a}), 2.28 (s, 3 H, S- CH_3^{b}), 0.66 (s, 3 H, Si- CH_3), -10.91 (dd, $J_{\text{H-Rh}} = 13.7$, $J_{\text{H-P}} = 23.4$ Hz, Rh-H).

$^{13}\text{C}\{^1\text{H}\}$ NMR (125 MHz, CDCl_3): δ 162.1 (q, $J_{\text{F-C}} = 50$ Hz, BAR_4^{F}), 135.1 (BAR_4^{F}), 129.3 (q, $J_{\text{F-C}} = 12$ Hz, BAR_4^{F}), 125.9 (q, $J_{\text{F-C}} = 273$ Hz, CF_3), 117.9 (s, BAR_4^{F}), 134.3-128.1 ($\text{C}_{\text{aromatics}}$), 33.6 (s, S- CH_3^{a}), 23.6 (s, S- CH_3^{b}), 2.5 (s, Si- CH_3).

$^{31}\text{P}\{^1\text{H}\}$ NMR (202 MHz, CDCl_3): δ 47.3 (d, $J_{\text{P-Rh}} = 136$ Hz).

ESI-MS (CH_3CN): calculated for $\{\text{C}_{33}\text{H}_{33}\text{PRhS}_2\text{Si}\}^+$: 655.06; found m/z 655.06.

Elemental Analysis: $\text{C}_{65}\text{H}_{45}\text{BF}_{24}\text{PRhS}_2\text{Si}$ Calculated C 51.36, H 3.05, S 4.22. Found C 51.17, H 3.31, S 4.24.

Synthesis of $[\text{IrCl}(\eta^3\text{-cyclooctenyl})(\text{SiMe}(\text{o-C}_6\text{H}_4\text{SMe})_2)]$ (7)

To a Schlenk charged with $[\text{Ir}(\text{cod})\text{Cl}]_2$ (50 mg, 0.07 mmol) and 2.2 equivalents of $\text{SiMe}(\text{o-C}_6\text{H}_4\text{SMe})_2$ (44 mg, 0.16 mmol) 5 mL of CH_2Cl_2 were added. The solution was stirred at room temperature overnight (16 h). The mixture was concentrated under vacuum, 20 mL of pentane were added and the mixture was stored at -20 °C overnight to complete the crystallization of the product. Yield 67 %.

$^1\text{H NMR}$ (500 MHz, CDCl_3): δ 7.61 (m, 4 $\text{H}_{\text{aromatic}}$), 7.29 (m, 4 $\text{H}_{\text{aromatic}}$), 5.15 (t, $J_{\text{H-H}} = 7.3$ Hz, 1 H, CH, cyclooctenyl), 3.68 (dt, $J_{\text{H-H}} = 8.3$ Hz, 8.4 Hz, 2 H, CH, cyclooctenyl), 3.17 (s, 6 H, S- CH_3), 2.59 (m, 2 H, CH_2 , cyclooctenyl), 1.99 (m, 2 H, CH_2 , cyclooctenyl), 1.90 (m, 2 H, CH_2 , cyclooctenyl), 1.55 (m, 2 H, CH_2 , cyclooctenyl), 1.38 (m, 2 H, CH_2 , cyclooctenyl), 0.70 (s, 3 H, Si- CH_3).

$^{13}\text{C}\{^1\text{H}\}$ NMR (125 MHz, CDCl_3): δ 133.0 (s, $\text{HC}_{\text{aromatic}}$), 130.0 (s, $\text{HC}_{\text{aromatic}}$), 128.9 (s, $\text{HC}_{\text{aromatic}}$), 87.0 (s, HC, cyclooctenyl), 49.3 (s, HC, cyclooctenyl), 29.0 (s, H_2C , cyclooctenyl), 28.4 (s, H_2C , cyclooctenyl), 27.0 (s, S CH_3), 25.6 (s, H_2C , cyclooctenyl), -1.3 (s, Si- CH_3).

ESI-MS (CH_3CN): calculated for $\{\text{M} - \text{Cl}\}^+$ or $\{\text{C}_{23}\text{H}_{30}\text{IrS}_2\text{Si}\}^+$: 591.12; found m/z 591.12.

Elemental Analysis: $\text{C}_{23}\text{H}_{30}\text{IrClS}_2\text{Si} \cdot 0.5(\text{CH}_2\text{Cl}_2)$ Calculated: C 42.20, H 4.67, S 9.59. Found: C 41.63, H 4.49, S 9.52.

Synthesis of [Ir(η^3 -cyclooctenyl)(SiMe(*o*-C₆H₄SMe)₂)]BAR^F₄ (**8**)

To a Schlenk charged with [IrCl(η^3 -cyclooctenyl)(SiMe(*o*-C₆H₄SMe)₂)] (**7**) (50 mg, 0.08 mmol) and 1.1 equivalents of NaBAR^F₄ (78 mg, 0.09 mmol) 2 mL of CH₂Cl₂ were added. The mixture was stirred for 30 minutes at room temperature, filtered off to another schlenk and concentrated under vacuum. Addition of 5 mL of pentane gave a white precipitate that was washed with pentane and dried under vacuum. Yield 65 %.

¹H NMR (500 MHz, CD₂Cl₂): δ 7.76 (s, 8 H, BAR^F₄), 7.59 (s, 4 H, BAR^F₄), 7.70-7.20 (m, 8 H_{aromatic}), 5.20 (t, J_{H-H} = 7.0 Hz, 1 H, CH, cyclooctenyl), 4.41 (m, 2 H, CH, cyclooctenyl), 3.33 (s, 3 H, S-CH₃), 2.43 (s, 3 H, S-CH₃), 2.33 (m, 2 H, CH₂, cyclooctenyl), 1.70 (m, 3 H, 2 CH₂, cyclooctenyl), 1.25 (m, 1 H, CH₂, cyclooctenyl), 0.99 (m, 2 H, CH₂, cyclooctenyl), 0.88 (m, 2 H, CH₂, cyclooctenyl), 0.65 (s, 3 H, Si-CH₃).

¹³C{¹H} NMR (125 MHz, CD₂Cl₂): δ 161.7 (q, J_{F-C} = 50 Hz, BAR^F₄), 134.7 (s, BAR^F₄), 128.7 (q, J_{F-C} = 31 Hz, BAR^F₄), 124.5 (q, J_{F-C} = 273 Hz, CF₃), 117.5 (s, BAR^F₄), 145.5-129.5 (s, C_{aromatic}), 97.6 (s, HC, cyclooctenyl), 66.9 (s, HC, cyclooctenyl), 62.3 (s, HC, cyclooctenyl), 34.5 (s, SCH₃), 32.5 (s, H₂C, cyclooctenyl), 31.5 (s, H₂C, cyclooctenyl), 29.9 (s, H₂C, cyclooctenyl), 28.5 (s, H₂C, cyclooctenyl), 24.1 (s, S-CH₃), 14.1 (s, H₂C, cyclooctenyl), -2.0 (s, Si-CH₃).

Elemental Analysis: C₅₅H₄₂IrS₂SiBF₂₄·0.25(CH₂Cl₂) Calculated: C 44.54, H 2.90, S 4.29. Found: C 44.05, H 3.12, S 4.78.

Synthesis of [IrH(η^4 -cod)(SiMe(*o*-C₆H₄SMe)₂)]BAR^F₄ (**9**)

Method a: To a Young NMR tube charged with [Ir(η^3 -cyclooctenyl)(SiMe(*o*-C₆H₄SMe)₂)]BAR^F₄ (**8**) (20 mg, 0.013 mmol) 0.5 mL of CDCl₃ were added. The solution was monitored by ¹H NMR during 18 h. Yield 50% (calculated by ¹H NMR).

Method b: To a Schlenk charged with [Ir(cod)Cl]₂ (30 mg, 0.04 mmol), 2.2 equivalents of SiMeH(*o*-C₆H₄SMe)₂ (29 mg, 0.10 mmol) and 2.1 equivalents of NaBAR^F₄ (83 mg, 0.09 mmol) 5 mL of CH₂Cl₂ were added. The solution was stirred at room temperature for 30 minutes and filtered off to another schlenk. The mixture was concentrated under vacuum, 20 mL of pentane were added and the mixture was stored at -20 °C overnight to allow the crystallization of the product. Yield 81 %.

^1H NMR (500 MHz, CDCl_3): δ 7.73 (s, 8 H, BAR^{F}_4), 7.56 (s, 4 H, BAR^{F}_4), 7.80-7.20 (m, 8 $\text{H}_{\text{aromatics}}$), 5.29 (dd, $J_{\text{H-H}} = 5.0$ Hz, 2.8 Hz, 2 H, CH, cod), 4.87 (ddd, $J_{\text{H-H}} = 8.8$ Hz, 6.4 Hz, 2.3 Hz, 1 H, CH, cod), 3.50 (m, 1 H, CH, cod), 3.07 (s, 3 H, S- CH_3), 3.06 (m, 1 H, CH_2 , cod), 2.81 (m, 1 H, CH_2 , cod), 2.75 (m, 1 H, CH_2 , cod), 2.61 (m, 1 H, CH_2 , cod), 2.55 (m, 1 H, CH_2 , cod), 2.42 (m, 1 H, CH_2 , cod), 2.40 (s, 3 H, S- CH_3), 2.15 (m, 1 H, CH_2 , cod), 2.06 (m, 1 H, CH_2 , cod), 0.90 (s, 3 H, Si- CH_3), -12.75 (s, 1 H, IrH).

$^{13}\text{C}\{^1\text{H}\}$ NMR (125 MHz, CDCl_3): δ 162.1 (q, $J_{\text{F-C}} = 50$ Hz, BAR^{F}_4), 134.9 (s, BAR^{F}_4), 129.3 (q, $J_{\text{F-C}} = 12$ Hz, BAR^{F}_4), 125.9 (q, $J_{\text{F-C}} = 273$ Hz, CF_3), 117.5 (s, BAR^{F}_4), 128.0-132.0 (s, $\text{C}_{\text{aromatics}}$), 101.7 (s, HC, cod), 96.9 (s, HC, cod), 79.7 (s, HC, cod), 75.6 (s, HC, cod), 37.5 (s, H_2C , cod), 35.1 (s, S- CH_3), 29.8 (s, H_2C , cod), 28.1 (s, H_2C , cod), 27.8 (s, H_2C , cod), 21.9 (s, S- CH_3), 1.4 (s, Si- CH_3).

ESI-MS (CH_3CN): calculated for $\{\text{C}_{23}\text{H}_{30}\text{IrS}_2\text{Si}\}^+$: 591.12; found m/z 591.12.

Elemental Analysis: $\text{C}_{55}\text{H}_{42}\text{IrS}_2\text{SiBF}_{24}\cdot 0.5(\text{CH}_2\text{Cl}_2)$ Calculated: C 44.54, H 2.90, S 4.29. Found: C 44.05, H 3.26, S 4.13.

Synthesis of $[\text{RhCl}(\text{ntyl})(\text{SiMe}(\text{o-C}_6\text{H}_4\text{SMe})_2)]$ (10)

To a Schlenk charged with $[\text{Rh}(\text{nbd})\text{Cl}]_2$ (50 mg, 0.11 mmol) and 2 equivalents of $\text{SiMeH}(\text{o-C}_6\text{H}_4\text{SMe})_2$ (**L2**) (64 mg, 0.22 mmol) 2 mL of CH_2Cl_2 were added. The solution was stirred at room temperature for 45 minutes. The mixture was concentrated under vacuum. Addition of 5 mL of pentane gave a white precipitate that was washed with pentane and dried under vacuum. Yield 72 %.

^1H NMR (500 MHz, CD_2Cl_2): δ 7.76-7.06 (8 $\text{H}_{\text{aromatics}}$), 2.88 (s, 3 H, S- CH_3), 2.42 (s, 3 H, S- CH_3), 2.37 (m, 1 H, RhCH, nortriciclyl), 1.93 (m, 1 H, CH_2 , nortriciclyl), 1.32 (m, 2 H, CH, nortriciclyl, CH_2 , nortriciclyl), 1.25 (m, 1 H, CH, nortriciclyl), 1.08 (m, 1 H, CH_2 , nortriciclyl), 1.01 (s, 3 H, Si- CH_3), 0.91 (m, 1 H, CH_2 , nortriciclyl), 0.88 (s, 1 H, CH, nortriciclyl) 0.13 (m, 1 H, CH, nortriciclyl).

$^{13}\text{C}\{^1\text{H}\}$ NMR (125 MHz, CD_2Cl_2): δ 124.7-148.3 (s, $\text{C}_{\text{aromatics}}$), 44.0 (d, $J_{\text{Rh-C}} = 23$ Hz, RhHC, nortriciclyl), 35.4 (s, HC, nortriciclyl), 33.4 (s, H_2C , nortriciclyl), 26.4 (s, S- CH_3), 22.3 (s, HC, nortriciclyl), 21.3 (s, S- CH_3), 16.0 (s, HC, nortriciclyl), 13.9 (s, H_2C , nortriciclyl), 12.3 (s, HC, nortriciclyl), -0.03 (s, Si- CH_3).

ESI-MS (CH_3CN): calculated for $\{\text{M} - \text{Cl}\}^+$ or $\{\text{C}_{22}\text{H}_{26}\text{RhS}_2\text{Si}\}^+$: 485.03; found m/z 485.03.

Elemental Analysis: $\text{C}_{22}\text{H}_{26}\text{RhClS}_2\text{Si}$ Calculated: C 50.72, H 5.03, S 12.31. Found: C 50.13, H 5.75, S 12.74.

Synthesis of [Rh(ntyI)(SiMe(*o*-C₆H₄SMe)₂)]BAR^F₄ (11)

To a Schlenk charged with [Rh(ntyI)(SiMe₂(*o*-C₆H₄SMe)₂)Cl] (**10**) (25 mg, 0.05 mmol) and 1.1 equivalents of NaBAR^F₄ (47 mg, 0.05 mmol) 2 mL of CH₂Cl₂ were added. The solution was stirred at room temperature for 30 minutes and filtered off to another schlenk. The mixture was concentrated under vacuum, 10 mL of pentane were added and the mixture was stored at -20 °C overnight to complete the crystallization of the product. Yield 55 %.

¹H NMR (500 MHz, CDCl₃): δ 7.73 (s, 8 H, BAR^F₄), 7.56 (s, 4 H, BAR^F₄), 7.65-7.38 (m, 8 H_{aromatics}), 5.50 (m, 1 H, CH, norbornenyl), 4.45 (m, 1 H, CH, norbornenyl), 3.77 (m, 1 H, CH, norbornenyl), 3.24 (m, 1 H, CH, norbornenyl), 2.61 (s, 3 H, S-CH₃), 2.29 (m, 1 H, RhCH, norbornenyl), 1.87 (s, 3 H, S-CH₃), 1.81 (s, 1 H, CH₂, norbornenyl) 1.76 (m, 1 H, CH₂, norbornenyl), 1.58 (m, 1 H, CH₂, norbornenyl), 1.48 (m, 1 H, CH₂, norbornenyl), 1.19 (s, 3 H, Si-CH₃).

¹³C{¹H} NMR (125 MHz, CDCl₃): δ 162.1 (q, J_{F-C} = 50 Hz, BAR^F₄), 134.9 (s, BAR^F₄), 129.3 (q, J_{F-C} = 12 Hz, BAR^F₄), 125.9 (q, J_{F-C} = 273 Hz, CF₃), 117.5 (s, BAR^F₄), 133.5-128.6 (s, C_{aromatic}), 107.9 (d, J_{Rh-C} = 6.7 Hz, HC, norbornenyl), 73.4 (s_{broad}, HC, norbornenyl), 56.9 (s, H₂C, norbornenyl), 48.9 (s, HC, norbornenyl), 45.8 (s, HC, norbornenyl), 26.5 (s, S-CH₃), 22.6 (s, S-CH₃), 20.1 (d, J_{Rh-C} = 11.2 Hz, HC, norbornenyl), 9.5 (s, H₂C, norbornenyl), 1.80 (s, Si-CH₃).

ESI-MS (CH₃CN): calculated for {C₁₈H₂₆RhS₂Si}⁺: 485.03; found m/z 485.03.

Elemental Analysis: C₅₄H₃₈RhS₂SiBF₂₄ Calculated: C 48.08, H 2.83, S 4.75. Found: C 47.62, H 2.91, S 4.71.

Synthesis of [Rh(cod)SiMe₂(*o*-C₆H₄SMe)₂]]BAR^F₄ (12)

To a Schlenk charged with [Rh(cod)Cl]₂ (30 mg, 0.06 mmol) in CH₂Cl₂ (5 ml) two equivalents of Me₂Si(*o*-C₆H₄SMe)₂ (**L3**) (37 mg, 0.12 mmol) and NaBAR^F₄ (108 mg, 0.12 mmol) were added. The mixture was stirred for 60 minutes, filtered into another schlenk and concentrated under vacuum. Addition of 20 mL of pentane gave a light orange precipitate that was washed with pentane twice and dried under vacuum. Yield 72 %.

¹H NMR (500 MHz, CD₂Cl₂): δ 7.64, 7.47 (m, 12 H, BAR^F₄), 7.60-7.40 (m, 8 H_{aromatics}), 4.75 (m, 2 H, CH, cod), 4.23 (m, 2 H, CH, cod), 2.48 (m, 2 H, CH₂, cod), 2.31 (s, 6 H, S-CH₃), 2.20 (m, 4 H, CH₂, cod), 1.91 (m, 2 H, CH₂, cod), 0.47 (s, 6 H, Si-CH₃).

¹³C{¹H} NMR (125 MHz, CDCl₃): δ 161.7 (q, J_{F-C} = 50 Hz, BAR^F₄), 135.1 (s, BAR^F₄), 129.5 (q, J_{F-C} = 31 Hz, BAR^F₄), 124.5 (q, J_{F-C} = 273 Hz, CF₃), 117.8 (s, BAR^F₄), 136.0-129.0 (12 C_{aromatics}), 90.1 (d, J_{Rh-C} =

10.8 Hz, 2 CH, cod), 86.8 (d, $J_{\text{Rh-C}} = 10.2$ Hz, 2 CH, cod), 32.3 (s, 2 CH₂, cod), 29.7 (s, 2 CH₂, cod), 16.2 (s, 2 S-CH₃), -0.51 (s, 2 C, Si-CH₃).

ESI-MS (CH₃CN): calculated for {C₂₄H₃₂RhS₂Si}⁺: 515.08; found m/z 515.09.

Elemental Analysis: C₅₆H₄₄RhS₂SiBF₂₄ Calculated: C 48.78, H 3.22. Found: C 48.86, H 3.18.

Synthesis of [Rh(nbd)SiMe₂(*o*-C₆H₄SMe)₂]BAr^F₄ (**13**)

To a Schlenk charged with [Rh(nbd)Cl]₂ (15 mg, 0.03 mmol) in CH₂Cl₂ (5 ml) two equivalents of Me₂Si(*o*-C₆H₄SMe)₂ (**L3**) (21 mg, 0.066 mmol) and NaBAr^F₄ (58 mg, 0.066 mmol) were added. The mixture was stirred for 60 minutes, filtered into another schlenk and concentrated under vacuum. Addition of 20 mL of pentane gave an orange precipitate that was washed twice with pentane and dried under vacuum. Yield 56 %.

¹H NMR (500 MHz, CD₂Cl₂): δ 7.64, 7.47 (m, 12 H, BAr^F₄), 7.60-7.40 (m, 8 H_{aromatics}), 4.19 (m broad, 4 H, CH, nbd), 3.92 (m, 2 H, CH, nbd), 2.16 (s, 6 H, S-CH₃), 1.44 (m, 2 H, CH₂, nbd), 0.44 (s, 6 H, Si-CH₃).

¹³C{¹H} NMR (500 MHz, CDCl₃): δ 161.7 (q, $J_{\text{F-C}} = 50$ Hz, BAr^F₄), 134.5 (s, BAr^F₄), 129.5 (q, $J_{\text{F-C}} = 31$ Hz, BAr^F₄), 124.5 (q, $J_{\text{F-C}} = 273$ Hz, CF₃), 117.8 (s, BAr^F₄), 136.0-127.0 (12 C_{aromatics}), 70.0 (m, 2 CH, nbd), 65.3 (m, CH₂, COD), 64.3 (d, $J_{\text{Rh-C}} = 6.3$ Hz, 2 CH, nbd), 53.1 (d, $J_{\text{Rh-C}} = 2.3$ Hz, 2 CH, nbd), 16.0 (s, 2 S-CH₃), -0.66 (s, 2 C, Si-CH₃).

ESI-MS (CH₃CN): calculated for {C₂₃H₂₈RhS₂Si}⁺: 499.05; found m/z 499.06.

Elemental Analysis: C₅₅H₄₀RhS₂SiBF₂₄ Calculated: C, 48.47; H, 2.96; Found: C, 48.53; H, 2.93.

Synthesis of [Ir(cod)SiMe₂(*o*-C₆H₄SMe)₂]BAr^F₄ (**14**)

To a Schlenk charged with [Ir(cod)Cl]₂ (30 mg, 0.05 mmol) in CH₂Cl₂ (5 ml) two equivalents of Me₂Si(*o*-C₆H₄SMe)₂ (**L3**) (27 mg, 0.09 mmol) and NaBAr^F₄ (80 mg, 0.09 mmol) were added. The mixture was stirred for 60 minutes, filtered into another schlenk and concentrated under vacuum. Addition of 20 mL of pentane gave an orange precipitate that was washed with pentane and dried under vacuum. Yield 64 %.

¹H NMR (500 MHz, CD₂Cl₂): δ 7.64, 7.47 (m, 12 H, BAr^F₄), 7.50-7.35 (m, 8 H_{aromatics}), 4.58 (m, 2 H, CH, cod), 3.91 (m, 2 H, CH, cod), 2.32 (m, 2 H, CH₂, cod), 2.04 (m, 2 H, CH₂, cod), 2.55 (s, 6 H, S-CH₃), 1.59 (m, 2 H, CH₂, cod), 0.51 (s, 6 H, Si-CH₃).

Elemental Analysis: C₅₆H₄₄IrS₂SiBF₂₄ Calculated: C 45.81, H 3.02. Found: C 45.69, H 2.81.

Synthesis of [Rh(Si(Me)₂(*o*-C₆H₄SMe)₂)Cl(DMSO)] (15)

To a schlenk charged with [Rh(coe)₂Cl]₂ (50 mg, 0.07 mmol) in CH₂Cl₂ (5 ml) two equivalents of Me₂Si(*o*-C₆H₄SMe)₂ (**L3**) (42.4 mg, 0.14 mmol) and an excess (60 μL) of dimethylsulfoxide were added. Stirring the mixture for 2 hours gave a yellow precipitate. This precipitate was washed with 20 mL of pentane and dried under vacuum. Yield 81 %.

¹H NMR (500 MHz, DMSO-d₆): δ 7.80-7.10 (m, 16 H_{aromatics}), 2.69 (s, 6 H, 2 S-CH₃), 2.77 (s, 6 H, 2 S-CH₃), 2.50 (s, 6H, DMSO), 0.82 (s, 6 H, 2 Si-CH₃), 0.59 (s, 6 H, 2 Si-CH₃).

Synthesis of [Rh(Me)(Si(Me)(*o*-C₆H₄SMe)₂)(MeCN)₂]BAR^F₄ (16)

To a schlenk charged with [Rh(coe)₂Cl]₂ (30 mg, 0.042 mmol) in 5 mL of CH₂Cl₂ two equivalents of Me₂Si(*o*-C₆H₄SMe)₂ (**L3**) (26 mg, 0.084 mmol) and NaBAR^F₄ (75mg, 0.084 mmol), and an excess of acetonitrile (60 μL) were added. The solution was stirred at room temperature for an hour and filtered off to another schlenk. The mixture was concentrated under vacuum and 10 mL of pentane were added. The resultant light yellow powder was washed with pentane and dried under vacuum. Yield 61 %.

¹H NMR (500 MHz, CDCl₃): δ 7.85-6.95 (m, 8 H_{aromatics}), 2.66 (s, 3 H, S-CH₃), 2.60 (s, 3 H, S-CH₃), 2.25 (m, 6 H, 2 CH₃, ACN), 0.80 (m, 3 H, Rh-CH₃), 0.61 (s, 3 H, Si-CH₃).

¹³C{¹H} NMR (500 MHz, CDCl₃): δ 161.7 (q, J_{F-C} = 50 Hz, BAR^F₄), 134.5 (s, BAR^F₄), 129.5 (q, J_{F-C} = 31 Hz, BAR^F₄), 124.5 (q, J_{F-C} = 273 Hz, CF₃), 117.8 (s, BAR^F₄), 136.0-127.0 (12 C_{aromatics}), 70.0 (m, 2 CH, cod), 65.3 (m, CH₂, cod), 64.3 (d, J_{Rh-C} = 6.3 Hz, 2 CH, cod), 53.1 (d, J_{Rh-C} = 2.3 Hz, 2 CH, cod), 16.0 (s, 2 S-CH₃), -0.66 (s, 2 C, Si-CH₃).

Elemental Analysis: C₅₂H₃₈RhS₂N₂SiBF₂₄ Calculated: C 46.17, H 2.83, N 2.07. Found: C 46.54, H 2.93, N 2.86.

Synthesis of [RhH(SiMe₂(*o*-C₆H₄SMe))(PPh₃)₂]BAR^F₄ (17)

To a Schlenk charged with [RhCl(PPh₃)₃] (100 mg, 0.11 mmol) in 5 mL of CH₂Cl₂, an equivalent of SiMe₂H(*o*-C₆H₄SMe) (**L1**) (20 mg, 0.11 mmol) and NaBAR^F₄ (98 mg, 0.11 mmol) were added. The mixture was stirred for 30 minutes, filtered off via cannula to another schlenk and

concentrated under vacuum. Addition of 20 mL of pentane gave a pale yellow precipitate that was washed with pentane and dried under vacuum. Yield 70 %.

^1H NMR (500 MHz, CD_2Cl_2): δ 7.73 (s, 8 H, BAr^{F}_4), 7.56 (s, 4 H, BAr^{F}_4), 7.61-7.10 (m, 34 H aromatics), 2.02 (s, 3 H, S- CH_3), 0.21 (s, 6 H, Si- CH_3), -9.65 (dt, $J_{\text{H-Rh}} = 22.9$ Hz, $J_{\text{H-P}} = 13.5$ Hz, HRh)

$^{13}\text{C}\{^1\text{H}\}$ NMR (125 MHz, CD_2Cl_2): δ 162.1 (q, $J_{\text{F-C}} = 50$ Hz, BAr^{F}_4), 135.1 (BAr^{F}_4), 129.3 (q, $J_{\text{F-C}} = 12$ Hz, BAr^{F}_4), 125.9 (q, $J_{\text{F-C}} = 273$ Hz, CF_3), 117.9 (s, BAr^{F}_4), 147.4-128.2 (42 $\text{C}_{\text{aromatics}}$), 21.9 (S- CH_3), 10.6 (Si- CH_3)

$^{31}\text{P}\{^1\text{H}\}$ NMR (202 MHz, CD_2Cl_2): δ 44.4 (d, $J_{\text{P-Rh}} = 118$ Hz)

$^{29}\text{Si}\{^1\text{H}\}$ NMR (99 MHz, CD_2Cl_2): δ 51.2 (obtained from correlation $^1\text{H}/^{29}\text{Si}$)

ESI-MS (CH_3OH): calculated for $\{\text{C}_{45}\text{H}_{44}\text{RhSP}_2\text{Si}\}^+$: 809.15; found m/z 809.15.

Elemental Analysis: $\text{C}_{77}\text{H}_{56}\text{RhSP}_2\text{SiBF}_4$ Calculated: C 55.28, H 3.37, S 1.92. Found: C 55.33, H 3.41, S 1.75.

Synthesis of $[\text{IrClH}(\text{SiMe}(\text{o-C}_6\text{H}_4\text{SMe})_2)(\text{PPh}_3)](\mathbf{18})$

To a Schlenk charged with $[\text{Ir}(\text{Cod})\text{Cl}]_2$ (50 mg, 0.07 mmol) in CH_2Cl_2 (5 mL), 2 equivalents of ligand $\text{SiMe}(\text{o-C}_6\text{H}_4\text{SMe})_2$ (**L2**) (44 mg, 0.15 mmol) and 2 equivalents of PPh_3 (40 mg, 0.15 mmol) were added. The mixture was stirred for 1 hour and concentrated under vacuum. Addition of 20 mL of pentane gave a pale yellow precipitate that was washed with pentane and dried under vacuum. Yield 87 %.

^1H NMR (500 MHz, CDCl_3): δ 7.70-7.05 (m, 8 $\text{H}_{\text{aromatics}}$), 3.41 (s, 3 H, S- CH_3^{a}), 2.65 (s, 3 H, S- CH_3^{b}), 0.07 (s, 3 H, Si- CH_3), -14.13 (dd, $J_{\text{P-H}} = 17.6$ Hz, Ir-H)

$^{13}\text{C}\{^1\text{H}\}$ NMR (125 MHz, CDCl_3): δ 127-153 (30 $\text{C}_{\text{aromatics}}$), 34.4 (s, S- CH_3^{a}), 21.6 (s, S- CH_3^{b}), 1.6 (s, Si- CH_3)

$^{31}\text{P}\{^1\text{H}\}$ NMR (202 MHz, CDCl_3): δ 13.3 (s)

ESI-MS (CH_3OH): Calculated for $\{\text{M} - \text{Cl}\}^+$ or $\{\text{C}_{33}\text{H}_{33}\text{IrPS}_2\text{Si}\}^+$: 745.12; found m/z 745.12.

Elemental analysis: $\text{C}_{33}\text{H}_{33}\text{IrCIPS}_2\text{Si}$ Calculated: C 50.78, H 4.26, S 8.22. Found: C 50.75, H 3.92, S 7.98.

Synthesis of $[\text{IrH}_2(\text{SiMe}(\text{o-C}_6\text{H}_4\text{SMe})_2)(\text{PPh}_3)]$ (**19**)

To a Schlenk charged with complex $[\text{IrClH}(\text{SiMe}(\text{o-C}_6\text{H}_4\text{SMe})_2)(\text{PPh}_3)]$ (**18**) (80 mg, 0.12 mmol) in 5 mL of CH_2Cl_2 an excess of 4 equivalents of LiAlH_4 (152 mg, 0.48 mmol) was added. The mixture was stirred overnight, concentrated to dryness and resuspended in benzene (5 mL). The mixture was filtered off to another schlenk and concentrated under vacuum. Addition of 20 mL of pentane gave a white precipitate that was washed with pentane and dried under vacuum. Yield 47 %.

^1H NMR (500 MHz, CDCl_3): δ 8.00-7.05 (m, 8 $\text{H}_{\text{aromatics}}$), 2.15 (s, 6 H, S- CH_3), 1.09 (s, 3 H, Si- CH_3), -15.44 (d, $J_{\text{P-H}} = 14.2$ Hz, Ir-H)

$^{13}\text{C}\{^1\text{H}\}$ NMR (125 MHz, CDCl_3): δ 154-127 (30 $\text{C}_{\text{aromatics}}$), 30.7 (s, S- CH_3), 3.4 (s, Si- CH_3)

$^{31}\text{P}\{^1\text{H}\}$ NMR (202 MHz, CDCl_3): δ 13.6 (s)

ESI-MS (CH_3OH): Calculated for $\{\text{M} - \text{H}\}^+$ or $\{\text{C}_{33}\text{H}_{33}\text{IrPS}_2\text{Si}\}^+$: 745.12; found m/z 745.12.

Elemental analysis: $\text{C}_{33}\text{H}_{34}\text{IrPS}_2\text{Si}$ Calculated: C 53.13, H 4.59, S 8.60. Found: C 52.87, H 4.41, S 7.94.

Synthesis of $[\text{IrH}(\text{SiMe}(\text{o-C}_6\text{H}_4\text{SMe})_2)(\text{PPh}_3)]\text{BAR}^{\text{F}_4}$ (**20**)

To a Schlenk charged with complex $[\text{Ir}(\text{H})(\text{SiMe}(\text{o-C}_6\text{H}_4\text{SMe})_2)\text{Cl}(\text{PPh}_3)]$ (**18**) (40 mg, 0.05 mmol) in CH_2Cl_2 (3 ml) an equivalent of $\text{NaBAR}^{\text{F}_4}$ (46 mg, 0.05 mmol) was added. The mixture was stirred for 5 minutes, filtered off to another schlenk and concentrated to dryness under vacuum. To the resultant solid 5 mL of THF were added, and the mixture was stirred for 20 minutes. Addition of 20 mL of pentane gave a pale yellow precipitate that was washed with pentane and dried under vacuum. Yield 60 %.

^1H NMR (500 MHz, THF-d_8): δ 8.00-7.00 (m, 20 $\text{H}_{\text{aromatics}}$), 3.57 (s, 4H, THF), 3.30 (s, 3 H, S- CH_3^{a}), 2.60 (s, 3 H, S- CH_3^{b}), 1.72 (s, 4H, THF), -0.06 (s, 3 H, Si- CH_3), -14.25 (d, $J_{\text{P-H}} = 14.8$ Hz, Ir-H)

$^{13}\text{C}\{^1\text{H}\}$ NMR (125 MHz, THF-d_8): δ 162.1 (q, $J_{\text{F-C}} = 50$ Hz, BAR^{F_4}), 134.9 (s, BAR^{F_4}), 129.3 (q, $J_{\text{F-C}} = 12$ Hz, BAR^{F_4}), 125.9 (q, $J_{\text{F-C}} = 273$ Hz, CF_3), 117.5 (s, BAR^{F_4}), 152.5-126.7 (30 $\text{C}_{\text{aromatics}}$), 32.7 (s, S- CH_3^{a}), 20.0 (s, S- CH_3^{b}), -2.7 (s, Si- CH_3)

$^{31}\text{P}\{^1\text{H}\}$ NMR (202 MHz, THF-d_8): δ 11,9 (s)

ESI-MS (CH_3OH): Calculated for $\{\text{C}_{33}\text{H}_{33}\text{IrPS}_2\text{Si}\}^+$: 745.12; found m/z 745.12.

Elemental analysis: C₆₅H₄₅BF₂₄PRhS₂Si Calculated: C 48.54, H 2.82, S 3.99. Found: C 48.11, H 3.01, S 4.24.

Synthesis of [Rh(SiMe(*o*-C₆H₄SMe)₂)₂]BAr^F₄ (21)

To a Schlenk charged with complex [RhH(SiMe(*o*-C₆H₄SMe)₂)(PPh₃)]BAr^F₄ (**6**) (50 mg, 0.033 mmol) in 5 mL of toluene, an excess of SiMe(*o*-C₆H₄SMe)₂ (**L2**) (15 mg, 0.05 mmol) was added. The mixture was refluxed for 2 h. Concentration under vacuum and addition of 20 mL of pentane gave a pale yellow precipitate that was washed with pentane and dried under vacuum. Yield 81 %.

¹H NMR (500 MHz, CD₂Cl₂): δ 7.95-7.00 (m, 28 H_{aromatics}), 2.90 (s, 6 H, S-CH^a₃), 2.46 (s, 6 H, S-CH^b₃), 0.27 (s, 6 H, Si-CH₃) ppm.

¹³C{¹H} NMR (125 MHz, CD₂Cl₂): δ 162.1 (q, J_{F-C} = 50 Hz, BAr^F₄), 135.2 (BAr^F₄), 129.3 (q, J_{F-C} = 12 Hz, BAr^F₄), 125.1 (q, J_{F-C} = 273 Hz, CF₃), 117.9 (s, BAr^F₄), 147.8-128.0 (24 C_{aromatics}), 26.7 (s, S-CH^a₃), 23.9 (s, S-CH^b₃), -1.7 (s, Si-CH₃) ppm.

ESI-MS (CH₃CN): calculated for {C₃₀H₃₄PRhS₂Si}⁺: 681.01; found m/z 681.01.

Elemental analysis: C₆₂H₄₆BF₂₄RhS₂Si Calculated; C 48.19, H 3.00, S 8.30. Found: C 48.45, H 3.20, S 8.09.

Synthesis of [RhClH(PPh₂(CH(Ph)CH₂CO))(py)₂] (22)

To a Schlenk charged with complex [Rh(cod)Cl]₂ (50 mg, 0.10 mmol) in CH₂Cl₂ (5 ml) 4 equivalents of pyridine (32 mg, 0.40 mmol) and a slight excess of PPh₂(CH(Ph)CH₂CHO) (75 mg, 0.25 mmol) were added. The mixture was stirred for 15 minutes and concentrated under vacuum. Addition of 20 mL of diethyl ether gave a pale yellow precipitate that was washed with diethyl ether and dried under vacuum. Yield 76 %.

¹H NMR (500 MHz, CDCl₃): δ -16.00 (dd, J_{Rh-H} = J_{P-H} = 20.0 Hz, RhH, **trans-H,Cl-22a**); -16.20 (m, RhH, **trans-H,Cl-22a'**); 8.80-6.73 (m, 25 H_{aromatics}); 3.86 (m, 1H, PhCH); 3.06 (m, 2H, CH₂).

³¹P{¹H} NMR (202 MHz, CDCl₃): δ 97.9 (d, J_{Rh-P} = 166 Hz, **trans-H,Cl-22a**); 93.9 (d, J_{Rh-P} = 169 Hz, **trans-H,Cl-22a'**).

IR (KBr, cm⁻¹): 2075 (m), ν(Rh-H); 1618 (s), ν(C=O).

ESI-MS (CH₃CN): Calculated for [M - py - H]⁺ or {C₂₆H₂₃ClNOPRh}⁺: 534.02; found m/z 534.02.

Elemental analysis: C₃₁H₂₉ClN₂OPRh Calculated: C 60.55, H 4.75, N 4.56. Found: C 61.06, H 4.82, N 4.14.

Synthesis of [Rh(Cl)₂(PPh₂(CH(Ph)CH₂CO))(py)₂] (23)

A chloroform solution of **22** (153 mg, 0.25 mmol) was left to stir for 24 hours at room temperature and concentrated under vacuum. Addition of 20 mL of diethyl ether gave a yellow precipitate that was washed with diethyl ether and dried under vacuum. Yield 61 %.

¹H NMR (500 MHz, CDCl₃): δ 9.05-6.75 (m, H_{aromatics}); 5.19 (m, PhCH); 4.87 (m, PhCH); 4.58 (m, CH₂); 4.25 (m, PhCH); 3.93 (m, CH₂); 3.80 (m, CH₂); 3.54 (m, CH₂); 3.45 (m, CH₂).

³¹P{¹H} NMR (202 MHz, CDCl₃): δ 74.4 (d, J_{Rh-P} = 135 Hz, *cis*-Cl-**23b**); 72.5 (d, J_{Rh-P} = 135 Hz, *cis*-Cl-**23b'**); 66.4 (d, J_{Rh-P} = 131 Hz, *trans*-py-**23a**).

¹³C{¹H} NMR (125 MHz, CDCl₃): δ 241.2 (d, J_{Rh-C} = 28 Hz) and 239.6 (d, J_{Rh-C} = 30 Hz) (C=O); 63.3 (d, J_{P-C} = 23 Hz), 57.3 (d, J_{P-C} = 16 Hz) and 57.0 (d, J_{P-C} = 19 Hz) (CH₂); 45.6 (d, J_{P-C} = 26 Hz), 44.1 (d, J_{P-C} = 25 Hz); 41.4 (d, J_{P-C} = 25 Hz) (PhCH).

IR (KBr, cm⁻¹): 1660 (s), ν(C=O).

ESI-MS (CH₃CN): Calculated for {M - py - Cl}⁺ or {C₂₆H₂₃ClNOPRh}⁺: 534.02; found m/z 534.02.

Elemental analysis: C₃₁H₂₈Cl₂N₂OPRh Calculated: C 57.02, H 3.95, N 4.06. Found: C 56.67, H 3.80, N 3.87.

Synthesis of [RhClH(PPh₂(CH(Ph)CH₂CO))(κ¹-PPh₂(CH(Ph)CH₂CHO))(py)] (24)

To a Schlenk charged with [Rh(cod)Cl]₂ (30 mg, 0.06 mmol) in CH₂Cl₂ (5 ml), pyridine (19 mg, 0.24 mmol) and PPh₂CH(Ph)CH₂CHO (117 mg, 0.37 mmol) were added. The mixture was stirred for 1 hour and concentrated under vacuum. Addition of 20 mL of diethyl ether gave a white precipitate that was washed with diethyl ether and dried under vacuum. Yield 82 %.

¹H NMR (500 MHz, CDCl₃): δ 8.30-6.30 (m, H_{aromatics}); 5.24 (m, PhCH); 4.30 (m, CH₂); 3.70 (m, PhCH); 3.13 (m, CH₂); 2.78 (m, CH₂); 2.60 (m, CH₂). **Data for 24a**: δ -14.75 (dd, J_{Rh-H} = 19.6 Hz, J_{P-H} = 10.9 Hz, 1H, RhH); 9.54 (d, J_{P-H} = 5 Hz, 1H, CH=O). **Data for 24a'**: δ -15.02 (dd, J_{Rh-H} = 18.8 Hz, J_{P-H} = 13.4 Hz, 1H, RhH); 9.43 (d, J_{P-H} = 3 Hz, 1H, CH=O).

$^{31}\text{P}\{^1\text{H}\}$ NMR (202 MHz, CDCl_3): **Data for 24a:** δ 80.5 (dd, $J_{\text{Rh-P}} = 136$ Hz, $P\sim\text{CO}$); 54.2 (dd, $J_{\text{Rh-P}} = 124$ Hz, $J_{\text{P-P}} = 360$ Hz, $P\sim\text{CHO}$). **Data for 24a':** δ 79.9 (dd, $J_{\text{Rh-P}} = 138$ Hz, $P\sim\text{CO}$); 52.0 (dd, $J_{\text{Rh-P}} = 126$ Hz, $J_{\text{P-P}} = 370$ Hz, $P\sim\text{CHO}$).

$^{13}\text{C}\{^1\text{H}\}$ NMR (125 MHz, CDCl_3): δ 66.1 (d, $J_{\text{P-C}} = 8$ Hz, CH_2); 45.9 (d, $J_{\text{P-C}} = 9$ Hz, CH_2); 41.1 (d, $J_{\text{P-C}} = 20$ Hz, PhCH); 36.7 (d, $J_{\text{P-C}} = 17$ Hz, PhCH). **Data for 24a:** δ 242.5 (d, $J_{\text{Rh-C}} = 32$ Hz, $P\sim\text{C=O}$); 202.9 (d, $J_{\text{P-C}} = 21$ Hz, CH=O). **Data for 24a':** δ 242.6 (d, $J_{\text{Rh-C}} = 30$ Hz, $P\sim\text{C=O}$); 201.9 (d, $J_{\text{P-C}} = 11$ Hz, CH=O).

IR (KBr, cm^{-1}): 2037 (m), $\nu(\text{Rh-H})$; 1718 (s), $\nu(\text{CHO})$; 1638 (s), $\nu(\text{C=O})$.

ESI-MS (CH_3CN): Calculated for $\{\text{M} - \text{py} - \text{Cl}\}^+$ or $\{\text{C}_{42}\text{H}_{38}\text{O}_2\text{P}_2\text{Rh}\}^+$: 739.14; found m/z 739.14.

Elemental analysis: $\text{C}_{47}\text{H}_{43}\text{ClNO}_2\text{P}_2\text{Rh}$ Calculated: C 66.09, H 5.07, N 1.64. Found: C 66.26, H 5.39, N 1.33.

Synthesis of $[\text{RhCl}(\text{PPh}_2(o\text{-C}_6\text{H}_4\text{CO}))(\kappa^1\text{-PPh}_2(\text{CH}(\text{Ph})\text{CH}_2\text{CHO}))(\text{py})]$ (25)

To a schlenk charged with compound $[\text{RhCl}(\text{H})(\text{PPh}_2(o\text{-C}_6\text{H}_4\text{CO}))(\text{py})_2]$ (35 mg, 0.26 mmol) in CH_2Cl_2 (5 ml) $\text{PPh}_2(\text{CH}(\text{Ph})\text{CH}_2\text{CHO})$ (120 mg, 0.38 mmol) was added. This solution was left to stir for 1 hour at room temperature and concentrated under vacuum. Addition of 20 mL of hexane gave a yellow precipitate that was washed with hexane and dried under vacuum. Yield 86 %.

^1H NMR (500 MHz, CDCl_3): δ -14.70 (ddd, $J_{\text{Rh-H}} = 19.4$ Hz, $J_{\text{P-H}} = 9.5$ Hz, $J_{\text{P-H}} = 4.9$ Hz, RhH); -15.06 (ddd, $J_{\text{Rh-H}} = 18.3$ Hz, $J_{\text{P-H}} = 11.9$ Hz, $J_{\text{P-H}} = 2.3$ Hz, RhH); 8.40-6.30 (m, $\text{H}_{\text{aromatics}}$). **Data for 25a:** 9.44 (d, $J_{\text{P-H}} = 3$ Hz, 1H, CH=O); 5.73 (m, 1H, PhCH); 3.05 (m, 1H, CH_2); 2.77 (m, 1H, CH_2). **Data for 25a':** 9.56 (d, $J_{\text{P-H}} = 5$ Hz, 1H, CH=O); 5.32 (m, 1H, PhCH); 4.28 (m, 1H, CH_2); 2.59 (m, 1H, CH_2).

$^{31}\text{P}\{^1\text{H}\}$ NMR (202 MHz, CDCl_3): δ 63.3 (dd, $J_{\text{Rh-P}} = 137$ Hz, $J_{\text{P-P}} = 363$ Hz, $P\sim\text{CO}$) and 55.2 (dd, $J_{\text{Rh-P}} = 125$ Hz, $J_{\text{P-P}} = 363$ Hz, $P\sim\text{CHO}$); 63.2 (dd, $J_{\text{Rh-P}} = 140$ Hz, $J_{\text{P-P}} = 372$ Hz, $P\sim\text{CO}$) and 53.2 (dd, $J_{\text{Rh-P}} = 126$ Hz, $J_{\text{P-P}} = 372$ Hz, $P\sim\text{CHO}$).

$^{13}\text{C}\{^1\text{H}\}$ NMR (125 MHz, CDCl_3): δ 237.1 (d, $J_{\text{Rh-C}} = 33$ Hz, $P\sim\text{C=O}$); 229.4 (d, $J_{\text{Rh-C}} = 32$ Hz, $P\sim\text{C=O}$). **Data for 25a:** δ 201.8 (d, $J_{\text{P-C}} = 21$ Hz, CH=O); 44.0 (s, CH_2); 34.9 (d, $J_{\text{P-C}} = 16$ Hz, PhCH). **Data for 25a':** δ 203.0 (d, $J_{\text{P-C}} = 11$ Hz, CH=O); 45.9 (d, $J_{\text{P-C}} = 9$ Hz, CH_2); 36.7 (d, $J_{\text{P-C}} = 16$ Hz, PhCH).

IR (KBr, cm^{-1}): 2046 (m), $\nu(\text{Rh-H})$; 1718 (s), $\nu(\text{CHO})$, 1621 (s), $\nu(\text{C=O})$.

ESI-MS (CH_3CN): Calculated for $\{\text{M} - \text{py} - \text{Cl}\}^+$ or $\{\text{C}_{40}\text{H}_{34}\text{O}_2\text{P}_2\text{Rh}\}^+$: 711.11; found m/z 711.11.

Elemental analysis: C₄₅H₃₉ClNO₂P₂Rh Calculated: C 65.41, H 4.76, N 1.70. Found C 64.99, H 4.71, N 1.92.

Synthesis of [RhH(PPh₂(*o*-C₆H₄CO))(κ¹-PPh₂(CH(Ph)CH₂CHO))(NN)]BPh₄ (NN = 1,10-phenantroline, **26; NN = 2,2'-bipyridine, **27**)**

To a methanol suspension of compound **25** (50 mg, 0.06 mmol) a slight excess of the corresponding NN ligand (0.07 mmol) was added. The mixture was left to stir for an hour (**26**) or 5 hours (**27**) at room temperature. The solution was concentrated under vacuum, and addition of the stoichiometric amount of NaBPh₄ (24 mg, 0.07 mmol) gave a pale yellow precipitate that was filtered off, washed with diethyl ether and dried under vacuum.

- Data for **26**. Yield 73 %.

¹H NMR (500 MHz): **Data for 26a (DMSO-d₆)**: δ -13.25 (ddd, J_{Rh-H} = 14.8 Hz, J_{P-H} = 7.2 Hz, J_{P-H} = 6.2 Hz, 1H, RhH); 9.50 (s, 1H, CH=O); 8.90-5.50 (m, 57 H_{aromatics}); 4.87 (m, 1H, PhCH); 3.30 (m, 1H, CH₂); 2.74 (m, 1H, CH₂). **Data for 26a' (CDCl₃)**: δ -12.85 (ddd, J_{Rh-H} = 18.0 Hz, J_{P-H} = 9.8 Hz, J_{P-H} = 7.0 Hz, 1H, RhH); 9.56 (s, 1H, CH=O); 8.40-5.70 (m, 57 H_{aromatics}); 5.40 (m, 1H, PhCH); 3.35 (m, 1H, CH₂); 2.86 (m, 1H, CH₂).

³¹P{¹H} NMR (202 MHz): **Data for 26a (DMSO-d₆)**: δ 238.8 (d, J_{Rh-C} = 34 Hz, C=O); 201.2 (d, J_{Rh-C} = 12 Hz, C=O); 44.7 (s, CH₂); 33.9 (d, J_{P-C} = 19 Hz, PhCH). **Data for 26a' (CDCl₃)**: δ 64.5 (dd, J_{Rh-P} = 129 Hz, P~CO); 54.0 (dd, J_{Rh-P} = 117 Hz, J_{P-P} = 321 Hz, P~CHO).

¹³C{¹H} NMR (125 MHz): **Data for 26a (DMSO-d₆)**: δ 237.1 (d, J_{Rh-C} = 33 Hz, P~C=O); 229.4 (d, J_{Rh-C} = 32 Hz, P~C=O); 201.8 (d, J_{P-C} = 21 Hz, CH=O); 44.0 (s, CH₂); 34.9 (d, J_{P-C} = 16 Hz, PhCH). **Data for 26a' (CDCl₃)**: δ 240.9 (d, J_{Rh-C} = 31 Hz, C=O); 199.6 (d, J_{P-C} = 19 Hz, CH=O); 45.8 (d, J_{P-C} = 12 Hz, CH₂); 34.0 (d, J_{P-C} = 19 Hz, PhCH).

IR (KBr, cm⁻¹): 2028 (m), ν(Rh-H); 1719 (s), ν(C=O), 1622 (s), ν(C=O).

ESI-MS (CH₃CN): Calculated for {C₅₂H₄₂N₂O₂P₂Rh}⁺: 891.18; found m/z 891.18.

Elemental analysis: C₇₆H₆₂N₂O₂P₂BRh Calculated: C 75.38, H 5.16, N 2.31. Found C 74.93, H 5.20, N 2.60.

- Data for **27**. Yield 83 %.

¹H NMR (500 MHz): δ 8.70-5.90 (m, H_{aromatics}). **Data for 27a (CDCl₃)**: δ -13.21 (ddd, J_{Rh-H} = 18.3 Hz, J_{P-H} = 10.2 Hz, J_{P-H} = 8.4 Hz, 1H, RhH); 9.52 (s, 1H, CH=O); 5.27 (m, 1H, PhCH); 3.20 (m, 1H,

CH₂); 2.79 (m, 1H, CH₂). **Data for 27a' (DMSO-d₆):** δ -13.53 (ddd, $J_{\text{Rh-H}} = 15.5$ Hz, $J_{\text{P-H}} = 7.5$ Hz, $J_{\text{P-H}} = 7.5$ Hz, 1H, RhH); 9.47 (s, 1H, CH=O); 4.78 (m, 1H, PhCH); 3.22 (m, 1H, CH₂); 2.67 (m, 1H, CH₂).

³¹P{¹H} NMR (202 MHz): **Data for 27a (CDCl₃):** δ 64.1 (dd, $J_{\text{Rh-P}} = 130$ Hz, P~CO); 54.3 (dd, $J_{\text{Rh-P}} = 118$ Hz, $J_{\text{P-P}} = 324$ Hz, P~CHO). **Data for 27a' (DMSO-d₆):** δ 65.0 (dd, $J_{\text{Rh-P}} = 131$ Hz, P~CO); 51.1 (dd, $J_{\text{Rh-P}} = 122$ Hz, $J_{\text{P-P}} = 329$ Hz, P~CHO).

¹³C{¹H} NMR (125 MHz): **Data for 27a (CDCl₃):** δ 241.6 (d, $J_{\text{Rh-C}} = 26$ Hz, P~C=O); 199.8 (d, $J_{\text{P-C}} = 20$ Hz, CH=O); 45.9 (d, $J_{\text{P-C}} = 11$ Hz, CH₂); 34.3 (d, $J_{\text{P-C}} = 20$ Hz, PhCH). **Data for 27a' (DMSO-d₆):** δ 239.2 (d, $J_{\text{Rh-C}} = 29$ Hz, P~C=O); 200.6 (d, $J_{\text{P-C}} = 19$ Hz, CH=O); 44.7 (s, CH₂); 33.8 (d, $J_{\text{P-C}} = 19$ Hz, PhCH).

IR (KBr, cm⁻¹): 2028 (m), $\nu(\text{Rh-H})$; 1719 (s), $\nu(\text{C=O})$, 1622 (s), $\nu(\text{C=O})$.

ESI-MS (CH₃CN): Calculated for {C₅₀H₄₂N₂O₂P₂Rh}⁺: 867.17; found m/z 867.17.

Elemental analysis: C₇₄H₆₂N₂O₂P₂BRh Calculated: C 74.88, H 5.26, N 2.36. Found C 74.47, H 5.10, N 2.31.

Separation of the mixture of [RhH(PPh₂(*o*-C₆H₄CO))(κ^1 -PPh₂(CH(Ph)CH₂CHO)) (Phen)]BPh₄ diastereomers 26a and 26a'

A CHCl₃ solution (3 mL) of compound **26** (20 mg) containing an equimolar mixture of **26a** and **26a'** was stirred for 12 hours. The quantitative precipitation of **26a** occurred, which was washed with diethyl ether and dried under vacuum. The remaining solution was evaporated to dryness, washed with diethyl ether and dried under vacuum to afford **26a'**.

Synthesis of [RhH(PPh₂(*o*-C₆H₄CO))(PNN)]BF₄ (PNN = κ^3 -PPh₂(CH(Ph)CH₂CNC₉H₆N, **28; κ^3 -PPh₂(CH(Ph)CH₂CNCH₂C₅H₄N, **29**)**

To a dichloromethane solution of compound **25** (50 mg, 0.06 mmol) a slight excess of the corresponding NNH₂ ligand (0.07 mmol) was added. The mixture was left to stir for 3 hours (**28**, NNH₂ = aqu) or 24 hours (**29**, NNH₂ = ampy) at room temperature. The addition of the stoichiometric amount of Et₃OBF₄ (13 mg, 0.07 mmol) gave a pale yellow precipitate that was concentrated under vacuum, filtered off, washed with diethyl ether and dried under vacuum.

- Data for **28**. Yield 73 %.

^1H NMR (500 MHz, CDCl_3): δ 9.00-5.90 (m, $\text{H}_{\text{aromatics}}$); 4.75 (m, PhCH); 4.20 (m, PhCH); 4.00 (m, CH_2); 3.60 (m, CH_2). **Data for 28a:** δ -13.55 (ddd, $J_{\text{Rh-H}} = 20.2$, $J_{\text{P-H}} = 12.9$ Hz, $J_{\text{P-H}} = 6.8$ Hz, RhH); 9.06 (s, CH=N). **Data for 28a':** δ -13.79 (ddd, $J_{\text{Rh-H}} = 22.4$, $J_{\text{P-H}} = 16.8$ Hz, $J_{\text{P-H}} = 6.2$ Hz, RhH); 9.36 (s, CH=N).

$^{31}\text{P}\{^1\text{H}\}$ NMR (202 MHz, CDCl_3): **Data for 28a:** δ 59.4 (dd, $J_{\text{Rh-P}} = 129$ Hz, P~CO); 52.6 (dd, $J_{\text{Rh-P}} = 119$ Hz, $J_{\text{P-P}} = 326$ Hz, P~NN). **Data for 28a':** δ 61.4 (dd, $J_{\text{Rh-P}} = 125$ Hz, P~CO); 45.7 (dd, $J_{\text{Rh-P}} = 120$ Hz, $J_{\text{P-P}} = 331$ Hz, P~NN).

$^{13}\text{C}\{^1\text{H}\}$ NMR (125 MHz, CDCl_3): δ 47.5 (d, $J_{\text{P-C}} = 22$ Hz, PhCH); 42.9 (d, $J_{\text{P-C}} = 10$ Hz, CH_2); 41.8 (d, $J_{\text{P-C}} = 5$ Hz, CH_2); 39.0 (d, $J_{\text{P-C}} = 22$ Hz, PhCH). **Data for 28a:** δ 239.9 (d, $J_{\text{Rh-C}} = 30$ Hz, C=O); 176.6 (s, C=N). **Data for 28a':** δ 239.2 (d, $J_{\text{Rh-C}} = 29$ Hz, C=O); 175.5 (d, $J_{\text{P-C}} = 8$ Hz, C=N).

IR (KBr, cm^{-1}): 2020 (m), $\nu(\text{Rh-H})$; 1624 (s), $\nu(\text{C=N})$.

ESI-MS (CH_3CN): Calculated for $\{\text{C}_{49}\text{H}_{40}\text{N}_2\text{OP}_2\text{Rh}\}^+$: 837.16; found m/z 837.16.

Elemental analysis: $\text{C}_{49}\text{H}_{40}\text{N}_2\text{OP}_2\text{BF}_4\text{Rh}$ Calculated: C 63.66, H 4.36, N 3.03. Found C 63.31, H 4.09, N 3.18.

- Data for 29. Yield 74 %.

^1H NMR (500 MHz, CDCl_3): δ 8.30-6.40 (m, $\text{H}_{\text{aromatics}}$); 4.85 (m, PhCH); 3.91 (m, PhCH); 3.60 (m, CH_2); 3.29 (m, CH_2). **Data for 29a:** δ -13.85 (ddd, $J_{\text{Rh-H}} = 19.6$ Hz, $J_{\text{P-H}} = 10.4$ Hz, $J_{\text{P-H}} = 9.2$ Hz, 1H, RhH); 8.79 (s, CH=N); 5.30 (d, $J_{\text{H-H}} = 16.2$ Hz, 1H, $\text{CH}_2\text{-N}$); 4.74 (d, $J_{\text{H-H}} = 16.2$ Hz, 1H, $\text{CH}_2\text{-N}$). **Data for 29a':** δ -14.08 (ddd, $J_{\text{Rh-H}} = 21.2$ Hz, $J_{\text{P-H}} = 15.2$ Hz, $J_{\text{P-H}} = 7.2$ Hz, 1H, RhH); 9.09 (s, CH=N); 5.35 (d, $J_{\text{H-H}} = 17.0$ Hz, 1H, $\text{CH}_2\text{-N}$); 4.83 (d, $J_{\text{H-H}} = 17.0$ Hz, 1H, $\text{CH}_2\text{-N}$).

$^{31}\text{P}\{^1\text{H}\}$ NMR (202 MHz, CDCl_3): **Data for 29a:** δ 56.8 (dd, $J_{\text{Rh-P}} = 125$ Hz, P~CO); 55.1 (dd, $J_{\text{Rh-P}} = 120$ Hz, $J_{\text{P-P}} = 328$ Hz, P~NN). **Data for 29a':** δ 56.6 (dd, $J_{\text{Rh-P}} = 125$ Hz, P~CO); 48.0 (dd, $J_{\text{Rh-P}} = 118$ Hz, $J_{\text{P-P}} = 333$ Hz, P~NN).

$^{13}\text{C}\{^1\text{H}\}$ NMR (125 MHz, CDCl_3): δ 46.1 (d, $J_{\text{P-C}} = 20$ Hz, PhCH); 40.7 (d, $J_{\text{P-C}} = 8$ Hz, CH_2); 39.8 (d, $J_{\text{P-C}} = 6$ Hz, CH_2); 38.7 (d, $J_{\text{P-C}} = 17$ Hz, PhCH). **Data for 29a:** δ 239.9 (d, $J_{\text{Rh-C}} = 30$ Hz, C=O); 175.0 (s, C=N); 67.7 (s, $\text{CH}_2\text{-N}$). **Data for 29a':** δ 241.2 (d, $J_{\text{Rh-C}} = 30$ Hz, C=O); 173.9 (d, $J_{\text{P-C}} = 8$ Hz, C=N); 68.8 (s, $\text{CH}_2\text{-N}$).

IR (KBr, cm^{-1}): 2029 (m), $\nu(\text{Rh-H})$; 1621 (s), $\nu(\text{C=N})$.

ESI-MS (CH_3CN): Calculated for $\{\text{C}_{46}\text{H}_{40}\text{N}_2\text{OP}_2\text{Rh}\}^+$: 801.16; found m/z 801.16.

Elemental analysis: C₄₆H₄₀N₂OP₂BF₄Rh Calculated: C 62.18, H 4.54, N 3.15. Found C 61.81, H 4.40, N 3.20.

Synthesis of [RhCl(ntyI)(PPh₂(CH(Ph)CH₂CO))(NN)] (NN = 1,10-phenantroline, **30; NN = 2,2'-bipyridine, **31**)**

To a Schlenk charged with [Rh(nbd)Cl]₂ (30 mg, 0.07 mmol) in CH₂Cl₂ (5 ml), a slight excess of phosphine PPh₂CH(Ph)CH₂CHO (47 mg, 0.15 mmol) was added. The solution was stirred for 45 min, and a stoichiometric amount of the corresponding NN ligand (0.15 mmol) was added. The mixture was stirred further for 15 min and concentrated under vacuum. Addition of diethyl ether gave red solids that were washed with diethyl ether and dried under vacuum.

- Data for **30**. Yield 75 %.

¹H NMR (500 MHz, DMSO-d₆): **Data for 30a**: δ 10.60-6.80 (m, 23 H_{aromatics}); 4.50 (m, 1H, PhCH); 3.92 (m, 1H, CH₂); 3.02 (m, 1H, CH₂); 1.77 (d, J_{H-H} = 9.4 Hz, 1H, CH₂); 1.10 (m, 2H, CH and RhCH); 0.44 (d, J_{H-H} = 9.4 Hz, 1H, CH₂); 0.36 (d, J_{H-H} = 9.4 Hz, 1H, CH₂); 0.00 (m, 1H, CH, cyclopropyl); -0.24 (d, J_{H-H} = 9.4 Hz, 1H, CH₂); -0.36 (m, 1H, CH, cyclopropyl); -1.17 (m, 1H, CH, cyclopropyl).

³¹P{¹H} NMR (202 MHz, DMSO-d₆): **Data for 30a**: δ 77.2 (d, J_{Rh-P} = 177 Hz). **Data for 30a'**: δ 80.9 (d, J_{Rh-P} = 178 Hz).

¹³C{¹H} NMR (125 MHz, DMSO-d₆): **Data for 30a**: δ 244.0 (dd, J_{Rh-C} = 22 Hz, J_{P-C} = 7 Hz, C=O); 58.0 (d, J_{P-C} = 23 Hz, CH₂); 45.5 (d, J_{P-C} = 22 Hz, PhCH); 39.0 (d, J_{Rh-C} = 6 Hz, RhCH); 38.0 (s, CH); 34.2 (s, CH₂); 31.7 (s, CH₂); 17.6 (s, CH, cyclopropyl); 12.5 (s, CH, cyclopropyl); 11.8 (s, CH, cyclopropyl).

IR (KBr, cm⁻¹): 1631 (s), ν(C=O)

ESI-MS (CH₃OH): Calculated for {M - Cl}⁺ or {C₄₀H₃₅N₂OPRh}⁺: 693.15; found m/z 693.15.

Elemental analysis: C₄₀H₃₅N₂OCIPRh Calculated: C 65.90, H 4.84, N 3.84. Found C 65.52, H 4.70, N 3.70.

- Data for **31**. Yield 76 %.

¹H NMR (500 MHz, CDCl₃): **Data for 31a**: δ 10.50-6.70 (m, 23 H_{aromatics}); 4.80 (m, 1H, PhCH); 3.62 (m, 1H, CH₂); 3.48 (m, 1H, CH₂); 1.65 (m, 1H, CH₂); 1.25 (m, 2H, RhCH and CH); 0.65 (m, 1H, CH₂); 0.60 (m, 1H, CH₂); 0.27 (m, 1H, CH, cyclopropyl); 0.09 (m, 1H, CH, cyclopropyl); 0.03 (m, 1H, CH₂); -0.64 (m, 1H, CH, cyclopropyl).

$^{31}\text{P}\{^1\text{H}\}$ NMR (202 MHz, CDCl_3): **Data for 31a:** δ 78.9 (d, $J_{\text{Rh-P}} = 177$ Hz). **Data for 31a':** δ 80.6 (d, $J_{\text{Rh-P}} = 176$ Hz).

$^{13}\text{C}\{^1\text{H}\}$ NMR (125 MHz, CDCl_3): **Data for 31a:** δ 245.8 (dd, $J_{\text{Rh-C}} = 32$ Hz, $J_{\text{P-C}} = 7$ Hz, C=O); 58.2 (d, $J_{\text{P-C}} = 22$ Hz, CH_2); 45.0 (d, $J_{\text{P-C}} = 23$ Hz, PhCH); 40.5 (d, $J_{\text{Rh-C}} = 28$ Hz, RhCH); 37.9 (s, CH); 34.3 (s, CH_2); 31.5 (s, CH_2); 17.6 (s, CH, cyclopropyl); 12.7 (s, CH, cyclopropyl); 12.1 (s, CH, cyclopropyl). **Data for 31a':** δ 247.0 (dd, $J_{\text{Rh-C}} = 27$ Hz, $J_{\text{P-C}} = 9$ Hz, C=O).

IR (KBr, cm^{-1}): 1632 (s), $\nu(\text{C}=\text{O})$.

ESI-MS (CH_3CN): Calculated for $\{\text{M} - \text{Cl}\}^+$ or $\{\text{C}_{38}\text{H}_{35}\text{N}_2\text{OPRh}\}^+$: 669.15; found m/z 669.15.

Elemental analysis: $\text{C}_{38}\text{H}_{35}\text{N}_2\text{OCIPRh}$ Calculated: C 64.74, H 5.00, N 3.97. Found C 64.43, H 4.87, N 3.63.

Synthesis of $[\text{RhCl}(\text{C}_9\text{H}_6\text{NCO})(\text{ntyl})(\text{PPh}_2(\text{CH}(\text{Ph})\text{CH}_2\text{CO})(\text{OCH}_3))] \text{ (32)}$

To a suspension of $[\text{Rh}(\text{nbd})\text{Cl}]_2$ (30 mg, 0.07 mmol) in methanol (5 mL) the phosphine $\text{PPh}_2\text{CH}(\text{Ph})\text{CH}_2\text{CHO}$ (41.5 mg, 0.13 mmol) was added. The mixture was stirred for 30 minutes at room temperature until total dissolution was obtained. An excess of $\text{C}_9\text{H}_6\text{NCHO}$ (25 mg, 0.16 mmol) was then added and the mixture was stirred for 1 hour. The solution was evaporated to dryness, redissolved in dichloromethane (1 mL) and precipitated by addition of diethyl ether (10 mL). This led to a yellow solid that was filtered off, washed with diethyl ether and dried under vacuum. Yield 91 %.

^1H NMR (500 MHz, CDCl_3): δ 9.40-6.60 (m, 21 $\text{H}_{\text{aromatics}}$); 4.48 (m, 1H, CH_2); 4.29 (m, 1H, PhCH); 4.01 (s, 3H, OCH_3); 2.92 (m, 1H, CH_2); 2.11 (d, $J_{\text{H-H}} = 10$ Hz, 1H, CH_2); 1.85 (m, 1H, CH); 1.05 (m, 1H, RhCH and 1H, CH_2); 0.83 (d, $J_{\text{H-H}} = 9$ Hz, 1H, CH_2); 0.35 (m, 1H, CH_2 and 1H, CH, cyclopropyl); 0.06 (m, 1H, CH, cyclopropyl); - 0.49 (dd, $J_{\text{H-H}} = 5$ Hz, 1H, CH, cyclopropyl).

$^{31}\text{P}\{^1\text{H}\}$ NMR (202 MHz, CD_3OD): δ 52.4 (d, $J_{\text{Rh-P}} = 184$ Hz).

$^{13}\text{C}\{^1\text{H}\}$ NMR (125 MHz, CDCl_3): δ 222.9 (d, $J_{\text{Rh-C}} = 39$ Hz, $\text{N}\sim\text{C}=\text{O}$); 180.2 (s, $\text{C}(\text{CH}_3)=\text{O}$); 53.6 (s, OCH_3); 42.6 (dd, $J_{\text{Rh-C}} = 28$ Hz, $J_{\text{P-C}} = 4$ Hz, RhCH); 38.4 (d, $J_{\text{P-C}} = 5$ Hz, CH_2); 37.8 (d, $J_{\text{P-C}} = 15$ Hz, PhCH); 37.5 (s, CH); 34.4 (s, CH_2); 32.7 (s, CH_2); 18.4 (s, CH, cyclopropyl); 13.5 (s, CH, cyclopropyl); 12.0 (s, CH, cyclopropyl).

IR (KBr, cm^{-1}): 1673 (s), $\nu(\text{C}=\text{O})$; 1642 (s), $\nu(\text{C}=\text{O})$.

ESI-MS (CH_3OH): Calculated for $\{\text{M} - \text{Cl}\}^+$ or $\{\text{C}_{39}\text{H}_{36}\text{NO}_3\text{PRh}\}^+$: 700.15; found m/z 700.15.

Elemental analysis: C₃₉H₃₆NO₃ClRh·0.5(CH₂Cl₂) Calculated: C 60.94, H 4.79, N 1.80. Found C 60.86, H 4.86, N 1.82.

Synthesis of [RhCl(C₉H₆NCO)(Hpz)(nbyl)]₂ (33)

To a suspension of [Rh(nbd)Cl]₂ (50 mg, 0.108 mmol) in methanol (5 mL) pyrazole (15 mg, 0.217 mmol) and C₉H₆NCHO (34 mg, 0.217 mmol) were added. Stirring for 2 hours at room temperature gave a yellow precipitate that was filtered off, washed with methanol and dried under vacuum. Yield 78 %.

¹H NMR (500 MHz, DMSO-d₆): **Data for 33a:** δ 14.12 (s, 2 H, NH, Hpz); 10.16-7.85 (m, 12 H_{aromatics}); 8.47 (m, 2 H, CH, Hpz); 8.13 (m, 2 H, CH, Hpz); 6.55 (d, J_{H-H} = 2 Hz, 2 H, CH, Hpz); 5.27 (dd, J_{H-H} = 3 Hz, 6 Hz, 2 H, =CH, nbyl), 4.13 (dd, J_{H-H} = 3 Hz, 6 Hz, 2 H, =CH, nbyl), 3.30 (m, 2 H, RhCH, nbyl), 2.41 (m, 2 H, CH, nbyl), 2.30 (m, 2 H, CH, nbyl), 0.92 (ddd, J_{H-H} = 4 Hz, 9 Hz, 12 Hz, 2 H, CH₂, nbyl), 0.86 (m, 4 H, CH₂, nbyl), 0.20 (dd, J_{H-H} = 5 Hz, 12 Hz, 2 H, CH₂, nbyl).

¹³C{¹H} NMR (125 MHz, DMSO-d₆): **Data for 33a:** δ 232.6 (d, J_{Rh-C} = 39 Hz, C=O), 155-122 (s, C_{aromatics}), 141.2 (s, CH, Hpz), 134.2 (s, =CH, nbyl), 133.1 (s, =CH, nbyl), 131.0 (s, CH, Hpz), 106.8 (s, CH, Hpz), 50.0 (s, CH₂, nbyl), 48.2 (s, CH, nbyl), 40.3 (s, CH, nbyl), 36.6 (d, J_{Rh-C} = 28 Hz, RhCH, nbyl), 30.6 (s, CH₂, nbyl).

IR (KBr, cm⁻¹): 1623 (s), ν(C=O); 3439 (s), ν(N-H).

ESI-MS (CH₃OH): Calculated for {M - Cl - Hpz}⁺ or {C₃₇H₃₄ClN₄O₂Rh₂}⁺: 807.48; found m/z 807.49.

Elemental analysis: C₄₀H₃₈N₆O₂Cl₂Rh₂ Calculated: C 52.71, H 4.20, N 9.22. Found C 51.56, H 3.97, N 9.34.

Synthesis of [RhCl(C₉H₆NCO)(nbyl)(Hpz)₂] (34)

Method a: To a dichloromethane (5 mL) suspension of complex **33** (35 mg, 0.038 mmol) pyrazole (5.5 mg, 0.08 mmol) was added, affording a yellow solution. The mixture was stirred for 2 hours, and concentrated under vacuum. Addition of pentane (10 mL) afforded a yellow solid that was filtered off, washed with pentane and vacuum-dried. Yield 68 %.

Method b: To a solution of complex [Rh(nbd)Cl]₂ (50 mg, 0.108 mmol) in dichloromethane (5 mL) pyrazole (30 mg, 0.434 mmol) and 8-quinolinecarbaldehyde (34 mg, 0.217 mmol) were added. The resultant yellow solution was stirred for 2 hours, and concentrated under vacuum.

Addition of pentane (10 mL) gave a yellow precipitate that was filtered off, washed with pentane and dried under vacuum. Yield 76 %.

$^1\text{H NMR}$ (500 MHz, CDCl_3 , 293 K): δ 14.50 (s, 1 H, NH, Hpz), 12.80 (s, 1 H, NH, Hpz), 10.25-7.50 (m, 6 $\text{H}_{\text{aromatics}}$), 8.35 (m, broad, CH, Hpz), 7.62 (m, 1 H, CH, Hpz), 7.20 (m, broad, CH, Hpz), 6.28 (m, 1 H, CH, Hpz), 6.00 (m, 1 H, CH, Hpz), 5.40 (dd, $J_{\text{H-H}} = 3 \text{ Hz}, 5 \text{ Hz}$, 1 H, CH, nbyl), 4.11 (dd, $J_{\text{H-H}} = 3 \text{ Hz}, 6 \text{ Hz}$, 1 H, CH, nbyl), 3.44 (m, 1 H, RhCH, nbyl), 2.45 (m, 1 H, CH, nbyl), 2.34 (m, 1 H, CH, nbyl), 1.10 (m, 1 H, CH_2 , nbyl), 1.03 (m, 1 H, CH_2 , nbyl), 0.94 (m, 1 H, CH_2 , nbyl), 0.26 (m, 1 H, CH_2 , nbyl).

$^1\text{H NMR}$ (500 MHz, CDCl_3 , 233 K): δ 14.50 (s, 1 H, NH, Hpz), 12.65 (s, 1 H, NH, Hpz), 10.40-7.50 (m, 6 $\text{H}_{\text{aromatics}}$), 8.50 (m, 1 H, CH, Hpz), 7.66 (m, 1 H, CH, Hpz), 7.28 (m, 1 H, CH, Hpz), 6.89 (m, 1 H, CH, Hpz), 6.32 (m, 1 H, CH, Hpz), 5.96 (m, 1 H, CH, Hpz), 5.40 (dd, $J_{\text{H-H}} = 3 \text{ Hz}, 5 \text{ Hz}$, 1 H, =CH, nbyl), 3.91 (dd, $J_{\text{H-H}} = 3 \text{ Hz}, 6 \text{ Hz}$, 1 H, =CH, nbyl), 3.49 (m, 1 H, RhCH, nbyl), 2.45 (m, 1 H, CH, nbyl), 2.34 (m, 1 H, CH, nbyl), 1.20 (m, 1 H, CH_2 , nbyl), 1.03 (m, 1 H, CH_2 , nbyl), 0.91 (m, 1 H, CH_2 , nbyl), 0.26 (m, 1 H, CH_2 , nbyl).

$^{13}\text{C}\{^1\text{H}\}$ NMR (125 MHz, CDCl_3 , 293 K): δ 237.8 (d, $J_{\text{Rh-C}} = 42 \text{ Hz}$, C=O), 155-122 (s, $\text{C}_{\text{aromatics}}$), 141.4 (s, CH, Hpz), 135.3 (s, =CH, nbyl), 133.6 (s, =CH, nbyl), 128.5 (s, CH, Hpz), 106.6 (s, CH, Hpz), 105.9 (s, CH, Hpz), 50.5 (s, CH_2 , nbyl), 49.8 (s, CH, nbyl), 41.3 (s, CH, nbyl), 32.2 (d, $J_{\text{Rh-C}} = 27 \text{ Hz}$, RhCH, nbyl), 32.1 (s, CH_2 , nbyl). The missing carbon signals corresponding to a pyrazole molecule cannot be found most likely due to the metallotropic tautomerism experimented by the ligand at room temperature.

IR (KBr, cm^{-1}): 1632 (s), $\nu(\text{C}=\text{O})$; 3365 (m), $\nu(\text{N-H})$.

ESI-MS (CH_3OH): Calculated for $\{\text{M} - \text{Cl} - 2\text{Hpz}\}^+$ or $\{\text{C}_{17}\text{H}_{15}\text{NORh}\}^+$: 352.02; found m/z 352.02.

Elemental analysis: $\text{C}_{23}\text{H}_{23}\text{N}_5\text{OCIRh}$ Calculated: C 52.74, H 4.43, N 13.37. Found C 52.24, H 4.43, N 13.39.

Synthesis of $[\text{Rh}(\text{C}_9\text{H}_6\text{NCO})(\text{Hpz})_3(\text{nbyl})]\text{BPh}_4$ (35)

To a methanol (5 mL) suspension of complex **34** (30 mg, 0.057 mmol) stoichiometric amounts of pyrazole (4 mg, 0.057 mmol) and NaBPh_4 (19.5 mg, 0.057 mmol) were added. The mixture was stirred for 2 hours, evaporated to dryness and redissolved in dichloromethane (5 mL). The resultant suspension was then filtered off to another schlenk, concentrated under vacuum and

pentane was added (10 mL) for precipitation. The resultant yellow solid was filtered off, washed with pentane and dried under vacuum. Yield 75 %.

$^1\text{H NMR}$ (500 MHz, CDCl_3 , 293 K): δ 15.00 (s, NH, Hpz), 8.22-6.88 (m, 6 $\text{H}_{\text{aromatics}}$), 7.80 (m, CH, Hpz), 6.38 (m, CH, Hpz), 5.45 (m, 1 H, =CH, nbyl), 3.90 (m, 1 H, =CH, nbyl), 2.98 (m, 1 H, RhCH, nbyl), 2.44 (m, 1 H, CH, nbyl), 2.27 (m, 1 H, CH, nbyl), 1.06 (m, 3 H, CH_2 , nbyl), 0.30 (dd, $J_{\text{H-H}} = 5$ Hz, 12 Hz, 1 H, CH_2 , nbyl).

$^{13}\text{C}\{^1\text{H}\}$ NMR (125 MHz, CDCl_3 , 293 K): δ 238.5 (d, $J_{\text{Rh-C}} = 30$ Hz, C=O), 152-125 ($\text{C}_{\text{aromatics}}$), 136.1 (s, =CH, nbyl), 133.5 (s, =CH, nbyl), 107.3 (s, CH, Hpz), 51.0 (s, CH_2 , nbyl), 50.1 (s, CH, nbyl), 41.5 (s, CH, nbyl), 33.4 (d, $J_{\text{Rh-C}} = 26$ Hz, RhCH, nbyl), 31.7 (s, CH_2 , nbyl).

IR (KBr, cm^{-1}): 1640 (s), $\nu(\text{C}=\text{O})$; 3229 (m), $\nu(\text{N-H})$.

ESI-MS (CH_3OH): Calculated for $\{\text{M} - 2\text{H}\}^+$ or $\{\text{C}_{26}\text{H}_{25}\text{N}_7\text{ORh}\}^+$: 554.12; found m/z 554.12.

Elemental analysis: $\text{C}_{50}\text{H}_{47}\text{N}_7\text{OBRh}$ Calculated: C 68.58, H 5.41, N 11.20. Found C 67.88, H 5.45, N 10.43.

Reaction of $[\text{RhCl}(\text{C}_9\text{H}_6\text{NCO})(\text{nbyl})(\text{Hpz})_2]$ (**34**) with triphenylphosphine

To a suspension of complex **34** (40 mg, 0.076 mmol) in dichloromethane a stoichiometric amount of triphenylphosphine (20 mg, 0.076 mmol) was added. The resultant yellow solution was stirred for 20 minutes and concentrated under vacuum. Addition of pentane (10 mL) gave a precipitate that was washed with pentane and dried under vacuum. The precipitate contains a mixture of quinolinylnorbornenyl-ketone and $[\text{RhCl}(\text{PPh}_3)_2]_2$.

Synthesis of $[\text{RhCl}(\text{C}_9\text{H}_6\text{N}(\text{C}(\text{nbyl})\text{OH}))(\text{Hpz})(\text{Ph}_2\text{PO})]$ (**36**)

Method a: To a dichloromethane (5 mL) solution of complex **34** (30 mg, 0.057 mmol) diphenylphosphine oxide $\text{Ph}_2\text{P}(\text{O})\text{H}$ (13 mg, 0.063 mmol) was added. The mixture was stirred for 16 hours, and concentrated under vacuum. Addition of pentane (10 mL) gave a yellow solid that was filtered off, washed with pentane and vacuum-dried. Yield 78 %.

Method b: To a suspension of complex **33** (70 mg, 0.077 mmol) in dichloromethane (5 mL) diphenylphosphine oxide $\text{Ph}_2\text{P}(\text{O})\text{H}$ (19 mg, 0.092 mmol) was added. The resultant solution was stirred for 16 hours. The mixture was then concentrated under vacuum, and addition of

pentane (10 mL) afforded a yellow precipitate that was filtered off, washed with pentane and dried under vacuum. Yield 85 %.

^1H NMR (500 MHz, CD_2Cl_2 , 293 K): δ 9.74-6.62 (m, 12 H, $\text{H}_{\text{aromatics}}$), 8.38 (m, 1H, CH, Hpz), 7.49 (m, 1 H, CH, Hpz), 6.10 (m, 1 H, CH, Hpz), 5.87 (dd, $J_{\text{H-H}} = 6 \text{ Hz}, 3 \text{ Hz}$, 1 H, =CH, nbyl), 5.19 (m, 1 H, =CH, nbyl), 3.15 (m, 1 H, CH, nbyl), 2.60 (m, 1 H, CH, nbyl), 2.56 (m, 1 H, CH, nbyl), 1.83 (m, 1 H, CH_2 , nbyl), 1.18 (m, 2 H, CH_2 , nbyl), 0.84 (m, 1 H, CH_2 , nbyl).

^1H NMR (500 MHz, CD_2Cl_2 , 243 K): δ 13.18 (s, 1 H, NH, Hpz), 9.83 (m, OH), 9.63-6.61 (m, 12 H, $\text{H}_{\text{aromatics}}$), 8.31 (m, 1H, CH, Hpz), 7.49 (m, 1 H, CH, Hpz), 6.09 (m, 1 H, CH, Hpz), 5.90 (m, 1 H, =CH, nbyl), 5.22 (m, 1 H, =CH, nbyl), 3.10 (m, 1 H, CH, nbyl), 2.52 (m, 2 H, CH, nbyl), 1.72 (m, 1 H, CH_2 , nbyl), 1.11 (m, 2 H, CH_2 , nbyl), 0.66 (m, 1 H, CH_2 , nbyl).

$^{31}\text{P}\{^1\text{H}\}$ NMR (202 MHz, CD_2Cl_2 , 293 K): δ 80.29 (d, $J_{\text{Rh-P}} = 150 \text{ Hz}$, **36a**).

$^{31}\text{P}\{^1\text{H}\}$ NMR (202 MHz, CD_2Cl_2 , 243 K): δ 81.92 (d, $J_{\text{Rh-P}} = 150 \text{ Hz}$, **36a**).

$^{31}\text{P}\{^1\text{H}\}$ NMR (202 MHz, CD_2Cl_2 , 193 K): δ 84.58 (d, $J_{\text{Rh-P}} = 150 \text{ Hz}$, **36a**), 82.96 (d, $J_{\text{Rh-P}} = 152 \text{ Hz}$, **36b**).

$^{13}\text{C}\{^1\text{H}\}$ NMR (125 MHz, CDCl_3 , 293 K): δ 155-121 (s, $\text{C}_{\text{aromatics}}$), 143.9 (s, CH, Hpz), 139.0 (s, =CH, nbyl), 130.4 (s, =CH, nbyl), 129.9 (s, CH, Hpz), 106.7 (s, CH, Hpz), 92.6 (d, $J_{\text{Rh-C}} = 26 \text{ Hz}$, C-OH), 51.3 (s, CH_2 , nbyl), 49.8 (s, CH, nbyl), 46.6 (s, CH, nbyl), 42.2 (s, CH, nbyl), 29.5 (s, CH_2 , nbyl).

IR (KBr, cm^{-1}): 1126 (m), $\nu(\text{P=O})$; 1625 (s), $\nu(\text{C=O})$; 3286 (m), $\nu(\text{N-H})$.

ESI-MS (CH_3OH): Calculated for $\{\text{M} - \text{Cl}\}^+$ or $\{\text{C}_{32}\text{H}_{30}\text{N}_3\text{O}_2\text{PRh}\}^+$: 622.11; found m/z 622.11.

Elemental analysis: $\text{C}_{32}\text{H}_{30}\text{N}_3\text{O}_2\text{PClRh}$ Calculated: C 58.42, H 4.60, N 6.39. Found C 57.97, H 4.45, N 5.88.

IV. 4. CATALYTIC PROCEDURES

IV. 4. 1. DEHYDROCOUPLING OF SILANES

To a boiling flask a solution of the silane (**L2**, 30 mg, 0.1 mmol or Et₃SiH, 16 μL, 0.1 mmol) in 1 mL of toluene was added. To this the [Rh] catalyst (0.005 mmol) was added.

The system was immediately sealed and heated at 110 °C for 24 h. Toluene was evaporated, and the silanes (organic phase) was extracted with pentane and filtered through silica. Pentane was removed under vacuum and the crude was checked by NMR spectroscopy.

IV. 4. 2. TÁNDEM ISOMERISATION-HYDROSILYLATION OR TÁNDEM ISOMERISATION-DEHYDROGENATIVE SILYLATION

Catalytic studies on the rhodium-catalysed alkene tandem isomerisation-hydrosilylation

General procedure for the hydrosilylation of hexene and octene isomers in CDCl₃. A Schlenck tube was charged with the catalyst (Wilkinson's, 2 mg, 0.002 mmol; **17**, 5 mg, 0.002 mmol; **5**, 2 mg, 0.002 mmol; **6**, 4 mg, 0.002 mmol), hexene (*trans*-2-, 32 μL, 0.25 mmol, 1-, 32 μL, 0.25 mmol; *cis*-2-, 32 μL, 0.25 mmol; *trans*-3-, 32 μL, 0.25 mmol) or octene (*trans*-2-, 39 μL, 0.25 mmol; *trans*-3-, 39 μL, 0.25 mmol; *trans*-4-, 39 μL, 0.25 mmol), Et₃SiH (40 μL, 0.25 mmol) and 0.5 mL of CDCl₃. The solution was stirred at room temperature (4 hours, 1-hexene; 12 hours, *trans*-2, *cis*-2- and *trans*-3- hexene). ¹H NMR of the reaction crude without previous treatment was carried out to calculate the conversion. Finally the reaction was filtered over silica to remove the catalyst and the solvent and the alkene remaining were removed under vacuum to obtain clean spectra to characterize the mixture of HexSiEt₃ and (Et₃Si)₂O.

General procedure for the hydrosilylation of alkenes without solvent. A Schlenck tube was charged with the catalyst (**17**, 5 mg, 0.002 mmol), alkene (1-hexene, 32 μL, 0.25 mmol; *trans*-2-hexene, 32 μL, 0.25 mmol; *cis*-2-hexene, 32 μL, 0.25 mmol; *trans*-3-hexene, 32 μL, 0.25 mmol; *trans*-2-heptene, 35 μL, 0.25 mmol; *trans*-2-octene, 39 μL, 0.25 mmol; *trans*-3-octene, 39 μL, 0.25 mmol; *trans*-4-octene, 39 μL, 0.25 mmol; cyclooctene, 33 μL, 0.25 mmol; *tert*-butylethylene, 32 μL, 0.25 mmol; allyltrimethylsilane, 40 μL, 0.25 mmol; styrene, 30 μL, 0.25 mmol; α-methylstyrene, 32 μL, 0.25 mmol; 4-chloro-α-methylstyrene, 36 μL, 0.25 mmol) and Et₃SiH (40 μL, 0.25 mmol). The solution was stirred at room temperature (4 hours: 1-hexene, *tert*-butylethylene, allyltrimethylsilane, styrene, α-methylstyrene, 4-chloro-α-methylstyrene; 12 hours: *trans*-2, *cis*-2- and *trans*-3- hexene, *trans*-2-, *trans*-3- and *trans*-4- octenes). ¹H NMR of the reaction crude without previous treatment was carried out to calculate the conversion. Finally the reaction was filtered over silica to remove the catalyst and the solvent and the alkene remaining were removed under vacuum to obtain clean spectra to characterize the products.

¹H NMR monitoring of the chlorination of Et₃SiH

A Young NMR tube was charged with Et₃SiH (40 μL, 0.25 mmol), **17** (5 mg, 0.002 mmol) and 0.5 mL of CDCl₃. The reaction was monitored by ¹H NMR. After 16 hours, the NMR tube was opened during 30 minutes and another ¹H NMR was carried out.

Catalytic studies on the isomerization of hexenes

1-hexene studies: In a NMR tube, 1-hexene (32 μL , 0.25 mmol) and **17** (5 mg, 0.002 mmol) were dissolved in 0.5 mL of CDCl_3 . The reaction was monitored by ^1H NMR during 2 hours. After 45 minutes the reaction was stabilized in an equilibrium mixture of hexene isomers.

Catalytic hydrosilylation of *trans*-2-octene using $(\text{EtO})_3\text{SiH}$. Formation of $\text{Oct}(\text{EtO})_3\text{Si}$

A Schlenk tube was charged with the catalyst (**17**, 5 mg, 0.002 mmol), *trans*-2-octene (39 μL , 0.25 mmol), $(\text{EtO})_3\text{SiH}$ (46 μL , 0.25 mmol) without any solvent. The solution was stirred for 3,5 hours at room temperature. ^1H NMR of the reaction crude without previous treatment was carried out to calculate the conversion. Finally the reaction was filtered over silica to remove the catalyst and the solvent and the alkene remaining were removed under vacuum to obtain clean spectra to characterize the hydrosilylation product.

Catalytic studies on the rhodium and iridium catalysed alkene tandem isomerisation-hydrosilylation or dehydrogenative silylation

General procedure for hydrosilylation of *trans*-2-octene. A Schlenk tube was charged with the catalyst (**6**, 3.8 mg, 0.0025 mmol; **18**, 2 mg, 0.0025 mmol; **19**, 1.9 mg, 0.0025 mmol; **20**, 4.2 mg, 0.0025 mmol), *trans*-2-octene (39 μL , 0.25 mmol) and Et_3SiH (40 μL , 0.25 mmol). The solution was stirred for 12 hours at room temperature (catalyst **6**) or 50 $^\circ\text{C}$ (catalysts **18**, **19** and **20**). ^1H NMR was carried out of the reaction crude without previous treatment to calculate the conversion. Finally the reaction was filtered over the silica to remove the catalyst and the solvent and the alkene remaining were removed under vacuum to obtain clean spectra to characterize the mixture of products. The conversion was determined by ^1H NMR of the crude of the reaction, by silane remaining. Selectivity was determined by ^1H NMR after being filtered over silica and removed the volatiles, by integration of the signals corresponding to the alkylsilane and allylsilane or vinylsilane products.

General procedure for hydrosilylation of alkenes with catalyst **6** and **20**. A Schlenk tube was charged with the catalyst (**6**, 3,8 mg, 0,0025 mmol); alkene (1-octene, 39 μL , 0.25 mmol; *trans*-3-octene, 39 μL , 0.25 mmol; *trans*-4-octene, 39 μL , 0.25 mmol; 1-hexene, 32 μL , 0.25 mmol; *trans*-2-hexene, 32 μL , 0.25 mmol; *trans*-3-hexene, 32 μL , 0.25 mmol; *tert*-butylethylene, 32 μL , 0.25 mmol; allyltrimethylsilane, 40 μL , 0.25 mmol; 4-bromo-1-butene, 26 μL , 0.25 mmol; styrene, 30 μL , 0.25 mmol; α -methylstyrene, 32 μL , 0.25 mmol; 4-chloro- α -methylstyrene, 36 μL , 0.25 mmol) and Et_3SiH (40 μL , 0.25 mmol). The solution was stirred for 12 hours at room

temperature (catalyst **6**) or at 50 °C (catalyst **20**). ^1H NMR was carried out of the reaction crude without previous treatment to calculate the conversion. Finally the reaction was filtered over the silica to remove the catalyst and the solvent and the alkene remaining were removed under vacuum to obtain clean spectra to characterize the mixture of the silylated product and $(\text{Et}_3\text{Si})_2\text{O}$. The conversion was determined by ^1H NMR of the crude of the reaction, by silane remaining. Selectivity was determined by ^1H NMR after being filtered over silica and removed the volatiles, by integration of the signals corresponding to the alkylsilane and allylsilane or vinylsilane products.

IV. 4. 3. DEHYDROGENATION OF AMMONIA-BORANE

Experiments were carried out in round bottom 40 ml flasks fitted with a gas outlet, with a side arm sealed with a tight-fitting septum cap. The flask was connected to a water-filled gas burette and warmed in a thermostatic bath to the required temperature. All experiments were performed at atmospheric pressure (1 atm), at a temperature of 303 K and in the presence of air, with the following proportions:

- Solvent: A 50/50 mixture of distilled THF and H₂O
- Total volume = 3 ml
- [Substrate] = 1.38 mmol (42.5 mg)

Both catalyst and substrate were weighted in tin boats, which were added into the reaction flask. Finally, the solvent mixture was syringed through the septum into the sealed flask, magnetic stirring was performed and timing started. Gas evolution began immediately and the amount of gas evolved was determined periodically by measuring the displacement of water in the burette.

IV. 5. BIBLIOGRAPHY

1. J. Chart, L. M. Venanzi, *J. Chem. Soc., A*, **1975**, 4735.
2. E. W. Abel, M. A. Bennett, G. Wilkinson, *J. Chem. Soc., A*, **1959**, 3178.
3. J. L. Herde, J. C. Lambert, C. V. Senoff, M. A. Cushing, *Cyclooctene and 1,5-Cyclooctadiene Complexes of Iridium(I)*, *Inorganic Syntheses, volume 15*, **1974**, 18-20.
4. A. van der Ent, A. L. Onderdelinden, R. A. Schunn, *Chlorobis(cyclooctene)rhodium(I) and -Iridium(I) Complexes*, *Inorganic Syntheses, volume 14*, **1973**, 92-95.
5. G. C. Anklin, P. S. Pregosin, *J. Organomet. Chem.*, **1983**, 243, 101-109.
6. S. Laue, L. Greiner, J. Wöltinger, A. Liese, *Adv. Synth. Catal.*, **2001**, 343, 711-720.
7. D. V. Moiseev, B. O. Patrick, B. R. James, *Inorg. Chem.*, **2007**, 46, 11467-11474.
8. M. A. Garralda, R. Hernández, L. Ibarlucea, E. Pinilla, M. R. Torres, M. Zarandona, *Organometallics*, **2007**, 26, 1031-1038.
9. M. Oba, Y. Kawahara, R. Yamada, H. Mizuta, K. Nishiyama, *J. Chem. Soc. Perkin Trans. 2*, **1996**, 1843-1848.

V. RESUMEN

Los compuestos organometálicos de rodio e iridio participan como catalizadores en una gran variedad de procesos de transformación de moléculas orgánicas. Entre estos procesos se encuentran las reacciones de funcionalización por adición de enlaces E-H a un enlace insaturado, tales como la hidroacilación (donde E = grupo acilo), la hidrosililación (E = SiR₃), la hidroboración (E = BR₂), la hidroaminación (E = NR₂), la hidrofosfinación (E = PR₂) o la hidrogenación (E = H). Estas reacciones de hidroelementación implican la activación previa del enlace E-H mediante adición oxidativa al centro metálico. Este primer paso conlleva, por lo general, la formación de un hidruro-compuesto.

Aunque la activación del enlace C-H en alcanos supone todavía un gran reto debido a su carácter inerte, el aldehído es un sustrato versátil que participa en un gran número de transformaciones. La adición oxidativa del enlace C-H de un aldehído a un complejo organometálico genera un derivado acilhidruro, el cual se considera intermedio en reacciones de formación de nuevos enlaces C-C como la hidroacilación. Los complejos acilhidruro presentan una baja estabilidad ya que pueden llevar a cabo la decarbonilación del aldehído, con la eliminación reductiva de un alcano. Un método que ha resultado muy útil frente a la descomposición del compuesto acilhidruro es la formación de un metalaciclo de cinco o seis miembros mediante el uso de ligandos quelantes. La 8-quinolinacarbaldehído C₉H₆NCHO y la *o*-(difenilfosfino)benzaldehído PPh₂(*o*-C₆H₄CHO) son dos ejemplos de aldehídos quelantes (Figura R1), los cuales quedarían coordinados al centro metálico a través del carbono del grupo acilo y de los átomos de nitrógeno y fósforo, respectivamente.

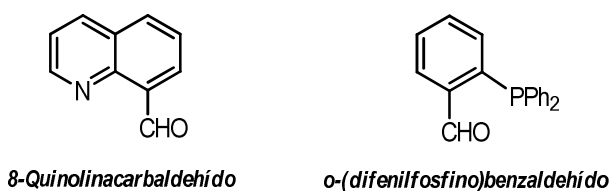
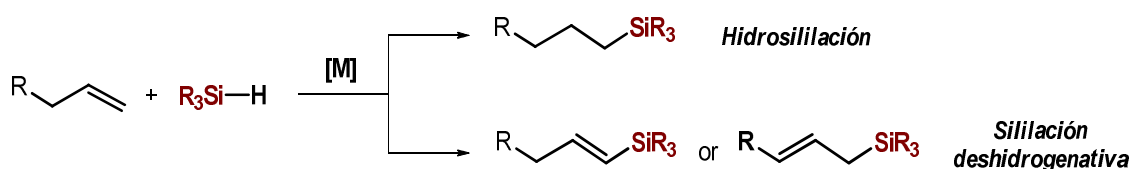


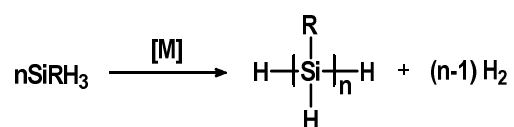
Figura R1. Estructuras de los aldehídos quelantes C₉H₆NCHO y PPh₂(*o*-C₆H₄CHO).

Por otro lado, la adición oxidativa del enlace Si-H a un centro metálico es un paso fundamental en reacciones de hidrosililación, sililación deshidrogenativa o acoplamiento deshidrogenativo de silanos. La hidrosililación es una de las reacciones más importantes en la química del silicio, e implica la adición del enlace Si-H a un enlace insaturado formando nuevos enlaces Si-C (Esquema R1). La reacción de sililación deshidrogenativa también implica la adición oxidativa del enlace Si-H, llegando a un producto alil o vinilsilano mediante un paso previo de eliminación de un átomo de hidrógeno en posición β (Esquema R1).



Esquema R1. Representación de las reacciones de hidrosililación y sililación deshidrogenativa de alquenos.

Las reacciones de acoplamiento deshidrogenativo de silanos primarios, secundarios o terciarios implican la activación del enlace Si-H por un centro metálico para la posterior formación de nuevos enlaces Si-Si (Esquema R2).



Esquema R2. Representación de acoplamiento deshidrogenativo de un silano primario.

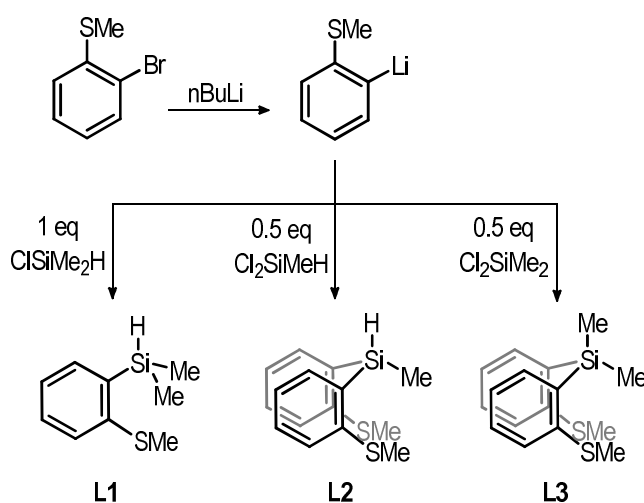
El estudio de la activación de estos enlaces Si-H y los derivados sililhidruro generados ayuda a elucidar los mecanismos implicados en este tipo de reacciones. Para ello, el uso de ligandos multidentados con enlaces Si-H capaces de formar quelatos ayuda a estabilizar el grupo sililo unido al centro metálico.

El objetivo de esta tesis es el del estudio de las activaciones de los enlaces C-H en aldehídos y Si-H en silanos por complejos organometálicos de rodio e iridio. Se describe la síntesis de varios preligandos sililo multidentados y su reactividad con varios compuestos de rodio(I) e iridio(I), así como la actividad catalítica que presentan los compuestos sililhidruro obtenidos en las reacciones de hidrosililación o acoplamiento deshidrogenativo de silanos. A su vez, se describe tanto la síntesis de compuestos acilhidruro por activación del enlace C-H en aldehídos quelantes como PPh₂CH(Ph)CH₂CHO y la 8-quinolinacetaldehído C₉H₆NCHO como su reactividad en presencia de varios ligandos nitrogenados, además del estudio de sus posibles aplicaciones catalíticas.

ACTIVACION DEL ENLACE Si-H

SINTESIS DE PRELIGANDOS MULTIDENTADOS SILIL-TIOETER Y REACTIVIDAD CON COMPLEJOS DIOLEFINICOS DE RODIO(I) E IRIDIO(I)

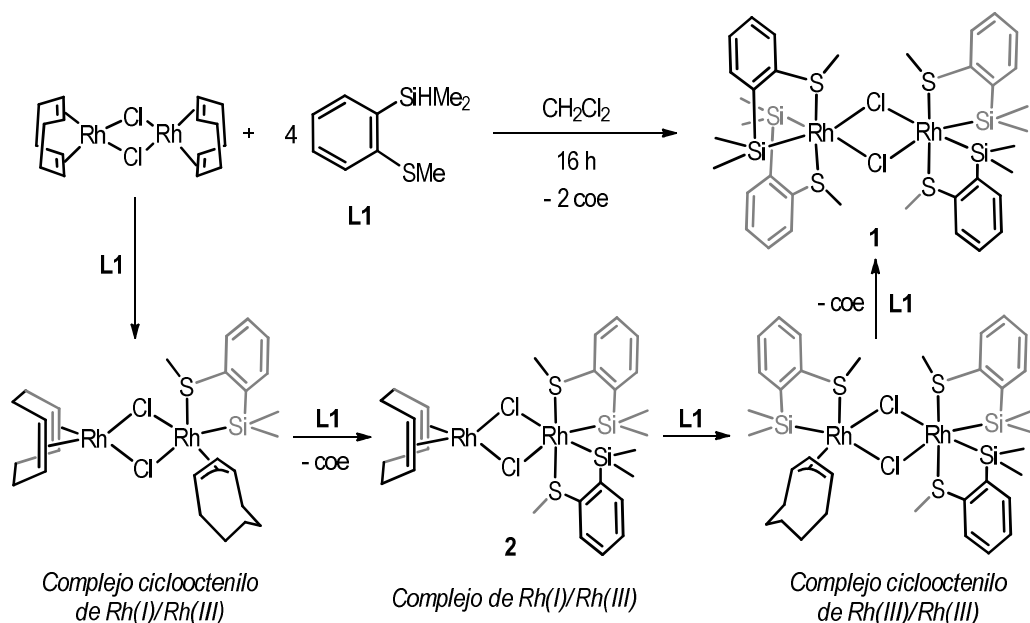
Se han sintetizado tres nuevos preligandos multidentados de tipo silano-tioeter, de formulación $\text{SiMe}_2\text{H}(o\text{-C}_6\text{H}_4\text{SMe})$ (**L1**), $\text{SiMeH}(o\text{-C}_6\text{H}_4\text{SMe})_2$ (**L2**) y $\text{SiMe}_2(o\text{-C}_6\text{H}_4\text{SMe})_2$ (**L3**), mediante la reacción de 2-MeS(C_6H_4 Br) con n-butillitio y la posterior adición del clorosilano correspondiente (Esquema R3). La reacción de estos preligandos con compuestos de rodio(I) e iridio(I) permiten estudiar reacciones de activación de enlaces Si-H o Si-C.



Esquema R3. Síntesis de ligandos multidentados silil-tioeter.

La reacción de $[\text{Rh}(\text{cod})\text{Cl}]_2$ con cuatro equivalentes de **L1** lleva a la formación de un complejo neutro dinuclear Rh(III)/Rh(III) de formulación $[\text{Rh}(\text{SiMe}_2(o\text{-C}_6\text{H}_4\text{SMe}))_2\text{Cl}]_2$ (**1**). Para la formación de **1** se propone un mecanismo que comienza con una primera activación del enlace Si-H por un centro de Rh(I), lo que generaría un compuesto de rodio-hidruro-ciclooctadieno no observable, seguido de la inserción de la diolefina en el enlace de Rh-H para dar un dímero mixto de Rh(I)ciclooctadieno/Rh(III)ciclooctenilo. La adición de otra unidad de **L1** permite una segunda activación de Si-H para dar el intermedio Rh(I)ciclooctadieno/Rh(III)bis(silano) $[(\text{cod})\text{Rh}(\mu\text{-Cl})_2\text{Rh}(\text{SiMe}_2(o\text{-C}_6\text{H}_4\text{SMe}))_2]$ (**2**). El segundo rodio, que sigue en estado de oxidación +1, seguiría el mismo proceso con la adición de una tercera molécula de **L1**, generando un compuesto de Rh(III)ciclooctenilo/Rh(III)bis(silano), y una última activación de Si-H en **L1** llevaría a la formación del producto final, Rh(III)bis(silano)/Rh(III)bis(silano) **1** (Esquema R4). Además del aislamiento del intermedio **2** de la mezcla de reacción de **L1** con $[\text{Rh}(\text{cod})\text{Cl}]_2$, la propuesta de mecanismo se apoya en la obtención de un complejo mononuclear de Rh(III)-

ciclooctenilo $[\text{Rh}(\eta^3\text{-ciclooctenyl})(\text{SiMe}(\text{o-C}_6\text{H}_4\text{SMe})_2\text{Cl})]$ (**3**) por reacción de $[\text{Rh}(\text{cod})\text{Cl}]_2$ con el preligando terdentado **L2**.



Esquema R4. Mecanismo propuesto para la formación de **1**.

La extracción del ligando cloruro del compuesto neutro **3** por reacción de éste con la sal, $\text{NaBAR}_4^{\text{F}}$, lleva a la formación del compuesto catiónico de 16e Rh(III)-ciclooctenilo, $[\text{Rh}(\eta^3\text{-ciclooctenyl})(\text{SiMe}(\text{o-C}_6\text{H}_4\text{SMe})_2)]\text{BAR}_4^{\text{F}}$ (**4**).

Con el objetivo de estudiar la posible obtención del mismo compuesto mediante la adición externa de una molécula de ciclooctadieno a un complejo de Rh(III), se han sintetizado el compuesto neutro $[\text{RhCl}(\text{H})(\text{SiMe}(\text{o-C}_6\text{H}_4\text{SMe})_2)(\text{PPh}_3)]$ (**5**) por reacción de **L2** con $[\text{RhCl}(\text{PPh}_3)_3]$, y el catiónico $[\text{Rh}(\text{H})(\text{SiMe}(\text{o-C}_6\text{H}_4\text{SMe})_2)(\text{PPh}_3)]\text{BAR}_4^{\text{F}}$ (**6**) por extracción de cloruro con $\text{NaBAR}_4^{\text{F}}$. La reacción del complejo insaturado **6** con 1,5-ciclooctadieno lleva a la coordinación y a la posterior inserción de la diolefina en el enlace Rh-H, para dar el compuesto ciclooctenilo **4** después de un reordenamiento. Esta reacción, la cual no se observa para el complejo saturado **5**, es posible gracias a la vacante coordinativa presente en el compuesto **6**.

El compuesto análogo de Ir(III) de 16e $[\text{Ir}(\eta^3\text{-ciclooctenyl})(\text{SiMe}(\text{o-C}_6\text{H}_4\text{SMe})_2)]\text{BAR}_4^{\text{F}}$ (**8**) se ha sintetizado de la misma manera que **4** por reacción de $[\text{Ir}(\text{cod})\text{Cl}]_2$ con **L2**, obteniéndose el complejo neutro $[\text{IrCl}(\eta^3\text{-ciclooctenyl})(\text{SiMe}(\text{o-C}_6\text{H}_4\text{SMe})_2)]$ y su posterior reacción con $\text{NaBAR}_4^{\text{F}}$. El compuesto **8** es inestable y se transforma en la especie hidruro $[\text{Ir}(\text{H})(\eta^4\text{-cod})(\text{SiMe}_2(\text{o-C}_6\text{H}_4\text{SMe})_2)]\text{BAR}_4^{\text{F}}$ (**9**) obteniendo la saturación coordinativa. Mediante cálculos DFT hemos podido estudiar teóricamente la transformación de **8** a **9**, la cual transcurre mediante

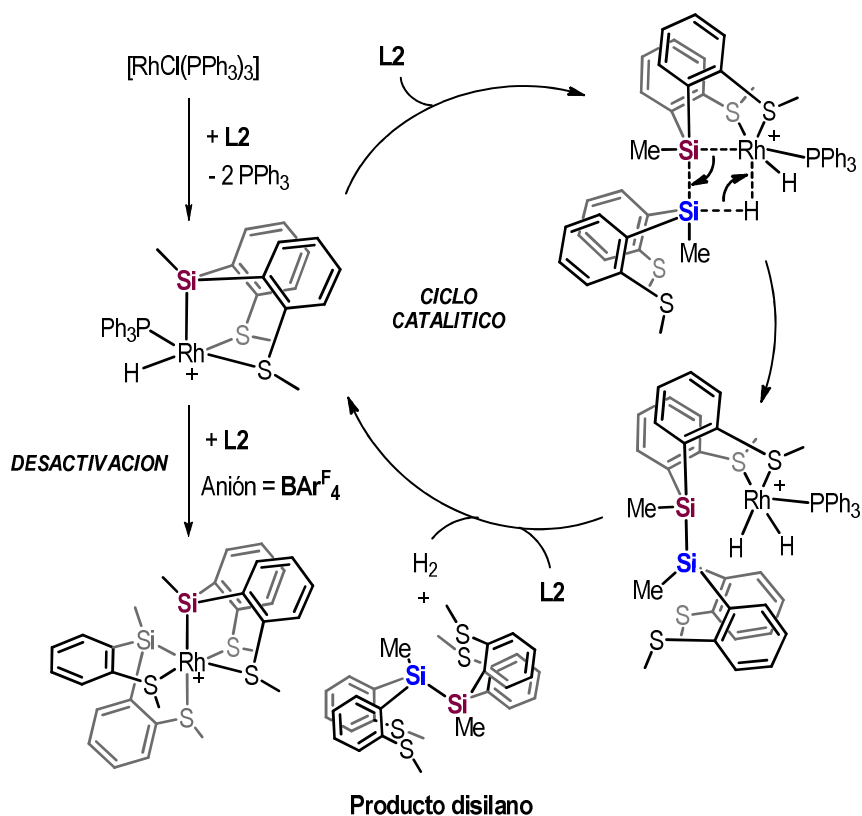
consecutivos pasos de eliminación de β-hidruro e inserción de olefina en el enlace Ir-H, en los que participan intermedios de Ir(III). La síntesis del compuesto **9** también ha sido posible por reacción directa de [Ir(cod)Cl]₂ con **L2** y NaBAR^F₄.

La reacción de [Rh(nbd)Cl]₂ con **L2** permite la formación de un compuesto de 16e [RhCl(ntyI)(SiMe₂(*o*-C₆H₄SMe)₂)] (**10**) por adición oxidativa del enlace Si-H. La inserción del ligando norbornadieno en el enlace Rh-H lleva a una especie σ-norbornenilo, la cual da lugar a un compuesto σ-nortricililo termodinámicamente favorecido mediante un reordenamiento. La extracción de cloruro no lleva a un compuesto de 14e, sino que promueve la isomerización del ligando σ-nortricililo a σ,π-norbornenilo mediante un reordenamiento inverso por la ruptura del fragmento ciclopropilo, obteniéndose el complejo de 16e [Rh(σ,π-nbyI)(SiMe₂(*o*-C₆H₄SMe)₂)]BAR^F₄ (**11**). Cálculos DFT revelan que esta transformación ocurre mediante una serie de sucesivos pasos de eliminación de β-hidruro e inserción de olefina.

La reacción de [Rh(cod)Cl]₂, [Rh(nbd)Cl]₂ y [Ir(cod)Cl]₂ con el preligando SiMe₂(*o*-C₆H₄SMe)₂ (**L3**) y NaBAR^F₄ lleva a la formación de compuestos catiónicos de 16 electrones de formulación [M(diolefina)SiMe₂(*o*-C₆H₄SMe)₂]⁺BAR^F₄⁻ por la coordinación del ligando únicamente mediante los dos fragmentos tioeter. Sin embargo, la reacción de [Rh(coe)₂Cl]₂ con **L3** y NaBAR^F₄ en presencia de acetonitrilo permite la inusual activación del enlace Si-CH₃ del ligando, generando el complejo Rh(III) de 18 electrones [Rh(Me)(Si(Me)(*o*-C₆H₄SMe)₂)(MeCN)₂]⁺BAR^F₄⁻ (**16**).

SINTESIS Y APLICACIONES CATALITICAS DE COMPUESTOS SILIL-HIDRURO DE RODIO(III) E IRIDIO(III)

La reacción de acoplamiento deshidrogenativo del silano terciario SiMeH(*o*-C₆H₄SMe)₂ (**L2**) es catalizada por el complejo neutro [RhClH(SiMe(*o*-C₆H₄SMe)₂)(PPh₃)] (**5**) para dar el producto disilano (*o*-C₆H₄SMe)₂MeSi-SiMe(*o*-C₆H₄SMe)₂. Se ha propuesto un mecanismo de reacción con la formación de **5** como la especie activa del ciclo catalítico, por la adición de una unidad del sustrato **L2** al compuesto [RhCl(PPh₃)₃]. Continúa con una metátesis de enlace σ, en el que intervendría un estado de transición de cuatro centros que permite la formación del enlace Si-Si, y el producto disilano se generaría mediante eliminación reductiva. El compuesto insaturado [Rh(H)[SiMe(*o*-C₆H₄SMe)₂](PPh₃)]BAR^F₄ (**6**) seguiría la misma ruta catalítica de metátesis de enlace σ para la formación del producto disilano, pero se observa una menor actividad catalítica por la formación de una especie inactiva de fórmula [Rh(SiMe(*o*-C₆H₄SMe)₂)₂]⁺BAR^F₄⁻ (**21**) por reacción de **6** con una segunda unidad de **L2** (Esquema R5).

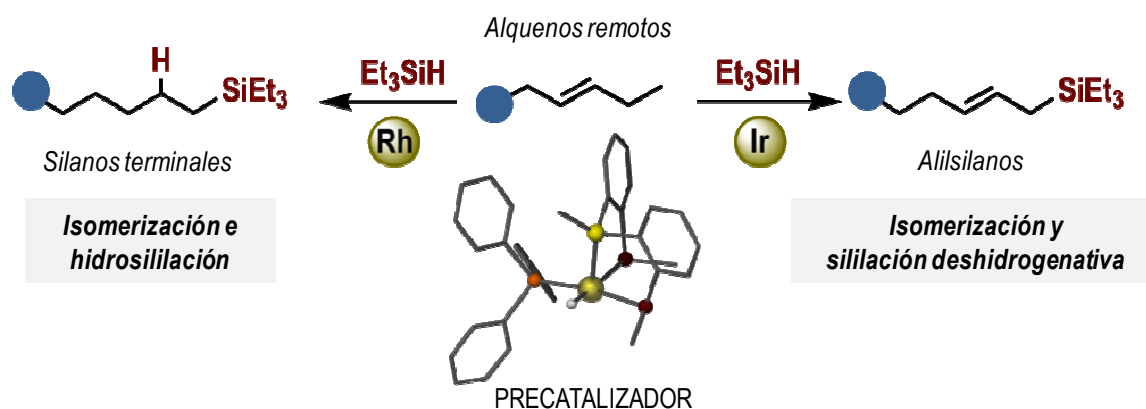


Esquema R5. Mecanismo propuesto para la formación del product disilano y el proceso de desactivación.

El complejo catiónico $[\text{RhH}(\text{SiMe}_2(o\text{-C}_6\text{H}_4\text{SMe}))(\text{PPh}_3)_2]\text{BAR}^{\text{F}_4}$ (**17**), preparado por reacción directa de $[\text{RhCl}(\text{PPh}_3)_3]$ con el preligando bidentado **L1** y $\text{NaBAR}^{\text{F}_4}$, ha resultado ser un catalizador eficiente en la reacción tándem de isomerización e hidrosililación de olefinas internas con Et_3SiH a temperatura ambiente y sin disolvente, en la que muestra una completa selectividad hacia el producto alquilsilano lineal. De esta manera, es posible la obtención de un solo producto de hidrosililación partiendo de una mezcla de varios isómeros de un mismo alqueno. El mismo complejo es capaz de catalizar la reacción de deshalogenación de CDCl_3 en presencia de Et_3SiH para dar lugar al clorosilano Et_3SiCl y a CHDCl_2 .

Por otra parte, se ha preparado el compuesto de Ir(III) $[\text{IrH}(\text{SiMe}(o\text{-C}_6\text{H}_4\text{SMe})_2)(\text{PPh}_3)(\text{THF})]\text{BAR}^{\text{F}_4}$ (**20**), estructuralmente análogo a la especie de Rh(III) $[\text{RhH}(\text{SiMe}(o\text{-C}_6\text{H}_4\text{SMe})_2)(\text{PPh}_3)]\text{BAR}^{\text{F}_4}$ (**6**), por reacción de $[\text{Ir}(\text{cod})\text{Cl}]_2$ con **L2** y PPh_3 y la posterior extracción del ligando cloruro con $\text{NaBAR}^{\text{F}_4}$ y coordinación de una molécula de THF. Los compuestos **6** y **20** también han sido utilizados como pre-catalizadores en reacciones en tándem de olefinas internas con Et_3SiH sin disolvente. El complejo de Rh(III) **6** promueve la reacción en tándem de isomerización e hidrosililación para obtener productos lineales a temperatura ambiente, mientras que el compuesto de Ir(III) **20** lleva a una reacción en tándem

de isomerización y sililación deshidrogenativa de las olefinas internas, para dar el producto alilsilano de forma mayoritaria (Esquema R6).



Esquema R6. Esquema general de la reacción de alquenos remotos con Et_3SiH catalizado por los compuestos análogos de Rh(III) e Ir(III) **6** y **20**.

ACTIVACION DEL ENLACE C-H EN ALDEHÍDOS

REACTIVIDAD DE LA FOSFINA-ALDEHIDO $\text{PPh}_2\text{CH}(\text{Ph})\text{CH}_2\text{CHO}$ CON COMPLEJOS DIOLEFINICOS DE RODIO(I)

Se ha visto que la reacción de $[\text{Rh}(\text{cod})\text{Cl}]_2$ con la mezcla racémica del fosfinoalquilaldehído $\text{PPh}_2\text{CH}(\text{Ph})\text{CH}_2\text{CHO}$ en presencia de piridina lleva a la activación del enlace C-H del grupo aldehído mediante adición oxidativa ayudada por la formación de un quelato acilfosfina, generando el complejo Rh(III)-hidrido(difenilfosfino)alquilacilo $[\text{RhClH}(\text{PPh}_2\text{CH}(\text{Ph})\text{CH}_2\text{CO})(\text{py})_2]$ (**22**) como una única especie, con una alta diastereoselectividad. Este comportamiento difiere del mostrado por fosfinoarilaldehídos similares, con los que se observa la inserción del grupo aldehído en el enlace Rh-H para generar derivados hidroxialquílicos. La reacción del acilcomplejo **22** con una molécula adicional de $\text{PPh}_2\text{CH}(\text{Ph})\text{CH}_2\text{CHO}$ no lleva a una segunda adición oxidativa, sino que genera un compuesto conteniendo un grupo aldehído libre y con los dos átomos de fósforo mutuamente *trans*, de formulación $[\text{RhClH}(\text{PPh}_2\text{CH}(\text{Ph})\text{CH}_2\text{CO})(\kappa^1\text{-PPh}_2\text{CH}(\text{Ph})\text{CH}_2\text{CHO})(\text{py})]$ (**24**), con notable diastereoselectividad. Sin embargo, la adición del arilaldehído $\text{PPh}_2(o\text{-C}_6\text{H}_4\text{CHO})$ a **22** provoca la eliminación reductiva del alquilaldehído para formar un metalacilo arilacilo de mayor estabilidad en el complejo $[\text{RhClH}(\text{PPh}_2(o\text{-C}_6\text{H}_4\text{CO}))(\kappa^1\text{-PPh}_2(\text{CH}(\text{Ph})\text{CH}_2\text{CHO}))(\text{py})]$ (**25**), como una mezcla equimolecular de dos diastereómeros. Estos resultados sugieren una barrera de activación menor para la reacción de diastereoisomerización en el caso de alquilaldehídos (**24**) que en el de arilaldehídos (**25**).

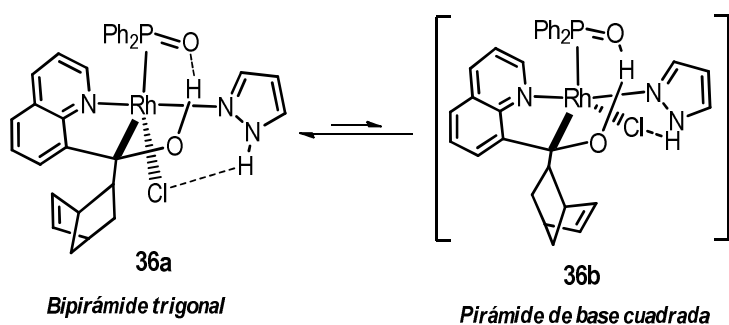
Se ha estudiado la reactividad del complejo **25** con las diiminas aromáticas 1,10-fenantrolina y 2,2'-bipiridina, con las que se consiguen complejos catiónicos de tipo $[\text{RhH}(\text{NN})(\text{PPh}_2(o\text{-C}_6\text{H}_4\text{CO}))(\kappa^1\text{-PPh}_2(\text{CH}(\text{Ph})\text{CH}_2\text{CHO}))]\text{BPh}_4$ como mezclas de dos diastereoisómeros, cuya separación física ha sido posible debido a la diferencia de solubilidad que presentan en cloroformo. En presencia de las amino-iminas, 8-aminoquinolina y 2-aminometilpiridina la fosfina P-monodentada en el complejo **25** experimenta una iminación completa para dar ligandos terdentados hemilábiles PNN en compuestos de tipo $[\text{RhH}(\text{PPh}_2(o\text{-C}_6\text{H}_4\text{CO}))(\text{PNN})]\text{BF}_4$. El comportamiento de **25** con la 2-aminometilpiridina difiere del mostrado por un compuesto similar derivado del arilaldehído $\text{PPh}_2(o\text{-C}_6\text{H}_4\text{CHO})$, el cual llevaba a la formación de un grupo hemiaminal $-\text{CH}(\text{OH})\text{NH}-$ estable. Esto puede ser debido a la mayor flexibilidad que presenta la cadena alifática de la alquilfosfina $\text{PPh}_2\text{CH}(\text{Ph})\text{CH}_2\text{CHO}$, la cual facilitaría la última etapa de condensación en la reacción entre el aldehído libre y los grupos amino.

Por último, se ha estudiado la reactividad de la fosfina $\text{PPh}_2\text{CH}(\text{Ph})\text{CH}_2\text{CHO}$ con $[\text{Rh}(\text{nbd})\text{Cl}]_2$, consiguiéndose derivados σ -norticiclilo de tipo $[\text{RhCl}(\text{NN})(\text{Ntyl})(\text{PPh}_2\text{CH}(\text{Ph})\text{CH}_2\text{CO})]$ cuando la reacción se lleva a cabo en presencia de diiminas N-dadoras, mediante la inserción del ligando norbornadieno en el enlace Rh-H y una posterior reorganización. En todos los casos se consigue una mezcla de diastereoisómeros de un solo isómero geométrico, en una proporción de 75:25. Si la reacción entre la fosfina y $[\text{Rh}(\text{nbd})\text{Cl}]_2$ se realiza en metanol y en presencia de 8-quinolinacarboxaldehído, se produce la transformación del alquilaldehído en alquilester y la adición oxidativa del arilaldehído generando el complejo $[\text{RhCl}(\text{Ntyl})(\text{C}_9\text{H}_6\text{NCO})(\kappa^2\text{-PPh}_2\text{CH}(\text{Ph})\text{CH}_2\text{CO}(\text{OCH}_3))]$ (**32**), pasando por un intermedio (difenilfosfino)hemiacetal con la fosfina coordinada como P-monodentada. El nuevo ligando hemilábil P,O permite una completa isomerización consiguiendo un único diastereoisómero.

REACTIVIDAD DE $[\text{Rh}(\text{nbd})\text{Cl}]_2$ CON 8-QUINOLINACARBOXALDEHIDO Y PIRAZOL. APLICACIONES CATALITICAS.

El acilaldehído $\text{C}_9\text{H}_6\text{NCHO}$ reacciona con $[\text{Rh}(\text{nbd})\text{Cl}]_2$ en presencia de pirazol para formar el compuesto dinuclear $[\text{RhCl}(\text{C}_9\text{H}_6\text{NCO})(\text{Hpz})(\text{nbyl})]_2$ (**33**), y los compuestos mononucleares neutro y catiónico $[\text{RhCl}(\text{C}_9\text{H}_6\text{NCO})(\text{Hpz})_2(\text{nbyl})]$ (**34**) y $[\text{Rh}(\text{C}_9\text{H}_6\text{NCO})(\text{Hpz})_3(\text{nbyl})]\text{BPh}_4$ (**35**) respectivamente, formados por inserción del norbornadieno en el enlace Rh-H para dar el derivado σ -norbornenilo, o el σ -norticiclilo en una menor proporción. La formación de enlaces de hidrógeno $\text{N-H}\cdots\text{O}$ y $\text{N-H}\cdots\text{Cl}$ entre el ligando pirazol y el grupo acilo o el ligando cloruro estabilizan estos compuestos.

La adición de trifenilfosfina al compuesto dinuclear **33** lleva a la eliminación reductiva del producto quinolinilnorbornenil-cetona $C_9H_6NC(O)Nbyl$. Sin embargo, con la adición del óxido de difenilfosfina se genera un fragmento quinolinil(norbornenilhidroxialquilo) en el compuesto insaturado $[RhCl(C_9H_6NC(nbyl)OH)](Hpz)(Ph_2PO)$ (**36a**), el cual presenta una estructura de bipirámide trigonal. Esto ocurre por la migración del ligando σ -norbornenilo hacia el átomo de carbono en la acilquinolina, con la formación de un nuevo enlace C-C y una transferencia de hidrógeno de esfera externa desde el ácido fosfínico hasta el fragmento carboxi coordinado. Al bajar la temperatura se revela un equilibrio entre la especie insaturada de estructura de bipirámide trigonal y una especie de estructura de pirámide de base cuadrada (**36b**) (Esquema R7).



Esquema R7. Equilibrio entre la especie bipirámide trigonal **36a** y la pirámide de base cuadrada **36b**.

Los cuatro compuestos Rh(III)-alquil(acilquinolina) han demostrado ser catalizadores homogéneos eficientes en la reacción de hidrólisis del aducto de amoniaco-borano en una mezcla de THF/ H_2O , a $30\text{ }^\circ\text{C}$ en presencia de aire. Con todos los complejos se genera casi el total de tres equivalentes de hidrógeno por mol de sustrato, siendo el compuesto dinuclear **33** el que muestra una mayor actividad catalítica.